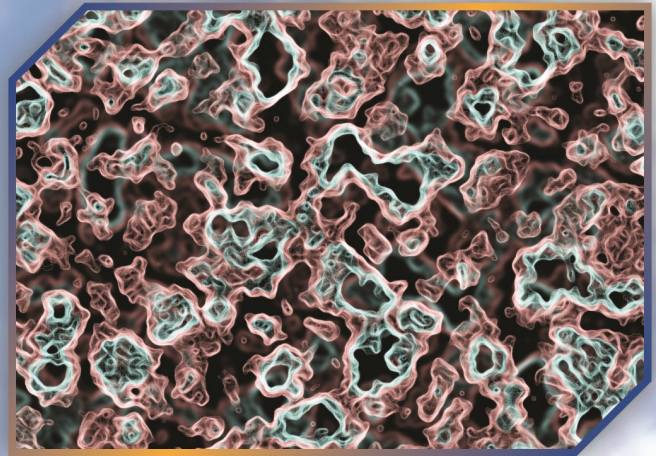


Environmental Research & Technology

YEAR : 2020 | VOLUME : 03 | ISSUE : 04

e-ISSN: 2636-8498





Environmental Research & Technology

<http://dergipark.gov.tr/ert>



ACADEMIC ADVISORY BOARD

Prof. Dr. Adem Basturk (Yildiz Technical University)

Prof. Dr. Mustafa Ozturk (Yildiz Technical University)

Prof. Dr. Lutfi Akca (Istanbul Technical University)

Prof. Dr. Oktay Tabasaran (Stuttgart University)

Prof. Dr. Ahmet Demir (Yildiz Technical University)

SCIENTIFIC DIRECTOR

Prof. Dr. Ahmet Demir (Yildiz Technical University)

EDITOR IN CHIEF

Prof. Dr. Mehmet Sinan Bilgili (Yildiz Technical University)

ASSISTANT EDITOR

Assoc. Prof. Dr. Hanife Sari Erkan (Yildiz Technical University)

CONTACT

Yildiz Technical University
Environmental Engineering Department, 34220 Esenler
Istanbul – Turkiye
Web: <http://dergipark.gov.tr/ert/>
E-mail: ert@yildiz.edu.tr



Environmental Research & Technology

<http://dergipark.gov.tr/ert>



Co-Editors (Air Pollution)

Prof. Dr. Arslan SARAL (Yildiz Technical University, Turkiye)
Prof. Dr. Mohd Talib LATIF (Universiti Kebangsaan, Malaysia)
Prof. Dr. Nedim VARDAR (Interamerican University of Puerto Rico, Puerto Rico)
Prof. Dr. Sait Cemil SOFUOGLU (Izmir Institute of Technology, Turkiye)
Prof. Dr. Wina GRAUS (Utrecht University, The Netherlands)

Co-Editors (Environmental Engineering and Sustainable Solutions)

Prof. Dr. Bulent Inanc (Istanbul Technical University, Turkiye)
Prof. Dr. Guleda ENGIN (Yildiz Technical University, Turkiye)
Prof. Dr. Hossein KAZEMIAN (The University of Northern British Columbia, Canada)
Prof. Dr. Raffaella POMI (Sapienza University of Rome, Italy)
Prof. Dr. Yilmaz YILDIRIM (Bulent Ecevit University, Turkiye)
Prof. Dr. Zenon HAMKALO (Ivan Franko National University of Lviv, Ukraine)

Co-Editors (Waste Management)

Prof. Dr. Bestami OZKAYA (Yildiz Technical University, Turkiye)
Prof. Dr. Bulent TOPKAYA (Akdeniz University, Turkiye)
Prof. Dr. Kahraman UNLU (Middle East Technical University, Turkiye)
Prof. Dr. Mohamed OSMANI (Loughborough University, United Kingdom)
Prof. Dr. Pin Jing HE (Tongji University, China)

Co-Editors (Water and Wastewater Management)

Prof. Dr. Ayse FILIBELI (Dokuz Eylul University, Turkiye)
Prof. Dr. Baris CALLI (Marmara University, Turkiye)
Prof. Dr. Marina PRISCIANDARO (University of L'Aquila, Italy)
Prof. Dr. Selvam KALIYAMOORTHY (Nagoya University, Japan)
Prof. Dr. Subramanyan VASUDEVAN (Central electrochemical Research Institute, India)



Editorial Board

Prof. Dr. Andjelka MIHAJLOV (University of Novi Sad, Serbia)

Prof. Dr. Aysegul PALA (Dokuz Eylul University, Turkiye)

Prof. Dr. Azize AYOL (Dokuz Eylul University, Turkiye)

Prof. Dr. Didem OZCIMEN (Yildiz Technical University, Turkiye)

Prof. Dr. Eyup DEBIK (Yildiz Technical University, Turkiye)

Prof. Dr. Gulsum YILMAZ (Istanbul Universtiy Cerrahpasa, Turkiye)

Prof. Dr. Hanife BUYUKGUNGOR (Ondokuz Mayıs University, Turkiye)

Prof. Dr. Ismail KOYUNCU (Istanbul Technical University, Turkiye)

Prof. Dr. Lucas Alados ARBOLEDAS (University of Granada, Spain)

Prof. Dr. Marcelo Antunes NOLASCO (University of São Paulo, Brazil)

Prof. Dr. Mehmet Emin AYDIN (Necmettin Erbakan University, Turkiye)

Prof. Dr. Mukand S. BABEL (Asian Institute of Technology, Thailand)

Prof. Dr. Mufide BANAR (Eskisehir Technical University, Turkiye)

Prof. Dr. Nihal BEKTAŞ (Gebze Technical University, Turkiye)

Prof. Dr. Osman ARIKAN (Istanbul Technical University, Turkiye)

Prof. Dr. Omer AKGIRAY (Marmara University, Turkiye)

Prof. Dr. Pier Paolo MANCA (University of Cagliari, Italy)

Prof. Dr. Saim OZDEMIR (Sakarya University, Turkiye)

Prof. Dr. Serdar AYDIN (Istanbul Universtiy Cerrahpasa, Turkiye)

Prof. Dr. Ulku YETIS (Middle East Technical University, Turkiye)

Prof. Dr. Yaşar NUHOGLU (Yildiz Technical University, Turkiye)



Environmental Research & Technology

<http://dergipark.gov.tr/ert>



- Prof. Dr. Artur J. BADA (Warsaw University of Technology, Poland)
- Prof. Dr. Aysen ERDINCLER (Bogazici University, Turkiye)
- Prof. Dr. Bulent KESKINLER (Gebze Technical University, Turkiye)
- Prof. Dr. Erwin BINNER (University of Natural Resources and Life Science, Austria)
- Prof. Dr. F. Dilek SANIN (Middle East Technical University, Turkiye)
- Prof. Dr. Hamdy SEIF (Alexandria University, Egypt)
- Prof. Dr. Ilirjan MALOLLARI (University of Tirana, Albania)
- Prof. Dr. Jaakko PUHAKKA (Tampere University Finland)
- Prof. Dr. Mahmoud A. ALAWI (University of Jordan, Jordan)
- Prof. Dr. Martin KRANERT (University of Stuttgart, Germany)
- Prof. Dr. Mesut AKGUN (Yildiz Technical University, Turkiye)
- Prof. Dr. Mustafa ODABASI (Dokuz Eylul University, Turkiye)
- Prof. Dr. Mufit BAHADIR (Technische Universität Braunschweig, Germany)
- Prof. Dr. Nurdan Gamze TURAN (Ondokuz Mayıs University, Turkiye)
- Prof. Dr. Osman Nuri AGDAG (Pamukkale University, Turkiye)
- Prof. Dr. Ozer CINAR (Yildiz Technical University, Turkiye)
- Prof. Dr. Recep BONCUKCUOGLU (Istanbul University Cerrahpasa, Turkiye)
- Prof. Dr. Sameer AFIFI (Islamic University of Gaza, Palestine)
- Prof. Dr. Timothy O. RANDHIR (University of Massachusetts Amherst, U.S.A.)
- Prof. Dr. Victor ALCARAZ GONZALEZ (University of Guadalajara, Mexico)



Environmental Research & Technology

<http://dergipark.gov.tr/ert>



TABLE OF CONTENTS

<i>Title</i>	<i>Pages</i>
Research Articles	
Treatment of dye-producing chemical industry wastewater by persulfate advanced oxidation DOI: https://doi.org/10.35208/ert.771190 <i>Deniz İzlen Cifci, Elçin Güneş, Yalçın Güneş</i>	149-156
Experimental evaluation of compressibility parameters of lime and silica fume stabilized dredged soil DOI: https://doi.org/10.35208/ert.782042 <i>Inci Develioglu, Hasan Fırat Pulat</i>	157-165
Preparation of coal-derived magnetic carbon material for magnetic solid-phase extraction of fungicides from water samples DOI: https://doi.org/10.35208/ert.788913 <i>Gizem Tarhan, Elif Yıldız, Atakan Toprak, Hasan Çabuk</i>	166-174
Evaluation of electrochemical treatment of real hospital wastewater with different electrode materials DOI: https://doi.org/10.35208/ert.785556 <i>Gülizar Kurtoğlu Akkaya</i>	175-181
The biosynthesis of silver nanoparticles with fungal cytoplasmic fluid obtained from <i>Phanerochaete chrysosporium</i> ME446 DOI: https://doi.org/10.35208/ert.788891 <i>Fatma Deniz, Mehmet Ali Mazmanlı</i>	187-192
Assessment of ship emissions through cold ironing method for Iskenderun Port of Turkey DOI: https://doi.org/10.35208/ert.794595 <i>Alper Kılıç, Mustafa Yolcu, Fuat Kılıç, Levent Bilgili</i>	193-201
Ecologically friendly production of copper powder and elimination of cupric ions from aqueous solutions using D-Glucose and ascorbic acid DOI: https://doi.org/10.35208/ert.802170 <i>Esmâ Mahfouf, Souad Djerad, Raouf Bouchareb</i>	202-208
Characterization of pistachio processing industry wastewater and investigation of chemical pretreatment DOI: https://doi.org/10.35208/ert.800721 <i>Sevtap Tırınk, Alper Nuhoglu, Sinan Kul</i>	209-216

Assessment of toxic and essential metals in fish feed ingredients available in different areas of Bangladesh 217-224

DOI: <https://doi.org/10.35208/ert.838481>

Biraj Saha, Md. Abdul Mottalib, A. N. M. Al-Razee

Spatiotemporal modeling of nutrient retention in a tropical semi-arid basin 225-237

DOI: <https://doi.org/10.35208/ert.782409>

Saheed Adekunle Raji, Shakirudeen Odunuga, Mayowa Fasona

Review Article

Bio-electroactive fuel cells and their applications 182-186

DOI: <https://doi.org/10.35208/ert.788183>

Afşin Çetinkaya, Sadullah Levent Kuzu, Ahmet Demir



RESEARCH ARTICLE

Treatment of dye-producing chemical industry wastewater by persulfate advanced oxidation

Deniz Izlen Cifci^{1,*}, Elçin Güneş¹, Yalçın Güneş¹

¹Tekirdağ Namık Kemal University, Environmental Engineering Department, 59860 Çorlu, Tekirdağ, TURKIYE

ABSTRACT

A dye-producing chemical industry wastewater in Çorlu (Tekirdağ) is treated by the coagulation-flocculation process of the wastewater. However, the wastewater discharged after coagulation-flocculation still has a very high COD (4402 mg L⁻¹) with very high proportion of dissolved COD (4316 mg L⁻¹). Therefore, the aim of this study is to achieve higher COD and color removal in wastewater using Fe²⁺/S₂O₈ or UV/S₂O₈ oxidation process after coagulation-flocculation. The processes in the oxidation of this industrial wastewater using Fe²⁺/S₂O₈ and UV/S₂O₈ were examined and the effect of COD/Fe²⁺/S₂O₈ ratio (in Fe²⁺/S₂O₈) or COD/S₂O₈ ratio (in UV/S₂O₈), pH and oxidation time were evaluated in the study. While high organic matter and color removal was observed in acidic conditions for both processes, optimum pH were 3 and 6 in Fe²⁺/S₂O₈ and UV/S₂O₈ oxidation processes, respectively. In Fe²⁺/S₂O₈ oxidation, 61.1% of COD removal and above 97% of color (UV₄₃₆, UV₅₂₅ and UV₆₂₀) removal was obtained at 1/8/8 of COD/Fe²⁺/S₂O₈ ratio and pH 3 after 1 h oxidation. In UV/S₂O₈ oxidation (COD/S₂O₈ ratio 1/8, pH 6), 54.4% of COD and 98% of color (UV₄₃₆, UV₅₂₅ and UV₆₂₀) removals were achieved after 4 h oxidation. As a result, both Fe²⁺/S₂O₈ and UV/S₂O₈ oxidation processes were applied to ensure discharge standards for color removal from this chemical industry wastewater are effective methods as they provide over 97% color removal. Moreover, COD removal efficiency was approximately 55-60% in both methods.

Keywords: Activation, kinetics, oxidation, persulfate, industrial wastewater treatment

1. INTRODUCTION

The chemical industry is considered a highly polluting sector. Generally, the chemical industry does not alter chemical products and processes and prefers to deal with the end of the pipe for the management of wastewater [1]. The chemical industry produces special chemicals such as adhesives, sealants, catalysts, coatings, plastic adhesives, and personal care products such as pharmaceuticals, soaps, detergents, shampoos, creams from various raw materials [1]. One of the chemical industries, the dye-producing chemical industry uses many different raw materials (aniline, soluble, etc.), auxiliary chemicals, dyes and intermediates, many of which can be toxic to the environment and have carcinogenic effects in humans [2]-[3]. Auxiliary chemicals, dyes and intermediates include many agents, phosphates, polyamide resins, acrylic coatings and the wastewaters formed have high organic matter, non-biodegradable and toxic substances [4].

Advanced oxidation technologies are suitable and effective method for the treatment of high non-biodegradable and persistent organic pollutants in industrial wastewaters [5]. Although hydroxyl (OH[•]) production processes such as Fenton and UV photocatalysis oxidation processes have been used as advanced oxidation processes for many years, interest in the persulfate oxidation processes for producing the sulfate radical has increased for persistent organic pollutant removal in recent years [6]. SO₄^{•-} has become an alternative to OH[•] radical for the organic compound degradation and wastewater treatment due to the high redox potential (2.5-3.1 V) and longer lifetime (3-4.10⁻⁵ s) [7].

Methods such as heat, UV, alkaline, metal ions and activated carbon is used to activate the persulfate to generate sulphate free radicals [8]-[9]. Many studies showed that the sulfate radical based treatment is very effective and promising results for various organic pollutants and dye treatment [9]-[10]. However, the

Corresponding Author: dicifci@nku.edu.tr (Deniz Izlen Cifci)

Received 18 June 2020; Received in revised form 24 September 2020; Accepted 28 September 2020

Available Online 2 November 2020

Doi: <https://doi.org/10.35208/ert.771190>

© Yildiz Technical University, Environmental Engineering Department. All rights reserved.

studies generally focused on leachate treatment, and it was stated that UV/S₂O₈, Fe/S₂O₈ oxidation processes were effective for the treatment of landfill leachate [11]-[16]. In addition, studies show that the UV/S₂O₈ or Fe/S₂O₈ oxidation processes can be used in the treatment of petrochemical wastewater that 66-69% of COD removal could be achieved up to 120 min oxidation [17]-[19]. Treatment of dye-producing chemical industry wastewater by UV/S₂O₈ or Fe/S₂O₈ persulfate oxidation has not been studied yet. Studies on the comparison of iron and UV activation methods for persulfate oxidation are insufficient and it could not be determined which method was more effective for organic matter removal. In this study, the chemically treated wastewater of a chemical industry, which produces dyes for textile, paper, plastic (masterbatch) and metal industries was trying to be treated by UV/S₂O₈ and Fe/S₂O₈ persulfate oxidation method. The wastewater of this industry is quite complex and much polluted in terms of organic matter and color so to treat it very hard. The aim of this study is to compare iron and UV activation methods for persulfate oxidation process in terms of COD and color removal efficiencies. For this purpose, the optimum pH, oxidation time and persulfate doses in both methods were determined and the kinetic evaluations of the processes were also made.

2. MATERIALS AND METHODS

2.1. Wastewater characterization

Wastewater was taken from dye-producing chemical industry. In this industry, dispersed dyes, reactive dyes, acrylic dyes, acid dyes, digital inks, digital auxiliaries, pigments and chemical groups of liquid, powder and dispersion products used in the textile industry are produced. Hybrid electrostatic powder paint for metal industry, and paper auxiliaries, brown paint, optical brightener and performance chemicals for the paper industry are also produced. The wastewater in this chemical industry is chemically treated using FeCl₃ as a coagulant and then transferred to the central wastewater treatment plant of the industrial zone in Çerkezköy, Tekirdağ. The wastewater used in the study was taken after the coagulation-flocculation process. The characterization of the wastewater is given in Table 1. As seen from Table 1, although the wastewater is the chemically treated, the COD concentration is quite high, but the majority of the COD is in soluble form. In addition, the low TSS concentration in the wastewater shows that the particulate matter in the wastewater is low due to chemical treatment as expected. The color (UV₄₃₆-UV₅₂₅-UV₆₂₀) values in the wastewater are quite high and the wastewater has a brown-red color.

Table 1. The characterization of the wastewater

Parameter	Unit	Concentration
pH	-	7.84
EC	mS cm ⁻¹	6.84
TSS	mg L ⁻¹	87±2.0
VSS	mg L ⁻¹	42±2.6
NH ₃ -N	mg L ⁻¹	12.1±1.6
TKN	mg L ⁻¹	37.3±1.6
Total COD	mg L ⁻¹	4402±135
Soluble COD	mg L ⁻¹	4316±41
UV ₂₅₄	abs.	13.2±0.53
UV ₂₈₀	abs.	10.4±0.34
UV ₄₃₆	abs.	4.79±0.33
UV ₅₂₅	abs.	0.91±0.03
UV ₆₂₀	abs.	0.65±0.02

2.2. Fe²⁺/S₂O₈ oxidation process

Jar test method was used for the treatment of wastewater with Fe²⁺/S₂O₈ oxidation process. 200 mL wastewater, required amount of FeSO₄·7H₂O (Sigma-Aldrich, 215422) and K₂S₂O₈ (Merck, 1.05091) were added to the 600 mL beaker. pH was adjusted to the desired value and wastewater were stirred for 60 min at 60 rpm. Then pH was adjusted to about 7.5 with 6 N NaOH to precipitate excess iron and settled for 1 h. After 1 h of precipitation, sample was taken from the supernatant and centrifuged for 5 min at 4000 rpm for the analysis. COD/Fe²⁺/S₂O₈ (as g/g/g) ratio was used

to evaluate the effect of the Fe²⁺ and S₂O₈ concentration. Also, effect of pH (2-7) and oxidation time (0.5-4 h) were investigated in the experiments.

2.3. UV/S₂O₈ Oxidation Process

UV/S₂O₈ oxidation experiments were conducted by using 500 mL graduated cylinder (active volume 300 mL). Required amount of K₂S₂O₈ were added to the wastewater and the pH was adjusted to the desired value. 12 watts of mercury vapor lamp (model Hg F15-05, Eurotech) at 254 nm was positioned in the center of the cylinder for the UV-C irradiation [20].

Wastewater was stirred with magnetic stirrer at about 60 rpm during the UV irradiation. The samples were taken at certain times and centrifuged for 5 min at 4000 rpm before the analysis. The effect of the COD/S₂O₈ (as g/g) ratio, pH and oxidation time were evaluated the oxidation studies.

2.4. Analysis

The pH was measured using a pH meter (WTW pH 315i). Color (UV₄₃₆-UV₅₂₅-UV₆₂₀) and humic substance (UV₂₅₄-UV₂₈₀) of the wastewater were determined using a UV spectrophotometer (Shimadzu UV-2401 PC instrument). UV₂₅₄ is used for aromatic and unsaturated organic compounds and UV₂₈₀ is represented aromaticity [21]. Total COD, soluble COD, total suspended solids (TSS), volatile suspended solids (VSS), total Kjeldahl nitrogen (TKN) and ammonia nitrogen (NH₃-N) was analyzed based on the Standard Methods for the Examination of Water and Wastewater [22]. The chemical oxygen demand (COD) was determined using a closed reflux colorimetric method. S₂O₈ concentration was measured according to Liang et al. [23]. The removal efficiencies of COD, UV₂₅₄, UV₂₈₀ or color were obtained using the following Eq. 1.

$$\text{Removal Efficiency(\%)} = \frac{C_0 - C_t}{C_0} \quad (1)$$

where C₀ is the initial COD (mg L⁻¹), UV₂₅₄, UV₂₈₀ or color (m⁻¹) concentration and C_t refer to the COD (mg L⁻¹), UV₂₅₄, UV₂₈₀ or color (m⁻¹) concentration at time t or at the end of the treatment, respectively.

The pseudo first order kinetics of COD, UV₂₅₄, UV₂₈₀, UV₄₃₆, UV₅₂₅ or UV₆₂₀ is calculated according to Eq. 2 [23];

$$\ln \frac{C_t}{C_0} = -k_1 \cdot t \quad (2)$$

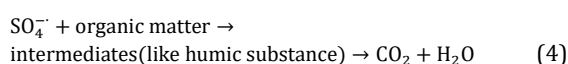
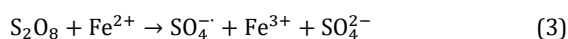
where C₀ is the initial pollutant as COD (mg L⁻¹), UV₂₅₄, UV₂₈₀, UV₄₃₆, UV₅₂₅ or UV₆₂₀ (m⁻¹) concentration and C_t refer to the pollutant as COD (mg L⁻¹), UV₂₅₄, UV₂₈₀, UV₄₃₆, UV₅₂₅ or UV₆₂₀ (m⁻¹) concentration at time t, respectively. k₁ is the pseudo first order kinetic constant rate as (h⁻¹).

3. RESULTS AND DISCUSSION

3.1. Fe²⁺/S₂O₈ oxidation process

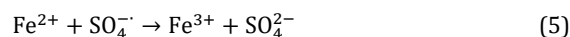
Effect of Fe²⁺ concentration for Fe²⁺/S₂O₈ oxidation process

Fe²⁺/S₂O₈ ratio is an important parameter for the persulfate oxidation. When the S₂O₈ activated with Fe²⁺ ion, sulfate radical (SO₄^{•-}) was generated in the system and then oxidation occurs by reacting organic matter with sulfate radicals. The reactions were given in Eq. 3 and Eq. 4 [14].



However, in the case of excessive amounts of Fe²⁺, a scavenging effect of sulfate radicals occurs due to the

reaction between Fe²⁺ and SO₄^{•-} and oxidation efficiency decreases (Eq. 5) [24]-[25].



The effect of Fe²⁺ ions on COD and color removal efficiencies were investigated by keeping COD/S₂O₈ ratio (1/5) constant of the COD/S₂O₈/Fe²⁺ ratio. It was observed that 25.4% COD removal was achieved at the lowest Fe²⁺ concentration (at COD/S₂O₈/Fe²⁺:1/5/1) and COD removal efficiency increased up to 57.2% (at COD/S₂O₈/Fe²⁺:1/5/8) as the Fe²⁺ concentration increased (Fig. 1). A slight decrease of COD removal (56.5%) showed in 1/5/9 ratio due to the scavenger effect of excessive Fe²⁺ on the sulfate radical. When the COD/S₂O₈/Fe²⁺ ratio is between 1/5/1 and 1/5/4, UV₂₅₄ removal is close to each other, while UV₂₈₀ removal is lower than UV₂₅₄ removal. This suggests that COD/S₂O₈/Fe²⁺ ≤ 1/5/4 is insufficient and further oxidation is needed to break down organic matter. After the COD/S₂O₈/Fe²⁺ > 1/5/4, UV₂₈₀ removal started to increase and in parallel UV₂₅₄ removal also enhanced.

When the examine of the consumed S₂O₈, observation of the residue S₂O₈ in treated wastewater up to 1/5/4 ratios indicated that Fe²⁺ concentration was insufficient to generate the sulfate radicals. 100% of S₂O₈ has been converted to the sulfate radicals between 1/5/5 and 1/5/9 ratios. UV₂₅₄ and UV₂₈₀ represent the aromatic organic compounds in water and are used as a humic substance concentration index in the literature [26]-[27]. UV₂₈₀ removal enhanced with increasing the Fe²⁺ while the removal of UV₂₅₄ showed no significant change between 1/5/8 and 1/5/9. Meanwhile, more than 90% color (UV₄₃₆-UV₅₂₅-UV₆₂₀) removal was observed above 1/5/5 ratio.

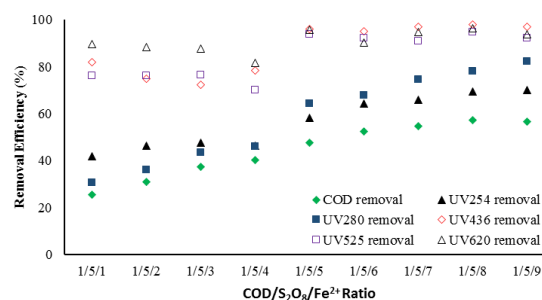


Fig 1. Effect of Fe²⁺ concentration on the COD, UV₂₅₄, UV₂₈₀ and color (UV₄₃₆-UV₅₂₅-UV₆₂₀) removal (pH: 2, oxidation time: 60 min)

Effect of S₂O₈ concentration on Fe²⁺/S₂O₈ oxidation process

S₂O₈ concentration is important in the sulfate oxidation process for wastewater treatment since sulfate radicals are generated by the S₂O₈. However, when the excessive amount of S₂O₈ is added into the system, the sulfate radicals formed can react with each other by the effect of collision and reformed to S₂O₈ [25].

When the amount of COD/S₂O₈/Fe²⁺ ratio increased from 1/4/8 to 1/8/8, COD removal efficiency increased from 54.9% to 61.1%, UV₂₅₄ removal efficiency increased from 67.6% to 72.8% and UV₂₈₀ removal efficiency enhanced from 77.7% to 82.8% (Fig 2).

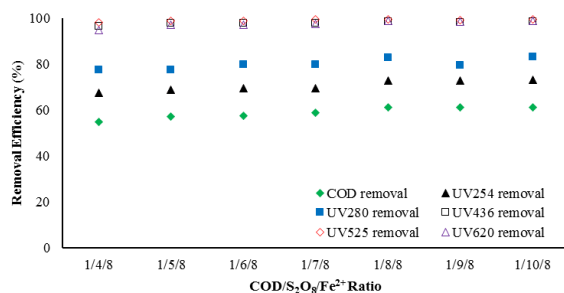


Fig 2. Effect of S_2O_8 concentration on the COD, UV_{254} , UV_{280} and color (UV_{436} - UV_{525} - UV_{620}) removal (pH: 2, oxidation time: 60 min)

The most appropriate $COD/S_2O_8/Fe^{2+}$ ratio was 1/8/8 due to the fact that no significant change in COD, UV_{254} and UV_{280} removal was observed in the applications after 1/8/8, and the residual S_2O_8 in the treated wastewater increased after the 1/8/8 ratio. In addition, color (UV_{436} - UV_{525} - UV_{620}) removal were higher than 95% between 1/4/8 and 1/10/8 of $COD/S_2O_8/Fe^{2+}$ ratios while UV_{436} , UV_{525} and UV_{620} removals in 1/8/8 ratio were 98.5%, 99.4% and 98.8%, respectively. This result was consistent with the literature that when the stabilized leachate was treated using Fe^{2+}/S_2O_8 oxidation process, the highest COD removal was observed at Fe^{2+}/S_2O_8 molar ratio 1:1 [12]. In the treatment of leachate using $COD/S_2O_8/Fe^{2+}$ oxidation process, the best COD removal was obtained as 76.2% at 90 mM Fe^{2+} with COD/S_2O_8 1/6.7 after 120 min oxidation [11].

Effect of pH for Fe^{2+}/S_2O_8 oxidation process

One of the critical factors in the treatment of wastewater by Fe^{2+}/S_2O_8 oxidation process is the solution pH due to the control of free sulfate radical and Fe^{2+} ions [28]. As can be seen from Fig. 3, the removal efficiencies of COD, UV_{254} and UV_{280} decreased as the pH of the wastewater increased. The decrease of the removal efficiencies between pH 2 and 4 was very negligible, but when the pH was increased from 4 to 7, the COD, UV_{254} and UV_{280} removal efficiency decreased from 57.7% to 44.0%, from 70.0% to 53.0% and from 78.9% to 68.5%, respectively. This finding is compatible with the literature.

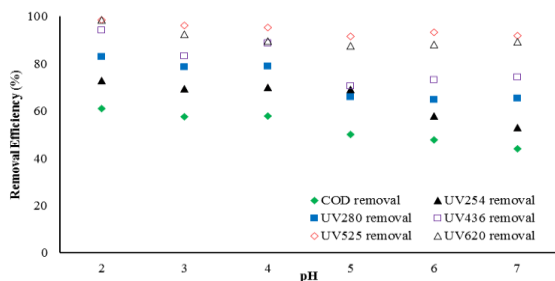


Fig 3. Effect of pH on the COD, UV_{254} , UV_{280} and color (UV_{436} - UV_{525} - UV_{620}) removal ($COD/Fe^{2+}/S_2O_8$ ratio 1/8/8, oxidation time: 60 min)

Asha et al. [12] achieved the highest COD removal for stabilized leachate treatment with Fe/S_2O_8 was in the range of pH 3-4 and stated that COD removal decreased when the pH was above 4 [12]. Likewise, the highest treatment efficiency of leachate with the Fe^{2+}/S_2O_8

process was obtained at pH 3, and the COD removal decreased as the pH increased [11]. In other study, maximum COD removal efficiency was found as 69% at pH 3 under Fe^{2+}/S_2O_8 ratio of 6 for the treatment saline recalcitrant petrochemical wastewater [18]. Because when the pH is above 4, iron deactivation occurs which leads to the formation of iron hydroxide complexes having the high stability and low catalytic activity [14], [28]-[29]. Another reason for increasing removal efficiencies at $pH \leq 4$ is that H_2O_2 is produced by the hydrolysis of S_2O_8 and together with H_2O_2 and Fe^{2+} may form extra OH radicals by Fenton reaction [30]. While the pH change did not have a significant effect on color (UV_{436} - UV_{525} - UV_{620}) removal, it can be seen that a slight color removal decreased with increasing pH.

Effect of oxidation time on Fe^{2+}/S_2O_8 oxidation process

The effect of oxidation time on Fe^{2+}/S_2O_8 oxidation process is shown in Fig 4. COD, UV_{254} and UV_{280} as well as color removal tended to increase rapidly up to 1 h reaction. After 1 h of oxidation, no significant change in color removal was observed. Similar to color removal, COD, UV_{254} and UV_{280} removal increased rapidly during the first hour oxidation period and no significant change was observed after 1 h of oxidation time.

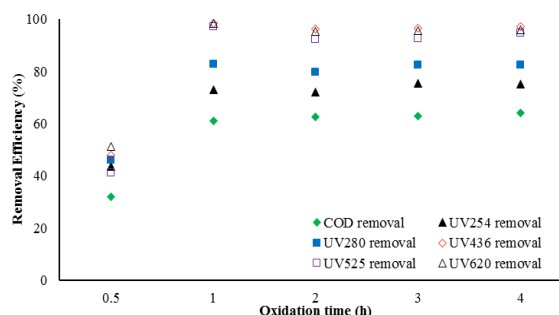


Fig 4. Effect of oxidation time on the COD, UV_{254} , UV_{280} and color (UV_{436} - UV_{525} - UV_{620}) removal ($COD/Fe^{2+}/S_2O_8$ ratio 1/8/8, pH:2, oxidation time: 60 min)

At the end of 1 h of oxidation, COD, UV_{254} and UV_{280} removal efficiencies were obtained as 61.1%, 72.8% and 82.8%, which increased to 64.1%, 75.0% and 82.5% after 4 h oxidation, respectively. UV_{436} , UV_{525} and UV_{620} removal efficiencies of 1/8/8 ratio were obtained as 47.7%, 40.9% and 51.1% after 0.5 h oxidation time and 98.4%, 97.1% and 98.4% removal efficiencies were obtained after 1 h oxidation, respectively. In a study for treating petroleum refinery wastewater using Fe^{2+}/S_2O_8 oxidation process, 66.6% of COD removal was observed at 302.9 mg L⁻¹ of $K_2S_2O_8$, 20.3 mg L⁻¹ $FeSO_4 \cdot 7H_2O$ and 4.8 of pH after 1 h oxidation [17]. Rahmat and Ahmadi [18] reported that maximum COD removal was achieved after 30 min oxidation time and COD concentration remained same up to 120 min oxidation time for the treatment of saline recalcitrant petrochemical wastewater using Fe^{2+}/S_2O_8 oxidation process [18].

3.2. UV/S₂O₈ oxidation process

Effect of COD/S₂O₈ ratio for UV/S₂O₈ oxidation process

To determine the effect of COD/S₂O₈ ratio on the COD, UV₂₅₄ and UV₂₈₀ removal efficiencies at initial pH 6, three different COD/S₂O₈ ratios (1/4, 1/6 and 1/8) were used (Fig 5). When the COD/S₂O₈ ratio was increased from 1/4 to 1/8 after 4 hours of oxidation, COD, UV₂₅₄ and UV₂₈₀ removal efficiencies increased from 17.4%, 17.1% and 31.3% to 54.4%, 54.3% and 66.5%, respectively. The increase in pollutant removal by UV/S₂O₈ is related to the formation of free sulphate radicals after activation of persulfate by UV irradiation. (Eq. 7) [15], [31].

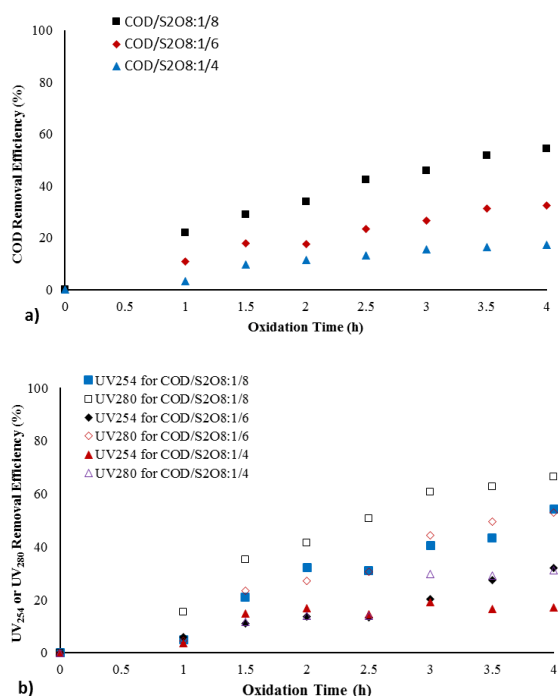


Fig 5. Effect of COD/S₂O₈ ratio (a) on the COD removal (pH:6); (b) on the UV₂₅₄ and UV₂₈₀ removal (pH:6)

UV₄₃₆, UV₅₂₅ and UV₆₂₀ removal efficiencies were increased after 4 hours oxidation (Fig 6). The UV₄₃₆, UV₅₂₅ and UV₆₂₀ removals were obtained over 95% after 2.5 h oxidation. The UV₄₃₆, UV₅₂₅ and UV₆₂₀ removal efficiencies were 97.5%, 97.2% and 98.2% at 1/8 of COD/S₂O₈ ratio after 2.5 h oxidation, respectively. At the end of 4 h oxidation, the UV₄₃₆, UV₅₂₅ and UV₆₂₀ removals were reached 92.9%, 85.2% and 86.3% at 1/6 of COD/S₂O₈ ratio, while they were remained 82.1%, 66.5% and 68.5% at 1/4 of COD/S₂O₈ ratio.

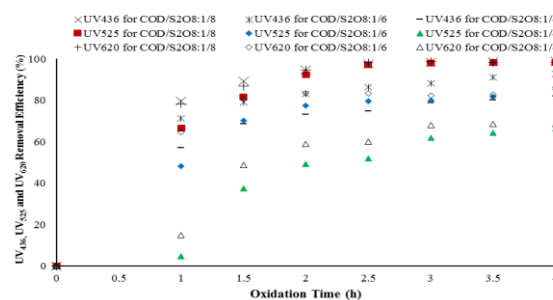


Fig 6. Effect of COD/S₂O₈ ratio on the color (UV₄₃₆-UV₅₂₅-UV₆₂₀) removal (pH:6)

Effect of pH for UV/S₂O₈ oxidation process

The effect of the initial pH on the removal of organic matter and color was investigated using the initial pH of 3, 6 and 10. The removal efficiencies of COD, UV₂₅₄ and UV₂₈₀ were increased by increasing the initial pH from 3 to 6 (Fig 7). However, when the initial pH increased to 10, the COD, UV₂₅₄ and UV₂₈₀ removal efficiencies decreased after 4 h of oxidation, they were 31.8%, 30.7% and 55.5% respectively.

Maximum COD, UV₂₅₄ and UV₂₈₀ removal efficiencies were obtained at pH 6. This finding is consistent with the literature that the highest pollutant removal with persulfate oxidation has been achieved at near neutral pH levels [32]-[34]. The highest COD removal was obtained at pH 6 and 8.2 values in the treatment of pulp and paper wastewater by UV/S₂O₈ oxidation [34]. In some studies related to oxidation of organic substances (1H-benzotriazole, N,N-diethyl-m-toluamide, chlorophene, 3-methylindole, and nortriptyline hydrochloride, trichloroethylene) with sulfate radicals, the activation energy of the reactions was found to be the lowest at pH 7 and therefore the removal efficiencies were reported to be higher at this pH [32], [35]. In this study, it is thought that a similar result was obtained because chemical industry wastewaters which contain many different organic materials were used. In the range of pH 7-10.5, SO₄^{•-} and OH^{•-} radicals are present in solution and the OH^{•-} radical is predominant, which may reduce the removal efficiency at basic conditions [33], [36]. Although the removal of UV₂₅₄ and UV₂₈₀ at pH 3 and 10 were close to each other, COD removal was higher at pH 10 than pH 3.

No significant change in color removal was observed at pH 6 and 10. The UV₄₃₆, UV₅₂₅ and UV₆₂₀ absorbances removal efficiencies were high at both pH 10 and pH 6, and over 90% removal of UV₄₃₆, UV₅₂₅ and UV₆₂₀ was achieved at pH 6 after 2 h of oxidation (Fig 8). UV₄₃₆ decolorization at pH 3 was close to that of pH 6 and 10; however UV₅₂₅ and UV₆₂₀ absorbances removal at pH 3 remained considerably lower than pH 6 and 10. Compared COD, UV₂₅₄, UV₂₈₀ removal with color removal efficiency, both organic matter removal and color removal at pH 3 remain low according to pH 6 and 10.

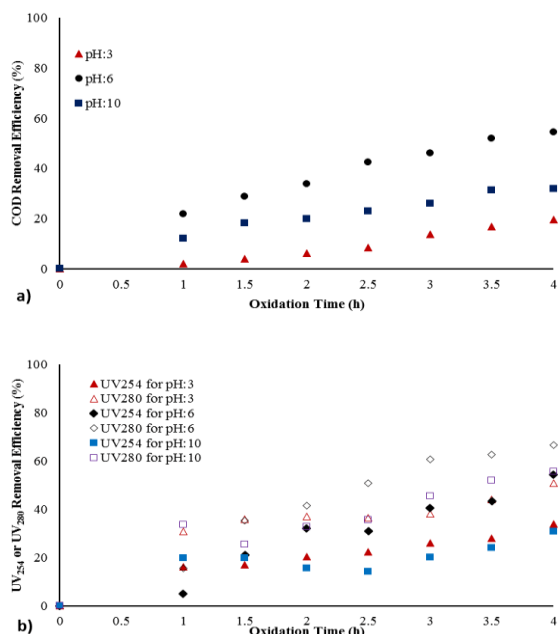


Fig 7. Effect of pH (a) on the COD removal (COD/S₂O₈ ratio 1/8); (b) on the UV₂₅₄ and UV₂₈₀ removal (pH:6) (COD/S₂O₈ ratio 1/8)

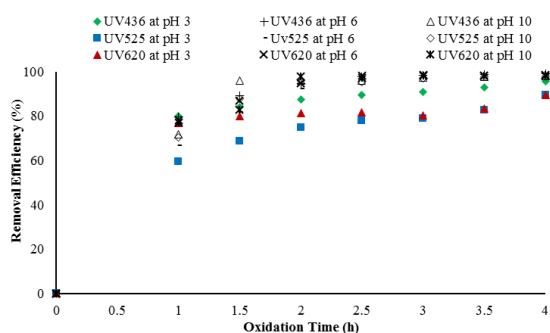


Fig 8. Effect of pH on the color (UV₄₃₆-UV₅₂₅-UV₆₂₀) removal (COD/S₂O₈ ratio 1/8)

3.3. Kinetic evaluation of Fe²⁺/S₂O₈ and UV/S₂O₈ oxidation process

Fe²⁺/S₂O₈ and UV/S₂O₈ oxidation of dye-producing chemical industrial wastewater is fitted better pseudo first order kinetic model for COD, UV₂₅₄, UV₂₈₀, UV₄₃₆, UV₅₂₅ and UV₆₂₀ removals. The pseudo first order rate constants (k₁) for Fe²⁺/S₂O₈ oxidation process were 0.9074 h⁻¹, 1.2689 h⁻¹, 1.6557 h⁻¹, 3.5816 h⁻¹, 3.0519 h⁻¹ and 3.5731 h⁻¹ for COD, UV₂₅₄, UV₂₈₀, UV₄₃₆, UV₅₂₅ and UV₆₂₀ removal at 1/8/8 COD/S₂O₈/Fe²⁺ ratio and pH 2, respectively (Table 2). The pseudo first order rate constants (k₁) for COD, UV₂₅₄, UV₂₈₀, UV₄₃₆, UV₅₂₅ and UV₆₂₀ removal were 0.2071 h⁻¹, 0.1731 h⁻¹, 0.2816 h⁻¹, 1.4335 h⁻¹, 1.3059 h⁻¹ and 1.4727 h⁻¹ at 1/8 ratio of UV/S₂O₈ and pH 6, respectively.

In a study by Pourehie and Saien [17], k₁ value of COD was calculated 0.0218 min⁻¹ under the optimum conditions as 302.9 mg/L K₂S₂O₈, 20.3 mg/L FeSO₄.7H₂O and 4.8 pH for treating petroleum refinery wastewater using UV/Fe²⁺/S₂O₈ oxidation process [17]. In addition, according to a study on the treatment of petrochemical wastewater by UV/S₂O₈ and UV/S₂O₈/Fe²⁺ oxidation processes, k₁ value for COD removal was calculated as 0.018 min⁻¹ and 0.0188 min⁻¹, respectively [19].

The oxidation rate in UV/S₂O₈ oxidation process was lower than Fe²⁺/S₂O₈ oxidation process. For COD, UV₂₅₄ and UV₂₈₀ using Fe²⁺/S₂O₈ treatment, k₁ values were 4.38, 7.33 and 5.88 times higher than UV/S₂O₈ treatment. In addition, the color (UV₄₃₆, UV₅₂₅ and UV₆₂₀) removal rates were found to be about 2.3-2.5 times higher in Fe²⁺/S₂O₈ process. Above 90% of color (UV₄₃₆, UV₅₂₅ and UV₆₂₀) removal efficiency could be achieved by Fe²⁺/S₂O₈ oxidation process in 1 h, while UV/S₂O₈ oxidation process was obtained in 2 h.

Table 2. Pseudo first order kinetic constants of Fe²⁺/S₂O₈ and UV/S₂O₈ oxidation

Parameter	Fe ²⁺ /S ₂ O ₈ oxidation process (COD/S ₂ O ₈ /Fe ²⁺ ratio 1/8/8)		UV/S ₂ O ₈ oxidation process (COD/S ₂ O ₈ ratio 1/8)	
	k ₁ (h ⁻¹)	R ²	k ₁ (h ⁻¹)	R ²
	COD	0.9074	0.9857	0.2071
UV ₂₅₄	1.2689	0.9937	0.1731	0.9372
UV ₂₈₀	1.6557	0.9645	0.2816	0.9793
UV ₄₃₆	3.5816	0.8366	1.4335	0.9924
UV ₅₂₅	3.0519	0.8301	1.3059	0.9818
UV ₆₂₀	3.5731	0.8510	1.4727	0.9841

4. CONCLUSIONS

The treatment of dye-producing chemical industrial wastewater using $\text{Fe}^{2+}/\text{S}_2\text{O}_8$ or $\text{UV}/\text{S}_2\text{O}_8$ oxidation process was investigated in this study. In $\text{Fe}^{2+}/\text{S}_2\text{O}_8$ oxidation process, optimum COD/ $\text{Fe}^{2+}/\text{S}_2\text{O}_8$ ratio, pH and oxidation time were found to be 1/8/8, 3 and 1 h. In these conditions, COD, UV_{254} , UV_{280} , UV_{436} , UV_{525} and UV_{620} removal efficiencies in this chemical industrial wastewater were obtained as 61.1%, 72.8%, 82.8%, 98.4%, 97.1% and 98.4%, respectively. In $\text{UV}/\text{S}_2\text{O}_8$ oxidation process, COD, UV_{254} , UV_{280} , UV_{436} , UV_{525} and UV_{620} removal efficiencies were 54.4%, 54.3%, 66.5%, 98.9%, 98.2% and 98.3% at 1/8 of COD/ S_2O_8 ratio and pH 6 after 4 h oxidation time, respectively. While more than 97% color removal can be achieved in both $\text{Fe}^{2+}/\text{S}_2\text{O}_8$ and $\text{UV}/\text{S}_2\text{O}_8$ oxidation processes, it was seen that organic matter removal was lower in $\text{UV}/\text{S}_2\text{O}_8$ oxidation process when COD, UV_{254} and UV_{280} parameters are examined. In the $\text{Fe}^{2+}/\text{S}_2\text{O}_8$ oxidation process, high COD and color removal efficiencies were achieved compared to $\text{UV}/\text{S}_2\text{O}_8$ oxidation process and also the oxidation time was shorter (the oxidation rate was higher). The results showed that both $\text{Fe}^{2+}/\text{S}_2\text{O}_8$ and $\text{UV}/\text{S}_2\text{O}_8$ oxidation processes were effective and suitable methods for removal of especially color parameter in this chemically treated dye-producing chemical industry wastewater. Although the organic matter removal (as COD, UV_{254}) was higher in the $\text{Fe}^{2+}/\text{S}_2\text{O}_8$ oxidation process, the amount of Fe^{2+} used in this process and the amount of sludge formed should also be taken into account for economic evaluation.

ACKNOWLEDGMENT

The authors would like to thank Yasemin Kayhan for her assistance in providing wastewater.

REFERENCES

- [1]. V. García, E. Pongrácz and R. Keiski, "Waste minimization in the chemical industry: From theory to practice", *Proceedings of the Waste Minimization and Resources Use Optimization Conference*, pp. 93-106, 2004.
- [2]. M. Kornaros and G. Lyberatos, "Biological treatment of wastewaters from a dye manufacturing company using a trickling filter", *Journal of Hazardous Materials*, Vol. 136, pp. 95-102, 2006.
- [3]. H.-Y. Shu and W.-P. Hsieh, "Treatment of dye manufacturing plant effluent using an annular $\text{UV}/\text{H}_2\text{O}_2$ reactor with multi-UV lamps", *Separation and Purification Technology*, Vol. 51, pp. 379-386, 2006.
- [4]. F. Sun, B. Sun, J. Hu, Y. He and W. Wu, "Organics and nitrogen removal from textile auxiliaries wastewater with A2O-MBR in a pilot-scale", *Journal of Hazardous Materials*, Vol. 286, pp. 416-424, 2015.
- [5]. E. Kattel, N. Dulova, M. Viisimaa, T. Tenno and M. Trapido, "Treatment of high-strength wastewater by Fe^{2+} -activated persulphate and hydrogen peroxide", *Environmental Technology*, Vol. 37 (3), pp. 352-359, 2016.
- [6]. I.A. Ike, K.G. Linden, J.D. and M. Orbell Duke, "Critical review of the science and sustainability of persulphate advanced oxidation processes", *Chemical Engineering Journal*, Vol. 338, pp. 651-669, 2018.
- [7]. P. Devi, U. Das and A.K. Dalai, "In-situ chemical oxidation: Principle and applications of peroxide and persulfate treatments in wastewater systems", *Science of the Total Environment*, Vol. 571, pp. 643-657, 2016.
- [8]. R. Guo, Q. Meng, H. Zhang, X. Zhang, B. Li, Q. Cheng and X. Cheng, "Construction of $\text{Fe}_2\text{O}_3/\text{Co}_3\text{O}_4$ /exfoliated graphite composite and its high efficient treatment of landfill leachate by activation of potassium persulfate", *Chemical Engineering Journal*, Vol. 355, pp. 952-962, 2019.
- [9]. L.W. Matzek and K.E. Carter, "Activated persulfate for organic chemical degradation: A review", *Chemosphere*, Vol. 151, pp. 178-188, 2016.
- [10]. S. Waclawek, H.V. Lutze, K. Grübel, V.V.T. Padil, M. Černík and D.D. Dionysiou, "Chemistry of persulfates in water and wastewater treatment: A review", *Chemical Engineering Journal*, Vol. 330, pp. 44-62, 2017.
- [11]. S. Yazici Guvenc, "Optimization of COD removal from leachate nanofiltration concentrate using $\text{H}_2\text{O}_2/\text{Fe}^{2+}/\text{heat}$ - Activated persulfate oxidation processes", *Process Safety and Environmental Protection*, Vol. 126, pp. 7-17, 2019.
- [12]. T.T. Asha, R. Gandhimathi, S.T. Ramesh and P.V. Nidheesh, "Treatment of stabilized leachate by ferrous-activated persulfate oxidative system", *Journal of Hazardous, Toxic, and Radioactive Waste*, Vol. 21 (2), pp. 1-6, 2017.
- [13]. E. Kattel and N. Dulova, "Ferrous ion-activated persulphate process for landfill leachate treatment: removal of organic load, phenolic micropollutants and nitrogen", *Environmental Technology*, Vol. 38 (10), pp. 1223-1231, 2017.
- [14]. Z. Liu, X. Li, Z. Rao and F. Hu, "Treatment of landfill leachate biochemical effluent using the nano- $\text{Fe}_3\text{O}_4/\text{Na}_2\text{S}_2\text{O}_8$ system: Oxidation performance, wastewater spectral analysis, and activator characterization", *Journal of Environmental Management*, Vol. 208, pp. 159-168, 2018.
- [15]. A.R. Ishak, F.S. Hamid, S. Mohamad and K.S. Tay, "Stabilized landfill leachate treatment by coagulation-flocculation coupled with UV-based sulfate radical oxidation process", *Waste Management*, Vol. 76, pp. 575-581, 2018.
- [16]. C. Chen, H. Feng and Y. Deng, "Re-evaluation of sulfate radical based advanced oxidation processes (SR-AOPs) for treatment of raw municipal landfill leachate", *Water Research*, Vol. 153, pp. 100-107, 2019.
- [17]. O. Pourehie and J. Saien, "Treatment of real petroleum refinery wastewater with alternative ferrous-assisted UV/persulfate homogeneous processes", *Desalination and Water Treatment*, Vol. 142, pp. 140-147, 2019.

- [18]. Z.G. Rahmat and M. Ahmadi, "Activation of persulfate by Fe²⁺ for saline recalcitrant petrochemical wastewater treatment: Intermediates identification and kinetic study", *Desalination and Water Treatment*, Vol. 166, pp. 35-43, 2019.
- [19]. A.A. Babaei and F. Ghanbari, "COD removal from petrochemical wastewater by UV/hydrogen peroxide, UV/persulfate and UV/percarbonate: biodegradability improvement and cost evaluation", *Journal of Water Reuse and Desalination*, Vol. 6 (4), pp. 484-494, 2016.
- [20]. E. Güneş, E. Demir, Y. Güneş and A. Hanedar, "Characterization and treatment alternatives of industrial container and drum cleaning wastewater: Comparison of Fenton-like process and combined coagulation/oxidation processes", *Separation and Purification Technology*, Vol. 209, pp. 426-433, 2019.
- [21]. I. Arslan-Alaton and I. Akmeahmet Balcioglu, "Biodegradability assessment of ozonated raw and biotreated pharmaceutical wastewater", *Archives of Environmental Contamination and Toxicology*, Vol. 43 (4), pp. 425-431, 2002.
- [22]. Standard Methods for the Examination of Water and Wastewater 21th edn, American Public Health Association/American Water Works Association/Water Environment Federation, Washington DC, USA, 2005.
- [23]. C. Liang, C.-F. Huang, N. Mohanty and R.M. Kurakalva, "A rapid spectrophotometric determination of persulfate anion in ISCO", *Chemosphere*, Vol. 73, pp. 1540-1543, 2008.
- [24]. H. Zhang, Z. Wang, C. Liu, Y. Guo, N. Shan, C. Meng and L. Sun, "Removal of COD from landfill leachate by an electro/Fe²⁺/peroxydisulfate process", *Chemical Engineering Journal*, Vol. 250, pp. 76-82, 2014.
- [25]. S. Zhu, Z. Zhou, H. Jiang, J. Ye, J. Ren, L. Gu and L. Wang, "Advanced treatment of effluents from an industrial park wastewater treatment plant by ferrous ion activated persulfate oxidation process", *Water Science & Technology*, Vol. 74 (2), pp. 535-541, 2016.
- [26]. C.S. Uyguner and M. Bekbolet, "Evaluation of humic acid photocatalytic degradation by UV-vis and fluorescence spectroscopy", *Catalysis Today*, Vol. 101 (3-4), pp. 267-274, 2005.
- [27]. D. Kulikowska, T. Józwiak, M. Kuczajowska-Zadrożna, T. Pokój and Z. Gusiatin, "Efficiency of nitrification and organics removal from municipal landfill leachate in the rotating biological contactor (RBC)", *Desalination and Water Treatment*, Vol. 33 (1-3), pp. 125-131, 2011.
- [28]. G. Barzegar, S. Jorfi, V. Zarezade, M. Khatebasreh, F. Mehdipour and F. Ghanbari, "Chlorophenol degradation using ultrasound/peroxymonosulfate/nanoscale zero valent iron: Reusability, identification of degradation intermediates and potential application for real wastewater", *Chemosphere*, Vol. 201, pp. 370-379, 2018.
- [29]. F. Ghanbari, M. Moradi and M. Manshouri, "Textile wastewater decolorization by zero valent iron activated peroxymonosulfate: Compared with zero valent copper", *Journal of Environmental Chemical Engineering*, Vol. 2 (3), pp. 1846-1851, 2014.
- [30]. J.M. Monteagudo, A. Duran, R. Gonzalez and A.J. Exposito, "In situ chemical oxidation of carbamazepine solutions using persulfate simultaneously activated by heat energy, UV light, Fe²⁺ ions, and H₂O₂", *Applied Catalysis B: Environmental*, Vol. 176-177, pp. 120-129, 2015.
- [31]. M. Hassan, X. Wang, F. Wang, D. Wu, A. Hussain and B. Xie, "Coupling ARB-based biological and photochemical (UV/TiO₂ and UV/S₂O₈) techniques to deal with sanitary landfill leachate", *Waste Management*, Vol. 63, pp. 292-298, 2017.
- [32]. J.L. Acero, F.J. Benítez, F.J. Real and E. Rodríguez, "Degradation of selected emerging contaminants by UV-activated persulfate: Kinetics and influence of matrix constituents", *Separation and Purification Technology*, Vol. 201, pp. 41-50, 2018.
- [33]. S. Dhaka, R. Kumar, M.A. Khan, K.-J. Paeng, M.B. Kurade, S.-J. Kim and B.-H. Jeon, "Aqueous phase degradation of methyl paraben using UV-activated persulfate method", *Chemical Engineering Journal*, Vol. 321, pp. 11-19, 2017.
- [34]. N. Jaafarzadeh, M. Omidinasab and F. Ghanbari, "Combined electro-coagulation and UV-based sulfate radical oxidation processes for treatment of pulp and paper wastewater", *Process Safety and Environmental Protection*, Vol. 102, pp. 462-472, 2016.
- [35]. C. Liang, Z.-S. Wang and C.J. Bruell, "Influence of pH on persulfate oxidation of TCE at ambient temperatures", *Chemosphere*, Vol. 66, pp. 106-113, 2007.
- [36]. Z. Wang, Y. Shao, N. Gao and N. An, "Degradation kinetic of dibutyl phthalate (DBP) by sulfate radical- and hydroxyl radical-based advanced oxidation process in UV/persulfate system", *Separation and Purification Technology*, Vol. 195, pp. 92-100, 2018.



RESEARCH ARTICLE

Experimental evaluation of compressibility parameters of lime and silica fume stabilized dredged soil

Inci Develioglu¹, Hasan Firat Pulat^{1,*}

¹ Izmir Katip Celebi University, Civil Engineering Department, Balaticik No:33/2, 35620, Izmir, TURKIYE

ABSTRACT

The use of alternative materials in civil engineering applications contributes to sustainable development and the economy. Large amounts of sediment are produced as waste material regarding to dredging activities in canals and ports. Storage or disposal of this material may cause some environmental and economic problems. To overcome these problems, dredged soils can be used for various civil engineering applications such as filling materials of road, foundation, and embankment. However, dredged soils generally have low bearing capacity, shear strength, and high compressibility due to their organic matter content. Therefore, these soils need to be improved with various additives before using as fillers. In this study, the index and compressibility parameters of a dredged soil were examined. The dredged soils were obtained from İzmir Bay. In the first part, Atterberg's limit test, sieve analysis, specific gravity, pH determination, scanning electron microscope analysis, Fourier transform infrared spectroscopy and consolidation test has been conducted for dredged samples which have various organic matter content (0, 4, 7 and 11%). In the next part, natural dredged soil samples were mixed with lime and silica fume in various proportions (5, 10, 15, and 20%), and compressibility performance was compared with the natural samples. It has been obtained that liquid and plastic limit, compression index, and void ratio change of natural dredged samples increased when organic matter content increased. While the silica fume has a negative effect on the compressibility behavior of dredged soil, the lime has a positive effect.

Keywords: *Compressibility, dredged soil, lime, silica fume*

1. INTRODUCTION

Advances in the industrial, urban, and tourism sectors cause the emergence of landmarks and high-rise buildings. As the number of lands becomes scarce, land reclamation has become more important. Therefore, more land is needed to expand this development.

Dredging is the operation of removing material from one part of the water environment such as rivers, lakes, seas, oceans and harbors, and relocating it to another. Dredging is carried out for many different purposes and in many different locations [1], [2], [3]. Dredged soil can be used in land reclamation applications such as wildlife habitat development, construction and filling materials, road and foundation embankments [4], [5], [6]. These types of soils have been known to have high compressibility and low shear strength because of their organic matter content (OM) [7], [8], [9]. Therefore, the geotechnical properties and

compressibility behavior of this dredged material should be examined in detail before using it in these applications.

When the literature is examined, there are many studies conducted to determine the geotechnical index properties of the dredged soils. Shahri and Chan [3] examined the geotechnical index parameters of dredged materials taken from three sites (Lumut, Marina Melaka, Tok Bali) in Malaysia. The obtained test results of dredged materials were compared with the sediment sample from the Pasir Gudang region. The liquid limits of the dredged and sediment materials were determined 37 and 95% and the plastic limits were 26 and 36%, respectively. The specific gravity values also were designated as 2.41 and 2.68 [3]. Yu et al. [10] investigated the physicochemical properties of dredged soil treated with self-cementing Class C fly ash. The dredged soil was supplied from Milwaukee Harbor, Wisconsin in the USA. Untreated samples were mixed at a rate of 10, 20, and 30% fly ash, and the

Corresponding Author: hfirat.pulat@ikcu.edu.tr (Hasan F. Pulat)

Received 18 August 2020; Received in revised form 23 September 2020; Accepted 28 September 2020

Available Online 2 November 2020

Doi: <https://doi.org/10.35208/ert.782042>

© Yildiz Technical University, Environmental Engineering Department. All rights reserved.

curing process was applied 2 hours, 7, and 28 days. The undrained compressive strength (UCS) values stayed constant up to 20% fly ash content then increased. The CBR values increased with an increase in the fly ash content and ranged between 1.5 and 20.0. Average UCS was proportional to the fly ash content and the rate of increase in UCS increased with the increasing curing time [10]. Rosman and Chan [11] attempted to examine the compressibility behavior of dredged marine sediment admixed with waste granular materials (coal bottom ash and palm oil clinker) and cement. Samples of 10, 15, and 20% cement and 50, 100, and 150% waste granular material were mixed with the dredged marine sediment and subjected to an oedometer experiment. The test results showed that compression index values decreased where the cement and waste granular materials ratio were increasing. Cement was found to be more effective than the waste granular materials. Compression index values were obtained between 0.009 and 0.3. The minimum compression index was obtained in 10% cement and 100% palm oil clinker added sample. Hence, the authors reported that reusing of coal bottom ash and palm oil clinker could provide better waste management for dredged marine sediment and be suitable as auxiliary materials to cement [11].

It is known that the OM of the dredged materials has many effects on the geotechnical and strength parameters of the soil. Thiyyakkandi and Annex [8] explored the effect of OM (7 to 11%) on geotechnical index properties of the Kuttanad clay. As a result of laboratory experiments, the consistency limits linearly increased with increasing OM. While the optimum moisture content was proportional to the OM, not much variation was observed in maximum dry density. As the OM increased, the angle of friction and undrained shear strength decreased. The compression index (C_c), initial void ratio, and rate of secondary compression (C_α) increased, the coefficient of primary consolidation (c_v) decreased with an increase in OM [8]. Malasavage et al. [7] used steel slag fines (SSF) as a stabilizer material. The dredged soil and SSF were mixed 80/20, 60/40, 50/50, 40/60, and 20/80 ratios, and laboratory tests were performed. The plastic limits and liquid limits varied between 37 and 49%, 74 and 140%, respectively. The clay fraction of samples was in the range of 21.7 and 98.8%. The internal friction angle of natural dredged soil was 27.3°, which increased to a peak value of 45° for the mixture of 50/50 ratio [7].

Increasing its resistance by mixing various additives to dredged materials is a popular method of soil improvement among researchers. Nguyen et al. [9] studied on the geotechnical index properties of untreated and treated clayey dredged material. Quicklime, hydrated lime, Portland cement, and Class F fly ash were used as a stabilizer material. These materials were mixed with the dry soil sample at a rate of 12, 6, 6, and 7.5%, respectively. Consistency limits, optimum moisture content, and UCS of both untreated and treated samples were determined. According to test results, liquid limit, plasticity index, and optimum moisture content values decreased with the quick lime, hydrated lime, fly ash increasing and Portland cement decreasing. The quick lime was the additive that increases the optimum water content the most. The UCS values increased with the addition of stabilizers.

While the Portland cement showed the most significant improvement, the fly ash had the least effect [9]. Lei et al. [12] focused on the effect of the polyacrylamide (PAM) addition on the compressibility behavior of the dredged clay. One dimensional consolidation tests were conducted with both normally consolidated (NC) and overconsolidated clay (OC) specimens. The PAM in certain proportions (0, 12.5, 25, 50, 75, and 120 mg L⁻¹) was first mixed with deionized water, and then this suspension was mixed with the dry sample so that the water content of the sample was 200%. Finally, the same consolidation tests were carried out with cement added samples (0, 2, 5, 8, and 10%) to compare the effects of PAM and cement. The test results showed that in the NC state, the structural yield stress, and the coefficient of consolidation increased, the coefficient of secondary compression decreased with the PAM content increasing. In the OC state minimum consolidation settlement and coefficient of secondary compression were obtained in the 50 mg L⁻¹ PAM suspension. The effects of PAM and cement on the consolidation behavior of dredged clay were found to be approximately similar [12]. Jaditager and Sivakugan [13] examined the compressibility behavior of dredged soil obtained from the Port of Townsville, Australia. The improvement application was made using a fly ash-based geopolymer binder. The samples were mixed with 6, 12, and 18% fly ash-based geopolymers by weight. The coefficient of volume compressibility (m_v) increased with the fly ash-based geopolymer decreasing and was ranged between 0.634×10^{-3} and 1.13×10^{-3} kPa⁻¹. The permeability values were proportional to the fly ash-based geopolymer and were ranged between 2.17×10^{-10} and 3.65×10^{-10} m s⁻¹ [13].

The effect of OM on the geotechnical and compressibility properties of dredged soil has been investigated within the scope of this study. In addition, it was aimed to improve the compressibility behavior of the dredged soil by using various additives (lime, silica fume). Scanning electron microscope (SEM) and Fourier transform infrared spectroscopy (FTIR) analyzes were performed to determine the internal structure of dredged soil. Geotechnical index properties were obtained from various laboratory tests such as sieve analysis, specific gravity, consistency limits, and pH tests. One dimensional consolidation test was conducted to determine the compressibility parameters of natural and stabilized dredged soil samples. The additives were mixed at 5, 10, 15, and 20% by dry weight of soil sample.

2. MATERIALS AND METHODS

Dredged soils used in the study were obtained from İzmir Bay. Turkish State Railways and İzmir Metropolitan Municipality carried out a project whose name is "Project of İzmir Bay and Harbor Rehabilitation". Circulation channel projected for the construction was 13 km and dredging has been made up to 8 m. At the end of the project, approximately 22.000.000 m³ of organic dredged materials have been obtained [14]. The general view of İzmir Bay is shown in Fig 1.



Fig 1. General view of İzmir Bay

The OM of dredged soil was defined by ignition at 440°C in a furnace according to ASTM D2974 [15]. Firstly, natural OM was determined (11%) then samples were ignited at 440°C for predefined times (1440, 70, and 20 minutes) to obtain different OM samples (0, 4, 7 and 11%) (Fig 2).



Fig 2. Dredged soil samples a) 0% OM, b) 4% OM, c) 7% OM, d) 11% OM

The specific gravity of samples was determined according to ASTM D854 with the pycnometer method [16]. The pH values of samples were obtained from a digital pH meter. The suspension was prepared by mixing 50 g sample and 125 ml distilled water. pH measurement was performed after 24 hours of preparation [17]. The particle size distributions for four dredged samples with different OM were defined using wet sieve analysis in accordance with ASTM D422 and ASTM D6913 [18], [19]. The liquid limit was determined by the fall cone method [20]. The plastic limit test was carried out according to ASTM D4318 [21]. The dredged soil samples were classified using Atterberg's limits and particle size analyses according to ASTM D2487 [22].

The FTIR analysis was conducted to obtain a molecular bond characterization of natural and stabilized samples in the mid-infrared region (4000 – 400 cm⁻¹). The analysis was performed at İzmir Katip Celebi University Central Research Laboratory with the dry sample passing from No.40 sieve (0.425 mm). The specimen was placed on the sample plate and the head was brought into contact with the sample after that the analysis was carried out with the Thermo iS50 FT-IR model device.

SEM analysis was performed to determine the internal structure of the dredged soil sieved from No. 40 (0.425 mm). The analysis was conducted at İzmir Katip Celebi University Central Research Laboratory with the Zeiss brand Sigma 300 VP model device. In this analysis, both microscopic image scanning and elemental analysis results were obtained.

The 1D consolidation test was turned out to obtain compressibility parameters of dredged soil according to ASTM D2435 [23]. Each test sample was prepared at their liquid limit to obtain uniform samples. The seating pressure of 5 kPa was applied before the experiment started. The specimen was loaded with 24.5, 49, 98, 196, 392, and 784 kPa of vertical stresses. Then the same specimen was unloaded with 196 and 49 kPa vertical stresses to determine the swelling behavior. The consolidation tests were repeated two times for each sample to check the repeatability.

Following the consolidation experiments with natural samples, consolidation experiments were carried out on additive samples (lime, silica fume). The specific gravities of lime and silica fume are 2.48 and 2.21, respectively. The dredged soil was mixed with the additive of 5, 10, 15, and 20% (dry weight additive by dry weight dredged soil) for one-dimensional consolidation test. The samples were prepared again at their liquid limits. The samples, mixture ratios, and abbreviations are listed in Table 1.

Table 1. Sample, abbreviations and mixture ratios

Dredged soil	Additive content (%)				
	Lime				
	5	10	15	20	
0% OM	00M5L	00M10L	00M15L	00M20L	
4% OM	40M5L	40M10L	40M15L	40M20L	
7% OM	70M5L	70M10L	70M15L	70M20L	
11% OM	110M5L	110M10L	110M15L	110M20L	
Dredged soil	Silica fume				
	0% OM	00M5S	00M10S	00M15S	00M20S
	4% OM	40M5S	40M10S	40M15S	40M20S
	7% OM	70M5S	70M10S	70M15S	70M20S
	11% OM	110M5S	110M10S	110M15S	110M20S

3. RESULTS AND DISCUSSION

3.1. Index and compressibility properties of natural dredged soil

The particle size distributions of dredged soil samples that have various OM have been shown in Fig 3. The particle size distribution curves of all samples were very similar to each other. The maximum particle size of the dredged soil sample is about 4.75 mm, it was also observed that more than half of the sample passed through No. 200 sieve.

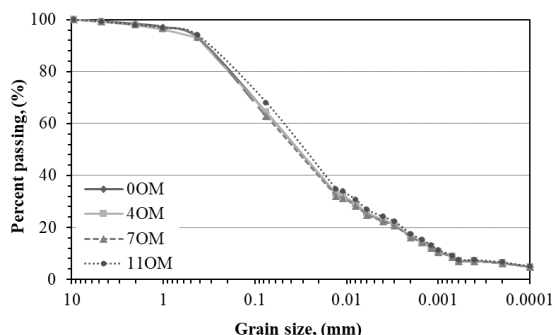


Fig 3. Particle size distributions of dredged soils

The natural dredged soil contains fine particles such as algae, branches, and bones that are much larger than the other two dimensions. Therefore, two-dimensional sieve analysis was insufficient for the particle size distribution of the dredged soil. For this reason, it is aimed to support the sieve analysis results with SEM analyzes. SEM analyzes were carried out with 0OM and 11OM samples to see the OM effect on particle size in detail. The SEM analyzes results have been shown in Fig 4. While the natural dredged sample contains organic materials (Fig 4b), there isn't any organic matter in the 0OM sample (Fig 4a).

According to FTIR analyzes, the peak positions (cm⁻¹) of the spectra were obtained as 711 – 713, 777 – 797, 872 – 874, 999 – 1005, 1409 – 1428 and 3391 – 3641. These spectra have been obtained very similarly to each other for samples with different OM. The boundary conditions which represent a chemical bond

and a functional group were adaptable with the studies in the literature [24], [25], [26].

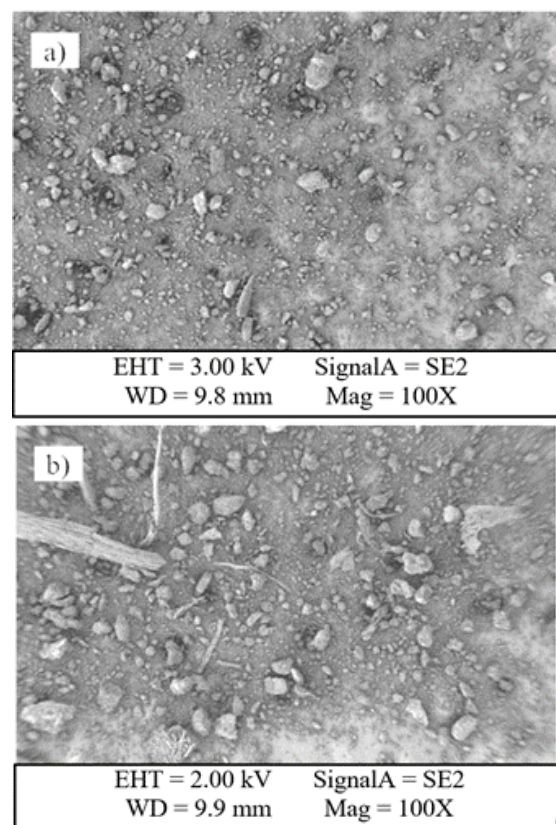


Fig 4. SEM analysis of a) 0OM sample, b) 11OM sample

The graph showing the change of specific gravity with respect to the OM has been given in Fig 5. As a result of specific gravity experiments, it was determined that there is an inverse relationship between OM and specific gravity. This situation can be explained by the increase in the amount of carbon content and the weakening of the internal structure with the increase of OM [7], [27], [28], [29], [30].

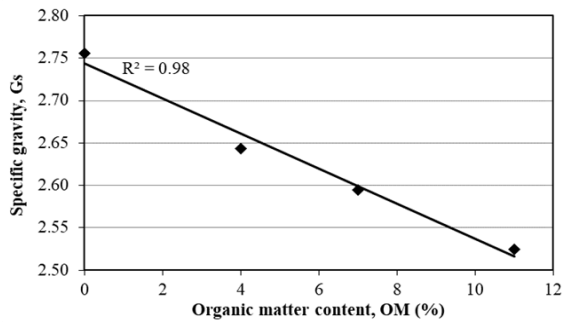


Fig 5. The relation between specific gravity and OM

The graph showing the change of liquid and plastic limit with respect to the OM has been given in Fig 6. As a result of the fall cone and plastic limit experiments, it was determined that there is a proportional relation between OM and liquid and plastic limit. This situation can be explained by the fact that the water covers the particles after the hydration of the organic materials is completed. As a result, an increase in liquid and plastic limits occurs [8], [31].

The pH values of the dredged soil samples were obtained in the range of 7.2 and 8.9, which are defined from slightly alkaline (7-8) to moderately alkaline (8-

9). The classification of the dredged soil sample was made using consistency limits and particle size distribution curves according to USCS [22]. In the plasticity chart, the place of OOM sample was above the A-line, other samples were under the A-line and liquid limits were in the range of 32.6 and 39.5%, indicated as OL (low plasticity organic soil) group for all samples.

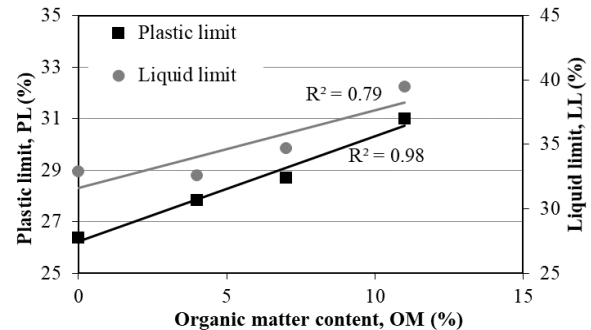


Fig 6. The relation between liquid limit, plastic limit, and OM

The results obtained from the literature studies investigating the index and compressibility properties of the dredged soils and the current study have been summarized in Table 2.

Table 2. Index and compressibility properties of dredged soils from different studies

Reference	G _s	OM (%)	LL (%)	PL (%)	C _c
Present study	2.76	0	32.9	26.4	0.097
	2.64	4	32.6	27.9	0.134
	2.60	7	34.7	28.7	0.189
	2.52	11	39.5	31.0	0.318
[2]	-	7.00	104	38	0.74
[7]	2.58	11.76	140	38	0.28
[32]	2.67	-	55.0	26.0	0.048
[3]	2.60	-	95.8	34.5	-
	2.63	-	58.5	30.72	-
	2.38	-	36.8	25.83	-
	2.41	-	46.1	35.6	-
[37]	2.53	6.27	76.1	35.3	-
[33]	2.71	-	78.8	28.3	-
	2.70	-	54.7	24.3	-
	2.65	-	39.8	21.0	-
[34]	2.45	-	56.5	16.92	-
	2.56	6.33	95.8	34.4	-
[35]	2.76	6.60	65.3	15.5	-
	2.75	4.20	61.2	20.7	-
	2.70	8.30	89.5	72.2	-
[13]	2.67	-	74	32	-
[36]	2.64	10.20	107.6	35.4	-
[11]	2.57	-	47.7	31.5	0.3
[10]	2.59	9.8	62	42	-
[12]	2.74	-	63.8	29.2	-
[9]	2.68	2.85	80	28	-

The specific gravity values were between 2.76 and 2.38 as shown in Table 2. Also, the plasticity indices were in the range of 5 and 102%. The geotechnical index properties' results of the current study were compatible with the results of the literature studies. This table also proves that the studies on the compressibility behavior of the dredged soil are very limited.

The void ratio (e) – effective vertical stress (σ') curves have been shown in Fig 7. The highest change in void ratio ($\Delta e = e_0 - e_1$) was obtained on the 11OM sample ($\Delta e_{11OM} = 0.38$). The change in void ratio were proportional with the OM ($\Delta e_{7OM} = 0.23$, $\Delta e_{4OM} = 0.20$, $\Delta e_{0OM} = 0.11$).

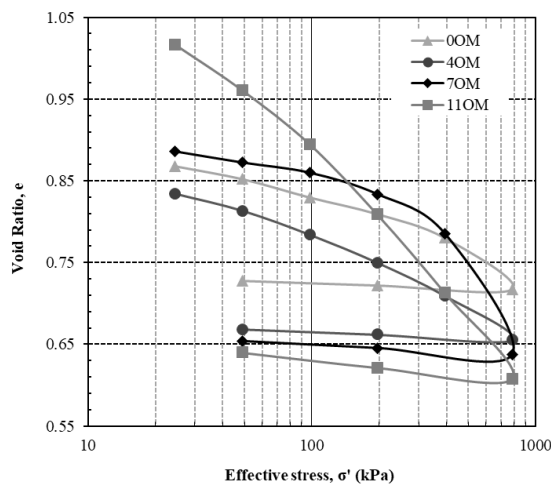


Fig 7. The compressibility curves of dredged soils

It was determined that the ignited dredged soil samples (0OM, 4OM, 7OM) did not have a breakpoint (the maximum curvature of the curve [the point where the slope of the curve increases sharply]) on the $e - \sigma'$ curve, whereas the natural dredged material (11OM) had a breakpoint. The steepest slope of the swelling curve and the maximum swelling potential belong to a natural dredged soil sample containing the highest OM. The graphs showing the change of the compression (C_c) and swelling index (C_s) depending on the OM obtained from one-dimensional consolidation tests has been given in Fig 8.

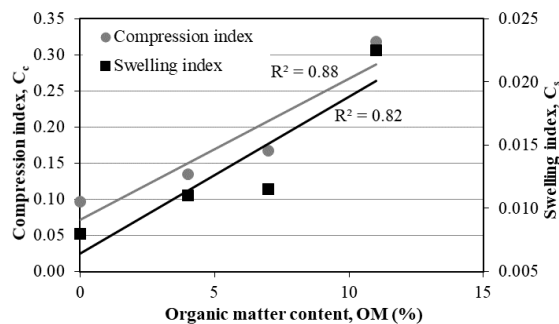


Fig 8. The relation between C_c , C_s , and OM

According to test results, it was determined that C_c and C_s were proportional to the OM. This can be explained

by the fact that organic particles are more deformable than solid particles and have high void ratios. Consequently, as OM increases, the change in void ratio increases.

3.2. Compressibility properties of lime stabilized dredged soil

The graph showing the change of the compression index depending on the lime content (LC) has been given in Fig 9 for all samples. The C_c values were inversely proportional to the LC and took values between 0.043 and 0.247.

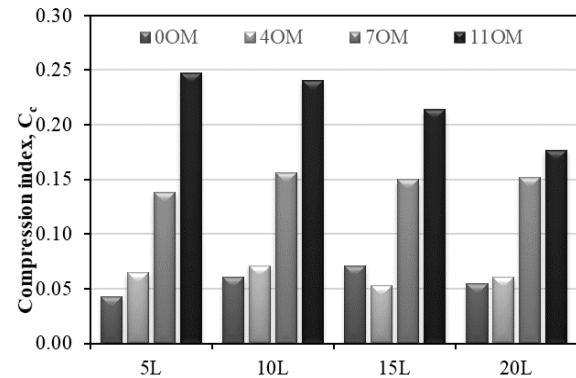


Fig 9. The relation between C_c and LC

3.3. Compressibility properties of silica fume stabilized dredged soil

The graph showing the change of the compression index depending on the silica fume content (SFC) has been given in Fig 10 for all samples. The C_c values were proportional to the SFC except for 11 OM samples and had values between 0.156 and 0.426.

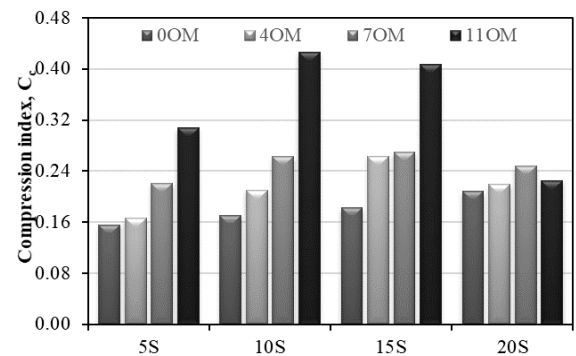


Fig 10. The relation between C_c with SFC

The axial strain values of lime and silica fume stabilized dredged soil samples have been listed in Table 3. The axial strains of the natural dredged soil samples were also as follows; 0.085, 0.102, 0.153, and 0.213, respectively.

Table 3. Axial strains of lime and silica fume stabilized dredged soil samples

OM (%)	Axial strain (ϵ)			
	LC (%)			
	5	10	15	20
0	0.030	0.035	0.048	0.064
4	0.031	0.043	0.047	0.053
7	0.075	0.077	0.142	0.091
11	0.121	0.139	0.133	0.087
	SFC (%)			
	5	10	15	20
	0	0.094	0.094	0.103
4	0.123	0.144	0.157	0.152
7	0.164	0.191	0.191	0.193
11	0.228	0.205	0.216	0.218

For lime added samples, in three out of four samples, the minimum axial strain was obtained in 5% lime stabilized sample except for 11OM. It was observed that the axial strain of the lime stabilized sample was lower than the axial strain of the natural sample for all samples. These results prove that the addition of lime positively affects the compressibility properties. However, it has been determined that the most effective contribution rate, in general, is 5%. The previous studies which are Önal [38] and Önal and Sariavcı [39] were also suggested 4% lime for improvement strength properties. For silica fume added samples, it was determined that the axial strain values increased with the SFC increasing. Also, it was observed that the axial strain of the silica fume stabilized sample was higher than the axial strain of the natural sample. These results prove that the addition of silica fume negatively affects the compressibility properties. This situation can be explained by the fact that the silica fume contains more fine-grained compared to the dredged soil, and therefore the silica fume has a higher void ratio.

The lime and silica fume were used in various ratios to improve the compressibility parameters of dredged soil. Axial strains and compression indices were measured, and results were compared. As a result of the consolidation experiments, it has been observed that while lime has a positive effect on the compressibility parameters, silica fume has a negative effect.

4. CONCLUSIONS

In the scope of this study, the geotechnical and compressibility properties of dredged soil obtained from İzmir Bay were investigated under different conditions. Initially, the organic matter content effect on both geotechnical and compressibility behavior of dredged soil was examined. Afterwards, the effect of lime and silica fume on the compressibility properties of the dredged soil was determined. For natural samples the test results showed that;

- Specific gravity was inversely proportional to the organic matter content.
- The compression index, swelling index, liquid, and plastic limit were proportional to the organic matter content.
- The change in the void ratio was proportional to the organic matter content.
- The maximum change in the void ratio was obtained from the 11OM sample.

For lime stabilized samples;

- The lime stabilization had a positive effect on the compressibility behavior of dredged soil.
- The compression index values were inversely proportional to the organic matter content.
- Lime contents of 5 – 10 % were more effective than the lime contents of 15 – 20 % on the compressibility performance.

For silica fume stabilized samples;

- The silica fume stabilization had a negative effect on the compressibility behavior of dredged soil.
- The compression index values were proportional to the silica fume content except for the 11OM sample.
- According to these results, this type of stabilizer is not appropriate to improve the compressibility behavior of dredged soil for the 0OM, 4OM, and 7OM samples but it is appropriate for the 11OM sample.

REFERENCES

- [1]. <https://www.european-dredging.eu/Dredging>, The European Dredging Association website. [Online]. Available: (2018).
- [2]. B. Rekik and M. Boutouil, "Geotechnical properties of dredged marine sediments treated at high water/cement ratio," *Geo – Marine Letters*, Vol.29, pp. 171 – 179, 2009.
- [3]. Z. Shahri and C.M. Chan, "On the characterization of dredged marine soils from Malaysian waters:

- physical properties," *Environment and Pollution*, Vol. 4, pp. 1 – 9, 2015.
- [4]. J. Limeria, L. Agullo, and M. Etxeberria, "Dredged marine sand as construction material," in *Proc. Journees Nationales Genie Cotier – Genie Civil*, 2010.
- [5]. D. Ganesalingam, A. Arulrajah, J. Ameratunga, P. Boyle, and N. Sivakugan, "Geotechnical properties of reconstituted dredged mud," in *Proc. Pan-AM CGS Geotechnical Conference*, pp. 1 – 7, 2011.
- [6]. L. Zeng, Z. Hong, and Y. Gao, "Practical estimation of compression behavior of dredged clays with three physical parameters," *Engineering Geology*, Vol. 217, pp. 102 – 109, 2017.
- [7]. N.E. Malasavage, S. Jagupilla, D.G. Grubb, M. Wazne, and W.P. Coon, "Geotechnical performance of dredged material – steel slag fines blends: laboratory and field evaluation," *Journal of Geotechnical and Geoenvironmental Engineering*, Vol. 8, pp. 981 – 991, 2012.
- [8]. S. Thiyyakkandi and S. Annex, "Effect of organic content on geotechnical properties of Kuttanan clay," *Electronic Journal of Geotechnical Engineering*, Vol. 16, pp. 1653 – 1663, 2011.
- [9]. T.T.M. Nguyen, S. Rabbanifar, N.A. Brake, Q. Qian, K. Kibodeaux, H.E. Crochet, S. Oruji, R. Whitt, J. Farrow, B. Belaire, P. Bernazzani, and M. Jao, "Stabilization of silty clayey dredged material," *Journal of Material in Civil Engineering*, Vol. 30 (9), pp. 1 – 11, 2018.
- [10]. H. Yu, J. Yin, A. Soleimanbeigi, and W.J. Likos, "Effects of curing time and fly ash content on properties of stabilized dredged material," *Journal of Materials in Civil Engineering*, Vol. 29 (10), pp. 1 – 11, 2017.
- [11]. M.Z. Rosman and C. Chan, "Settlement reduction of dredged marine soils (DMS) admixed with cement & waste granular materials (WGM): 1-D compressibility study," *International Journal of GEOMATE*, Vol. 13 (38), pp. 104 – 110, 2017.
- [12]. H. Lei, Y. Xu, X. Li, G. Zheng, and G. Liu, "Effects of polyacrylamide on the consolidation behaviour of dredged clay," *Journal of Materials in Civil Engineering*, Vol. 30 (3), pp. 1 – 10, 2018.
- [13]. M. Jaditager and N. Sivakugan, "Consolidation behaviour of fly ash-based geopolymer-stabilized dredged mud," *Journal of Waterway, Port, Coastal and Ocean Engineering*, Vol. 144 (4), pp. 1 – 7, 2018.
- [14]. B. Ozkırılı and O. Urker, "İzmir Körfezi ve Limanı Rehabilitasyon Projesi kapsamında, Gediz Deltası sulak alanı içerisinde yapılması planlanan tarama malzemesi depolanması ve işlenmesi sürecinin ekolojik ve hukuki olarak incelenmesi," *Doğa Derneği*, 2012.
- [15]. ASTM D2974 – 14, "Standard test methods for moisture, ash, and organic matter of peat and other organic soils," *ASTM International*, 2014, www.astm.org.
- [16]. ASTM D854-14, "Standard test methods for specific gravity of soil solids by water pycnometer," *ASTM International*, 2014, www.astm.org.
- [17]. G. Kocasoy. Atıksu arıtma çamuru ve katı atık ve kompost örneklerinin analiz yöntemleri, 1st ed., *Boğaziçi Üniversitesi Yayınları*, İstanbul, Turkey, 1994.
- [18]. ASTM D422-63(2007)e2, "Standard test method for particle-size analysis of soils (Withdrawn 2016)," *ASTM International*, 2007, www.astm.org.
- [19]. ASTM D6913-04(2009)e1, "Standard test methods for particle-size distribution (Gradation) of soils using sieve analysis," *ASTM International*, 2009, www.astm.org.
- [20]. BS 1377-1, "Methods of test for soils for civil engineering purposes," *British Standard Institution*, London, 2016.
- [21]. ASTM D4318-10e1, "Standard test methods for liquid limit, plastic limit, and plasticity index of soils," *ASTM International*, 2010, www.astm.org.
- [22]. ASTM D2487-11, "Standard practice for classification of soils for engineering purposes (Unified Soil Classification System)," *ASTM International*, 2011, www.astm.org.
- [23]. ASTM D2435/D2435M-11, "Standard test methods for one-dimensional consolidation properties of soils using incremental loading," *ASTM International*, 2011, www.astm.org.
- [24]. C. Huang and P.F. Kerr, "Infrared study of the carbonate minerals," *Am. Mineral*, Vol. 45, pp. 311 – 324, 1960.
- [25]. T. Nguyen, L.J. Janik, and M. Raupach, "Diffuse reflectance infrared Fourier transform (DRIFT) spectroscopy in soil studies," *Soil Research*, Vol. 29(1), pp. 49 – 67, 1991.
- [26]. R. Ravisankar, A. Chandrasekaran, S. Kalaiarsi, P. Eswaran, C. Rajashekhar, K. Vanasundari, and A. Athavale, "Mineral analysis in beach rocks of Andaman Island, India by spectroscopic techniques," *Archives of Applied Science Research*, Vol. 3(3), pp. 77 – 84, 2011.
- [27]. C. Chan, "Geo-parametric study of dredged marine clay with solidification for potential reuse as good engineering soil," *Environmental Earth Sciences*, Vol. 75, pp. 941 – 955, 2016.
- [28]. G. Kang, T. Tsuchida, and A.M.R. Athapaththu, "Engineering behaviour of cement-treated marine dredged clay during early and later stages of curing," *Engineering Geology*, Vol. 209, pp. 163 – 174, 2016.
- [29]. G. Kang, T. Tsuchida, and Y. Kim, "Strength and stiffness of cement-treated marine dredged clay at various curing stages," *Construction and Building Materials*, Vol. 132, pp. 71 – 84, 2017.
- [30]. D. Wang, N.E. Abriak, and R. Zentar, "One-dimensional consolidation of lime-treated dredged harbour sediments," *European Journal of Environmental and Civil Engineering*, Vol. 19, pp. 199 – 218, 2015.
- [31]. I. Develioglu, and H.F. Pulat, "Geotechnical Properties and Compressibility Behavior of Organic Dredged Soils," in *Proc. 19th*

- International Conference on Earthquake Geotechnical Engineering*, pp. 194 –198, 2017.
- [32]. A. Federico, C. Vitone, and A. Murianni, "On the mechanical behaviour of dredged submarine clayey sediments stabilized with lime or cement," *Canadian Geotechnical Journal*, Vol. 52, pp. 2030 – 2040, 2015.
- [33]. G. Xu, Y. Gao, J. Yin, R. Yang, and J. Ni, "Compression behaviour of dredged slurries at high water contents," *Marine Georesources & Geotechnology*, Vol. 33, pp. 99 – 108, 2015.
- [34]. C. Chan, "Strength improvement characteristic of cement-solidified dredged marine clay with relation to water-cement ratio," *International Journal of GEOMATE*, Vol. 11, pp. 2734 – 2740, 2016.
- [35]. G. Kang, T. Tsuchida, and A. M. R. G. Athapaththu, "Engineering behaviour of cement-treated marine dredged clay during early and later stages of curing," *Engineering Geology*, Vol. 209, pp. 163 – 174, 2016.
- [36]. G. Kang, T. Tsuchida, and Y. Kim, "Strength and stiffness of cement-treated marine dredged clay at various curing stages," *Construction and Building Materials*, Vol. 132, pp. 71 – 84, 2017.
- [37]. D. Wang, N.E. Abriak, and R. Zentar, "One-dimensional consolidation of lime-treated dredged harbour sediments," *European Journal of Environmental and Civil Engineering*, Vol. 19, pp. 199 – 218, 2015.
- [38]. O. Önal, "Lime Stabilization of Soils Underlying a Salt Evaporation Pond: A Laboratory Study," *Marine Georesources and Geotechnology*, Vol. 33(5), pp. 391 – 402, 2015.
- [39]. O. Önal, and Ç. Sariavcı, "Stabilization of Meles Delta soils using cement and lime mixtures," *Geomechanics and Engineering*, Vol. 19(6), pp. 543 – 554, 2019.



RESEARCH ARTICLE

Preparation of coal-derived magnetic carbon material for magnetic solid-phase extraction of fungicides from water samples

Gizem Tarhan Zengin¹ , Elif Yildiz¹ , Atakan Toprak² , Hasan Cabuk^{1,*}

¹Zonguldak Bulent Ecevit University, Faculty of Arts and Sciences, Department of Chemistry, 67100, Zonguldak, TURKIYE

²Zonguldak Bulent Ecevit University, Department of Chemistry and Chemical Process Technology, 67800, Zonguldak, TURKIYE

ABSTRACT

A magnetic solid-phase extraction method has been developed for the extraction and analysis of some fungicides in environmental water samples. Azoxystrobin, chlorothalonil, cyprodinil and trifloxystrobin were the target fungicides selected. First, a carbon material was obtained from the raw coal sample collected from Zonguldak region by ash removal process and then a magnetic C/Fe₃O₄ composite was produced from the carbon material using a single-step thermal method. The magnetic C/Fe₃O₄ composite was characterized by N₂ adsorption-desorption, X-ray diffraction, Fourier transform infrared spectroscopy and scanning electron microscopy. This composite was then used as an adsorbent for the magnetic solid-phase extraction of fungicides from water samples followed by high-performance liquid chromatographic analysis. Experimental parameters affecting the extraction efficiency such as adsorbent amount, type and volume of desorption solvent, adsorption and desorption time, ionic strength, and pH were optimized. Under the optimized conditions, the extraction efficiency for azoxystrobin, chlorothalonil, cyprodinil and trifloxystrobin was found to be 71%, 44%, 41% and 70%, respectively. The method detection limits for fungicides were found to be in the range of 0.4-1.1 µg L⁻¹. The relative standard deviations were found to be lower than 6.6% and 6.9% for intra-day and inter-day precisions, respectively. The extraction of related fungicides from water samples collected from Zonguldak region was carried out efficiently. The recoveries obtained from spiked water samples were in the range of 71-106%.

Keywords: Fungicides, liquid chromatography, magnetic solid-phase extraction, water samples

1. INTRODUCTION

Today, despite significant advances in instrument technology, a sample preparation step is still needed prior to instrumental analysis for target analytes particularly in environmental, food, and biological samples, which are described as complex matrices [1]. In this sense, the sample preparation is an important step for extracting and concentrating the analytes from various matrices as well as making the analytes more compatible for the instrumental system [2]. For years, the most commonly used sample preparation methods for aqueous samples have been liquid-liquid extraction (LLE) and solid-phase extraction (SPE). The disadvantages of the LLE method include excessive use of solvent, formation of emulsions during extraction, and most importantly, production of large quantities of environmental pollutants. The SPE method, on the

other hand, spends a lower amount of solvents and gives higher extraction efficiency compared to LLE. However, traditional SPE is also time-consuming as it involves different steps such as column conditioning, sample loading, column washing and elution [3]. Over the past few years, several miniaturized and simplified versions of SPE have been developed in order to make SPE faster and more environmentally friendly.

Magnetic solid-phase extraction (MSPE) is a promising method based on the use of magnetic adsorbents for separation and enrichment of organic and inorganic analytes from large volumes of aqueous samples. In MSPE, the magnetic adsorbent is placed in a sample solution containing analytes. The target analytes are adsorbed on to the surface of the magnetic adsorbent with the aid of mechanical stirring or ultrasonication. The magnetic adsorbent containing the analytes is separated from the sample solution by an external

Corresponding Author: cabukhasan@hotmail.com (Hasan Cabuk)

Received 1 September 2020; Received in revised form 28 September 2020; Accepted 29 September 2020

Available Online 2 November 2020

Doi: <https://doi.org/10.35208/ert.788913>

© Yildiz Technical University, Environmental Engineering Department. All rights reserved.

magnetic field applied to the outside surface of the extraction vessel. Next, the analytes are eluted from the magnetic adsorbent with a suitable solvent and then analyzed [1]. The MSPE is a rapid and simple extraction method in which some steps needed in traditional SPE methods such as filling the adsorbent into a column, centrifugation or filtration are eliminated [4]. In MSPE, the separation of adsorbent from aqueous solution and also from desorption solvent is performed with a very practical approach. This process is easy and effortless thanks to a magnet held outside the extraction vessel. Although the mechanism of magnetic separation has been known for many years, the first analytical application was carried out by Šafaříková and Šafařík in 1999. In this study, some selected organic dyes were extracted from high volume samples (100-800 mL) using copper phthalocyanine modified silanized magnetite and magnetic charcoal as adsorbents, with an enrichment of up to 460-fold [5]. In the years following this study, a great deal of research has been carried out on the development of new magnetic adsorbents for the extraction/preconcentration of wide variety of analytes.

As a class of pesticides, fungicides are used to control mold and fungal diseases, especially for vegetables and fruits. Under good farming practices, fungicides need to be applied regularly to vegetables and fruits during the growing season, regardless of whether a fungal infection is present [6]. As a result, significant amounts of fungicides are used in places where vegetables and fruits are grown, resulting in fungicide contamination of nutrients, water, and environmental resources in the food chain. It is known that these chemicals can have significant negative effects on human health. In the European Union, the allowable amount of fungicides in drinking water is set to $0.1 \mu\text{g L}^{-1}$ for any single residue and $0.5 \mu\text{g L}^{-1}$ for total residues [7]. Therefore, determination of fungicide residues in environmental waters is of great importance for human health and environmental safety. In this sense, the development of reliable, precise and rapid analytical methods for the determination of fungicides at trace levels in environmental waters is a significant matter.

In this study, a MSPE method has been developed for the extraction and analysis of some fungicides in water samples. First, a carbon material was obtained from the raw coal sample collected from Zonguldak region by ash removal process and then a magnetic C/Fe₃O₄ composite was produced from the carbon material using a single-step thermal method. The feasibility of the C/Fe₃O₄ composite as a green and effective adsorbent in the MSPE of some selected fungicides was investigated.

2. MATERIALS AND METHODS

2.1. Chemicals and solutions

Standard fungicides (azoxystrobin, chlorothalonil, cyprodinil and trifloxystrobin) were obtained from Sigma-Aldrich. Acetonitrile ($\geq 99.9\%$), acetone ($\geq 99\%$), methanol ($\geq 99.7\%$) and NaCl were purchased from Sigma-Aldrich, whereas NaOH, HCl, HF, NaH₂PO₄·2H₂O, and Fe(NO₃)₃·9H₂O were obtained from Merck. Water

was used in experiments after purification with Zeener Power I Scholar-UV (18.2 M Ω) system.

Stock standard solutions were prepared with acetonitrile, containing fungicides at a concentration of $100 \mu\text{g mL}^{-1}$. The working solutions at different concentrations were prepared by diluting stock solution with acetonitrile. These solutions were used in different stages of the experimental studies. All standard solutions were kept in the refrigerator at 4 °C. The tap water sample was taken from our laboratory and other water samples were collected from different streams located in Zonguldak city, Turkey. Water samples were placed in capped glass containers and stored in the refrigerator at 4 °C until processed. The raw coal sample used in the preparation of magnetic composite material was obtained from Kilimli district of Zonguldak province.

2.2. Instrumentation and chromatographic conditions

A Thermo Finnigan high-performance liquid chromatography with UV detector (HPLC-UV) was used in the chromatographic analysis of fungicides. The components of the HPLC-UV system were P1000 pump, UV1000 detector, S3000 automatic injection unit, SCM1000 degasser and SN4000 control system. ChromQuest 4.0 software was used to process the data. Chromatographic separation of fungicides was performed using C₁₂ Max-RP (250×4.6 mm i.d., 4.0 μm) column. Acetonitrile and water were used as the mobile phase. The optimal separation for fungicides was obtained by isocratic elution. The mobile phase was prepared as a mixture containing 65% acetonitrile and 35% water and this solvent mixture was passed through the HPLC system for 30 min. The flow rate of the mobile phase was 1 mL min^{-1} , the UV wavelength was 250 nm, and the sample injection volume was 20 μL .

A Protech Lab KF-6 electric furnace was used for preparing magnetic composite material, a Kern ABJ 220-4m precision scale was used for weighing samples and chemicals, and a Protech ultrasonic bath was used for sample preparation. The N₂ adsorption-desorption measurement was carried out using a Quantachrome Autosorb 1C apparatus. A Fourier-transform infrared (FT-IR) spectrometer (Perkin Elmer), an X-ray diffraction (XRD) device (Pananalytical Empyrean), and a scanning electron microscope (SEM) (FEI Quanta 450 FEG) were used to characterize the magnetic composite material.

2.3. Preparation of magnetic composite material

After grinding the raw coal sample in the grinding machine, the grain size was kept at 100-300 μm using a sieve, and then the sample was dried in an oven at 110 °C for 24 h. The coal sample was treated for 4 h under a condenser at 70 °C with 20% (v/v) HCl to remove its inorganic content. After the acid treatment, the coal sample was washed with hot water to remove chloride ions. In order to minimize the ash content in the coal sample, the same treatment mentioned above was repeated with 20% HF (v/v). After washing with hot water again, the sample was dried for 24 h at 110

°C and taken to a desiccator [8]. The ash and volatile matter content of raw coal and ash-removed coal samples were determined in accordance with ASTM D 3174 and ASTM D 3175 standards. The fixed carbon percentage was calculated by subtracting the sum of volatile matter and ash percentages from 100. Fixed carbon, volatile matter, and ash percentages were 63.1%, 31.3%, and 5.6% in the raw coal sample, whereas in the ash-removed coal sample were 67.4%, 32.0%, and 0.6%, respectively.

The magnetic C/Fe₃O₄ composite was produced from the ash-removed coal sample using a single-step thermal method based on the procedures described in the literature [9, 10]. Firstly, 3 g of ash-removed coal sample, 6 g Fe(NO₃)₃·9H₂O, and 10 mL ethanol were stirred in a crucible at 45 °C with a magnetic stirrer for 2 h. Then the mixture was re-stirred at 60 °C for 1 h. After the stirring process, the ethanol in the mixture was removed in the oven. The crucible containing the mixture was closed with a lid and placed in the electric oven, and the temperature was raised to 800 °C using a ramp of 20 °C min⁻¹. After waiting 10 min at this

temperature, the furnace was cooled to room temperature. The mixture was washed with hot water and then dried to obtain the C/Fe₃O₄ composite.

2.4. Magnetic solid-phase extraction procedure

For MSPE, 8 mL of the standard solution or water sample was transferred to 20 mL glass baker and 0.4 g NaCl was dissolved in the solution. Subsequently, 20 mg of C/Fe₃O₄ composite was added to the solution and the extraction was performed under sonication for 15 min. Next, an external magnet was placed to outside surface of the glass beaker to separate the composite material. After removing the aqueous solution, 200 µL of acetonitrile was used for desorption of analytes by sonication for 4 min. After separated with magnet, the desorption solution was transferred a vial for HPLC-UV analysis. Fig 1 shows a schematic of the C/Fe₃O₄-MSPE procedure.

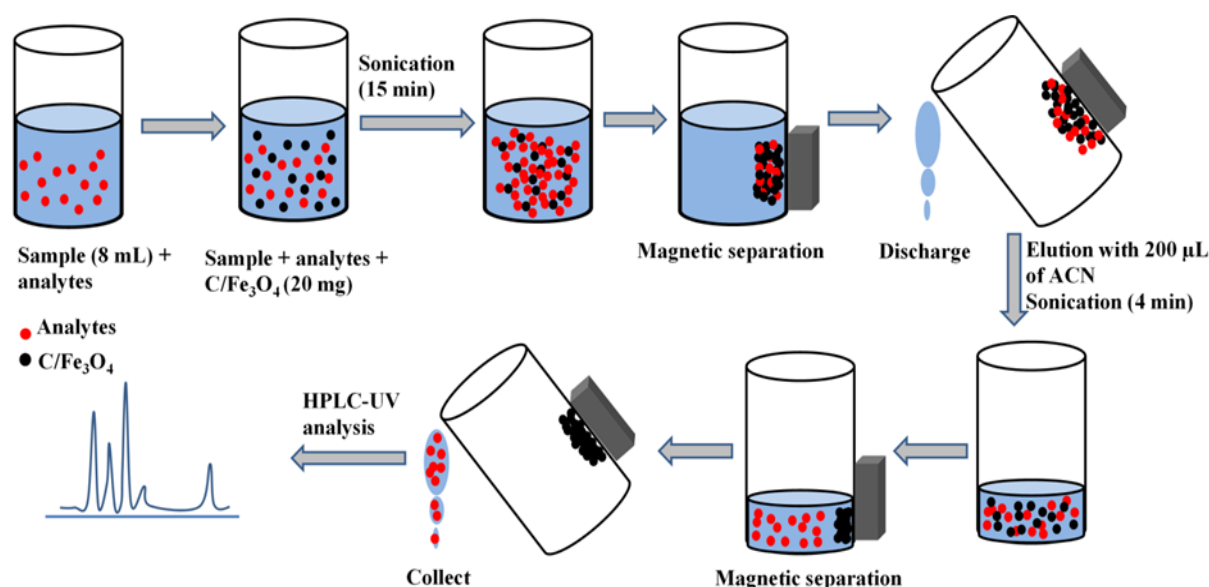


Fig 1. Schematic diagram of the C/Fe₃O₄-MSPE procedure.

3. RESULTS AND DISCUSSION

3.1. Characterization of the C/Fe₃O₄ composite

The surface properties of the C/Fe₃O₄ composite were investigated by adsorption-desorption experiments with N₂ gas at 77 K. The N₂ isotherm of the C/Fe₃O₄ composite fits the type I and II isotherms according to IUPAC classification (Figure 2a), which is usually associated with both microporous and mesoporous structures [11]. Additionally, the isotherm presents a type H4 hysteresis in the 0.99-0.4 relative pressure (P/P₀) range indicating narrow slit-like pores [12]. The BET (Brunauer-Emmett-Teller) surface area of the C/Fe₃O₄ composite was found to be 75.7 m² g⁻¹. The total pore volume and average pore width for C/Fe₃O₄ composite were 0.057 cm³ g⁻¹ and 1.475 nm, respectively.

Figure 2b shows the XRD spectrum of the C/Fe₃O₄ composite. The diffraction peaks of 2θ = 30.3°, 35.5°, 43°, 53.5°, 57°, and 62° correspond to the crystal planes of 220, 311, 400, 422, 511, and 440, respectively. These results indicate that the cubic Fe₃O₄ particles are present within the composite structure. Additionally, the dimensions of the Fe₃O₄ particles were determined using the Debye-Scherrer equation [13]. The average particle size calculated based on the diffraction peaks of 2θ = 30.3° and 35.5° was found to be approximately 42 nm.

The surface morphology and elemental composition of the C/Fe₃O₄ composite were determined by scanning electron microscopy (SEM) coupled with energy-dispersive X-ray spectroscopy (EDX). The resulting SEM image and EDX spectrum for the C/Fe₃O₄ composite can be seen in Figure 2c. The SEM image shows that the outer surfaces of the C/Fe₃O₄ composite

have irregularly dispersed slits and pores of different sizes. It also shows that Fe₃O₄ nanoparticles accumulate in the outer and inner surface pores of the composite. The EDX spectrum reveals that the C/Fe₃O₄ composite is composed of carbon, oxygen, and iron elements and that there are no additional impurities in the material.

Figure 2d shows the FT-IR spectrum of the C/Fe₃O₄ composite. The broad peak observed at 3448 cm⁻¹ is due to O-H stretching vibrations, indicating the presence of hydroxyl groups on the surface. The peaks

observed at 2923 and 2853 cm⁻¹ are due to asymmetric and symmetric C-H stretching vibrations, respectively. The peak observed at 1635 cm⁻¹ is due to aromatic C=C stretching vibrations and the peak observed at 1384 cm⁻¹ is due to aliphatic C-H bending vibrations [14,15]. The peak observed at 560 cm⁻¹ in the FT-IR spectrum is due to Fe-O-Fe stretching vibrations, proving that Fe₃O₄ nanoparticles are present in the composition of the material [16]. The results reveal that both hydrophilic (O-H) and hydrophobic groups (C=C) are present on the surface of C/Fe₃O₄ composite [17].

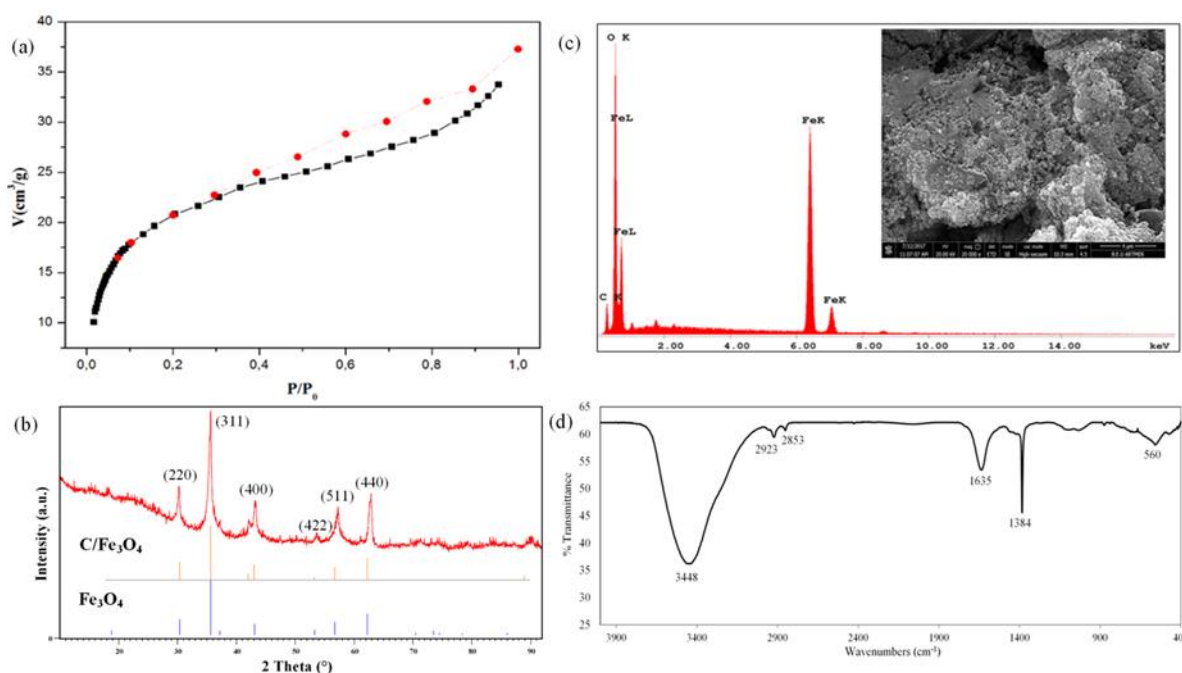


Fig 2. a) N₂ adsorption-desorption isotherm, b) XRD spectrum, c) SEM image with EDX spectrum, and d) FTIR spectrum of C/Fe₃O₄ composite.

3.2. Optimization of MSPE parameters

Some parameters such as the amount of adsorbent (C/Fe₃O₄), type and volume of desorption solvent, ionic strength, pH, adsorption and desorption time were optimized to determine the optimal MSPE conditions. Spiked water samples containing each fungicide at a fixed concentration of 12.5 µg L⁻¹ were used in the optimization experiments. Enrichment factor (EF) and extraction recovery (ER) were calculated for each fungicide and ERs were considered in selecting the optimum conditions. Equation 1 and 2 were used to calculate EF and ER, respectively.

$$EF = \frac{C_a}{C_b} \quad (1)$$

$$ER = \frac{(C_a \times V_a)}{(C_b \times V_b)} \times 100 = EF_x \frac{(V_a)}{(V_b)} \times 100 \quad (2)$$

C_a and C_b are the concentration of analytes expressed in µg L⁻¹ in the organic phase and in the sample solution, respectively. V_a and V_b are the volumes of the organic phase and sample solution, respectively.

The ideal amount of C/Fe₃O₄ was evaluated by increasing the dosage of C/Fe₃O₄ from 10 to 60 mg, while the other experimental parameters were kept constant. Acetonitrile was used as a desorption solvent with a fixed volume of 300 µL. The adsorption and desorption times were fixed at 5 and 2 min, respectively. Figure 3a shows the ERs obtained for fungicides by changing the amount of C/Fe₃O₄. The highest ERs for fungicides were achieved when 20 mg adsorbent was used, and a slight decrease in the extraction efficiency occurred over 20 mg. Therefore, 20 mg was selected as the optimal amount of C/Fe₃O₄ composite.

Acetonitrile, methanol, acetone and ethanol were tested to select the most appropriate desorption solvent. The other parameters including the amount of C/Fe₃O₄, the volume of desorption solvent, adsorption time and desorption time were fixed at 20 mg, 300 µL, 5 min and 2 min, respectively. Figure 3b shows the ERs obtained for the fungicides using different desorption solvents. The highest ERs were achieved when acetonitrile and acetone were used as desorption solvents. However, acetonitrile was chosen as desorption solvent since it was more compatible with

the mobile phase used in the chromatographic analysis.

Selecting the optimal desorption solvent volume is an important step in MSPE methods. The use of high volumes of desorption solvent decreases the sensitivity of the method due to the dilution effect. As the volume of desorption solvent is reduced, the extraction efficiency for the analytes decreases due to the lower rate of solvent-adsorbent interaction. The effect of desorption solvent volume on the extraction efficiency was investigated in the range of 100-500 μL . Figure 3c shows the ERs obtained for fungicides with varying volumes of desorption solvent. By increasing desorption solvent volume from 100 μL to 200 μL , the extraction efficiency for some fungicides increased. No significant change occurred over 200 μL . For this reason, 200 μL was chosen as the most appropriate desorption solvent volume.

In order to investigate the effect of ionic strength on the extraction of fungicides, NaCl was added to the sample solution at various concentrations (0-8%, w/v) and the MSPE method was applied with keeping the other parameters constant. Figure 3d shows the ERs obtained for fungicides with varying salt concentrations. The ERs increased slightly with increasing salt concentration up to 5%, and remained nearly unchanged with further increase. Increased salt concentration decreases the solubility of analytes in aqueous solution, thus making it easier for the analytes to transfer from the sample solution to the adsorbent [18]. Therefore, the subsequent experiments were carried out in the presence of 5% NaCl.

Another important parameter affecting the extraction efficiency of analytes is the pH of the water samples. This is because the analytes are present in different forms under different pH conditions. Generally, pH value of the samples is kept lower than the pK_a values of analytes in order to keep the analytes in their molecular state. In this way, the solubility of analytes in water decreases, while their interaction with the adsorbent surface increases [19]. The pH value of the aqueous solutions containing fungicides varied from 3 to 11 and the MSPE method was applied to these solutions. Figure 3e shows the ERs obtained for the fungicides at different pH values. The pH did not show any significant influence on the extraction efficiency of analytes in the range from 3 to 7, but when the pH value was above 7, there was a decrease in the ERs. The pH values of the water samples analyzed in this study were

generally lower than 7. Hence, initial pH adjustment was not required.

To determine the optimal adsorption time, several experiments with varying sonication times from 3 to 30 min were carried out. According to the results (Figure 3f), the highest ERs were achieved with sonication for 15 min. Longer sonication periods did not produce a significant improvement in the extraction efficiency. Since the adsorption of fungicides reached equilibrium within 15 min, this time was selected as the most appropriate adsorption time. In addition, the optimal desorption time was also tested with varying sonication times in the range of 2-10 min. The best ERs for the fungicides were obtained under sonication for 4 min. The higher sonication times did not improve extraction efficiency. Thus, 4 min was selected as optimal desorption time.

Under the optimal MSPE conditions, the average extraction efficiencies ($n=3$) for azoxystrobin, chlorothalonil, cyprodinil and trifloxystrobin were found to be 71%, 44%, 41% and 70%, and the average enrichment factors ($n=3$) were 28, 18, 16, and 27, respectively.

3.3. Analytical performance

The analytical performance of the C/Fe₃O₄-MSPE method was assessed under optimized experimental conditions. The linearity, limit of detection (LOD), limit of quantification (LOQ), and intra-day and inter-day precisions of the method were assessed. Table 1 shows the analytical performance parameters of the C/Fe₃O₄-MSPE method for the determination of fungicides in water samples. Good linearity was obtained for all analytes in the concentration range of 1-50 $\mu\text{g L}^{-1}$ with the coefficients of determination (r^2) higher than 0.9969. LODs and LOQs were calculated by considering the signal to noise ratio (S/N) as 3 and 10, respectively. LODs and LOQs were found to be in the range of 0.4-1.1 $\mu\text{g L}^{-1}$ and 1.3-3.5 $\mu\text{g L}^{-1}$, respectively. The intra-day and inter-day precisions of the method were calculated as relative standard deviation (RSD), based on the repeated analysis of standard solutions (5 $\mu\text{g L}^{-1}$) in the same day (intra-day, $n = 5$) and in the consecutive days (inter-day, $n = 5$). The intra-day and inter-day precisions for the fungicides varied between 5.3-6.6% and 3.6-6.9%, respectively.

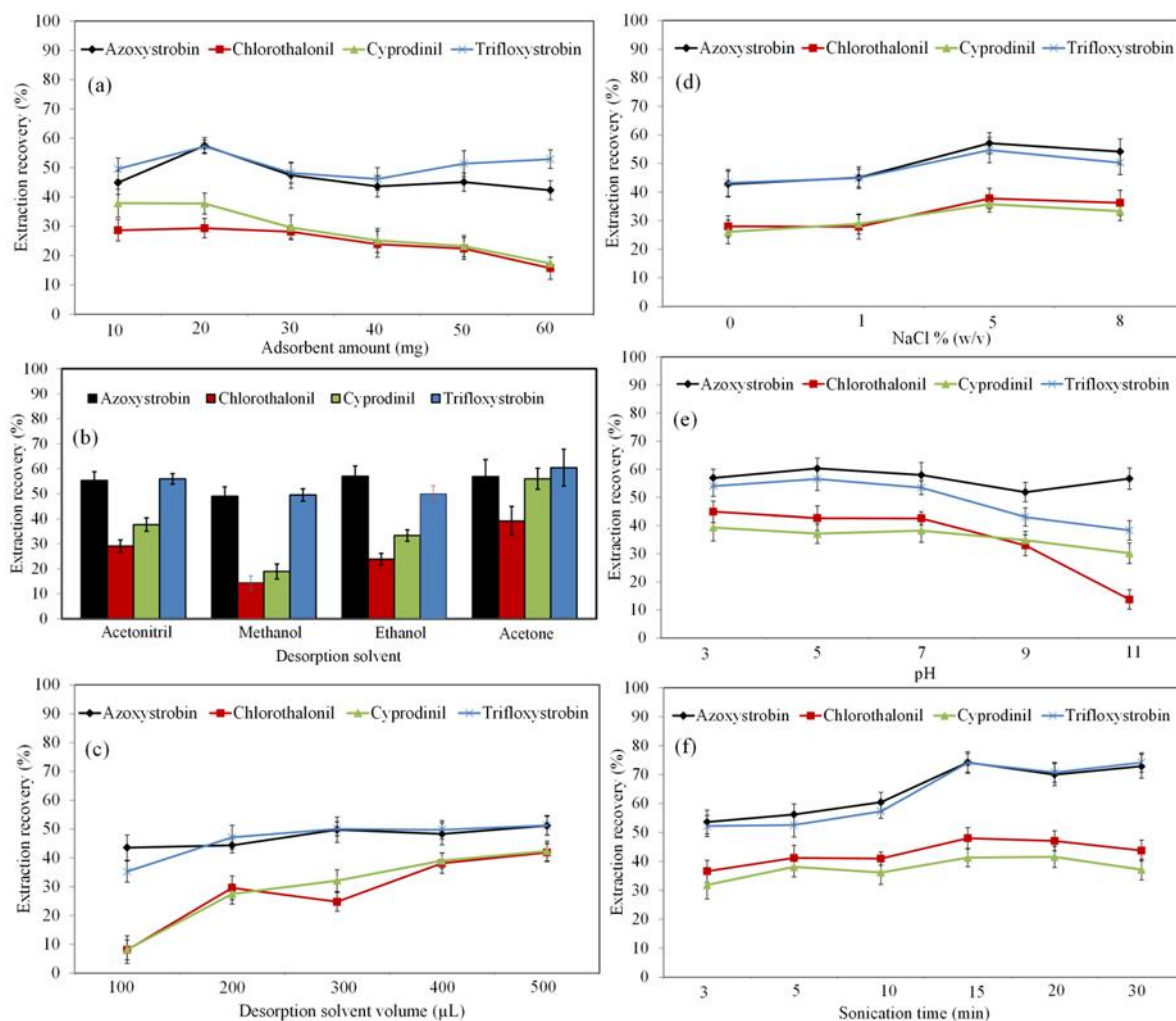


Fig 3. Effect of a) adsorbent amount, b) desorption solvent type, c) desorption solvent volume, d) ionic strength e) pH, and f) adsorption time on the extraction of fungicides using C/Fe₃O₄-MSPE method.

Table 1. Analytical performance of the C/Fe₃O₄-MSPE method for the determination of fungicides in water samples.

Analytes	Linear range (µg L ⁻¹)	r ²	LOD (µg L ⁻¹)	LOQ (µg L ⁻¹)	RSD ^a (%)	RSD ^b (%)	EF ^c	ER ^d (%)
Azoxystrobin	1-50	0.9976	0.4	1.3	5.3	3.6	28	71
Chlorothalonil	1-50	0.9979	0.6	2.0	6.6	6.9	18	44
Cyprodinil	1-50	0.9987	1.1	3.5	6.3	6.8	16	41
Trifloxystrobin	1-50	0.9969	0.8	2.8	6.3	5.9	27	70

^aIntra-day relative standard deviation (5 µg L⁻¹, n = 5)

^bInter-day relative standard deviation (5 µg L⁻¹, n = 5)

^cMean enrichment factor (12.5 µg L⁻¹, n = 3)

^dMean extraction recovery (12.5 µg L⁻¹, n = 3)

3.4. Real samples analysis

The applicability of the C/Fe₃O₄-MSPE method to different water samples was investigated. Tap water and stream water samples were analyzed both before and after spiking with standard fungicides at concentrations of 2.5 µg/L and 12.5 µg/L. No fungicides were detected in any of the non-spiked samples. The recovery values for fungicides were calculated using analysis results of the spiked samples, which was based on the ratio between the concentrations found after extraction and initially spiked. The recoveries were in the range of 71–106%

with RSDs between 2.5 and 8.6%. Fig. 4 shows the HPLC chromatograms obtained from extraction and subsequent analysis of the stream water sample before and after spiking with standard fungicides.

The C/Fe₃O₄-MSPE method developed for the extraction of fungicides in water samples was compared with the sample preparation methods available in the literature. Sample volume, extraction solvent type and volume, extraction time, and some analytical performance parameters were selected for the comparison. Table 2 shows the comparison details between methods.

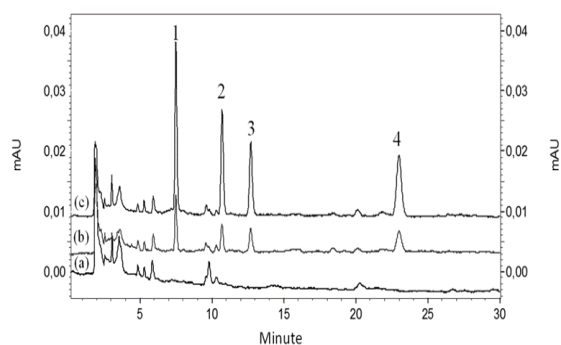


Fig 4. HPLC-UV chromatograms obtained after C/Fe₃O₄-MSPE of stream water sample (a) before and after spiking with fungicides at (b) 2.5 µg L⁻¹ and (c) 12.5 µg L⁻¹. Peaks, 1:Azoxystrobin, 2:Chlorothalonil, 3:Cyprodinil, 4:Trifloxystrobi

The C/Fe₃O₄-MSPE method has advantages over existing methods in terms of the type and volume of the extraction solvent used. Some of the methods use

expensive solvents such as 1-dodecanol [20], [C₈MIM][PF₆] [21] and [HMIM]NTf₂ [22,23], whereas the C/Fe₃O₄-MSPE uses only little volume of acetonitrile, which has much lower cost. The solvent volume of 200 µL used in the C/Fe₃O₄-MSPE method is lower than the solvent volumes used in some other methods [22,24]. Additionally, the extraction time of the C/Fe₃O₄-MSPE method (15 min) is shorter than the extraction time of some existing methods [20,25]. Those mentioned above make the newly developed C/Fe₃O₄-MSPE method more economical and rapid. Moreover, the C/Fe₃O₄-MSPE method uses a practical process to separate the magnetic adsorbent from both aqueous solution and desorption solvent, and therefore, as in some existing methods, the adsorbent must be filled into a column [24] or an additional centrifugation step to separate the extraction solvent [21,23] is not needed. In terms of accuracy, precision and sensitivity, the C/Fe₃O₄-MSPE method gives similar recovery, RSD and LOD values with all other methods.

Table 2. Comparison of C/Fe₃O₄-MSPE with other methods for the determination of fungicides in aqueous samples

Method	Analytes	Sample Volume (mL)	Extraction solvent and its volume	Extraction time (min)	Recovery (%)	RSD (%)	LOD (µg L ⁻¹)	Ref.
DS-SFO - HPLC-DAD	Chlorothalonil Cyprodinil Trifloxystrobin	3	1-dodecanol (20 µL)	90	93-110	>7.0	0.2-1.1	[20]
IL-USAEME-HPLC-VWD	Azoxystrobin	5	[C ₈ MIM][PF ₆] (40 µL)	15	106-115	>5.4	2.2	[21]
FPSE-HPLC-DAD	Azoxystrobin Chlorothalonil Cyprodinil Trifloxystrobin	8	[HMIM]NTf ₂ Acetonitrile (500 µL)	2	78-101	>7.3	0.09-0.23	[22]
AALLME-HPLC-UV	Azoxystrobin Cyprodinil	5	[HMIM]NTf ₂ (45 µL)	~ 1	75-115	>6.2	0.4-1.8	[23]
SPE-HPLC-UV	Azoxystrobin Chlorothalonil	12.5	Acetonitrile (~1 mL)	-	75-95	>7.3	0.05	[24]
SPME-GC-MS/MS	Azoxystrobin Chlorothalonil Cyprodinil Trifloxystrobin	19	Thermal desorption	60	88-115	>20.7	2.3-72.3	[25]
C/Fe ₃ O ₄ -MSPE-HPLC-UV	Azoxystrobin Chlorothalonil Cyprodinil Trifloxystrobin	8	Acetonitrile (200 µL)	15	71-106	> 6.9	0.4-1.1	This method

DS-SFO: Directly suspended-solidified floating organic droplet microextraction, IL-USAEME: Ionic liquid-based ultrasound-assisted emulsification microextraction, FPSE: Fabric phase sorptive extraction, AALLME: Air-assisted liquid-liquid microextraction, SPE: Solid-phase extraction, SPME: Solid-phase microextraction, C/Fe₃O₄-MSPE: Magnetic solid-phase extraction with C/Fe₃O₄ composite, HPLC: High-performance liquid chromatography, DAD: Diode array detector, VWD: Variable wavelength detector, UV: Ultraviolet detector, GC: Gas chromatography, MS/MS: Tandem mass spectrometry, [C₈MIM][PF₆]: 1-octyl-3-methylimidazolium hexafluorophosphate, [HMIM]NTf₂: 1-hexyl-3-methylimidazolium bis(trifluoromethanesulfonimide).

4. CONCLUSIONS

A coal-derived magnetic C/Fe₃O₄ composite was successfully prepared and used as a MSPE adsorbent for the extraction of fungicides from water samples prior to HPLC-UV analysis. The C/Fe₃O₄-MSPE method was rapid, and the adsorbent was practically separated from the water samples. The method displayed low detection limits, good precisions and satisfied spiked recoveries for trace fungicides in water samples. In conclusion, this technique expands the application of

liquid-liquid microextraction techniques and is expected to be extended to other analytes as well as other types of samples.

ACKNOWLEDGMENTS

This study was supported by the Scientific Research Projects (BAP) Coordination Unit of Zonguldak Bulent Ecevit University by the project number of 2016-72118496-03.

REFERENCES

- [1] M. Wierucka and M. Biziuk, "Application of magnetic nanoparticles for magnetic solid-phase extraction in preparing biological, environmental and food samples," *TrAC Trends in Analytical Chemistry*, Vol. 59, pp. 59, 50–58, 2014.
- [2] Y. Chen, Z. Guo, X. Wang and C. Qiu, "Sample preparation," *Journal of Chromatography A*, Vol. 1184, pp. 191–219, 2008.
- [3] S.M. Wille and W.E. Lambert, "Recent developments in extraction procedures relevant to analytical toxicology," *Analytical and Bioanalytical Chemistry*, Vol. 388, pp. 1381–1391, 2007.
- [4] J. Płotka-Wasyłka, N. Szczepańska, M. de La Guardia and J. Namieśnik, "Miniaturized solid-phase extraction techniques," *TrAC Trends in Analytical Chemistry*, Vol. 73, pp. 19–38, 2015.
- [5] M. Šafaříková and I. Šafařík, "Magnetic solid-phase extraction," *Journal of Magnetism and Magnetic Material*, Vol. 194, pp. 108–112, 1999.
- [6] A.M. Wightwick, A.D. Bui, P. Zhang, G. Rose, M. Allinson, J.H. Myers, S.M. Reichman, N.W. Menzies, V. Pettigrove and G. Allinson, "Environmental fate of fungicides in surface waters of a horticultural-production catchment in southeastern Australia," *Archives of Environmental Contamination and Toxicology*, Vol. 62, pp. 380–390, 2012.
- [7] M. Yang, X. Xi, X. Wu, R. Lu, W. Zhou, S. Zhang and H. Gao, "Vortex-assisted magnetic β -cyclodextrin/attapulgite-linked ionic liquid dispersive liquid-liquid microextraction coupled with high-performance liquid chromatography for the fast determination of four fungicides in water samples," *Journal of Chromatography A*, Vol. 1381, pp. 37–47, 2015.
- [8] P. Davini, "SO₂ adsorption by activated carbons with various burnoffs obtained from a bituminous coal," *Carbon*, Vol. 39, pp. 1387–1393, 2001.
- [9] N. Yang, S. Zhu, D. Zhang and S. Xu, "Synthesis and properties of magnetic Fe₃O₄-activated carbon nanocomposite particles for dye removal," *Materials Letters*, Vol. 62, pp. 645–647, 2008.
- [10] B. Qiu, H. Gu, X. Yan, J. Guo, Y. Wang, D. Sun, Q. Wang, M. Khan, X. Zhang and B.L. Weeks, "Cellulose derived magnetic mesoporous carbon nanocomposites with enhanced hexavalent chromium removal," *Journal of Materials Chemistry A*, Vol. 2, pp. 17454–17462, 2014.
- [11] K.Y. Foo and B.H. Hameed, "Microwave assisted preparation of activated carbon from pomelo skin for the removal of anionic and cationic dyes," *Chemical Engineering Journal*, Vol. 173, pp. 385–390, 2011.
- [12] J. Serafin, U. Narkiewicz, A.W. Morawski, R.J. Wróbel and B. Michalkiewicz, "Highly microporous activated carbons from biomass for CO₂ capture and effective micropores at different conditions," *Journal of CO₂ Utilization*, Vol. 18, pp. 73–79, 2017.
- [13] A.A. Asgharinezhad, S. Karami, H. Ebrahimzadeh, N. Shekari and N. Jalilian, "Polypyrrole/magnetic nanoparticles composite as an efficient sorbent for dispersive micro-solid-phase extraction of antidepressant drugs from biological fluids," *International Journal of Pharmaceutics*, Vol. 494, pp. 102–112, 2015.
- [14] J. Zhang, Z. Zhong, D. Shen, J. Zhao, H. Zhang, M. Yang and W. Li, "Preparation of bamboo-based activated carbon and its application in direct carbon fuel cells," *Energy and Fuels*, Vol. 25, pp. 2187–2193, 2011.
- [15] Y.-J. Zhang, Z.-J. Xing, Z.-K. Duan, M. Li and Y. Wang, "Effects of steam activation on the pore structure and surface chemistry of activated carbon derived from bamboo waste," *Applied Surface Science*, Vol. 315, pp. 279–286, 2014.
- [16] X. Yu, Y. Sun, C.-Z. Jiang, Y. Gao, Y.-P. Wang, H.-Q. Zhang and D.-Q. Song, "Magnetic solid-phase extraction and ultrafast liquid chromatographic detection of Sudan dyes in red wines, juices, and mature vinegars," *Journal of Separation Science*, Vol. 35, pp. 3403–3411, 2012.
- [17] L. Bai, B. Mei, Q.-Z. Guo, Z.-G. Shi and Y.-Q. Feng, "Magnetic solid-phase extraction of hydrophobic analytes in environmental samples by a surface hydrophilic carbon-ferromagnetic nanocomposite," *Journal of Chromatography A*, Vol. 1217, pp. 7331–7336, 2010.
- [18] S. Zhang, Z. Jiao and W. Yao, "A simple solvothermal process for fabrication of a metal-organic framework with an iron oxide enclosure for the determination of organophosphorus pesticides in biological samples," *Journal of Chromatography A*, Vol. 1371, pp. 74–81, 2014.
- [19] Q. Zhou, M. Lei, Y. Wu, X. Zhou, H. Wang, Y. Sun, X. Sheng and Y. Tong, "Magnetic solid phase extraction of bisphenol A, phenol and hydroquinone from water samples by magnetic and thermo dual-responsive core-shell nanomaterial," *Chemosphere*, Vol. 238, pp. 124621, 2020.
- [20] S. Li, X. Yang, L. Hu, X. Cui, S. Zhang, R. Lu, W. Zhou and H. Gao, "Directly suspended-solidified floating organic droplets for the determination of fungicides in water and honey samples," *Analytical Methods*, Vol. 6, pp. 7510–7517, 2014.
- [21] P. Liang, F. Wang and Q. Wan, "Ionic liquid-based ultrasound-assisted emulsification microextraction coupled with high performance liquid chromatography for the determination of four fungicides in environmental water samples," *Talanta*, Vol. 105, pp. 57–62, 2013.
- [22] M. Yang, Y. Gu, X. Wu, X. Xi, X. Yang, W. Zhou, H. Zeng, S. Zhang, R. Lu and H. Gao, "Rapid analysis of fungicides in tea infusions using ionic liquid immobilized fabric phase sorptive extraction with the assistance of surfactant fungicides analysis using IL-FPSE assisted with surfactant," *Food Chemistry*, Vol. 239, pp. 797–805, 2018.
- [23] X. You, X. Chen, F. Liu, F. Hou and Y. Li, "Ionic liquid-based air-assisted liquid-liquid microextraction followed by high performance liquid chromatography for the determination of

- five fungicides in juice samples," *Food Chemistry*, Vol. 239, pp. 354–359, 2018.
- [24] M. Catalá-Icardo, C. Gómez-Benito, E.F. Simó-Alfonso and J.M. Herrero-Martínez, "Determination of azoxystrobin and chlorothalonil using a methacrylate-based polymer modified with gold nanoparticles as solid-phase extraction sorbent," *Analytical and Bioanalytical Chemistry*, Vol. 409, pp. 243–250, 2017.
- [25] J. Martins, C. Esteves, T. Simões, M. Correia and C. Delerue-Matos, "Determination of 24 pesticide residues in fortified wines by solid-phase microextraction and gas chromatography–tandem mass spectrometry," *Journal of Agricultural and Food Chemistry*, Vol. 59, pp. 6847–6855, 2011.



RESEARCH ARTICLE

Evaluation of electrochemical treatment of real hospital wastewater with different electrode materials

Gülizar Kurtoğlu Akkaya ^{1,*}

¹ Necmettin Erbakan University, Department of Environmental Engineering, Meram, 42140, Konya, TURKIYE

ABSTRACT

In this paper, the treatment of real hospital wastewater (HWW) by electrocoagulation process (EC), which is one of the electrochemical treatment methods, has been evaluated. In the EC process, aluminum (Al) and iron (Fe) plates as anode and cathode are used. Experimental studies were conducted at 5, 10, 20, 30 voltage (V) and 5, 10, 20, 30, 45 minutes (min) exposure times. pH, temperature, and conductivity were monitored. COD and phenol removal were evaluated. As a result of experimental studies, Al and Fe electrodes were effective in the treatment of HWW with EC. The highest COD removal efficiency was 93% at 30V 10 min and 95% at 30V 5 min for Al and Fe electrode, respectively. The highest phenol removal efficiency is 97% at 10V 10 min and 97% at 10V 5 min for Al and Fe electrode. When all parameters are evaluated, optimum electro kinetic conditions for treatment of HWW was obtained for 10V 5 min by the Fe electrode.

Keywords: Hospital wastewater, electrocoagulation, aluminum electrode, iron electrode

1. INTRODUCTION

Hospital wastewater (HWW) is a wastewater similar to the quality of domestic wastewater, whose properties are not well known [1], [2], [3]. HWW contains many hazardous ingredients, including hazardous chemical components, heavy metals, disinfectants, and special detergents used in laboratories and research [4], [5], [6]. HWW is a wastewater obtained from all hospital activities, both medical and non-medical, including activities such as radiology cafeterias and examination rooms. In addition, higher concentrations of pharmaceutical ingredients can be found than are found in domestic wastewater [7], [8]. The degree of pollution of HWW and its polluting properties can vary from day to day from hour to hour [1]. Therefore, treatment disposal and proper management of HWW is an increasing international concern. HWW is generally discharged into city sewer systems. In domestic wastewater treatment facilities, it has to be treated together with domestic wastewater. In different countries, specific treatment methods have been used for HWW output [9], [10], [11], [12].

In recent years, electrochemical treatment methods, which provide more economical and high treatment efficiency, are widely preferred in the treatment of wastewater. Electrocoagulation (EC) is one of the simple and effective electrochemical methods for water and wastewater treatment [13]. In this technique, which is characterized by simple equipment and easy operation, soluble metal hydroxide is produced by electrolytic oxidation of a suitable anode material to a coagulant at a suitable pH to remove large contaminants [14]. These types of metal hydroxides neutralize electrostatic charges on suspended solids to facilitate their separation from the aqueous phase, flocculation and coagulation [15], [16].

This method is used efficiently in various types of wastewater. In this study, the treatment of wastewater obtained from a real hospital with two different electrode types by EC method was evaluated. Also, pH, conductivity changes, COD and total phenol removals were evaluated at different voltage (V) and exposure times and a comparison was made for two electrodes.

Corresponding Author: ka.gulizar@gmail.com (Gülizar Kurtoğlu Akkaya)

Received 25 August 2020; Received in revised form 3 October 2020; Accepted 4 October 2020

Available Online 2 November 2020

Doi: <https://doi.org/10.35208/ert.785556>

© Yildiz Technical University, Environmental Engineering Department. All rights reserved.

2. MATERIALS AND METHODS

2.1. Experimental setup

EC sets of HWW were conducted to plexiglass reactor (9 cm diameterx13 cm height) (Fig 1). Used wastewater volume was 600-mL for a set. Electrodes were preferred aluminum (Al-Al) and iron and (Fe-Fe) plate as anode and cathode. Electrode dimensions were 6 cm width, 11.5 cm height, 0.1 cm thickness, and their effective areas were 46.2 cm². Distance between electrodes was 2 cm. Before each set, electrodes were cleaned after distilled water and before acetone on electrodes. With DC power supply, an electric field were supplied by between 5 and 30 V in exposure times in EC (Table 1). At the end of each set, coagulated materials allowed to settle for a few hours in Imhoff and then supernatants were taken from Imhoff and analyzed.

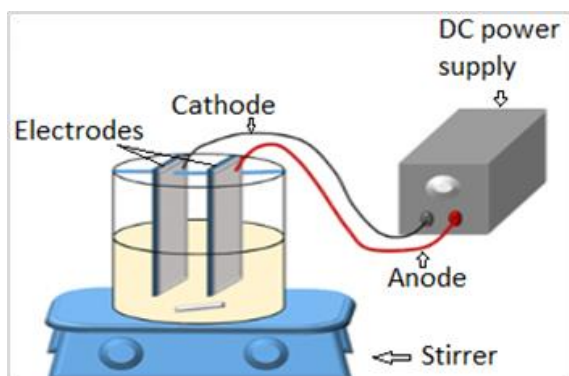


Fig 1. Experimental setup

Table 1. Experiment sets for Al and Fe electrodes

Experiment Sets	Exposure Time (min)	Voltage (V)
Control	0	0
1	5	5
2	10	5
3	20	5
4	30	5
5	45	5
6	5	10
7	10	10
8	20	10
9	30	10
10	45	10
11	5	20
12	10	20
13	20	20
14	30	20
15	45	20
16	5	30
17	10	30
18	20	30
19	30	30
20	45	30

2.2. Analytic procedure

In real HWW by EC, pH, temperature and conductivity parameters were measured by a pH 510 Eutech Inst. meter in end of EC sets. COD and phenol were analyzed in supernatants. COD and phenol were analyzed according to Standard Methods 5220-D and 5530-D, respectively (APHA, 2005). In the direct photometric method for phenol, samples were measured at 500 nm by UV/VIS Spectrophotometer. The removal rates of COD and phenol were calculated using the following equation: (%) = $(A_0 - A_1)/A_0 \times 100$ where A_0 and A_1 represent influent and effluent concentrations of the parameter, respectively. All analyses were conducted in triplicate. All chemicals used analyzed were analytical reagent grade.

2.3. HWW characterization

HWW samples were collected from the discharge point of the HWW to the sewer system in Sisli Hamidiye Etfal Training and Research Hospital, Istanbul, Turkey. Top [1] determined that the pollutant load density of the HWW sent to the sewerage systems is at noon. Therefore, the wastewater sample was taken at 13:00. All experiments have been done on the same wastewater. HWW characterization was given Table 2.

Table 2. Characteristics of used real HWW

Parameters	Value
COD (mg L ⁻¹)	772
TP (mg L ⁻¹)	0.345
Suspended Solids (mg L ⁻¹)	185
Phenol (mg L ⁻¹)	3.26
Sulfate (mg L ⁻¹)	174
Chloride (mg L ⁻¹)	158
pH	6.87
Temperature (°C)	20.6
Conductivity (µS cm ⁻¹)	929

3. RESULTS AND DISCUSSION

3.1. pH

The pH is one of parameters affected EC process. It is responsible for the speciation and solubility of metal oxides and hydroxide in wastewater. Also, pH change in EC contributes to the removal of pollutants in wastewater. Changes in pH during an EC are related to the electrolysis of water and the chemistry of the coagulation process. The rise in the final pH with applying electric field can be easily explained by Equations (Table 3).

The pH values obtained as a result of EC treatment of HWW with Al and Fe electrodes and the first wastewater pH range is wider at the Fe electrode, indicating that a different chemical process will occur with two reagents (Al and Fe) in the coagulation of pollutants. Fig 2 shows the pH change in HWW with Al-Al and Fe-Fe electrodes. According to the results, it was seen that pH gradually increased with the increase in voltage and duration due to the dominant activities of

the cathode, depending on the activities of the anode and cathode.

Table 3. Reactions occurred by EC in Wastewater [17]

Anode	Cathode
$4OH^- + 4e^- = 2H_2O + O_{2(g)}$	$2H_3O^+ + 2e^- = H_{2(g)} + 2H_2O$ (in aside solution)
$2H_2O + 4e^- = O_{2(g)} + 4H^+$	$2H_2O + 2e^- = H_{2(g)} + 2OH^-$ (in alkali solution)
$2Cl^- + 2e^- = Cl_{2(g)}$	$O_{2(g)} + 2H_2O + 4e^- = 4OH^-$
Al-anode	
$Al_{(k)} + 3e^- = Al_{(aq)}^{3+}$	$Al_{(k)} + 4OH^- = [Al(OH)_4]^- + 3e^-$ (in very-high pH)
$Al_{(aq)}^{3+} + 3H_2O = Al(OH)_3 + 3H^+$	
Fe-anode	
$Fe_{(k)} + 2e^- = Fe_{(aq)}^{2+}$	
$Fe_{(aq)}^{2+} + 2H_2O = Fe(OH)_2 + 2H_2O$	$Fe(OH)_3 + OH^- = [Fe(OH)_4]^-$
$Fe^{2+} + e^- = Fe^{3+}$ $Fe^{3+} + 3H_2O = Fe(OH)_3 + 3H^+$	$[Fe(OH)_4]^- + 2OH^- = [Fe(OH)_6]^{3-}$ (in very-high pH)

During the exposure period, the lowest pH increases occurred at 5V. The longest exposure time at 45 min was 7.18 for Al and 8.2 for Fe. When the voltage was 30, the pH increased from 6.87 to 8.57 with the Al-electrode, and from 6.87 to 9.32 with the Fe electrode. The pH increase in the Fe-electrode was higher than in the Al electrode. The higher the pH level, the higher the dose of coagulants in the solution.

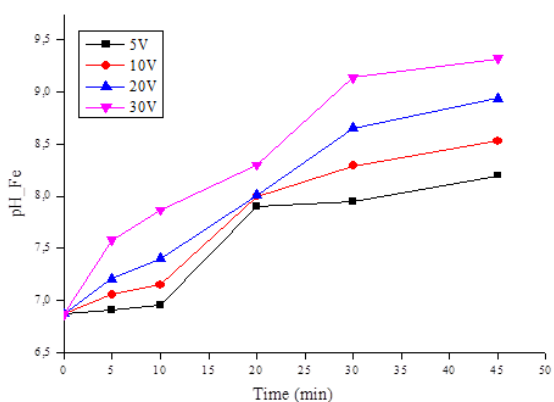
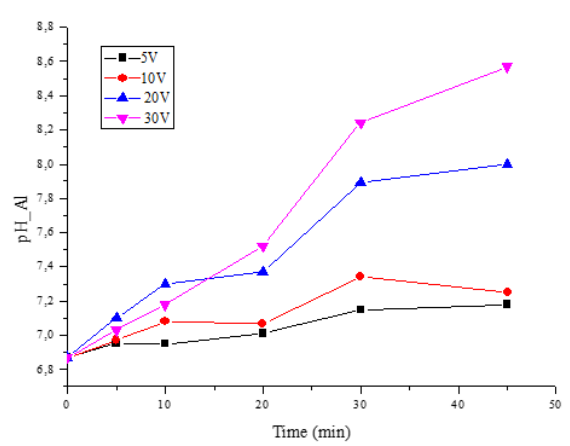


Fig 2. pH changes in Al and Fe electrodes

3.2. Temperature and conductivity

Temperature changes in HWW during EC are given in Fig 3. Temperature increase with time is an expected

situation arising from electrolytic reactions in EC processes [18]. Wang et al. [19] and Ilhan [18] found that there was an increase in temperature depending on the time in EC in their study. Depending on the contact time, the type of electrode, and the applied electrical field, temperatures increase as a result of electrolytic reactions. In these studies, when Al and Fe electrodes were used, the highest temperature was measured at 30V and 41 °C at the Fe electrode. The temperature of the two electrode types varied between 20-41 °C at different voltages and exposure times.

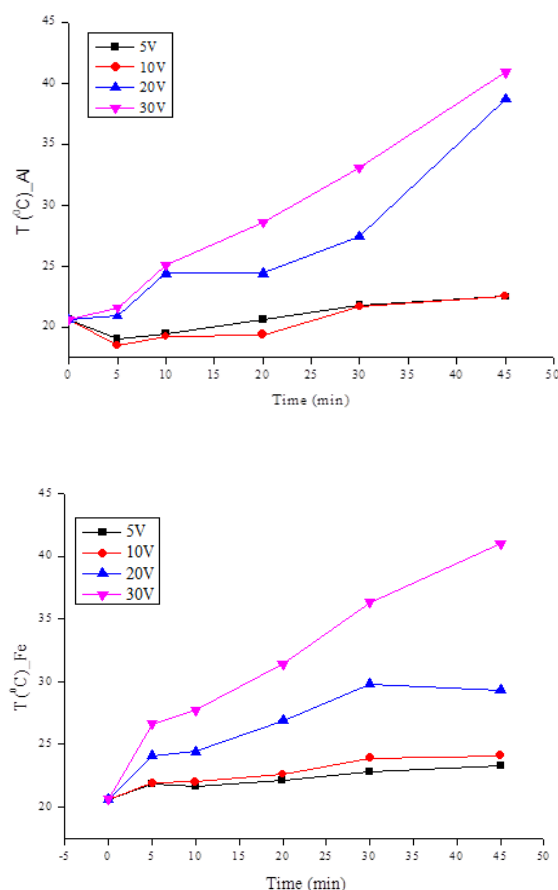


Fig 3. Temperature changes in Al and Fe electrodes

Also, the electrical conductivity changes depending on the contact time and the applied electrical field. The conductivity change is shown in Fig 4. The electric field applied in EC reduces conductivity [20]. In addition, the conductivity is higher in acidic pH than neutral pH. The reason for this is related to hydroxide compounds produced by the presence of Al and Fe ions emitted from the electrode surface, which can adsorb cations and anions into the solution. As a matter of fact, this is the case here. Conductivity starts to decrease with the increase of pH in the Al electrode, this situation is seen more clearly in the Fe electrode. Conductivity decreased at all voltage values after 20 min. of exposure. However, an increase was observed in the conductivity values of Al and Fe electrodes between 0-20 min. In some EC studies, it has been reported that disinfectants or dissolved ions in wastewater may cause an increase in conductivity [21], [22]. Consequently, it is estimated that disinfectants or dissolved ions in HWW may have caused an increase in conductivity.

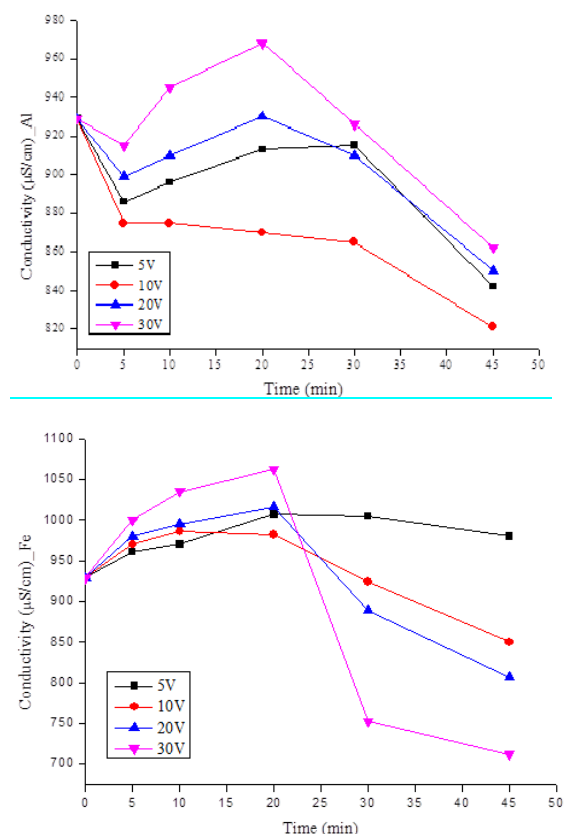


Fig 4. Conductivity changes in Al and Fe electrodes

3.3. COD removal

Under different voltage, the effect of COD concentration on the treatment of HWW with different electrodes was investigated. In Fig 5, the percentages of COD removal with both Al and Fe electrodes are given. The high removal efficiency was achieved with both electrode materials. The performances of the electrodes varied under the same conditions. Fe electrodes were obtained more COD removal efficiency than Al. For example, the lowest exposure time is 5 min. and the Al and Fe COD removal efficiencies at 5V are 88% and 94%, respectively. However, COD removal efficiencies during the highest voltage and highest exposure (30V 45 min) were 85% and 87% for Al and Fe, which were the lowest removal efficiencies obtained in the study. The reason for this is that high rates of metal coagulants are produced with the increase of pH in EC processes.

Maximum COD removal efficiency was achieved faster at low voltages than at higher voltages [23]. However, in this study, the highest COD removal was obtained at the highest voltage. The reason for this is that the conductivity of HWW is lower than that of other wastewater, so Al(OH)_3 compounds and Fe(OH)_2 formation have been achieved more in the wastewater at the highest voltage. The increase in pH with the exposure time also increased the bubbles formed in EC and these bubbles caused an increase in COD removal efficiency by increasing the buoyancy of the cell [24]. After 10 min of exposure time at the Al electrode, COD removal efficiency decreased at all voltage values. The decrease in the COD yield at the Al electrode at high pH

may be due to the $[\text{Al(OH)}_n]$ complex formations and the dissolution of Al(OH)_3 in solution (Table 3). After 10 min of exposure for Al, more bubbles are produced from the anode, which means a higher oxygen generation. Therefore, competition occurs between Al dissolution and oxygen formation. Thus, Al(OH)_3 formation was reduced, leading to a decrease in COD removal efficiency [25], [26]. In their study, Verma et al [27] determined that the maximum removal efficiency occurred at neutral pH and the decrease in removal efficiency was due to amphoteric Al(OH)_3 at acidic pH.

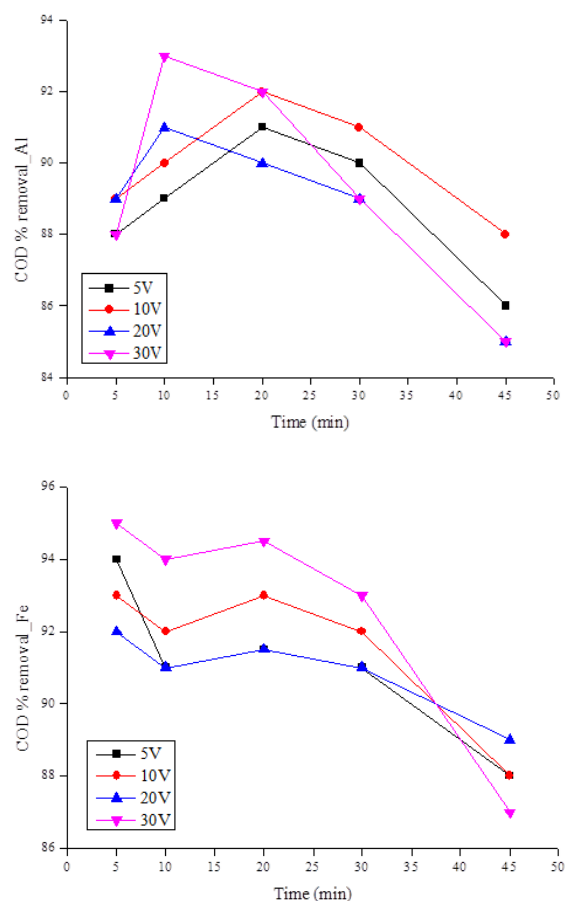


Fig 5. COD % removal of HWW with Al and Fe electrodes with EC processes

A different situation occurred in the Fe electrode compared to Al (Fig 5). After exposure time 5 min., the COD removal efficiency started to decrease. As is known, there is a relationship between solution pH and COD removal. The higher the solution pH, the more coagulants (Fe(OH)_2 and Fe(OH)_3) were formed [28]. Subsequently, they adsorbed the contaminant, thus achieving COD removal efficiency at higher solution pH. However, it has been stated that when the solution pH at the Fe electrode is higher than 8.00, the COD removal efficiency will decrease [29], [30]. COD removal efficiencies at all voltages decreased as the reaction time increased. It has been stated that the decrease in efficiency at higher reaction time and voltage may be associated with high production of drug degradation products, competition with major contaminants for coagulant, and reactive species. Similar results have been reported in the study conducted by Ahmadzadeh et al. [31] for the treatment

of HWW by EC process. The highest COD removal efficiency was 93% at 30V 10 min and 95% at 30V 5 min for Al and Fe electrode, respectively.

3.4. Phenol removal

Phenol is very soluble in water. If the phenol in wastewater is not removed, it may pose a risk in receiving environments. Due to their toxic effects, phenolic contaminants can damage sensitive cells. Phenolic micropollutants in HWW can cause health and environmental problems. For this reason, it is important to eliminate phenolic compounds in HWW. In Fig 6, phenol removal efficiencies of HWW with Al and Fe electrodes with EC processes are given. Phenol removal increased at all voltages during the 10 min exposure with Al electrodes. Treatment efficiency continued to increase up to the 20 min exposure time, except 20 and 30 V. The highest phenol removal efficiency was achieved at 10V 10 min at 97%. In the Fe electrode, it is 97% in 10V 5 minutes. It has been reported that phenols and organic acids can chemically interact with trivalent cations to form insoluble species through compound complexing, precipitation or coagulation processes [32]. The resulting $\text{Fe}(\text{OH})_3$ and $\text{Al}(\text{OH})_3$ and phenol molecules were removed from the water through the formation of surface complexes. Phenol molecules undergo physical adsorption by Van der Waals forces to gelatinous amorphous $\text{Fe}(\text{OH})_3$ flocs, which are found on the surfaces of hydroxide flocs (co-precipitation) [33].

Phenol removal efficiency trend from wastewater was found to be similar to COD. Efficiency decreased as the voltage and contact time increased. The low phenol removal efficiency was obtained at high pH. Similar results were found in Abdelwahab et al. [34] was also obtained in the study.

Removal efficiency is very low at low pH or high pH. The higher phenol removal efficiency was obtained with a neutral pH. This behavior has been attributed to the amphoteric character of $\text{Al}(\text{OH})_3$, which does not precipitate at very low pH [14]. It has also been determined that high pH leads to the formation of $\text{Al}(\text{OH})_4^-$, which is soluble and useless for the adsorption of phenol [35]. Therefore, it has been reported that further increasing the initial pH value decreases the phenol removal efficiency.

According to Faraday's Law, the electrolysis time in the EC process affects the rate of metal ions released into the system, therefore, as the EC time increased in this study, the COD and phenol removal efficiencies decreased compared to the low voltage and EC time [36]. Therefore, the treatment of HWW with a Fe electrode has been found more appropriate economically and environmentally.

In addition, the total suspended solids determination in the study was made at the end of EC, but the effluent TSS concentration was $<0.1 \text{ mg L}^{-1}$ in most of the experiment sets. The positively charged metal ions generated during EC can reduce the TSS concentration by destabilizing the negatively surface charged colloidal pigment particles by scavenging [37], [38].

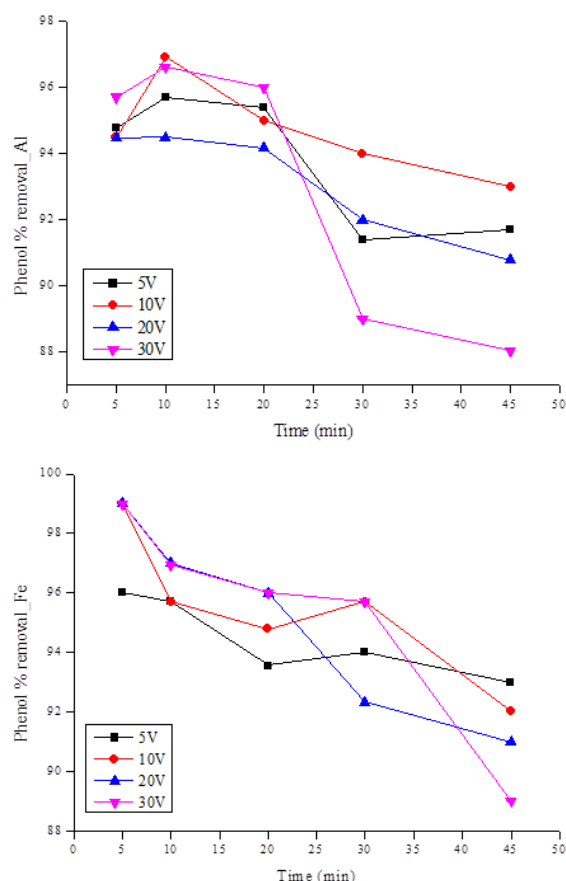


Fig 6. Phenol % removal of HWW with Al and Fe electrodes with EC processes

4. CONCLUSIONS

In the study, the treatment of real HWW by EC was evaluated using Al-Al and Fe-Fe electrodes. During EC, both electrode materials increased with increasing pH exposure time and voltage. Similarly, the temperature change was between 20-41 °C in all sets with increased temperature. The highest COD removal efficiency from wastewater was 93% at 30V 10min and 95% at 30V 5min for Al and Fe electrode, respectively. The highest phenol removal efficiency is 97% at 10V 10 min and 97% at 10V 5 min for Al and Fe electrode. High voltage and EC time increase the operating cost in EC studies. Accordingly, when COD and phenol removal efficiencies were evaluated, the optimum electrokinetic conditions in the treatment of HWW were 10V 10 min and 10V 5 min for Al and Fe, respectively. Therefore, economically and environmentally, optimum electro kinetic conditions in treatment of HWW was obtained for 10V 5min by Fe electrode.

REFERENCES

- [1]. S. Top, "Characterization of hospital wastewater and investigation of treatment alternatives," *Ph.D. Thesis*, Graduate School of Science and Engineering, YTÜ, İstanbul, Turkey, 2016
- [2]. A.R. Mesdaghinia, K. Naddafi, R. Nabizadeh, R. Saeedi and M. Zamanzadeh, "Wastewater

- characteristics and appropriate methods for wastewater management in the hospitals," *Iran J Public Health*, Vol. 38, pp. 34-40, 2009.
- [3]. H.A. Abd El-Gawad, A.M. Aly, "Assessment of aquatic environmental for wastewater management quality in the hospitals: a case study," *Aust J Basic Appl Sci*, Vol. 5(7), pp. 474-482, 2011.
- [4]. C. Boillot, C. Bazin, F. Tissot-Guerraz, J. Droguet, M. Perraud, J.C. Cetre, D. Trepo, Y. Perrodin, "Daily physicochemical, microbiological and ecotoxicological fluctuations of a hospital effluent according to technical and care activities," *Science of The Total Environment*, Vol. 403, pp. 113-129, 2008.
- [5]. H.A. Duong, N.H. Pham, H.T. Nguyen, T.T. Hoang, H. V. Pham, V.C. Pham, M. Berg, W. Giger, A.C. Alder, "Occurrence, fate and antibiotic resistance of fluoroquinolone antibacterials in hospital wastewaters in Hanoi, Vietnam," *Chemosphere*, Vol. 72, pp. 968-973, 2008.
- [6]. P. Verlicchi, M. Al Aukidy, A. Galletti, M. Petrovic, D. Barcelo', "Hospital effluent: investigation of the concentrations and distribution of pharmaceuticals and environmental risk assessment," *Science of The Total Environment*, Vol. 430, pp. 109-118, 2012.
- [7]. S. Yuan, X. Jiang, X. Xia, H. Zhang, S. Zheng, "Detection, occurrence and fate of psychiatric pharmaceuticals in psychiatric hospital and municipal wastewater treatment plants in Beijing, China," *Chemosphere*, Vol. 90(10), pp. 2520-2525, 2013.
- [8]. V.P. Prabhasankar, D.I. Joshua, K. Balakrishna, I.F. Siddiqui, S. Taniyasu, N. Yamashita, K. Kannan, M. Akiba, Y. Praveenkumarreddy, K.S. Guruge, "Removal rates of antibiotics in four sewage treatment plants in South India," *Environmental Science and Pollution Research*, Vol. 23(9), pp. 8679-8685, 2016.
- [9]. M. Al Aukidy, S. Al Chalabi, P. Verlicchi, "Hospital wastewater treatments adopted in Asia, Africa, and Australia," *In Hospital Wastewaters*, Springer, Cham., pp. 171-188, 2017.
- [10]. A. Khan, N.A. Khan, S. Ahmed, A. Dhingra, C.P. Singh, S.U. Khan, S. Vambol, "Application of advanced oxidation processes followed by different treatment technologies for hospital wastewater treatment," *Journal of Cleaner Production*, Vol. 269, No. 122411, 2020.
- [11]. S. Ahmadzadeh, M. Dolatabadi, "Removal of acetaminophen from hospital wastewater using electro-Fenton process," *Environmental earth sciences*, Vol. 77(2), pp. 53, 2018.
- [12]. S. Top, M. Akgün, E. Kıpçak, M.S. Bilgili, "Treatment of hospital wastewater by supercritical water oxidation process," *Water Research*, Vol. 185, No. 116279, 2020.
- [13]. Ü.T. Ün, S. Uğur, A.S. Kopalal, Ü.B. Ögütveren, "Electrocoagulation of olive mill wastewaters," *Separation and Purification Technology*, Vol. 52(1), pp. 136-141, 2006.
- [14]. N. Adhoum, L. Monser, "Decolourization and removal of phenolic compounds from olive mill wastewater by electrocoagulation," *Chemical Engineering and Processing: Process Intensification*, Vol. 43(10), pp. 1281-1287, 2004
- [15]. M.Y.A. Mollah, R. Schennach, J.R. Parga, D.L. Cocke, "Electrocoagulation (EC)—science and application," *Journal Hazardous Material*, Vol. 84(1), pp. 29-41, 2001.
- [16]. C. Feng, N. Sugiura, S. Shimada, T. Maekawa, "Development of a high performance electrochemical wastewater treatment system," *Journal Hazardous Material*, Vol. 103(1-2), pp. 65-78, 2003.
- [17]. P. Song, Z. Yang, G. Zeng, X. Yang, H. Xu, L. Wang, K. Ahmad, "Electrocoagulation treatment of arsenic in wastewaters: a comprehensive review", *Chemical Engineering Journal*, Vol. 317, pp. 707-725, 2017.
- [18]. F. İlhan, "Sızıntı Sularının Elektrokoagülasyon Yöntemiyle Arıtılması," Yüksek Lisans Tezi, *YTÜ Fen Bilimleri Enstitüsü*, İstanbul, 2006.
- [19]. C.T. Wang, W.L. Chou, Y.M. Kuo, "Removal of COD from Laundry Wastewater by Electrocoagulation/Electroflotation," *Journal of Hazardous Materials*, Vol. 164, pp. 81-86, 2009.
- [20]. M. Kobya, O.T. Can, M. Bayramoglu, M., "Treatment of Textile Wastewaters by Electrocoagulation Using Iron and Aluminum Electrodes," *Journal of Hazardous Materials*, Vol. 100, pp. 163-178, 2003.
- [21]. M.A. Ahangarnokolaei, H. Ganjidoust, B. Ayati, "Optimization of parameters of electrocoagulation/flotation process for removal of Acid Red 14 with mesh stainless steel electrodes," *Journal of Water Reuse and Desalination*, Vol. 8(2), pp. 278-292, 2018.
- [22]. S.R. Patel, S.P. Parikh, "Statistical optimizing of electrocoagulation process for the removal of Cr (VI) using response surface methodology and kinetic study," *Arabian Journal of Chemistry*, Vol. 13(9), pp. 7032-7044, 2020.
- [23]. Q. Nguyen, T. Watari, T. Yamaguchi, Y. Takimoto, K. Niihara, J. Wiff, T. Nakayama, "COD Removal from Artificial Wastewater by Electrocoagulation Using Aluminum Electrodes," *International Journal of Electrochemical Science*, Vol. 15, pp. 39-51, 2020.
- [24]. Z. Zaroual, H. Chaair, A.H. Essadki, K. El Ass, M. Azzi, "Optimizing the removal of trivalent chromium by electrocoagulation using experimental design," *Chemical Engineering Journal*, Vol. 148(2-3), pp. 488-495, 2009.
- [25]. I. Heidmann, W. Calmano, "Removal of Zn (II), Cu (II), Ni (II), Ag (I) and Cr (VI) present in aqueous solutions by aluminium electrocoagulation," *Journal of hazardous materials*, Vol. 152(3), Vol. 934-941, 2008.
- [26]. P. Canizares, M. Carmona, J. Lobato, F. Martinez, M.A. Rodrigo, "Electrodissolution of aluminum electrodes in electrocoagulation processes," *Industrial & engineering chemistry research*, Vol. 44(12), pp. 4178-4185, 2005.
- [27]. A.K. Verma, "Treatment of textile wastewaters by electrocoagulation employing Fe-Al composite

- electrode," *Journal of Water Process Engineering*, Vol. 20, pp. 168-172, 2017.
- [28]. S. Garcia-Segura, M.M.S. Eiband, J.V. de Melo, C.A. Martínez-Huitle, "Electrocoagulation and advanced electrocoagulation processes: A general review about the fundamentals, emerging applications and its association with other technologies," *Journal of Electroanalytical Chemistry*, Vol. 801, pp. 267-299, 2017.
- [29]. E. Demirbas, M. Kobya, "Operating cost and treatment of metalworking fluid wastewater by chemical coagulation and electrocoagulation processes," *Process Safety Environmental Protection*, Vol. 105, pp. 79-90, 2017.
- [30]. M.E. Olya, A. Pirkarami, "Electrocoagulation for the removal of phenol and aldehyde contaminants from resin effluent," *Water Science Technology*, Vol. 68(9), pp. 1940-1949, 2013.
- [31]. S. Ahmadzadeh, A. Asadipour, M. Pournamdari, B. Behnam, H.R. Rahimi, M. Dolatabadi, "Removal of ciprofloxacin from hospital wastewater using electrocoagulation technique by aluminum electrode: optimization and modelling through response surface methodology," *Process Safety and Environmental Protection*, Vol. 109, pp. 538-547, 2017.
- [32]. P. Canizares, F. Martinez, J. Garcia-gomez, C. Saez, M.A. Rodrigo Combined electrooxidation and assisted electrochemical coagulation of aqueous phenol wastes," *Journal of Applied Electrochemistry*, Vol. 32(11), pp. 1241-1246, 2002.
- [33]. C.A. Martínez-Huitle, E. Brillas, "Decontamination of wastewaters containing synthetic organic dyes by electrochemical methods: a general review," *Applied Catalysis B: Environmental*, Vol. 87, pp. 105-145, 2009.
- [34]. O. Abdelwahab, N.K. Amin, E.Z. El-Ashtouky, "Electrochemical removal of phenol from oil refinery wastewater," *Journal of Hazardous Materials*, Vol. 163(2-3), pp. 711-716, 2009.
- [35]. J. Zhu, H. Zhao, J. Ni, "Fluoride distribution in electrocoagulation defluoridation process," *Separation Purification Technology*, Vol. 56, pp. 184-191, 2007.
- [36]. M.M. Emamjomeh and M. Sivakumar, "Fluoride removal by a continuous flow electrocoagulation reactor," *Journal Environmental Management*, Vol. 90, pp. 1204-1212, 2009.
- [37]. J.N. Hakizimana, B. Gourich, M. Chafi, Y. Stiriba, C. Vial, P. Drogui, J. Naja, "Electrocoagulation process in water treatment: A review of electrocoagulation modeling approaches," *Desalination*, Vol. 404, pp. 1-21, 2017.
- [38]. V. Kuokkanen, T. Kuokkanen, J. Rämö, U. Lassi, "Recent applications of electrocoagulation in treatment of water and wastewater—a review," *Green and Sustainable Chemistry*, Vol. 3(2), pp. 33 2013.



REVIEW ARTICLE

Bio-electroactive fuel cells and their applications

Afşın Yusuf ÇETİNKAYA^{1,*} , S. Levent KUZU¹ , Ahmet DEMİR¹ 

¹Department of Environmental Engineering, Yildiz Technical University, Istanbul, TURKIYE

ABSTRACT

Bio-electroactive fuel cells are systems that produce useful products from renewable sources without causing environmental pollution and treating waste. In this study, general design properties, operation mechanisms, application areas, and historical advancement of the bio-electroactive fuel cell was reviewed. Electricity generating microbial fuel cells offer new opportunities as with hydrogen and methane-producing microbial electrolysis cells due to their attractive variety of electroactive microorganisms and operating situations. This article provides an up-to-date review for Bio-electroactive fuel cells and outlines instructions for future studies.

Keywords: Bioelectronics, biofuel cells, microbial fuel cell, microbial electrolysis cell, microbial desalination cell

1. INTRODUCTION

Bio-electroactive fuel cells are described as fuel cells based on enzymatic catalysis for a certain part of their activity [1, 2]. Basically, Bio-electroactive fuel cells are devices that can convert chemicals directly into electrical energy through electrochemical reactions involving biochemical stages and the bio-electroactive fuel cell may be of micro size because it uses chemical energy sources [3, 4, 5]. These fuel cells consist of 2 parts as anode and cathode compartments. Oxidation and reduction reactions occur at anode and cathode, respectively. Oxidation releases electrons that is transferred owing to the external circuit to the cathode by doing electrical work. The circuit is completed by moving a compensating charge along the electrolyte, usually in the form of positive ions [6, 7]. Traditionally, fuel cells systems utilizes hydrogen or methanol (MeOH) as fuel and produce energy, water, and carbon dioxide (in the presence of MeOH) [8]. Biodegradable organic matters supply essential nutrients for living organisms [9, 10]. Consequently microbial catalytic oxidation of degradable organic compounds, free electrons are released through the electron transport chain (ETC) [11]. Under anaerobic conditions, the released electrons are transferred to compounds such as nitrate or sulfate, which are different from oxygen. In the Microbial Electrochemical System (MES), bacteria utilize their

catalytic activities to transfer the released electrons to an electrode (as an electron acceptor) and hereby, electric current is produced [12, 13].

Increasing consumption as the world population increases threatens natural resources and the earth. For this reason, research teams continue to work to obtain sustainable and renewable energy. Currently, alternative fuel sources such as solar energy, hydrogen, biomass, biofuels, and fuel cells [14, 15]. These devices consist of a system capable of generating electrical energy from electrochemical reactions involving oxidation and reduction of chemical species [16, 17]. Great interest in the field of biofuels can be considered as a mission to produce sustainable green energy from living systems to set against the global energy crisis in the future. These devices consist of a system capable of generating electrical energy from electrochemical reactions involving oxidation and reduction of chemical species [18]. Great interest in the field of biofuels can be considered as a mission to produce sustainable green energy from living systems to withstand the global energy crisis in the future [19]. Bio-electroactive fuel cells technology is considered a renewable and environmentally friendly technology that aims to be applied as a small power source for common applications [20]. The main advantages of Bio-electroactive fuel cells are that they can be operated at room temperature, have high fuel conversion

Corresponding Author: afsincetinkaya@gmail.com (Afşın Yusuf ÇETİNKAYA)

Received 31 August 2020; Received in revised form 30 September 2020; Accepted 4 October 2020

Available Online 5 November 2020

Doi: <https://doi.org/10.35208/ert.788183>

© Yildiz Technical University, Environmental Engineering Department. All rights reserved.

efficiency and scale up. Microorganisms are the main point of modern bio electrochemical systems.

Fuel cells can be classified according to the biocatalyst as Microbial Fuel Cell (MFC), microbial electrolysis cell (MEC), microbial desalination cells (MDCs), and microbial solar cells (MSC).

2. ANALYTICAL APPLICATIONS OF BIO-ELECTROACTIVE FUEL CELLS

2.1. Microbial fuel cell

The idea of producing electricity from bacteria was first proposed by Potter in 1911, which is the basis of the MFC system [21]. With these initial studies, significant progress was achieved in understanding electron transfer mechanisms, developing efficient bio-electrocatalytic interfaces, and developing new, low-cost and resistant electrode materials, but there is still deficiencies that should be improved. Prior to full-scale applications of MFCs, advancement of the system was made with the participation of NASA, some national agencies, and vehicle manufacturers [22]. In the 1960s Biofuel cells (BFC) gained some popularity due to NASA's interest in these units. NASA aimed to convert organic waste into electricity in space missions. But the interest ended in a short time. Since the start of the 21st century, increase in the number of scientific studies on MFC indicates that there is an increasing interest on the topic. Accordingly, several fuel cells have been developed and classified according to the function of utilized electrolyte (polymeric membrane, ceramic, liquid electrolyte). MFC is a bio-electrochemical utility that converts bio-sources into electricity [23]. MFC can be treat wastewater and generate electricity at the same time. This is the most known property of the system. MFC system consists of anode and cathode departments separated by a cation-specific membrane. The bacteria in the anode zone oxidizes the substrate [24, 25]. Electrons are transferred to the cathode through an external circuit, whereas protons are transferred to cathode from anode through a proton exchange membrane. Due to the fact that many MFCs are electrochemically inactive, electron transfer from MFC to the electrode can be expedited by mediators something like thionine, methyl cello, humic acid and etc. A MFC system is shown in Fig 1.

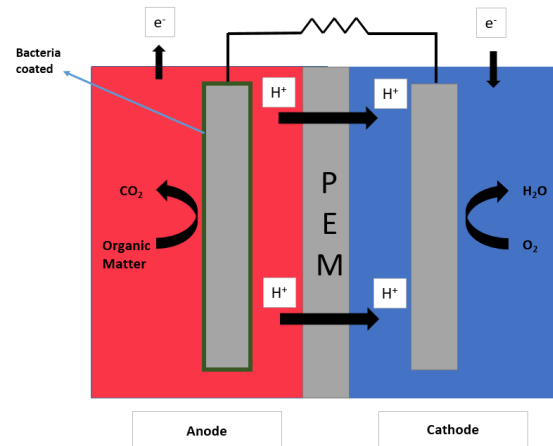


Fig. 1. The principle for microbial fuel cell [26]

In MFC applications, substrates (eg wastewater) are oxidized by exoelectrogenic microorganisms. The highest current densities to date usually generated by mixed cultures dominated by *Deltaproteobacteria* of the *Geobacter* genus. However, many other microorganism can transfer electrons to an anode.

MFCs represent a next-generation technology that allows not only energy generation but also recovery of useful products with wastewater treatment. MFCs allow the conversion of conventional wastewater treatment processes, which are characterized as energy intensive and purification-oriented, into integrated systems that allow the production of value-added products when wastewater treatment.

2.2. Microbial electrolysis cell (MEC)

MECs are a comparatively new method to produce hydrogen from electrohydrogenesis, acetate and other fermentation end products. In MEC, bacteria called exoelectrogens oxidize a substrate and release electrons on the anode [27, 28]. Generally, in the existence of oxygen at the cathode in an MFC, the current is produced by oxygen reduction, but in the MEC, the cathode is anaerobic and therefore, without oxygen, spontaneous current production is not possible [29]. MEC system is shown in Fig 2.

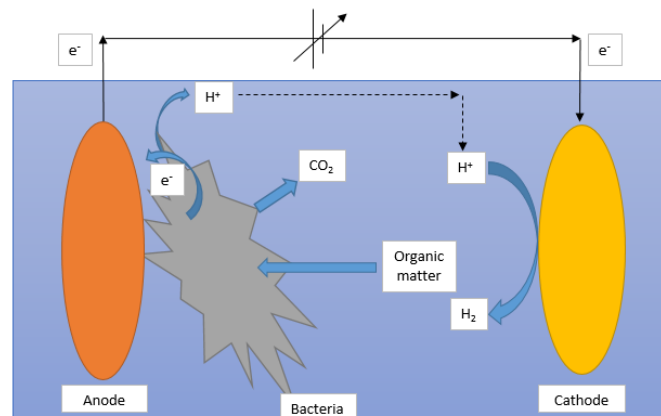


Fig. 2. The mechanism for a MEC system [30]

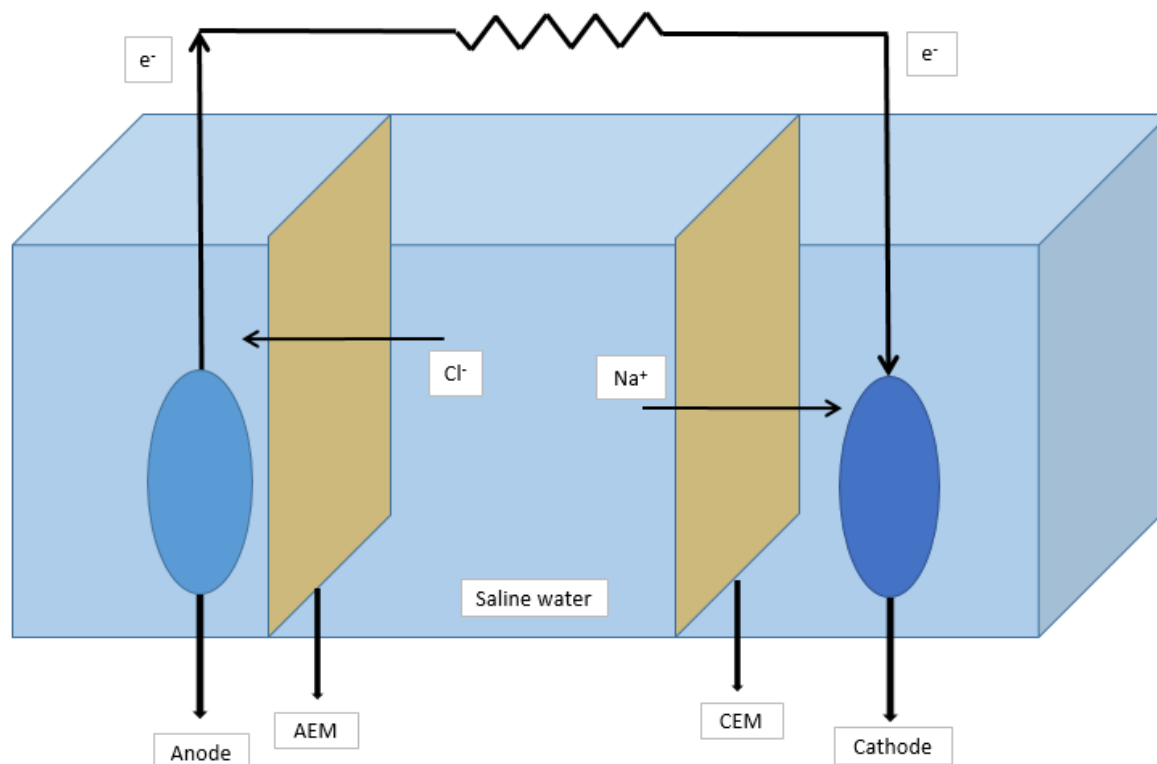


Fig. 3. General scheme of Microbial Desalination Cell [32]

Thus, a small voltage is applied externally to the circuit and allows the production of hydrogen at the cathode by reducing the proton. In MEC, hydrogen is produced at the cathode by electrolysis. However, an external electricity source is required for this production. Fortunately, this energy requirement is a relatively small amount. Because, most of the energy produced by the chemical energy at the anode during the oxidation of substrates.

2.3. Microbial desalination cell (MDC)

The microbial desalination cell (MDC) has been successfully developed for decisive purposes in order to purify wastewater, generate electricity and desalinate water simultaneously [31]. A general diagram of the microbial desalination cell is shown in Fig 3.

The increasing number of publications in MDC shows the growing interest to this topic. General accepted configurations in MDCs in current studies are air breathing, bio-cathodes and osmotic membranes. MEC systems are commonly used in studies with bio-cathodes and osmotic membranes [32, 33].

3. CONCLUSIONS

In the past two decades, researchers have tried to use more complex and higher energy containing fuels for conventional products. Bioelectroactive fuel cells can generate electric current in the presence of biological substances. Bio-electroactive fuel cells are released as

microbial electro synthesis devices, where the production of valuable products from other compounds, including CO₂ or gas conversion, with the help of specific bacteria. In order to make an easy-to-use and practical biofuel cell, many efforts have been made. These efforts include improving immobilization, electrode structure and electrolyte, and introducing multi-enzyme system and stabilization. This relatively new method, attracts attention of the researchers due to its off-grid energy supply potential.

REFERENCES

- [1] P. Pinyou, V. Blay, L. M. Muresan, T. Noguier, "Enzyme-modified electrodes for biosensors and biofuel cells", *Materials Horizons*, Vol. 6(7), pp. 1336-1358, 2019.
- [2] A. Kisieliute, A. Popov, R. M. Apetrei, G. Cârâc, I. Morkvenaite-Vilkonciene, A. Ramanaviciene, A. Ramanavicius, "Towards microbial biofuel cells: Improvement of charge transfer by self-modification of microorganisms with conducting polymer-Polypyrrole", *Chemical Engineering Journal*, Vol. 356, pp. 1014-1021, 2019.
- [3] S. R. Higgins, C. Lau, P. Atanassov, S. D. Minteer, M. J. Cooney, "Hybrid biofuel cell: microbial fuel cell with an enzymatic air-breathing cathode", *ACS Catalysis*, Vol. 1(9), pp. 994-997, 2011.
- [4] R. A. Escalona-Villalpando, K. Hasan, R. D. Milton, A. Moreno-Zuria, L. G. Arriaga, S. D. Minteer, J. Ledesma-García, "Performance comparison of

- different configurations of Glucose/O₂ microfluidic biofuel cell stack”, *Journal of Power Sources*, Vol. 414, pp. 150-157, 2019.
- [5] A. Pizzariello, M. Stred'ansky, S. Miertuš, “A glucose/hydrogen peroxide biofuel cell that uses oxidase and peroxidase as catalysts by composite bulk-modified bioelectrodes based on a solid binding matrix”, *Bioelectrochemistry*, Vol. 56(1-2), pp. 99-105, 2002.
- [6] S. Hao, X. Sun, H. Zhang, J. Zhai, S. Dong, “Recent development of biofuel cell based self-powered biosensors”, *Journal of Materials Chemistry B*, Vol. 8(16), pp. 3393-3407, 2020.
- [7] M. Goor, S. Menkin, E. Peled, “High power direct methanol fuel cell for mobility and portable applications”, *International Journal of Hydrogen Energy*, Vol. 44(5), pp. 3138-3143, 2019.
- [8] Y. H. Kwok, Y. Wang, M. Wu, F. Li, Y. Zhang, H. Zhang, D. Y. C. Leung, “A dual fuel microfluidic fuel cell utilizing solar energy and methanol”, *Journal of Power Sources*, Vol. 409, pp. 58-65, 2019.
- [9] J. Yang, S. Cheng, C. Li, Y. Sun, H. Huang, “Shear Stress Affected Biofilm Structure and Consequently Current Generation of Bioanode in Microbial Electrochemical Systems (MESs)”, *Frontiers in Microbiology*, Vol. 10, pp. 398, (2019).
- [10] J. Yang, Cheng, Li, P., Huang, H., Cen, K. “Sensitivity to oxygen in microbial electrochemical systems biofilms”, *iScience*, Vol. 13, pp. 163-172, 2019.
- [11] B. Liu, H. Zhai, Y. Liang, Ji, M., R. Wang, “Increased power production and removal efficiency of polycyclic aromatic hydrocarbons by plant pumps in sediment microbial electrochemical systems: A preliminary study,” *Journal Of Hazardous Materials*, Vol. 380, pp. 120896, 2019.
- [12] Q. Yang, F. Zhang, J. Zhan C.Gao, M. Liu, “Perchlorate removal in microbial electrochemical systems with iron/carbon electrodes”, *Frontiers in Chemistry*, Vol. 7, pp. 19, 2019.
- [13] A. Hagen, H. Langnickel, X. Sun, “Operation of solid oxide fuel cells with alternative hydrogen carriers”, *International Journal of Hydrogen Energy*, Vol. 44(33), pp. 18382-18392, 2019.
- [14] D. P. Strik, H. V. Hamelers, C. J. Buisman, “Solar energy powered microbial fuel cell with a reversible bioelectrod” *Environmental science & technology*, Vol.44(1), pp. 532-537, 2010.
- [15] Y. H. Kwok, Y. Wang, M. Wu, F. Li, Y. Zhang, H. Zhang, D. Y. C. Leung, “A dual fuel microfluidic fuel cell utilizing solar energy and methanol”, *Journal of Power Sources*, Vol. 409, pp. 58-65, 2019.
- [16] B. Tanç, H. T. Arat, E. Baltacıoğlu, K. Aydın, “Overview of the next quarter century vision of hydrogen fuel cell electric vehicles”, *International Journal of Hydrogen Energy*, Vol. 44(20), pp. 10120-10128, 2019.
- [17] Y. B. Vogel, J. J. Gooding, S. Ciampi, “Light-addressable electrochemistry at semiconductor electrodes: Redox imaging, mask-free lithography and spatially resolved chemical and biological sensing”, *Chemical Society Reviews*, Vol. 48(14), pp. 3723-3739, 2019.
- [18] D. Ivniński, B. Branch, P. Atanassov, C. Apblett, “Glucose oxidase anode for biofuel cell based on direct electron transfer”, *Electrochemistry Communications*, Vol. 8(8), pp.1204-1210, 2006.
- [19] Y. Kamitaka, S. Tsujimura, N. Setoyama, T. Kajino, K. Kano, “Fructose/dioxygen biofuel cell based on direct electron transfer-type bioelectrocatalysis”, *Physical Chemistry Chemical Physics*, Vol. 9(15), pp. 1793-1801, 2007.
- [20] E. Katz, M. Pita, “Biofuel cells controlled by logically processed biochemical signals: towards physiologically regulated bioelectronic devices”, *Chemistry—A European Journal*, Vol. 15(46), pp. 12554-12564, 2009.
- [21] A. Y. Cetinkaya, O. K. Ozdemir, E. O. Koroglu, A. Hasimoglu, B. Ozkaya, “The development of catalytic performance by coating Pt-Ni on CMI7000 membrane as a cathode of a microbial fuel cell”, *Bioresource Technology*, Vol. 195, pp. 188-193, 2015.
- [22] A. Y. Cetinkaya, O. K. Ozdemir, A. Demir, B. Ozkaya, “Electricity production and characterization of high-strength industrial wastewaters in microbial fuel cell”. *Applied Biochemistry and Biotechnology*, Vol. 182(2), pp. 468-481, 2017.
- [23] J.S. K. Butti, G. Velvizhi, M. L. Sulonen, J. M. Haavisto, E. O. Koroglu, A. Y. Cetinkaya, A. Verma “Microbial electrochemical technologies with the perspective of harnessing bioenergy: maneuvering towards upscaling”, *Renewable and Sustainable Energy Reviews*, Vol. 53, pp. 462-476, 2016.
- [24] Y. Zhang, M. Liu, M. Zhou, H. Yang, L. Liang, T. Gu, “Microbial fuel cell hybrid systems for wastewater treatment and bioenergy production: synergistic effects, mechanisms and challenges”, *Renewable and Sustainable Energy Reviews*, Vol.103, pp. 13-29, 2019.
- [25] M. I. San-Martín, A., Sotres, R. M., Alonso, J., Díaz-Marcos, A., Morán, A. Escapa, “Assessing anodic microbial populations and membrane ageing in a pilot microbial electrolysis cell”, *International Journal of Hydrogen Energy*, Vol. 44(32), pp.17304-17315, 2019.
- [26] M. H. Do, H. H. Ngo, W. Guo, S. W. Chang, D. D. Nguyen Y. Liu M., Kumar, “Microbial fuel cell-based biosensor for online monitoring wastewater quality: A critical review.” *Science of The Total Environment*, Vol.7 12, pp. 135612, 2020.
- [26] K. Guo, A. PrévotEAU, K. Rabaey, “A novel tubular microbial electrolysis cell for high rate hydrogen production” *Journal of Power Sources*, Vol. 356, pp. 484-490, 2017.
- [27] Zhen, X, Lu, G. Kumar, P, Bakonyi, K. Xu, Y. Zhao, “Microbial electrolysis cell platform for simultaneous waste biorefinery and clean electrofuels generation: Current situation, challenges and future perspectives”, *Progress in*

- Energy and Combustion Science*, Vol.63, pp. 119-145, 2017.
- [28] Y. Li, J. Styczynski, Y. Huang, Z. Xu, J. McCutcheon, B. Li, "Energy-positive wastewater treatment and desalination in an integrated microbial desalination cell (MDC)-microbial electrolysis cell (MEC)", *Journal of Power Sources*, Vol. 356, pp. 529-538, 2017.
- [29] C. Santoro, F. B. Abad, A. Serov, M. Kodali, K. J. Howe, F. Soavi, P. Atanassov, "Supercapacitive microbial desalination cells: new class of power generating devices for reduction of salinity content" *Applied Energy*, Vol. 208, pp. 25-36, 2017.
- [30] A. Kadier, Y. Simayi, M. S. Kalil, P. Abdeshahian, A. A. Hamid, "A review of the substrates used in microbial electrolysis cells (MECs) for producing sustainable and clean hydrogen gas", *Renewable Energy*, Vol.71, pp. 466-472, 2014.
- [31] A. C. Sophia, V. M. Bhalambaal, E. C. Lima, M. Thirunavoukkarasu, "Microbial desalination cell technology: contribution to sustainable wastewater treatment process, current status and future applications" *Journal of Environmental Chemical Engineering*, Vol. 4(3), pp.3468-3478, 2016.
- [32] H. M. Saeed, G. A. Hussein, S. Yousef, J. Saif, S. Al-Asheh, A. A. Fara, A. Aidan. "Microbial desalination cell technology: a review and a case study". *Desalination*, Vol. 359, pp. 1-13, 2015.
- [33] S. M. Iskander, J. T. Novak, Z. He, "Enhancing forward osmosis water recovery from landfill leachate by desalinating brine and recovering ammonia in a microbial desalination cell". *Bioresource Technology*, Vol. 255, pp.76-82, 2018.



RESEARCH ARTICLE

The biosynthesis of silver nanoparticles with fungal cytoplasmic fluid obtained from *Phanerochaete chrysosporium* ME446

Fatma Deniz^{1,*} , M. Ali Mazmanci¹ 

¹Mersin University, Department of Environmental Engineering, 33110, Mersin, TURKIYE

ABSTRACT

Over the last few years, the green synthesis of metal nanoparticles (NPs) has become the center of attention of researchers. There are eco-friendly techniques to determine the properties of metal nanoparticles, produced by microorganisms or their cytoplasmic fluids. In the present study, fungal cytoplasmic fluid of white-rot fungi *Phanerochaete chrysosporium* ME446 was used for the biosynthesis of Ag NP. The pH value of growing media of fungi, AgNO₃ concentration and fungal cytoplasmic fluid of *Phanerochaete chrysosporium* ME446 (PC-FCF) ratio were optimized to determine the most effective conditions. The formation of Ag NPs was monitored by UV visible spectrophotometer at a wavelength of 420 nm. Synthesized Ag NPs were characterized at scanning electron microscope (SEM). Optimum conditions for the pH value, AgNO₃ concentration and PC-FCF ratio were determined as 6.0, 1.50 mM and 100%, respectively. The shape and the sizes of nanoparticles, synthesized at optimum conditions, were confirmed by SEM. The shape was spherical, and the sizes were ranged from 26 to 63 nm.

Keywords: Biosynthesis, *Phanerochaete chrysosporium* ME446, silver nanoparticles

1. INTRODUCTION

Nano-sized materials were ranged from 1 to 100 nm and called nanoparticles (NPs). NPs are applied to the area of nanoscience and nanotechnology [1]. These materials have different magnetic effects from macro materials. [2, 3]. NPs have applied to many areas thanks to their important optical, thermal, and electrical properties. Drug, diagnosis, detection, imaging, artificial implants, genetic and tissue engineering are examples of these areas [4].

Metallic NPs have a large surface area/volume ratio and attracted the researchers' attention. Metals such as silver, gold and copper are generally utilized for the synthesis of metallic NPs. These syntheses are applied in many fields such as catalysis, photography, SERS (surface-enhanced Raman scattering), biological labeling, optoelectronics [1].

Silver NPs (Ag NPs), which have antibacterial properties, are used in many fields such as food packaging, food shelf life extension, cosmetics, medicine, and biomedical [4, 5]. When compared with

other metallic nanoparticles, Ag NPs are more effective against microorganisms such as viruses, bacteria [6, 7].

Metallic Ag is an inert material. However, ionized silver is reactive because it binds to tissue proteins and causes structural changes in bacterial cells. Silver binds to bacterial DNA and RNA, preventing bacterial growth [6, 8].

Various methods have been used for the synthesis of NPs. The selection of the synthesis method of a metallic nanoparticle is important because it affects the structure and size stability, and physicochemical properties of NPs [9]. The NP synthesis takes place in a short time with the high resolution and desired size when used the different physical and chemical methods such as electrochemical techniques, chemical and photochemical reduction. However, because of the disadvantages of these methods, such as high cost, toxic content, or inadequate particle stability, the development of eco-friendly synthesis methods and technology has been the subject of recent research [4-10].

Corresponding Author: fatmadeniz@mersin.edu.tr (Fatma Deniz)

Received 1 September 2020; Received in revised form 19 October 2020; Accepted 30 October 2020

Available Online 5 November 2020

Doi: <https://doi.org/10.35208/ert.788891>

© Yildiz Technical University, Environmental Engineering Department. All rights reserved.

Biological synthesis methods or biosynthesis are eco-friendly NP synthesis methods, used different microorganisms or plants. Silver NP biosynthesis using plant extracts [4, 11-13], bacteria [14, 15], algae [16], fungi [17, 18] was studied by many researchers.

Fungi are used for NP synthesis because their enzymes and proteins function as reducing agents to the metallic compound [9, 19]. AgNPs synthesis method using fungi, compared with other biological methods, is accepted as a more effective method due to dimensional stability [20]. *Trichoderma reesei*, *Aspergillus fumigates*, *Fusarium oxysporum* and *Fusarium oxysporum* are fungi types that are commonly used [9, 19].

In this study, the cytoplasmic fluid of the white-rot fungi *Phanerochaete chrysosporium* was used for the biosynthesis of Ag NP. Parameters such as pH, AgNO₃ concentration, and fungal cytoplasmic fluid (FCF) ratio were optimized.

2. MATERIALS AND METHODS

2.1. Materials

The white-rot fungi *Phanerochaete chrysosporium* ME446 (PC) was obtained from Mersin University Department of Environmental Engineering Microbiology Laboratory.

2.2. Methods

Preparing of PC-Fungal Cytoplasmic Fluid (PC-FCF)

The *Phanerochaete chrysosporium* ME446 (PC) was cultivated (the first cultivation) in Stok Basal Mineral Medium (SBM) at 39 °C, dark conditions, and shaken at 160 rpm [21, 22]. PC pellets were washed with sterile ultrapure water after 10 days. Pellets were added in a

tube containing ultrapure water (1:1 v/v) and incubated (the second incubation) at the same conditions for 5 days to obtain PC-fungal cytoplasmic fluid (PC-FCF). After the second incubation, pellets were separated from ultrapure water, and PC-FCF was obtained (Fig. 1).

Optimization studies

Optimization studies consisted of three steps. The first optimization step was pH optimization. At this step, the PC-FCF was obtained from PC pellets that were grown at different pH values (5.0; 6.0; 7.0). AgNO₃ concentration was adjusted 1mM.

The second step was AgNO₃ concentration optimization. The PC-FCF, obtained from PC pellets that were grown at optimum pH value, was used. Different amount of AgNO₃ (0.50, 0.75, 1.00, 1.50 mM) was added to samples.

The last step was PC-FCF dilution ratio optimization. The PC-FCF, obtained from PC pellets that were grown at optimum pH value and added optimum amount of AgNO₃, was used. The ratio of PC-FCF (25, 50, 75, and 100%) was adjusted using sterile ultrapure water.

Two different control groups were used. The first group was ultrapure water containing AgNO₃ and the second group was PC-FCF without AgNO₃.

All samples incubated at 39 °C, dark conditions, and shook at 160 rpm for two weeks. Color changes were measured with a UV spectrophotometer at 420 nm wavelength in every two days interval for 14 days.

After the optimization study, Ag NPs synthesized at optimum conditions were centrifuged at 12000 rpm, washed with ultrapure water, and characterized at SEM.

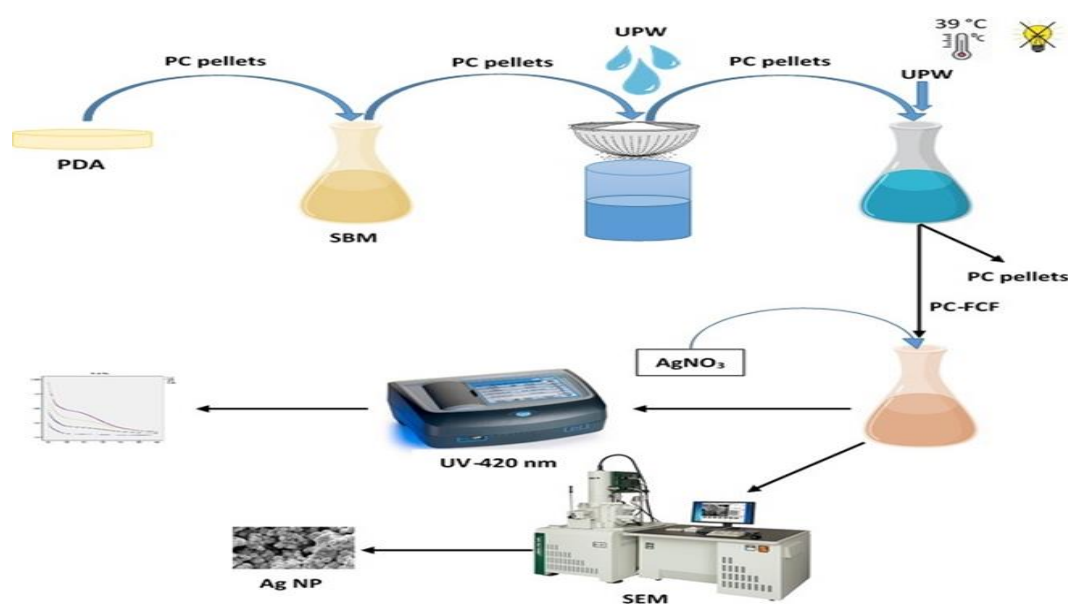


Fig 1. Scheme of the Ag NP biosynthesis method

3. RESULTS AND DISCUSSION

At the biosynthesis of metallic NPs, metal ions are reduced in the presence of biomolecules and enzymes [17, 23]. Toxic metal ions transform into nontoxic metal nanoparticles due to the catalytic effect of enzymes and metabolites of the fungi [20]. This formation is due to the excitation of surface plasmon vibrations in the nanoparticles [17, 24-26]. There are two different forms of biosynthesis: Intracellular and extracellular [23]. Intracellular synthesis of silver nanoparticles (Ag NPs) occurs inside microbial cells [27-30], while extracellular synthesis takes place on the outer surface of cells by reducing metal ions in the presence of biomolecules or enzymes [28, 29, 31-35]. Extracellular synthesis is preferred since it is inexpensive and simple, and large-scale production is possible [23, 36].

In the current study, extracellular synthesis was aimed. At all experiments, the nearly colorless PC-FCF turned to pale yellow as soon as AgNO_3 added. This observation showed that Ag NP synthesis was started immediately by reducing of Ag^+ . The media color changed from pale yellow to brown depending on the time (Fig. 2).

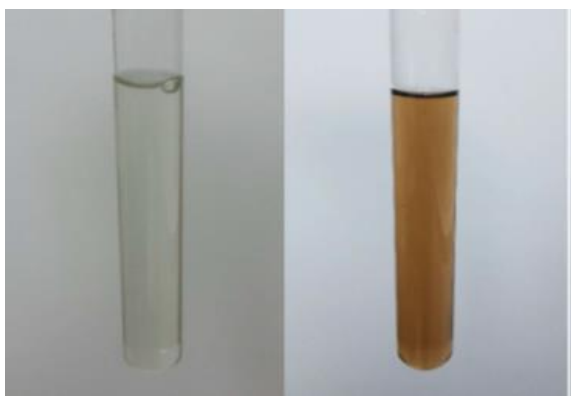


Fig 2. PC-FCF without and with Ag NP

Different pH values (2.0 - 9.0) were used in the previous studies that used various types of fungi such as *S. commune*, *P. sanguineus*, *L. sajour caju*, *T. pocas*, *T. feei*, *Verticillium sp.*, *Humicola*, *Penicillium fellutanum*, *R. oryzae* [18, 37-40] and bacteria such as *Streptomyces sp.*, *Streptomyces sp.* AOA21 [31, 41-43].

In this study, Ag NP formation was observed in all PC-FCFs obtained from fungi grown in three different pH (5.0; 6.0; 7.0) (Fig. 3a). A similar result was reported in the previous study [44]. While the best pH value for the growth of the PC was specified as 4.5-5.0 [45, 46], PC-FCF obtained at pH 6.0 was more effective in Ag NP synthesis (Fig. 3b). It was observed that the pH value of the growing medium of the fungus was an effective factor in Ag NP synthesis.

Different amount of AgNO_3 (0,5-1,5 mM) was used to observe the effect of AgNO_3 concentration on the Ag NP biosynthesis at pH 6. Adiguzel et. al. (2018) and Kathiresan et. al. (2009) reported that 1mM AgNO_3 was the optimal concentration for the Ag NP synthesis [38, 41]. But, in this study, maximum absorbance was obtained with 1,5 mM AgNO_3 (Fig. 4).

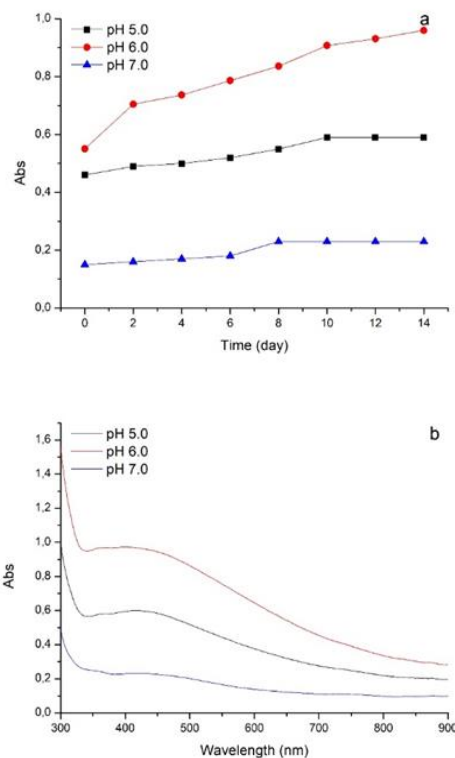


Fig 3. The effect of pH value during AgNP biosynthesis (a) and spectrum of synthesized AgNP on day 14 (b)

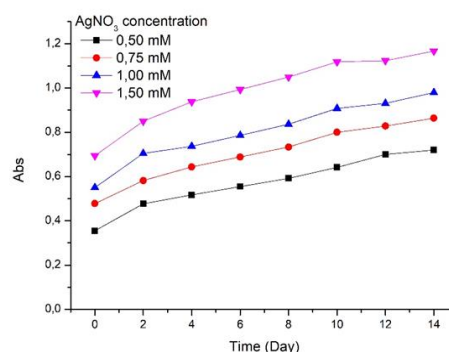


Fig 4. The effect of AgNO_3 concentration on the Ag NP biosynthesis

At the PC-FCF ratio optimization, pH 6.0 and 1,5 mM AgNO_3 was used. The absorbance value of the samples containing 25-50% PC-FCF increased until the second day, while other media (75-100% PC-FCF) until the 10th day. After two weeks, 0.28, 0.63, 0.88, and 1.13 abs were obtained in the samples containing 25, 50, 75, and 100% PC-FCF, respectively. The synthesized AgNP amount increased as the PC-FCF ratio increased (Fig. 5).

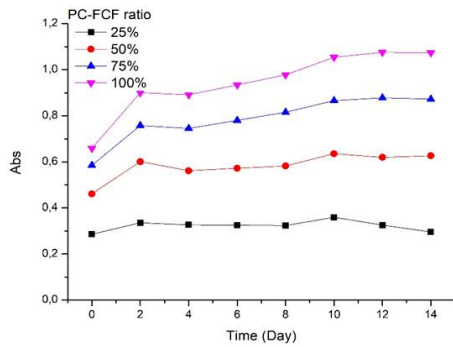


Fig 5. The change of Abs overtime on PC-FCF dilution ratio optimization

The size of the synthesized Ag NP changed from 26 to 63 nm. The shape of the Ag NP was spherical (Fig. 6-7). Similar fungi have been studied by some researchers. The size of Ag NP by using *P. chrysosporium* (MTCC 787/ATCC 24725) and *P. chrysosporium* (MTCC-787) was reported between 50-200 nm and 34-90 nm, and their shape was pyramidal and spherical/oval, respectively [27, 47]. In a previous study, *Coriolus versicolor* was used and synthesized Ag NP sizes ranged from 15-35 nm [44]. These results indicated that the microorganism type affects the Ag NP size and shape.

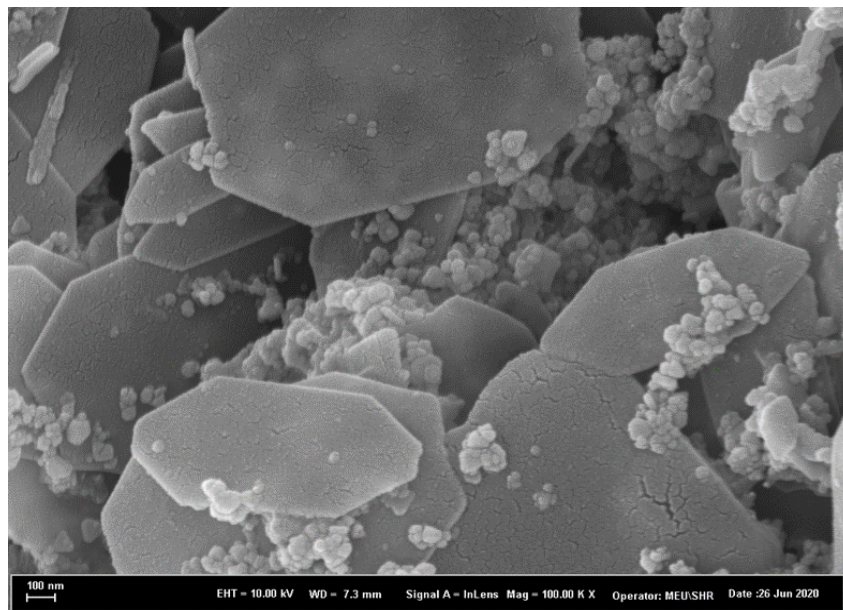


Fig 6. SEM images of the synthesized Ag NP (day 14)

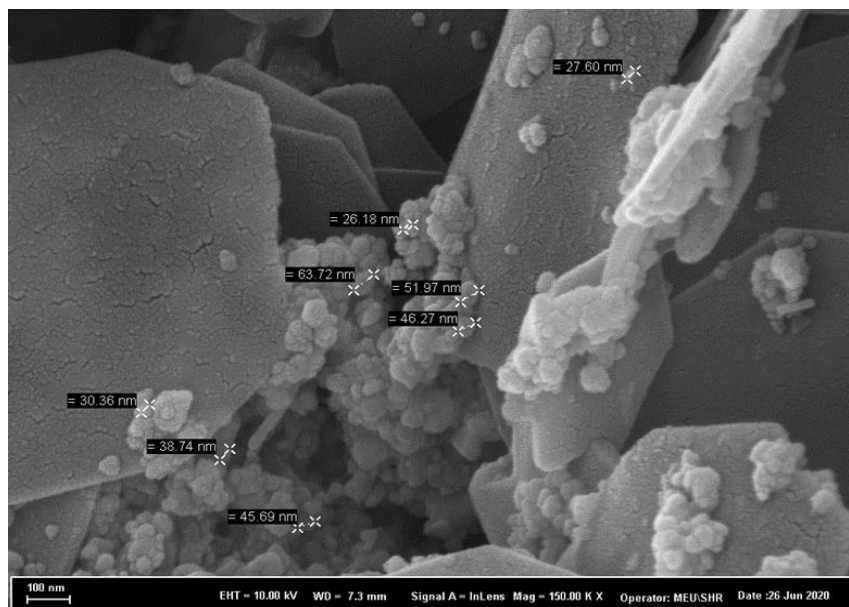


Fig 7. SEM images of the synthesized Ag NP (day 14)

4. CONCLUSIONS

In the present study, silver nanoparticles were synthesized by using PC-FCF. Optimization results showed that the optimum conditions were pH 6.0, 1.50 mM AgNO₃ and 100% PC-FCF. The size and shape of silver nanoparticles were measured by SEM. The size was between 26-63 nm, and the shape was spherical.

REFERENCES

- [1]. V. K. Sharma, R. A. Yngard, Y. Lin, "Silver nanoparticles: green synthesis and their antimicrobial activities," *Advances in colloid and interface science*, Vol. 145, pp. 83-96, 2009.
- [2]. M. Yer, "Gümüş nanopartikül sentezi ve karakterizasyonu," Selçuk Üniversitesi Fen Bilimleri Enstitüsü, Konya, Turkey, 2012.
- [3]. Y. Murthy, T. K. Rao, R. Singh, "Synthesis and characterization of nano silver ferrite composite," *Journal of Magnetism and Magnetic Materials*, Vol. 322, pp. 2071-2074, 2010.
- [4]. M. Beykaya, A. Çağlar, "Bitkisel özütler kullanılarak gümüş-nanopartikül (AgNP) sentezlenmesi ve antimikrobiyal etkinlikleri üzerine bir araştırma," *Afyon Kocatepe Üniversitesi Fen ve Mühendislik Bilimleri Dergisi*, Vol. 16, pp. 631-641, 2016.
- [5]. R. Karamian, J. Kamalnejad, "Green synthesis of silver nanoparticles using Cuminum cyminum leaf extract and evaluation of their biological activities," *Journal of Nanostructures*, Vol. 9, pp. 74-85, 2019.
- [6]. M. Rai, A. Yadav, A. Gade, "Silver nanoparticles as a new generation of antimicrobials," *Biotechnology Advances*, Vol. 27, pp. 76-83, 2009.
- [7]. P. Gong, H. Li, X. He, K. Wang, J. Hu, W. Tan, et al., "Preparation and antibacterial activity of Fe₃O₄@ Ag nanoparticles," *Nanotechnology*, Vol. 18, pp. 285604, 2007.
- [8]. J. J. Castellano, S. M. Shafii, F. Ko, G. Donate, T. E. Wright, R. J. Mannari, et al., "Comparative evaluation of silver-containing antimicrobial dressings and drugs," *International Wound Journal*, Vol. 4, pp. 114-122, 2007.
- [9]. P. G. Jamkhande, N. W. Ghule, A. H. Bamer, M. G. Kalaskar, "Metal nanoparticles synthesis: An overview on methods of preparation, advantages and disadvantages, and applications," *Journal of Drug Delivery Science and Technology*, Vol. 53, pp. 101174, 2019.
- [10]. T. V. Duncan, "Applications of nanotechnology in food packaging and food safety: barrier materials, antimicrobials and sensors," *Journal of Colloid and Interface Science*, Vol. 363, pp. 1-24, 2011.
- [11]. H. Tolouietabar, A. A. Hatamnia, R. Sahraei, E. Soheyli, "Biologically green synthesis of high-quality silver nanoparticles using scrophularia striata boiss plant extract and verifying their antibacterial activities," *Journal of Nanostructures*, Vol. 10, pp. 44-51, 2020.
- [12]. M. Kalaiselvi, R. Subbaiya, M. Selvam, "Synthesis and characterization of silver nanoparticles from leaf extract of Parthenium hysterophorus and its anti-bacterial and antioxidant activity," *Int J Curr Microbiol Appl Sci*, Vol. 2, pp. 220-227, 2013.
- [13]. S. CG Kiruba Daniel, K. Nehru, M. Sivakumar, "Rapid biosynthesis of silver nanoparticles using Eichornia crassipes and its antibacterial activity," *Current Nanoscience*, Vol. 8, pp. 125-129, 2012.
- [14]. P. Sivasankar, P. Seedeve, S. Poongodi, M. Sivakumar, T. Murugan, L. Sivakumar, et al., "Characterization, antimicrobial and antioxidant property of exopolysaccharide mediated silver nanoparticles synthesized by Streptomyces violaceus MM72," *Carbohydrate Polymers*, Vol. 181, pp. 752-759, 2018.
- [15]. S. Gurunathan, K. Kalishwaralal, R. Vaidyanathan, D. Venkataraman, S. R. K. Pandian, J. Muniyandi, et al., "Biosynthesis, purification and characterization of silver nanoparticles using Escherichia coli," *Colloids and Surfaces B: Biointerfaces*, Vol. 74, pp. 328-335, 2009.
- [16]. M. Mohseniazar, M. Barin, H. Zarredar, S. Alizadeh, D. Shanebandi, "Potential of microalgae and lactobacilli in biosynthesis of silver nanoparticles," *BiolImpacts: BI*, Vol. 1, pp. 149-152, 2011.
- [17]. A. Ahmad, P. Mukherjee, S. Senapati, D. Mandal, M. I. Khan, R. Kumar, et al., "Extracellular biosynthesis of silver nanoparticles using the fungus Fusarium oxysporum," *Colloids and Surfaces B: Biointerfaces*, Vol. 28, pp. 313-318, 2003.
- [18]. M. Sastry, A. Ahmad, M. I. Khan, R. Kumar, "Biosynthesis of metal nanoparticles using fungi and actinomycete," *Current Science*, Vol. 85, pp. 162-170, 2003.
- [19]. N. Pantidos, L. E. Horsfall, "Biological synthesis of metallic nanoparticles by bacteria, fungi and plants," *Journal of Nanomedicine & Nanotechnology*, Vol. 5, pp. 1000233, 2014.
- [20]. A. U. Khan, N. Malik, M. Khan, M. H. Cho, M. M. Khan, "Fungi-assisted silver nanoparticle synthesis and their applications," *Bioprocess and Biosystems Engineering*, Vol. 41, pp. 1-20, 2018.
- [21]. M. Mazmanci, A. Unyayar, H. Ekiz, "Decolorization of methylene blue by white rot fungus Coriolus versicolor," *Fresenius Environmental Bulletin*, Vol. 11, pp. 254-258, 2002.
- [22]. X. Fujian, C. Hongzhang, L. Zuohu, "Solid-state production of lignin peroxidase (LiP) and manganese peroxidase (MnP) by Phanerochaete chrysosporium using steam-exploded straw as substrate," *Bioresource Technology*, Vol. 80, pp. 149-151, 2001.
- [23]. K. S. Siddiqi, A. Husen, R. A. Rao, "A review on biosynthesis of silver nanoparticles and their biocidal properties," *Journal of Nanobiotechnology*, Vol. 16, pp. 14, 2018.
- [24]. A. Henglein, "Physicochemical properties of small metal particles in solution: microelectrode reactions, chemisorption, composite metal particles, and the atom-to-metal transition," *The Journal of Physical Chemistry*, Vol. 97, pp. 5457-5471, 1993.

- [25]. M. Sastry, K. Mayya, K. Bandyopadhyay, "pH Dependent changes in the optical properties of carboxylic acid derivatized silver colloidal particles," *Colloids and Surfaces A: Physicochemical and Engineering Aspects*, Vol. 127, pp. 221-228, 1997.
- [26]. M. Sastry, V. Patil, S. Sainkar, "Electrostatically controlled diffusion of carboxylic acid derivatized silver colloidal particles in thermally evaporated fatty amine films," *The Journal of Physical Chemistry B*, Vol. 102, pp. 1404-1410, 1998.
- [27]. N. Vigneshwaran, A. A. Kathe, P. Varadarajan, R. P. Nachane, R. Balasubramanya, "Biomimetics of silver nanoparticles by white rot fungus, *Phanerochaete chrysosporium*," *Colloids and Surfaces B: Biointerfaces*, Vol. 53, pp. 55-59, 2006.
- [28]. R. Sanghi, P. Verma, "Biomimetic synthesis and characterisation of protein capped silver nanoparticles," *Bioresource Technology*, Vol. 100, pp. 501-504, 2009.
- [29]. E. Castro-Longoria, A. R. Vilchis-Nestor, M. Avalos-Borja, "Biosynthesis of silver, gold and bimetallic nanoparticles using the filamentous fungus *Neurospora crassa*," *Colloids and Surfaces B: Biointerfaces*, Vol. 83, pp. 42-48, 2011.
- [30]. P. Mukherjee, A. Ahmad, D. Mandal, S. Senapati, S. R. Sainkar, M. I. Khan, et al., "Fungus-mediated synthesis of silver nanoparticles and their immobilization in the mycelial matrix: a novel biological approach to nanoparticle synthesis," *Nano Letters*, Vol. 1, pp. 515-519, 2001.
- [31]. N. F. Zonooz, M. Salouti, "Extracellular biosynthesis of silver nanoparticles using cell filtrate of *Streptomyces* sp. ERI-3," *Scientia Iranica*, Vol. 18, pp. 1631-1635, 2011.
- [32]. R. Singh, U. U. Shedbalkar, S. B. Nadhe, S. A. Wadhvani, B. A. Chopade, "Lignin peroxidase mediated silver nanoparticle synthesis in *Acinetobacter* sp.," *AMB Express*, Vol. 7, pp. 226, 2017.
- [33]. K. AbdelRahim, S. Y. Mahmoud, A. M. Ali, K. S. Almaary, A. E.-Z. M. Mustafa, S. M. Husseiny, "Extracellular biosynthesis of silver nanoparticles using *Rhizopus stolonifer*," *Saudi Journal of Biological Sciences*, Vol. 24, pp. 208-216, 2017.
- [34]. K. Gudikandula, P. Vadapally, M. S. Charya, "Biogenic synthesis of silver nanoparticles from white rot fungi: Their characterization and antibacterial studies," *OpenNano*, Vol. 2, pp. 64-78, 2017.
- [35]. D. Philip, "Biosynthesis of Au, Ag and Au-Ag nanoparticles using edible mushroom extract," *Spectrochimica Acta Part A: Molecular and Biomolecular Spectroscopy*, Vol. 73, pp. 374-381, 2009.
- [36]. N. Durán, P. D. Marcato, O. L. Alves, G. I. De Souza, E. Esposito, "Mechanistic aspects of biosynthesis of silver nanoparticles by several *Fusarium oxysporum* strains," *Journal of Nanobiotechnology*, Vol. 3, pp. 8, 2005.
- [37]. Y. San Chan, M. M. Don, "Biosynthesis and structural characterization of Ag nanoparticles from white rot fungi," *Materials Science and Engineering: C*, Vol. 33, pp. 282-288, 2013.
- [38]. K. Kathiresan, S. Manivannan, M. Nabeel, B. Dhivya, "Studies on silver nanoparticles synthesized by a marine fungus, *Penicillium fellutanum* isolated from coastal mangrove sediment," *Colloids and Surfaces B: Biointerfaces*, Vol. 71, pp. 133-137, 2009.
- [39]. A. Syed, S. Saraswati, G. C. Kundu, A. Ahmad, "Biological synthesis of silver nanoparticles using the fungus *Humicola* sp. and evaluation of their cytotoxicity using normal and cancer cell lines," *Spectrochimica Acta Part A: Molecular and Biomolecular Spectroscopy*, Vol. 114, pp. 144-147, 2013.
- [40]. S. K. Das, M. M. R. Khan, A. K. Guha, A. R. Das, A. B. Mandal, "Silver-nano biohybrid material: synthesis, characterization and application in water purification," *Bioresource Technology*, Vol. 124, pp. 495-499, 2012.
- [41]. A. O. Adiguzel, S. K. Adiguzel, B. Mazmanci, M. Tunçer, M. A. Mazmanci, "Silver nanoparticle biosynthesis from newly isolated streptomyces genus from soil," *Materials Research Express*, Vol. 5, pp. 045402, 2018.
- [42]. R. Nithya, R. Ragunathan, "Synthesis of silver nanoparticles using a probiotic microbe and its antibacterial effect against multidrug resistant bacteria," *African Journal of Biotechnology*, Vol. 11, pp. 11013-11021, 2012.
- [43]. R. Ramanathan, A. P. O'Mullane, R. Y. Parikh, P. M. Smooker, S. K. Bhargava, V. Bansal, "Bacterial kinetics-controlled shape-directed biosynthesis of silver nanoplates using *Morganella psychrotolerans*," *Langmuir*, Vol. 27, pp. 714-719, 2011.
- [44]. F. Deniz, A. O. Adiguzel, M. A. Mazmanci, "The biosynthesis of silver nanoparticles by cytoplasmic fluid of *Coriolus versicolor*," *Turkish Journal of Engineering*, Vol. 3, pp. 92-96, 2019.
- [45]. S. R. Couto, D. Moldes, M. A. Sanromán, "Optimum stability conditions of pH and temperature for ligninase and manganese-dependent peroxidase from *Phanerochaete chrysosporium*. Application to in vitro decolorization of Poly R-478 by MnP," *World Journal of Microbiology and Biotechnology*, Vol. 22, pp. 607-612, 2006.
- [46]. R. Ozturk Urek, N. Pazarlioglu, "Enhanced production of manganese peroxidase by *Phanerochaete chrysosporium*," *Brazilian Archives of Biology and Technology*, Vol. 50, pp. 913-920, 2007.
- [47]. M. Saravanan, S. Arokiyaraj, T. Lakshmi, A. Pugazhendhi, "Synthesis of silver nanoparticles from *Phanerochaete chrysosporium* (MTCC-787) and their antibacterial activity against human pathogenic bacteria," *Microb Pathog*, Vol. 117, pp. 68-72, 2018.



RESEARCH ARTICLE

Assessment of ship emissions through cold ironing method for Iskenderun Port of Turkey

Alper Kılıç¹, Mustafa Yolcu², Fuat Kılıç³, Levent Bilgili^{4,*}

¹Bandirma Onyedi Eylul University, Dept. of Maritime Business Manag., 10200, Balıkesir, TURKIYE

²Port Authority, Iskenderun, TURKIYE

³Balıkesir University, Dept. of Mechatronic Eng., 10145, Balıkesir, TURKIYE

⁴Bandirma Onyedi Eylul University, Dept. of Naval Arch. and Marine Eng., 10200, Balıkesir, TURKIYE

ABSTRACT

Ships are significant emissions sources, especially in port areas. Besides other emission sources, they have remarkable air pollution impacts on residential areas near ports. It is well known that these emissions have deleterious impacts on both human health, and ecosystems. The biggest ports are generally located near highly populated cities. Therefore, emissions occurred due to shipping activities in ports have a significant importance. This study examines shipping emissions at berth by using data of ships calling in Iskenderun Port in 2013 and compares the environmental performance of using shore side electricity. The study also investigates the external costs associated with the impacts of emissions on climate change, air quality, and human health. According to the results, utilization of shore side electricity instead of auxiliary engines in ports provide significant benefits on environmental and economic issues. In case of Iskenderun Port, it is concluded that shore side electricity eliminates approximately \$ 23 million of external costs per year.

Keywords: Ship, port, emission, cold ironing, air pollution

1. INTRODUCTION

As a result of industrial and technological developments in addition to growth in population and global networks, energy demand and consumption have increased throughout the years by showing an absolute dependency to the fossil fuels especially to the oil. It is clear that the transport sector has a growing share of approximately 20% in oil consumption among other sectors such as housing, petrochemicals, agriculture, and industry [1]. Accordingly, transportation constitutes a significant portion of the carbon dioxide (CO₂) emissions from fossil fuels on a global scale. While total CO₂ emissions caused by fossil fuels increased 37.8% from 1990 to 2007, transport modes' share increases approximately 45% [2]. The relationship between consumption of oil and CO₂ emissions is well known. In this respect, maritime transport is the mode of transport that has the highest energy efficiency and generates the least greenhouse gas emissions. International Maritime Organization (IMO) estimated that the total CO₂ and CO₂ equivalent

(CO₂e) emission amounts increased by 31,309 to 35,640 Mt and 34,881 to 39,113 Mt, respectively, which corresponds a 3.1% and 2.8% increasing rate annually [3].

Harmful emissions such as sulphur dioxide (SO₂), nitrogen oxides (NO_x), CO₂, hydrocarbons (HC), and particulate matter (PM) are produced by the main (ME) and auxiliary (AE) engines of the ships. These emissions have potential impacts on the environment by contributing to acid rain, eutrophication, greenhouse effect, ozone, and smog formation etc. In addition, ship flue gas emissions have significant contributions to air quality of the port-cities, which are located close to densely populated areas. For example, [4] emphasized that PM from ocean-going ships caused about 60,000 deaths a year due to cardiac diseases and lung cancer in Europe, East, and South Asia coastlines. IMO therefore calls for rapid action to control ship emissions. Estimates show that if no measures are taken, the greenhouse gas contribution of maritime transport can be around 18% by 2050.

Corresponding Author: lbilgili@bandirma.edu.tr (Levent Bilgili)

Received 14 September 2020; Received in revised form 9 November 2020; Accepted 12 November 2020

Available Online 1 December 2020

Doi: <https://doi.org/10.35208/ert.794595>

© Yildiz Technical University, Environmental Engineering Department. All rights reserved.

Several reports have outlined that shipping emissions are significant air pollution sources in port areas worldwide [5-11]. There is increasing interest in adopting green shipping practices and reducing environmental externalities in ship and port operations. The main objective of emission reduction is to adopt a green port policy that includes a variety of approaches and methods for the sustainable maritime industry to improve air quality at port sites [12]. In this context, cold ironing has been a promising technique which is used to decrease emissions due to the ship hoteling process in port areas [13-14]. It is a basic process that provides shore side electrical power to the vessels at the dock by enabling them to shut down their AE [15].

Different methods can be applied to reduce emissions from vessels in port areas. For example, scrubbing systems can be used for SO_x emissions or selective catalytic reduction systems (SCR) can be used for NO_x emissions. However, such emission reduction methods are designed to eliminate only a particular type of emission. The vast majority of shipping emissions occur in hoteling mode where only the auxiliary generators of the ships run. Scrubber or SCR-like systems are used in the exhaust systems of the ship's main engines. Therefore, the shore connection system is the most convenient way to reduce all types of emissions from ships.

The analyses on cold ironing show that there are several cold ironing feasibility studies in which different types of source for the shore side electrical power has been evaluated. For example, an analysis was realized by applying cold ironing method to the vessels that visited Kaohsiung harbour. They stated that they could reduce SO₂ (63.2%), NO_x (49.2%), CO₂ (57.2%), HC (29.2%), and PM (39.4%) emissions by shutting down the AEs at specified rates [12]. The consequences of replacing diesel fuel with electrical power for gantry cranes and yard equipment in port operations was analysed and it was resulted that cold ironing might be a feasible solution for many ports to reduce emissions [16]. LNG fuel option for cold ironing was also evaluated by making it available for the usage of local port delivery trucks, locomotives, ferries a commercial harbour crafts in industrial port complexes and terminals [17]. It was stated that hybrid battery-diesel-electric propulsion and energy storage systems as a cold ironing approach can reduce fuel consumption and emissions as these systems supply sufficient energy to vessel for a certain voyage speed. It is also emphasized that cargo handling operations can also use the stored energy without running ship engines [18]. Compared to on-board generators, cold ironing systems reduce CO₂ emissions by more than 30%, NO_x and PM emissions by more than 95%, and also reduce local pollution and noise [19]. Cold ironing method was analysed by 12 different plug positions in the marine areas and showed that 10,000 tons of CO₂ emissions could be reduced annually for €13 million investments in ferry and container terminals [20]. In order to reduce the environmental impact of berthing ships, cold ironing or coastal power plants are installed in a number of cruise terminals [21]. The prospects of cold ironing were investigated considering all stakeholders and concluded that cold ironing provides significant economic benefits for the case of medium

and high fuel prices. Consequently, it can be concluded that cold ironing approach has been placed in governmental policies in Europe, but it can be said that the practice is still quite limited in worldwide as in Turkey [22]. One of the last methods used to adopt green maritime practices and achieve the objective of reducing the environmental externalities of maritime activities was to reduce emissions at ports. Combining cold ironing with wind and solar energy is more effective solution to shipping emissions in port areas [23].

Turkey's coastline is more than 8,000 kilometres. Mediterranean, Aegean Sea, Marmara Sea, and Turkish Straits and Black Sea are the coasts of the country. There are many ports and shipyard facilities located on each sea for cargo, passenger, and fishing boats. Although there are some studies have been carried out for Turkish ports and straits [24-25], cold ironing method has been investigated for Turkish Ports in limited studies [26].

The main purpose of this study is to evaluate the application of cold ironing method as an alternative to AEs by calculating the ship emissions and their external costs in the vicinity of Iskenderun Port.

2. MATERIALS AND METHODS

2.1. Economic analysis of cold ironing method

An economic analysis (i.e. a CBA) and a discussion of the results in terms of the potential positive socioeconomic benefits related to the reduction of pollutant air emissions as a result of using cold ironing technology were carried out.

Due to the electrification of ship systems, fuel saving, and emission reduction can be achieved. The operations of the vessels during their stay in the port are handled with three approaches: energy storage, auxiliary drives, and on shore power supply. The results demonstrate significant fuel and emission reductions during port operations and the importance of the ship's operational profile [27]. The environmental impact of an electric generator on a Ro-Ro ship was estimated using the Life Cycle Assessment (LCA) and determined that the environmental load caused by the generator was significant. Also, they indicated that a number of environmental impacts could be reduced by using facilities with suitable developing technologies (eg. photovoltaic systems, lithium-ion batteries, cold ironing, and PTOs supported by variable frequency drives installed in frequency converters and existing frequency plants) [28]. In another study conducted by LCA, the operations of diesel generators and the hybrid power system were compared and demonstrated the environmental benefits of a newly built hybrid power system [29]. A previous study found out that if the ships draw electricity from national electricity grids instead of generating electricity with their own generators, CO₂ emissions will be significantly reduced [30]. The cost of hoteling emissions from ships in the Port of Bergen was estimated between €10 and €21.5 million per year [31]. In another study, it was concluded that the use of a built-in power supply in ports is beneficial to the port

area as the use of generators decreases [32]. Another study examined the applicability of medium-sized cold ironing to several small piers at a port in Aberdeen. Reimbursement scenarios were examined through SCBA based on the external costs of potential emission savings, and in the best-case scenario showed that the system would be reimbursed in just 7 years [33]. A recent study proposed an innovative power supply solution for the ports. This solution consists of an advanced static compensator with a rotating converter instead of a static converter [34]. Quantitative calculations show that in the long term, the use of coastal power has significant financial, environmental, and socio-economic benefits, while the cost of implementation is high. Furthermore, according to the qualitative interview data, perceptions of the current

political and global economic climates are currently hampering such an initiative, despite being aware of these benefits [35]. As a result of the analysis of cruise ship traffic data in Copenhagen in 2012, assuming that 60% of the ships use cold iron, the total potential external health cost is estimated to be around €2.8 million per year [36].

Iskenderun is a district in the province of Hatay on the East Mediterranean coast of Turkey. Iskenderun Port is located in the North East of the Mediterranean Sea and provides transit sea transportation services to Middle East countries. The port is also connected to the national railway system. Fig 1 presents the Iskenderun Port Region.

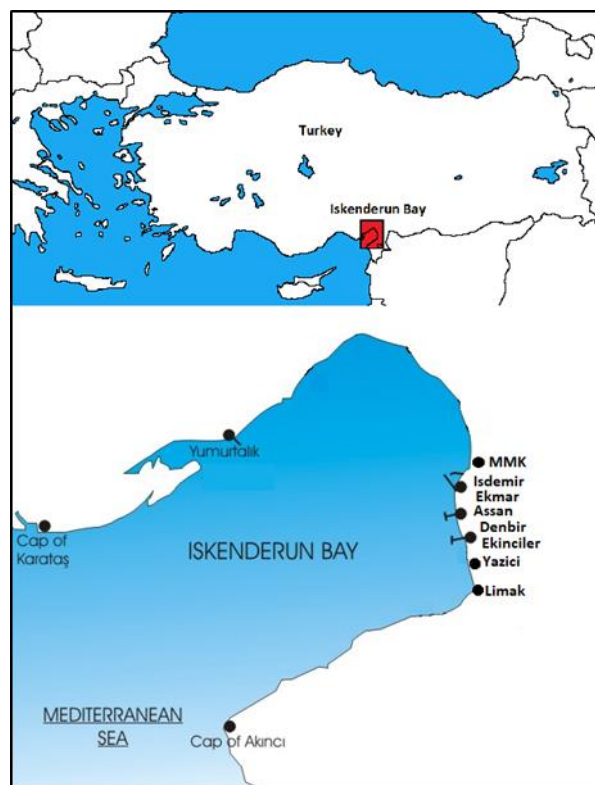


Fig 1. Iskenderun Port region

There are three numbers of pilotage points in Iskenderun Port area, which are called North, East, and South. Properties of ports are listed in Table 1.

Number of ships calling at these ports are given in Table 2 below. According to port statistics, 2,839 number of ships called at this port area in 2013. In 2014 number of ships call decreased to 2,787.

Table 1. Overview of Iskenderun Port area

Pilot Area	Berth number	Berth length (m)	Max Capacity (DWT)	Cargo Handling capacity (t year ⁻¹)	Ship Type
North	8	1,800	100,000	12,000,000	Bulk, Gen. Cargo, Ro-Ro, Container
	6	1,536	180,000	16,000,000	Bulk, Gen. Cargo
East	2	680	250,000(TEU)	n/a	Container
	6	812	55,000	n/a	Bulk, Gen. Cargo
	2	422	70,000	n/a	Bulk, Gen. Cargo
	10	1,150	n/a	7,500,000	Bulk, Gen. Cargo
South	8	1,652	n/a	2,000,000 1,300,000(TEU)	Bulk, Gen Cargo, Ro-Ro, Container

Table 2. Number of ships called in Iskenderun Port region

Port	Bulk Carrier	General Cargo	Container	Ro-Ro/Container	Chemical/Oil Tanker
North	93	436	10	-	-
North	166	416	32	-	21
East	3	72	-	204	-
East	8	106	-	-	17
East	49	317	-	6	-
East	39	127	3	-	-
South	25	299	-	251	-
Total	383	1773	45	461	38

2.2. Ship particulars

The general particulars of ships that called to Iskenderun Port region are summarized in Table 3. Totally 34 number of different ships surveyed on board while they were at port according to sample of technical file which is in the Appendix 1 of RESOLUTION MEPC.214(63), 2012 Guidelines on Survey and Certification of the Energy Efficiency Design Index (EEDI) (MEPC 63/23/Add.1).

Survey values of 34 different ships called at Iskenderun Port are used to create average values for each ship type. Survey values of ships include not only ship particulars such as ship length, gross tonnage, engine power but also additional information about ship's stay

at Iskenderun port such as arrival and departure times, running hours of auxiliary engine and auxiliary boilers (AB), fuel consumption values for these auxiliary machineries. Table 4 below present average ME, AE, and AB at maximum continuous rating (MCR) values for each ship type.

Marine type fuels have different sulphur content values and there are different regulations on sulphur content in marine fuel for different port areas. Therefore, total amount of different fuels at ship's tank and consumption values are monitored carefully in ship surveys at port and recorded. Table 5 below show the average running hours and fuel consumption values of auxiliary machinery for each ship type based on survey data of ships called at Iskenderun Port.

Table 3. Ships particulars in Iskenderun Port region

Ship Type	Number of ships	Average Ship Speed at 75% MCR (knots)	Average L _{0A} (m)	Average GRT	Average DWT
Bulk Carrier	14	13.4	175	20,748	34,775
Container	2	20.6	195	26,128	30,722
General Cargo	11	11.5	99.8	3,706	5,701
Heavy Lift Cargo	2	13.3	177	22,923	27,703
Multi-purpose Dry Cargo	2	13.8	158.4	15,041	20,170
Oil & Chemical Tanker	1	12.5	122	4,347	6,276

Table 4. Average ME, AE and AB powers of ship types

Ship Type	Average ME MCR (kW)	Average AE MCR (kW)	Average AB Power (kW)
Bulk Carrier	7,368	515	341
Container	20,888	1,178	485
General Cargo	2,453	214	303
Heavy Lift Cargo	4,904	560	931
Multi-purpose Dry Cargo	5,330	443	1,493
Oil & Chemical Tanker	2,642	400	2,001

Table 5. Average running hours and consumptions of auxiliary machinery

Ship Type	Running hours at port (h)		Consumptions at port (t)	
	Aux. Eng.	Aux. Boiler	Aux. Eng.	Aux. Boiler
Bulk Carrier	170.14	60.28	10.05	4.42
Container	28.50	22	5.6	3.31
General Cargo	150	59.63	2.88	1.7
Oil Chemical	67	35	2.51	7
Multipurpose Dry Cargo	100.5	59.5	10.6	1.05
Heavy Lift Cargo	107	23.5	8.07	4.7

2.3. Methodology

Ship emissions are estimated mainly based on two different methodologies. The first one is top-down approach which relies on marine bunker statistics. The second method is the recommended ship movement methodology when detailed technical information on ships is available in addition to detailed ship movement data. In this study, emission estimation methodology offered by Trozzi (2013) (Tier 3) is applied for a sample group of ships called to Iskenderun Port. In this study, berthing emissions were calculated based on the time spent at the port, the number of arrivals at the port, the average fuel consumption of the auxiliary machinery and the pollutant emission factors of AE. Average values of ship types are illustrated in Table 4, but emissions were calculated for each ship individually [37].

Tier 3 emission factors from Trozzi (2013) are used for estimating the emissions from ships in Iskenderun Port based on real and detailed information of ships such as ships movements, powers of main and auxiliary engines, fuel types, and fuel consumptions of each fuel types at manoeuvring and hoteling modes by engine technology as units of mass of pollutant per tonne of fuels. Emission factors are calculated in two different ways. First method is to calculate emission values by derived power (kWh) by using machine power (kW) and machine working hours (h). Second method is based on calculation of emission values by consumed fuel per capita.

Tier 3 approach calculates the emissions on each operation modes [38]:

$$E_{trip} = E_{Hotelling} + E_{Manoeuvring} + E_{Cruising} \quad (1)$$

The emission of pollutant *i* for a trip can be calculated as follows:

$$E_{Trip,i,j,m} = \sum_p (FC_{j,m,p} \times EF_{i,j,m,p}) \quad (2)$$

where;

E_{trip} : emission over a complete trip (tonnes)

FC: fuel consumption (tonnes)

EF: emission factor (kg tonne⁻¹)

i: pollutant

m: fuel type

j: engine type

p: operation mode

Tier 3 calculation method of Trozzi includes hoteling, manoeuvring, and cruising modes. As the scope of this study is to investigate port emissions and socio-economic benefits of using alternative shore-based electricity at ports, emission calculations are conducted for only hoteling mode. Average emission factors have been developed by conducting literature review of the marine emissions studies and presented in Table 6 below.

Table 6. Emission factors (kg ton⁻¹ fuel)

Emission Type	Main EF Kg ton ⁻¹	Aux EF Kg ton ⁻¹	Reference
CO ₂	3.114	3.114	[3]
NO _x	44.3	59.7	[27]
PM	4	1.4	[27]
CO	2.51	2.38	[3]
VOC	6.6	1.8	[27]
SO _x	52.7	52.7	[3]

3. RESULTS AND DISCUSSION

3.1. Shipping activities at Iskenderun Port

At open sea, ships are propelled by main engine(s) at economic load which is generally equal to 80-85% of MCR. For the requirement of the generation of electricity for light, pumps, air conditioning etc., normally one generation is enough for energy demand. Vessels are usually equipped with super-heaters that generate steam using the waste heat from the exhaust gases of the main engines. The resulting steam is converted to work using the turbine or to electrical energy via a generator. In addition, there are shaft generators on the ships which generate electrical energy by means of an alternator connected to the propeller shaft which are operated only during the cruising of the ship.

In port regions, two operation modes, manoeuvring and hoteling, appear as emission sources: At manoeuvring mode, unlike the cruising mode at open sea ships use main engines at reduced power, but the power demand varies due to changing the ships' course, reducing and increasing the ships speed. Thus, in this mode, ships consume more energy than cruising mode at the same distance. Furthermore, ships use additional auxiliary diesel engines which are synchronized for prevention of accidents may result from possible black outs. At hoteling mode, ships require electricity for dock activities such as handling of the cargo by means of cranes or pumps. Except for shifting operations inside the ports, ships do not use main engines at hoteling modes. According to the survey conducted on ships in Iskenderun Port, main engines of all ships use heavy fuel oil (HFO) and marine diesel oil (MDO). However, not every ship use dual fuel for AE and AB. Although HFO is cheaper than MDO, it requires heating to decrease the viscosity. Thus, using HFO at ports is not a common practice. Besides, local legislation requires marine engines of ocean-going ships to be run on low sulphur fuel at ports. In this section, emission estimation results are discussed and investment in adapting cold ironing system for Iskenderun Port is analysed.

3.2. Annual emission estimations for ships

Emission estimations based on fuel consumption values of auxiliary machinery at port are presented in Table 7 below. In 2013, approximately 19,796 tons of fuel have been consumed by ships docked at Iskenderun Port based on hoteling mode calculations.

Table 7. Emission estimations by ship type for Iskenderun Port in 2013

Ship Type	Total emissions (t)					
	NO _x	PM	CO	VOC	SO _x	CO ₂
Bulk Carrier	331	8	13	10	292	17,258
Container	24	1	1	1	21	1,249
General Cargo	485	12	19	15	428	25,287
Oil & Chemical Tanker	22	1	1	1	19	1,126
Multipurpose Dry Cargo	321	8	13	10	283	16,725
Total	1,183	30	47	37	1,043	61,645

For a fair comparison, environmental damage costs should be considered as well as fuel prices. Therefore, it would be possible to calculate real costs of fossil fuel usage by analysing external costs of emissions. Some studies have been conducted regarding to damage cost issue for Europe. Based on these studies, external costs of emission types per ton are given in Table 8.

Table 8. Unit costs per pollutant emission ton [26]

Pollutant	Unit costs per pollutant emission ton (USD)			
	Human health	Ecosystem	Climate change	Total
NO _x	7002	1228	0	8,230
PM	429,936	0	0	429,936
CO	36	0	41	76
VOC	1,155	86	0	1,241
CO ₂	0	0	26	26
SO ₂	7,739	246	0	7,985

Based on above unit costs of pollutants, total external cost of emissions by ships calling at Iskenderun Port in 2013 were calculated and results are presented in Table 9 below.

The results were compared with two previous studies, which focused on the calculation of emission inventories and dispersion modelling of these emissions.

First study was conducted on Ambarli and Kocaeli ports, which both are located in the Marmara Sea. During the period of 2017-2018, while Ambarli Port has 629 ship calls, Kocaeli Port has 2798 ship calls. The shipping activities cause 41,190.8 t of CO₂, 706.8 t of NO_x, 388 t of SO₂, 1 t of VOC and PM, and 32.2 t of CO in Ambarli Port. Similarly, the shipping activities cause 76,307.0 t of CO₂, 1353.8 t of NO_x, 718.8 t of SO₂, 1.7 t of VOC and PM, and 59.7 t of CO in Kocaeli Port. Considering that Iskenderun Port has 2700 ship calls, it is obvious that the emission amounts changes. The results occur in accordance with the number of ship calls [39].

Another study was carried out an emission inventory calculation of shipping activities occurred in Bandirma Port, which is located in the south of the Marmara Sea. During the study period, the port has 1577 ship calls of different types of ships. It was estimated that these ships cause 272,301 t of CO₂, 7,997 t of NO_x, 1,682 t of SO₂, 182 t of PM, and 240 t of CO. Although Iskenderun Port has almost twofold of ship calls than Bandirma Port, it can be seen that the shipping activities in Bandirma Port cause much more emissions. This difference may be caused by the hoteling duration or the fuel types [40].

Table 9. Total emission costs (USD)

Pollutant	Cost (USD)
NO _x	9,726,189
PM	11,915,009
CO	3,588
VOC	44,204
CO ₂	1,590,381
SO ₂	426,752
Total	23,706,122

Total fuel consumption for the auxiliary machinery of ships are calculated as 19,796 tons within 2013. Average MGO price for that year was 995 \$ ton⁻¹ in the Mediterranean region. Therefore, total cost of fuel is \$19,696,324 [41]. It indicates that external costs of emissions are much higher than the total cost of consumed fuel.

Since the total fuel consumption data are available, the total power can be calculated using the lower heating value of the fuel consumed (MGO) and the thermal efficiency of the diesel engine [42]. As shown in Table 10, the required total power of the ships in the port is calculated using the total fuel consumption. The table also shows that the total power required for ship operations such as lighting, pumping, loading, unloading and heating is 81 million kWh.

Table 10. Total emission costs (USD)

Total fuel consumption	19,796 ton
Lower heating value	42,700 kJ kg ⁻¹
	11.9 kWh kg ⁻¹
Thermal efficiency of AE	36%
Efficiency of alternator	95%
Overall efficiency	34.2%
Total required power	80,562,912 kWh

Cost of electricity in 2013 is provided by Turkish Energy Market Regulatory Authority (EPDK) as 0.12 USD/kWh for industrial use [43]. Therefore, total cost of electricity would be \$9,667,549.433. Table 11 below summarizes the comparison of total fuel consumption values and total power requirements and their costs.

In case of meeting electricity energy demand by renewable sources, it would be possible to eliminate the approximately \$23 million per year external costs of emissions. Table 11 below presents the total consumption and cost values.

Table 11. Total consumption and cost values (USD)

Consumption Values		
Power Source	Value	Cost (USD)
Total LS MGO (ton)	19,795.33	19,696,323.5
Total Electricity (kWh)	80,562,911.94	9,667,549.433
Cost Difference		10,028,774.07

3.3. Port investment on electricity supply

It is not enough to build the electricity distribution infrastructure on the land side to implement coastal

power. At the same time, a number of transformations are needed to connect ships to shore electricity. These transformations are often more complex than building new vessels designed for cold ironing. In addition, the size of the power supplies and the proximity to the port are important factors in determining the power distribution infrastructure on the shore [44]. Since the electrical infrastructure of a terminal with cold ironing is more than a conventional terminal, emission reduction credits may be used to help cover this expense [45]. Possible configuration of cold-ironing system is illustrated in figure below.

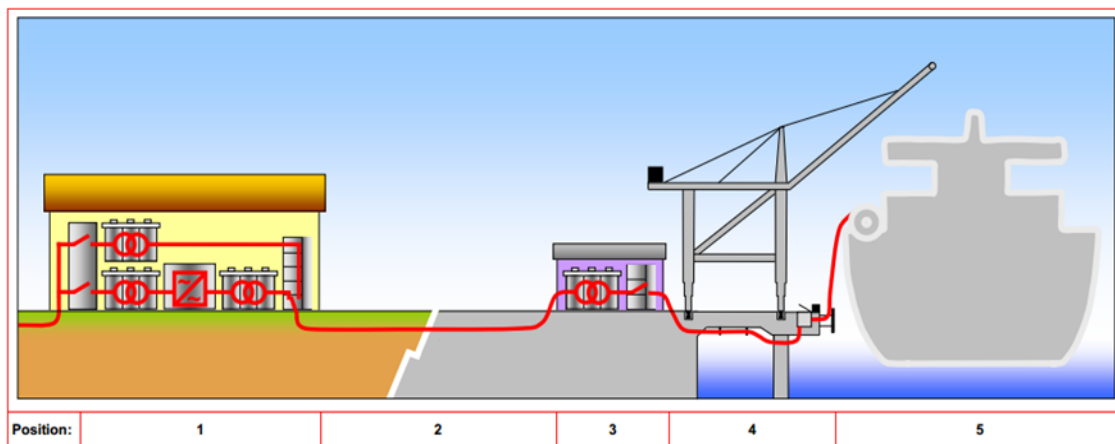


Fig 2. Overview illustration of cold-ironing system design [46]

Positions and descriptions of each facility are given in Table 12. Position 1 is the main substation building which represents the centre of the system. Main components of the shore side power system are located in this building. Technical details are presented in the table for each equipment.

Position 2 shows the cable arrangement, preferably consisting of underground cables above 24 kV, to reduce the current in the conductors as much as possible. mEU grid system is 380 kV-50 Hz, regional grid system is 150 kV-50 Hz and Euromax grid is 25 kV-50 Hz. Ports usually have 3.5 MVA-6.6 kV-60 Hz

systems for bigger tonnage ships and 3.5 MVA-6.3 kV-50 Hz for smaller feeder ships. In Turkey national grid is 380 kV-180 kV and main substitution output is 34.5 kV. Frequency converter output should be 6.6 kV with 50-60 Hz option. The use of coastal power does not completely eliminate emissions from ships due to the necessity of operating boilers or the use of propellants in port manoeuvres. However, the use of coastal power will greatly reduce atmospheric emissions from ships in the port. Developing a renewable energy supply for cold ironing clearly requires national efforts [47].

Table 12. Descriptions of related equipment for model cold ironing system design

Position	Description	Size/Length	Scope	Properties
1	Main Substation Building	28*15 m= 420 m2	Frequency converter	6-11 MVA 6.6 kV
		One station for each port	Double bus bar switchgear	Enable 50-60 Hz, Suitable up to 24 kV
2	Cable arrangement	5 km	Circuit-Breaker	-
			Underground cables	Preferably 24 kV Min. size
3	Shore-side transformer station	5*2,6m = 13 m2	Transformer	50 Hz&60 Hz 7.5 MVA 6.6 kV
		One station for each berth	Shore side Switchgear	
4	Shore-side connection arrangement	Three sets for each berth	Connection box	Placed along the berth at regular distances approx. 70 m
			Connection cable	350 A, 4MVA 6.6 kV
5	Vessel connection requirements			
6	Shore side power supply control: SCADA control system			

4. CONCLUSIONS

The annual shipping emission calculations have been carried out according to hoteling operation modes of various ship types (bulk carriers, chemical tankers, container ships, general cargo ships, heavy lift cargo, multipurpose dry cargo, and oil tankers) in Iskenderun Port region for the year 2013. It is concluded that, diesel engines have much lower thermal efficiency than electrical engines therefore use of direct shore power instead of auxiliary diesel engines at ports would provide crucial benefits on economic and environmental perspective.

In Iskenderun Port Area, external cost of burned fuels are much higher than the total cost of consumed fuel. In case of meeting electricity energy demand by renewable sources, it would be possible to eliminate the approximately \$23 million of external emission costs per year. Adaptation of a cold ironing system requires both ports and shipping companies to invest in power transmission equipment.

REFERENCES

- [1]. IEA. World Energy Outlook, ISBN: 978-92-64-08624-1, 2010.
- [2]. IEA. World Energy Outlook, ISBN: 978-92-64-06130-9, 2009.
- [3]. IMO. Third IMO GHG Study, International Maritime Organization, London, UK. 2014.
- [4]. J.J. Corbett, J.J. Winebrake, E.H. Green, P. Kasibhatla, V. Eyring, and A. Lauer, "Mortality from ship emissions: A global assessment", *Environment Science and Technology*, Vol. 41 (24), 8512-8518, 2007.
- [5]. K. Poplawski, E. Setton, B. McEwen, D. Hrebennyk, M. Graham, and P. Keller, "Impact of cruise ship emissions in Victoria, BC, Canada", *Atmospheric Environment*, Vol. 45, pp. 824-833, 2011.
- [6]. C. Dong, K.L. Huang, C.W. Chen, C.W. Lee, H.Y. Lin, and C.F. Chen, "Emission of air pollutants emissions from ships in the Kaohsiung Harbour Area", *Aerosol and Air Quality Research*, Vol. 2 (1), pp. 31-40, 2002.
- [7]. D.A. Cooper, "Exhaust emissions from ships at berth" *Atmospheric Environment*, Vol. 37, pp. 3817-3830, 2003.
- [8]. H. Saxe and T. Larsen, "Air pollution from ships in three Danish ports", *Atmospheric Environment*, Vol. 38, pp. 4057-4067, 2004.
- [9]. L.L. Marr, D.P. Rosser, and C.A. Meneses, "An air quality survey and emissions inventory at Aberdeen Harbour", *Atmospheric Environment*, Vol. 41, pp. 6379-6395, 2007.
- [10]. D.Q., Yang, S.H. Kwan, T. Lu, Q.Y. Fu, J.M.S. Cheng, Y.M. Wu, and J.J. Li, "An emission inventory of marine vessels in shanghai in 2003", *Environment Science and Technology*, Vol. 41 (15), pp. 5183-5190, 2007.
- [11]. P. De Meyer, F. Maes, and A. Volckaert, "Emissions from international shipping in the Belgian Part of the North Sea and Belgian Ports", *Atmospheric Environment*, Vol. 42, pp. 196-206, 2008.
- [12]. C.C. Chang and C.M. Wang, "Evaluating the effects of green port policy: Case study of Kaohsiung Harbor in Taiwan", *Transportation Research Part D: Transport and Environment*, Vol. 17, pp. 185-189, 2012.
- [13]. F. Adamo, G. Andria, G. Cavone, C. De Capua, A.M. Lanzolla, R. Morello, and M. Spadavecchia, "Estimation of ship emissions in the port of Taranto", *Measurement*, Vol. 47, pp. 982-988, 2014.
- [14]. G. Chen, K. Govindan, and M.M. Golias, "Reducing truck emissions at container terminals in a low carbon economy: proposal of a queueing-based bi-objective model for optimizing truck arrival pattern", *Transportation Research Part E: Logistics and Transportation Review*, Vol. 55, pp. 3-22, 2013.
- [15]. T.G. Papoutsoglou, "A cold ironing study on modern ports, implementation and benefits thriving for worldwide ports", Thesis, School of Naval Architecture and Marine Engineering, National Technical University of Athens, 2012.
- [16]. B. Slack, "Battening down the hatches: How should the maritime industries weather the financial tsunami?", *Research in Transportation Economics*, Vol. 27, pp. 4-9, 2010.
- [17]. S. Kumar, H.T. Kwon, K.H. Choi, W. Lim, J.H. Cho, K. Tak, and I. Moon, "LNG: An eco-friendly cryogenic fuel for sustainable development", *Applied Energy*, Vol. 88, pp. 4264-4273, 2011.
- [18]. E.K. Dedes, D.A. Hudson, and S.R. Turnock, "Assessing the potential of hybrid energy technology to reduce exhaust emissions from global shipping", *Energy Policy*, Vol. 40, pp. 204-218, 2012.
- [19]. ENEL. ENEL delivers "cold ironing" project for the marittima area to the Venice Port Authority. <https://www.enel.com/media/explore/search-press-releases/press/2011/10/enel-delivers-cold-ironing-project-for-the-marittima-area-to-the-venice-port-authority> Access Date: 01.09.2020.
- [20]. M. Acciaro, H. Ghiara, and M.I. Cusano, "Energy management in seaports: A new role for port authorities", *Energy Policy*, Vol. 7, pp. 4-12, 2014.
- [21]. J.P. Rodrigue, and T. Notteboom, "The geography of cruises: Itineraries, not destinations", *Applied Geography*, Vol. 38, pp. 31-42, 2013.
- [22]. T.P.V. Zis, "Prospects of cold ironing as an emissions reduction option", *Transportation Research Part A: Policy and Practice*, Vol. 119, pp. 82-95, 2019.
- [23]. A.M. Kotrikla, T. Lilas, and N. Nikitakos, "Abatement of air pollution at an Aegean Island Port utilizing shore side electricity and renewable energy", *Marine Policy*, Vol. 75, pp. 238-248, 2017.
- [24]. U. Kesgin and N. Vardar, "A study on exhaust gas emissions from ships in Turkish Straits", *Atmospheric Environment*, Vol. 35, pp. 1863-1870, 2001.

- [25]. A. Kılıç and C. Deniz, "Inventory of shipping emissions in Izmit Gulf, Turkey", *Environmental Progress and Sustainable Energy*, Vol. 29 (2), pp. 221-232, 2010.
- [26]. N.H. Peksen, D.Y. Peksen, and A. Olcer, "Cold ironing method: Marport port application", *Journal of ETA Maritime Science*, Vol. 2 (2), pp. 11-30 (in Turkish), 2014.
- [27]. E.A. Sciberras, B. Zahawi, and D.J. Atkinson, "Reducing shipboard emissions – assessment of the role of electrical technologies", *Transportation Research Part D: Transport and Environment*, Vol. 51, pp. 227-239, 2017.
- [28]. J. Ling-Ching and A.P. Roskilly, "Investigating a conventional and retrofit power plant on-board a roll-on/roll-off cargo ship from a sustainability perspective-a life cycle assessment case study", *Energy Conversion and Management*, Vol. 117, pp. 305-318, 2016a.
- [29]. J. Ling-Ching and A.P. Roskilly, "Investigating the implications of a new-build hybrid power system for roll-on/roll-off cargo ships from a sustainability perspective-a life cycle assessment case study", *Applied Energy*, Vol. 181, pp. 416-434, 2016b.
- [30]. W.J. Hall, "Assessment of CO2 and priority pollutant reduction by installation of shoreside power", *Resources, Conservation & Recycling*, Vol. 54, pp. 462-467, 2010.
- [31]. D.P. McArthur and L. Osland, "Ships in a city harbour: An economic valuation of atmospheric emissions", *Transportation Research Part D: Transport and Environment*, Vol. 21, pp. 47-52, 2013.
- [32]. E.A., Sciberras, B. Zahawi, and D.J. Atkinson, "Electrical characteristics of cold ironing energy supply for berthed ships", *Transportation Research Part D: Transport and Environment*, Vol. 39, pp. 31-43, 2015.
- [33]. A. Innes and J. Monios, "Identifying the unique challenges of installing cold ironing at small and medium ports-the case of Aberdeen", *Transportation Research Part D: Transport and Environment*, Vol. 62, pp. 298-313, 2018.
- [34]. T. Coppola, M. Fantauzzi, D. Lauria, C. Pisani, and F. Quaranta, "A sustainable electrical interface to mitigate emissions due to power supply in ports", *Renewable and Sustainable Energy Reviews*, Vol. 54, pp. 816-823, 2016.
- [35]. P.H. Tseng and N. Pilcher, "A study of the potential of shore power for the port of Kaohsiung, Taiwan: To introduce or not to introduce?", *Research in Transportation Business and Management*, Vol. 17, pp. 83-91, 2015.
- [36]. F. Ballini and R. Bozzo, "Air pollution from ships in ports: The socio-economic benefit of cold-ironing technology", *Research in Transportation Business and Management*, Vol. 17, pp. 92-98, 2015.
- [37]. C. Trozzi, EMEP/EEA emission inventory guidebook, 2013.
- [38]. C. Trozzi, "Emission estimate methodology for maritime navigation", *19th International Emission Inventory Conference*, 27-30 September 2010, San Antonio, USA, 2010.
- [39]. Ekmekçioğlu, A., Kuzu, S.L., Ünlügençoğlu, K., Çelebi, U.B., "Assessment of shipping emission factors through monitoring and modelling studies", *Science of the Total Environment*, Vol. 743, pp. 140742, 2020.
- [40]. Kuzu, S.L., Bilgili, L., Kılıç, A., "Estimation and dispersion analysis of shipping emissions in Bandırma Port, Turkey", *Environment, Development and Sustainability*, In-Press, Available Online.
- [41]. Bunker Index. 2013. <https://www.bunkerindex.com/> Access Date: 01.09.2020
- [42]. Y. Wild, "Determination of energy cost of electrical energy on board sea-going vessels", Dr.-Ing. Yves Wild Ingenieurbüro GmbH, Hamburg, Germany, 2005.
- [43]. Energy Market Regulatory Authority. 2013.
- [44]. C.H. Han, "Strategies to reduce air pollution in shipping industry", *The Asian Journal of Shipping and Logistics*, Vol. 26 (1), pp. 7-30, 2010.
- [45]. G. Arduino, R. Aronietis, Y. Crozet, K. Frouws, C. Ferrari, L. Guihéry, et al., "How to turn an innovative concept into a success? An application to seaport-related innovation", *Research in Transportation Economics*, Vol. 42, pp. 97-107, 2013.
- [46]. P. Ericsson and I. Fazlagic, "Shore-side power supply-A feasibility study and a technical solution for an on-shore electrical infrastructure to supply vessels with electric power while in port", M.Sc. Thesis prepared in Chalmers University of Technology, Department of Energy and Environment, Division of Electric Power Engineering, Masters Program in Electric Power Engineering, Göteborg, Sweden, 2008.
- [47]. P. Gilbert and A. Bows, "Exploring the scope for complementary sub-global policy to mitigate CO2 from shipping", *Energy Policy*, Vol. 50, pp. 613-622, 2012.



RESEARCH ARTICLE

Ecologically friendly production of copper powder and elimination of cupric ions from aqueous solutions using D-Glucose and ascorbic acid

Esma Mahfouf Bouchareb^{1,2,*}, Souad Djerad², Raouf Bouchareb^{1,*}

¹Department of Environmental Engineering, Process Engineering Faculty, Saleh Boubnider University, Constantine, 25000, Algeria

²Laboratory of Environmental Engineering, Chemical Engineering Department, Badji Mokhtar University, Annaba, 23000, Algeria

ABSTRACT

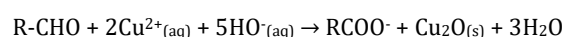
Copper(II) ions (Cu^{2+}) in copper sulfate solutions (CuSO_4) can be reduced with several carbohydrates to produce copper metal powder. In this study glucose was used as a reducing agent. The big challenge in this study was to find the optimum conditions for copper ions reduction because they were entwined with positive conditions for degradation and hydrolyses of sugar (D-glucose). For that reason, the impact of several parameters on these conditions was investigated in a series of experiments in this research study. The glucose concentration (0.2-1.6M), the temperature (30-70 °C), initial sodium hydroxide concentration (0.2-0.4M), the role of adding sulfuric acid (H_2SO_4) at different volumes (0.6-3 mL) and the addition of ascorbic acid at different doses (4-20 mL) were the considered key parameters that were studied in this research. The synthesis of copper was restricted due to organic acid build up and reactions of the degradation products and copper. Under optimum conditions using glucose as a reducing agent, maximum of 48% of copper ions were transformed to copper metal (Cu). By adding ascorbic acid at the end of the experiment process, reduction efficiency was 100% where total and complete copper reduction was achievable. Most of solid particles were analyzed and the characterization and nature of the produced solid was achieved by X-Ray Diffraction.

Keywords: Copper (II), glucose, ascorbic acid, copper metal synthesis, aqueous solution, X-ray diffraction analysis

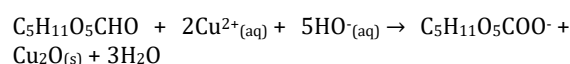
1. INTRODUCTION

Hydrometallurgy has always a remarkable reputation in view of its ability to treat ores with lowest environmental pollution issues [1], [2]. One of the most important hydrometallurgy areas is metal compound recovery by precipitation or chemical reduction [3]. In the past years, a great interest for copper powder synthesis has improved because of its high demands and high quality characteristics [4]. It is known that copper ions can be reduced chemically by different carbohydrates as glucose, fructose and sucrose [5], [6].

In fact, copper ion (Cu^{2+}) is considered as an oxidant of ores (Kasaie et al 2016). It is also used in Fehling liquor destined to determine blood sugar level [8]. Furthermore, during reaction, copper ions containing in Fehling solution oxidize blood sugar giving carboxylic acid under its basic form (ion carboxylate) and brick red precipitate (Cu_2O) according to the following reaction [9], [10]:



The aldehyde group -CHO is present in the linear form of reducing sugars. Glucose is qualified as a reducing sugar, i.e. its open form D(+)-glucose can be oxidized selectively to glycolic acid or to ion gluconate according to solution pH. In this case, the reaction in an alkaline environment can be written as follows [11], [12]:



According to the reaction, it seems that glucose triggered only one step of reduction of copper ions where copper ion passed from Cu^{2+} to Cu^{+} . However, the ultimate objective of this study is synthesizing copper metallic powder from copper ions which requires two successive reductions [13]. For these reasons several experiments were conducted in this

Corresponding Author: boucharebraouf@yahoo.fr (Raouf Bouchareb)

Received 29 September 2020; Received in revised form 12 November 2020; Accepted 16 November 2020

Available Online 1 December 2020

Doi: <https://doi.org/10.35208/ert.802170>

© Yildiz Technical University, Environmental Engineering Department. All rights reserved.

research study to determine optimal conditions for copper ions transformation.

The benefits of combinatorial approaches for better and complete metal recovery from aqueous solutions are unquestionable [14], [15]. The development of a new combination between two different reducing agent has improved copper ions reduction from copper sulfate solution [15], [16]. In addition of glucose, another known reducing agent was added to improve copper recovery efficiency.

2. MATERIALS AND METHODS

2.1. Preparation of solutions

The experiment was directed as follows: 10 mL of 0.8M glucose solution (pH of 6.5) was mixed with 10 mL of

0.3M sodium hydroxide (NaOH) i.e. 1.5 times the glucose concentration. (pH of NaOH solution was 12.9). The mixture was stirred mechanically in a bain-marie of 60°C as illustrated in the dispositive shown in Fig 1. After few minutes, the solution became clear yellow (pH of the mixture was 12) (Fig 2). According to the literature [17], [18], this color indicates that the glucose hydrolyze has taken place. After that, 10 mL of 0.2M copper sulfate (CuSO_4) was added drop by drop. After 10 min of the adding of CuSO_4 , particles of brick color appeared (as shown in Fig 2b) indicating the creation of Cu_2O particles (at this level pH of the solution was 4). The next step was adding 0.6 mL (equivalent to 12 droplets) of pure sulfuric acid (H_2SO_4). pH of the final solution decreased to 1 and its color transformed to pink/brown as illustrated in Fig 2c.

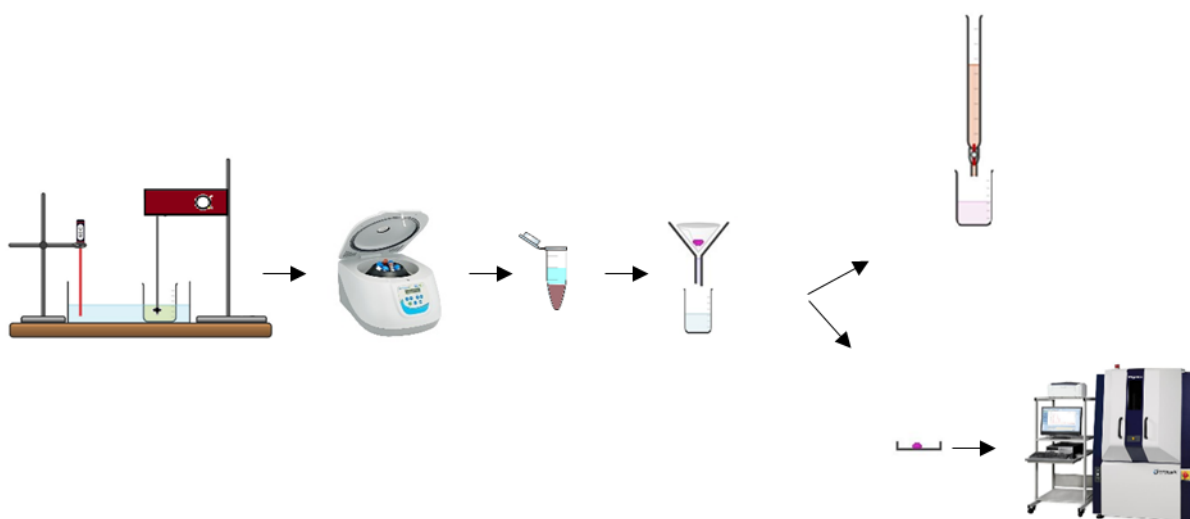


Fig 1. Schematic representative experimental dispositive of the research study.

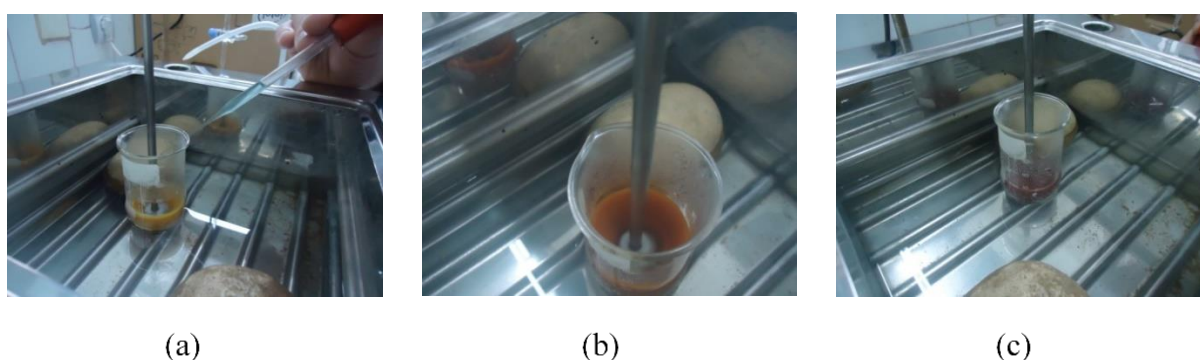


Fig 2. Solution color variation during copper ions reduction using D-glucose in an alkaline environment (a) clear yellow solution, (b) brick color solution and (c) pink/brown solution

2.2. Analytical methods

The pink/brown solution obtained at the end of experiment was left for settling. The supernatant solution was taken to determine the remaining copper ions concentration. Ions quantity was determined by

calorimetric dosage with Titriplex III and the presence of Murexide ($\text{C}_8\text{H}_8\text{N}_6\text{O}_6$) as color indicator. The solution was centrifuged at 6000 rpm for 05 min and the obtained solid particles were washed carefully by distillate water several times, filtrated using a standard paper filter and then dried in the open air. The ultimate powder was visually monitored and did not show any

sign of oxidation. The characterization of solid powder was determined by X-ray diffraction (XRD) analysis.

3. RESULTS AND DISCUSSION

3.1. Effect of glucose concentration

10 mL of 0.2M copper sulfate and glucose volumes were kept constant while glucose concentration was varied as follows: 0.2M, 0.4M, 0.6M, 0.8M, and 1.6M corresponding to (glucose/Cu²⁺) molar ratios of 1,2,3,4, and 8 subsequently. After settling, the final solution was dosed and the transformed copper ions were determined (Fig 3).

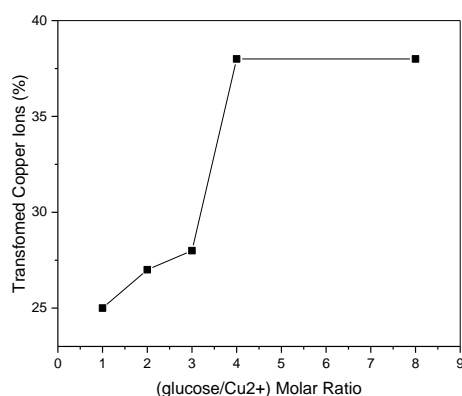


Fig3. Copper ions reduction efficiency in function of (glucose/Cu²⁺) molar ratios

Results represented in the graph shown in figure 03 demonstrate that in all cases copper ions were partially reduced and transformed to copper solid. The best results were for 0.8M of initial glucose concentration (molar ratio of 4) where 38% of copper ions were reduced and deposited as dark pink solid particles. Molar ratios of 1, 2 and 3 showed copper ions reduction efficiency of 25, 27 and 28% consequently and the deposited solid was of brown color.

The increase of glucose concentration up to 1.6M (molar ratio of 8) did not show any advantage. Based on this result, it is evident that excessive electrons arising from glucose did not enhance copper ions reduction capacity [13]. However, the obtained deposited particles were of black color indicating the formation of copper monoxide (CuO) characterized by its coal color [19]. Therefore, at this concentration glucose oxidized copper ions instead of reducing them.

Consequently, glucose concentration is found of a great importance because it can orient to either a reduction or oxidation of copper ions containing in the aqueous solution. In order to determine the allotropic nature of the obtained solid particle, two samples of 2 and 4 molar ratios were analyzed by XRD. The obtained results are illustrated in Fig 4 and 5.

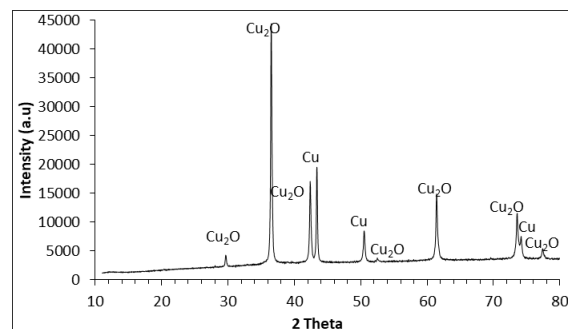


Fig 4. XRD specters of solid particles analysis obtained by 0.4M of glucose as reducing agent (glucose/Cu²⁺ molar ratio of 2)

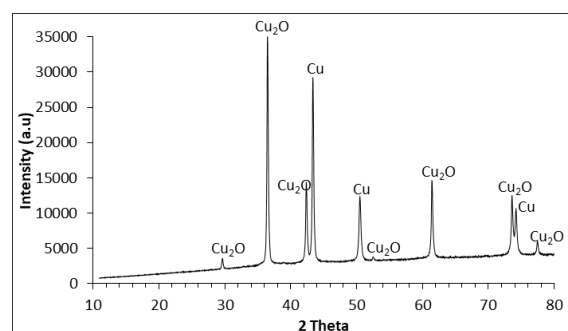


Fig 5. XRD specters of solid particles analysis obtained by 0.8M of glucose as reducing agent (glucose/Cu²⁺ molar ratio of 4)

The above results demonstrate that obtained solid particles given by both concentrations 0.4M and 0.8M of glucose are a mixture between copper metal (Cu) and cuprite (Cu₂O). Actually, there are few articles in the literature on the synthesis of copper metal using glucose; however, most of the literature studied the production of Cu₂O rather than Cu as confirmed in [6]. In addition, copper metal intensity peaks are lower than cuprite ones signifying weaker ability to transform copper ions to copper metal. However, glucose concentration played an important role of generated copper metal quantity. In fact, the peak observed a 42 in Fig 5 has got a bigger intensity than the one observed in Fig 4.

3.2. Effect of temperature

A range of temperatures was studied in this research to determine the optimum conditions for better copper metal synthesis from an aqueous solution. The different experiments were conducted under 30, 50, 60 and 70°C of temperature and 0.8M of glucose concentration. The rest of reactants concentrations and volumes were kept the same as the previous section. The obtained results are represented in Fig 6.

Results show that copper ions reduction using glucose as a reducing agent requires heat confirming previous studies in the literature [5, 20]. At nearly ambient temperature, 30 °C, the solution remained blue and did not change color. The dosage revealed very low transformation of copper ions. By increasing temperature, the quantity of produced solid particles has enhanced and became more important gradually.

Only a small increase of Cu^{2+} reduction was noticed for temperature increase from 30 °C to 50 °C. The maximum copper ions reduction efficiency was 48% obtained at 70 °C of temperature. Two samples of the best results, those of 60 and 70 °C, were analyzed and XRD specters are represented in Fig 7 and 8 continuously.

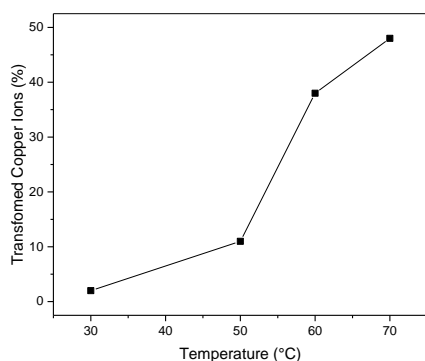


Fig 6. Copper ions reduction efficiency in function of reaction temperature

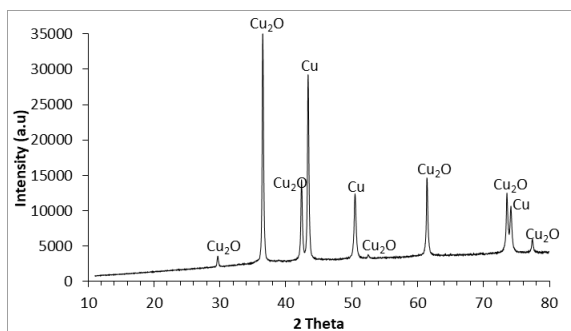


Fig 7. XRD specters of solid particles analysis obtained by 0.8M of glucose as reducing agent and 60 °C of reaction temperature

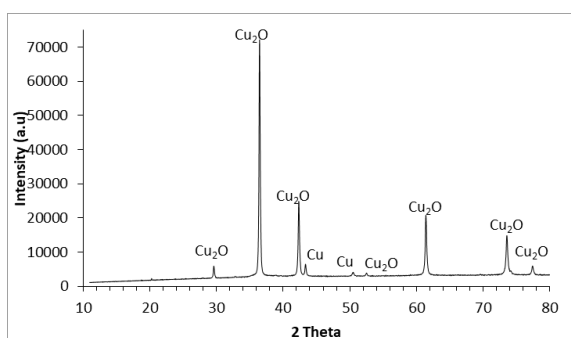


Fig 8. XRD specters of solid particles analysis obtained by 0.8M of glucose as reducing agent and 70 °C of reaction temperature

Comparing previous results, it is remarked that indeed temperature was in the favor of generating more solid particles; however, it did not act well to transform copper ions to metallic copper. At 70 °C, peaks which correspond to copper metal (Cu) are neglected compared to the ones of copper(I) oxide Cu_2O . On the other hand, the produced solid particles at 70 °C were more crystalline than the one of 60 °C. Furthermore, the temperature of 70 °C allowed the creation of crystallized precipitate formed mainly of Cu_2O . As a result,

60 °C of temperature was maintained for afterward experiments.

3.3. Effect of sodium hydroxide (NaOH) concentration

It is known that reduction of copper(II) to Cu by glucose requires high pH, where the metal species responds as insoluble oxides [13]. In this part of the study, 10 mL of three different sodium hydroxide concentrations were investigated: 0.2M, 0.3M and 0.4M, giving pH solution of 12.7, 12.9 and 13 respectively. The same experiences previously conducted were repeated using 10 mL of 0.8M glucose solution at 60 °C of temperature. Then, 10 mL of 0.2M copper sulfate (CuSO_4) was added to glucose-NaOH solution. In the three cases, when glucose was added to sodium hydroxide, pH of the mixture solution was nearly the same around 12. After adding CuSO_4 , pH decreased to around 4, 4.5 and 5.5 for the different initial NaOH concentration 0.2M, 0.3M and 0.4M consecutively indication the consumption of OH^- ions. At this level of reduction, the color of the three solutions passes from yellow-green to brown-green. By adding the droplets of sulfuric acid (12 droplets equivalent to 0.6 mL), orange particles appeared demonstrating that a formation of Cu_2O has occurred. However, the particle color has instantly changed to pink-brown signifying that the second reduction has happened [18].

Solid particles obtained from the reaction under three different initial sodium hydroxide concentrations were analyzed and characterized by XRD. The results are illustrated in Fig 9, 10 and 11.

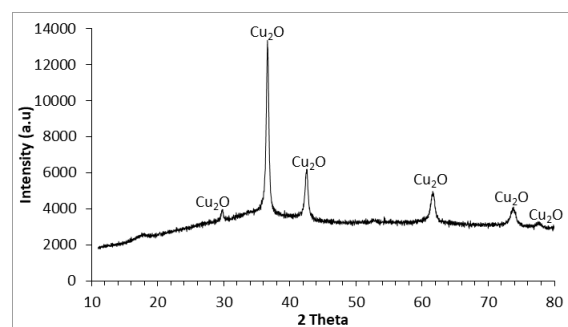


Fig 9. XRD specters of solid particles analysis obtained by 0.8M of glucose as reducing agent and 60 °C of reaction temperature and 0.2M of NaOH initial concentration

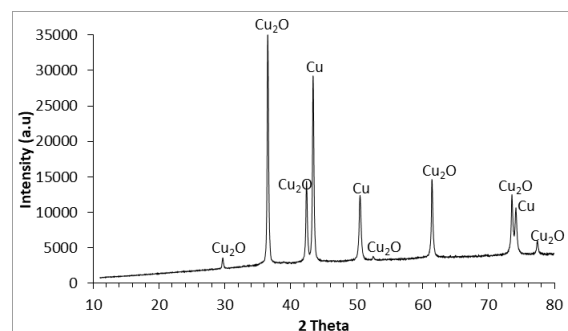


Fig 10. XRD specters of solid particles analysis obtained by 0.8M of glucose as reducing agent and 60 °C of reaction temperature and 0.3M of NaOH initial concentration

Fig 9 shows that the produced solid given by 0.2M of NaOH initial concentration is of amorphous form with the presence of cuprite (Cu_2O) particles only. By increasing sodium hydroxide initial concentrations, there was an apparition of metallic copper peaks with different intensities (Fig 10 and 11). Increasing the amount of NaOH resulted the decrease of Cu^{2+} reduction to Cu (Fig 11). From Fig 10, we can conclude that there are more important and stronger peaks corresponding to Cu showing that the optimum sodium hydroxide concentration for this experiment is 0.3M matching a solution of pH equal to 12.9. Although, considered pH in this study were close (12.7, 12.9 and 13); however, results were relatively different. As a result, pH is a key parameter to push the second copper ions reduction to occur.

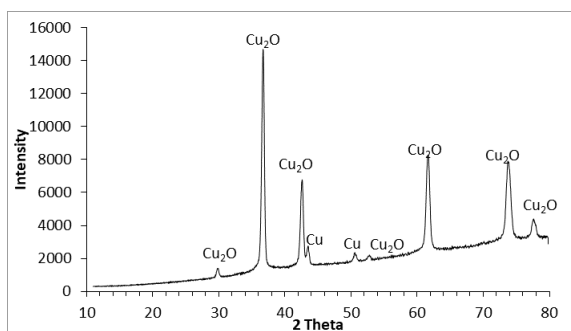


Fig 11. XRD specters of solid particles analysis obtained by 0.8M of glucose as reducing agent and 60 °C of reaction temperature and 0.4M of NaOH initial concentration

3.4. Effect of sulfuric acid volume

The objective of adding H_2SO_4 at the end of reaction was in order to promote the second reduction. When adding glucose solution to copper hydroxide solution, the mixture solution turns to orange color indicating the formation of Cu_2O particles and remains stable without changing its color even after a while. References [21] and [22] show the use of sulfuric acid for metals chemical reduction. The addition of sulfuric acid has provoked the change in color to dark pink. This color indicates that probably metallic copper has been produced. To determine the nature and characterize solid particles that were formed, two different sulfuric acid volumes were investigated, 0.6 mL (12 droplets) and 3 mL (60 droplets). The XRD results are shown in Fig 12 and 13 respectively.

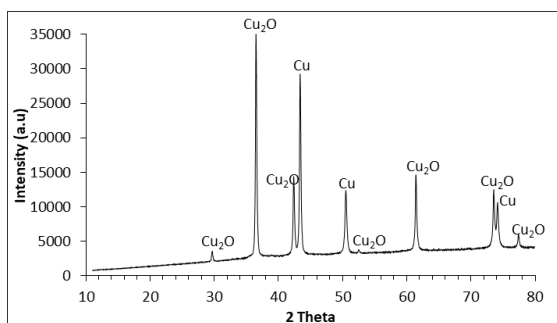


Fig 12. XRD specters of solid particles analysis obtained by adding 12 droplets of sulfuric acid H_2SO_4

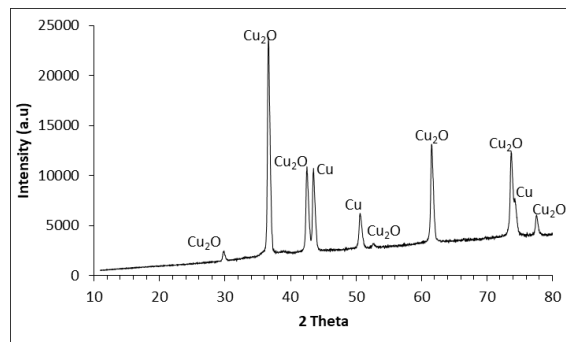


Fig 13. XRD specters of solid particles analysis obtained by adding 60 droplets of sulfuric acid H_2SO_4

The above results show that the concentration of sulfuric acid is a crucial parameter for copper ions reduction and copper metal synthesis. However, copper metal (Cu) peak intensity in Fig 12 (added H_2SO_4 volume is 0.6 mL) is more important than the one in Fig 13 (added H_2SO_4 volume is 3 mL). These results can be explained by the excessive use of acid, where copper can be solubilized in the acid solution [23].

3.5. Effect of adding ascorbic acid

It is perceived in all the previous experiments results that copper ions were not totally reduced to copper metal. For such reason, it is suggested that the second reduction reaction is difficult to achieve using glucose alone as a reducing agent. In the literature [24], glucose was used to reduce silver cations (Ag^+) which requires only one reduction. The combination of two reducing agents seems to be a good idea to enhance copper ions reduction efficiency. Ascorbic acid is known to be an environmentally friendly reducing agent widely used for copper reduction from aqueous solutions [15, 25].

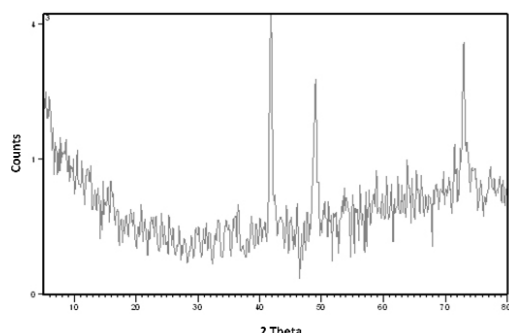
The experiment was conducted under the optimum conditions previously proved. 10 mL of glucose at 0.8M of concentration and 10 mL of NaOH 0.3M were heated up to 60 °C and mechanically mixed. 10 mL of CuSO_4 0.2M was added to the mixture drop by drop. At the end of reaction, four different doses of ascorbic acid: 4, 10, 16 and 20 mL, were added. The obtained results are illustrated in Table 1.

Table 1. Impact of ascorbic acid addition on copper ions reduction to metallic copper. From Table 1, the addition of ascorbic acid has highly increased copper ions reduction efficiency. A complete Cu^{2+} degradation was achieved for 16 and 20 mL of ascorbic acid. The powder sample obtained by adding 16 mL of ascorbic acid was analyzed and the given XRD spectra is illustrated in Fig 14.

Table 1. Impact of ascorbic acid addition on copper ions reduction to metallic copper

Ascorbic acid volume (mL)	Transformed Cu ²⁺ efficiency (%)	Observations
04	45	At the beginning, the supernatant solution was of dark green color and deposited solid particles were orange. After a week at ambient temperature, particles color changed to pink. After the change of color, Cu ²⁺ dosage was redone and found that the total of copper ions were reduced
10	60	Pink solid particles were formed rapidly and the supernatant solution was light blue
16	100	Pink solid particles were formed rapidly and the supernatant solution was transparent
20	100	

Fig 14 shows that the produced solid is mainly formed by metallic copper (Cu) since the main important three pics correspond to copper metal particles. The presence of other copper species could not be verified because unfortunately spectrum could not be processed to eliminate noise and detect lower intensity peaks. Therefore, the addition of ascorbic acid has highly helped the reduction of copper ions and pushed the second reduction reaction to take place.

**Fig 14.** XRD specters of solid particles analysis obtained by adding 16 mL of ascorbic acid

4. CONCLUSIONS

Copper powder was synthesized from copper sulfate aqueous solution using glucose and ascorbic acid as a combination of reducing agents. Both reducers played an integrated role to obtain a total degradation of copper(II) ions. The first reduction reaction was conducted by glucose, where the second reduction was taken in charge after the addition of ascorbic acid. The initial glucose concentration affected significantly the efficiency of copper ions reduction. Increasing temperature to 70 °C, enhanced copper reduction efficiency. However, XRD analyses demonstrated that produced solid particles at this temperature was mainly composed of copper(I) oxide (Cu₂O). pH was a key parameter for Cu²⁺ ions reduction as well. Sodium hydroxide was added at different concentrations; however, a concentration of 0.3M headed to better

results where copper metal peaks were more important and significant.

The addition of sulfuric acid did not help the second reduction to take place. Quite the opposite, when additional volume of H₂SO₄ was used, most of the powder was characterized by the presence of Cu₂O. Eventually, ascorbic acid was more effective by adding 16 mL at the end of reaction process, copper ions containing in the aqueous solution were completely transformed to solid particles. The nature of the formed product was confirmed by XRD analysis and it was mainly or totally made of copper metal. As a result, combination between the two reducing agents, glucose and ascorbic acid, can be affective approach to synthesis copper metal by chemical reduction and recover copper ions from polluted waters.

REFERENCES

- [1]. F. Habashi, "Dissolution of minerals and hydrometallurgical processes." Springer, *Naturwissenschaften*, Vol. 70, pp. 403–411, 1983.
- [2] A. Chagnes, "Recent advances in hydrometallurgy for the development of a sustainable production of lithium-ion batteries." *ALTA 2019 - Lithium Processing Conference*, Perth, Australia, 2019.
- [3] F. Habashi, "A short history of hydrometallurgy." *Hydrometallurgy*, Vol. 79, pp. 15–22, 2018.
- [4] W. Songping and M. Shuyuan, "Preparation of micron size copper powder with chemical reduction method", *Materials Letters*, Vol. 60, pp. 2438–2442, 2006.
- [5] R. D. Van Der Weijden, J. Mahabir, A. Abbadi, and M. A. Reuter, "Copper recovery from copper (II) sulfate solutions by reduction with carbohydrates." *Hydrometallurgy*, Vol. 64, pp. 131–146, 2002.
- [6] M. Jin, G. He, H. Zhang, J. Zeng, Z. Xie, and Y. Xia, "Shape-controlled synthesis of copper nanocrystals in an aqueous solution with glucose as a reducing agent and hexadecylamine as a capping agent." *Angewandte International Edition Chemie*, Vol. 50 (45), pp. 10560–10564, 2011.
- [7] M. Kasaie, H. Bahmanyar, and M. A. Moosavian, "Investigation of copper extraction from aqueous

- solution in a rotating disc contactor." *Brazilian Chemical Society*, Vol. 27 (5), pp. 866–876, 2016.
- [8] N. Verma, B. Vermani, N. Verma, and K. Rehani, "Comprehensive practical chemistry." *LAXMI Publications*, New Delhi, India, 2008.
- [9] F. Meira, G. L. Charles, and D. L. Mark, "Responses of insulin to oral glucose and fructose loads in marginally copper- deficient rats fed starch or fructose." *Nutrition*, Vol. 12, pp. 524–528, 1996.
- [10] G. Buxton and J. Green, "Reactions of some simple a- and b- hydroxyalkyl radicals with Cu²⁺ and Cu⁺ ions in aqueous solution." *Journal of the Chemical Society, Faraday Transactions 1: Physical Chemistry in Condensed Phases*, Vol. 01 (74), pp. 697–714, 1978.
- [11] U.S. Shenoy and A.N. Shetty, "Simple glucose reduction route for one-step synthesis of copper nanofluids." *Applied Nanoscience*, Vol. 4, pp. 47–54, 2014.
- [12] J. Li and C. Liu, "Carbon-coated copper nanoparticles: synthesis, characterization and optical properties." *Royal Society of Chemistry, New Journal of Chemistry*, Vol. 33 (07), pp. 1474–1477, 2009.
- [13] G. Granata, A. Onoguchi, and C. Tokoro, "Preparation of copper nanoparticles for metal-metal bonding by aqueous reduction with D-glucose and PVP." *Chemical Engineering Science*, Vol. 209, no. 115210, 2019.
- [14] S. Bao, Y. Tang, Y. Zhang, and L. Liang, "Recovery and separation of metal ions from aqueous solutions by solvent-impregnated resins." *Chemical Engineering & Technology*, Vol. 39, pp. 1377–1392, 2016.
- [15] S. Yokoyama, K. Motomiya, B. Jayadevan, and K. Tohji, "Environmentally friendly synthesis and formation mechanism of copper nanowires with controlled aspect ratios from aqueous solution with ascorbic acid." *Journal of Colloid and Interface Science*, Vol. 531, pp. 109–118, 2018.
- [16] S. Lotfian, H. Ahmed, and A.A.E.C. Samuelsson, "Alternative reducing agents in metallurgical processes: Gasification of shredder residue material." *Journal of Sustainable Metallurgy*, Vol. 3 (02), pp. 336–349, 2017.
- [17] U. Schmid, H.U. Guedel, and R.D. Willett, Origin of the red color in copper(II)-doped ethylenediammonium tetrachloromanganate(II). American Chemical Society, Inorganic Chemistry, Vol. 21 (08), pp. 2977–2982, 1982.
- [18] X. Qingling, M. L. Kyung, W. Fang, and Y. Juyoung. "Visual detection of copper ions based on azide- and alkyne-functionalized polydiacetylene vesicles." *Journal of Materials Chemistry*, Vol. 21 (39), pp. 15065–15820, 2011.
- [19] T. Huang and D. Tsai, "CO oxidation behavior of copper and copper oxides." *Catalysis Letters*, Vol. 87, pp. 173–178, 2003.
- [20] J. Vazquez-arenas, R. Cruz, and L. H. Mendoza-Huizar, "The role of temperature in copper electrocrystallization in ammonia – chloride solutions." *Electrochimica Acta*, Vol. 52, pp. 892–903, 2006.
- [21] J. Xue, H. Zhong, S. Wang, C. Li, J. Li, and F. Wu, "Kinetics of reduction leaching of manganese dioxide ore with *Phytolacca americana* in sulfuric acid solution: Kinetics of reduction leaching of manganese dioxide ore." *Journal of Saudi Chemical Society*, Vol. 20 (04), pp. 437–442, 2016.
- [22] D. Kim, S. J. Yang, Y. S. Kim, H. Jung, and C. R. Park, "Simple and cost-effective reduction of graphite oxide by sulfuric acid." *Carbon*, Vol. 50 (09), pp. 3229–3232, 2012.
- [23] F. Mended and A. Martins, "A statistical approach to the experimental design of the sulfuric acid leaching of gold-copper ore." *Brazilian Chemical Society*, Vol. 20 (03), 2003.
- [24] J. Belloni, "Transient and stable silver clusters induced by radiolysis in methanol." *Journal of Physical Chemistry A*, Vol. 106 (43), pp. 10184–10194, 2002.
- [25] E. Mahfouf, S. Djerad, and R. Bouchareb, "Synthesis of copper particles and elimination of cupric ions by chemical reduction." *Environmental Research & Technology*, Vol. 3 (02), pp. 46–49, 2020.



RESEARCH ARTICLE

Characterization of pistachio processing industry wastewater and investigation of chemical pretreatment

Sevtap Tırınk¹, Alper Nuhuğlu², Sinan Kul^{3,*}

¹Iğdır University, Environmental Health Program, 76000 Iğdır, TURKIYE

²Atatürk University, Department of Environmental Engineering, 25240 Erzurum, TURKIYE

³Bayburt University, Department of Emergency Aid and Disaster Management, 69010 Bayburt, TURKIYE

ABSTRACT

This study was carried out in two stages; in the first stage of the study, wastewater characterization of wastewater originating from the pistachio industry was primarily completed, and in the second stage, chemical pre-treatment studies were completed. Pistachio wastewater used in the study was obtained from a pistachio processing factory located in Gaziantep province. In chemical treatment studies, montmorillonite clay, $AlCl_3$, $Al_2(SO_4)_3$, $Fe_2(SO_4)_3$ and $FeCl_3$ were used as coagulants. As a result of chemical treatability tests, $AlCl_3$ was determined to be the best coagulant. With $AlCl_3$ at optimum dosage and optimum pH value, 99.6% suspended solid (SS) removal efficiency, 65.8% chemical oxygen demand (COD) removal efficiency and 85.5% total phenol (TP) removal efficiency were obtained.

Keywords: Pistachio industry wastewater, chemical treatment, coagulation, flocculation, precipitation

1. INTRODUCTION

Currently, dangerous material containing different structures and concentrations sourced in a variety of industrial and agricultural activities continuously pollute the environment. In spite of the contribution of these pollutants to modern life, most may accumulate in water, soil or air and if precautions are not taken to protect the environment and appropriate technologies are not used, an imbalance problem will occur leading to negative outcomes for the environment. Pollutants in receiving water environments may cause esthetic pollution and toxicity, just as basal accumulation may disrupt living conditions for aquatic organisms. Additionally, due to oxygen consumed by biological degradation or decomposition this may lead to dangerous situations for human groups or other living organisms using this aquatic environment. Though it appears that complete removal of environmental pollution is impossible when examined in terms of current technological and economic facilities and environmental awareness, on one hand further pollution of the environment should be prevented, while on the other it is necessary to ameliorate pollution that is present. Wastewater from the

pistachio processing industry is among pollutants requiring treatment in order not to harm receiving environments in Turkey.

Pistachio processing industry wastewater is wastewater as a result of processing 10 or more species of the Pistacia genus Pistacia vera L. (pistachio). The products have commercial value and are sold as dried nuts and nuts are accepted as an edible fruit [1]. With cultivation dating to ancient times, pistachio was first cultivated by Hittites living in southeast Anatolia and is known to have spread to Rome in the 1st century and then to Spain and later France. The transition to America occurred in 1853-54 [2].

Pistachio grows in suitable microclimates at the 30-45° parallels in the northern and southern hemispheres of the earth. Countries producing pistachio globally are found in the northern hemisphere generally [3, 4, 5]. In Turkey, 94% of production comes from the southeast Anatolian region, with pistachio cultivation in 56 provinces according to latest statistics [6]. In 1990, pistachio was produced from 33 343 ha area and this reached 70 087 ha in 2018. Parallel to this increase in production area, there has been a large increase in fruit

Corresponding Author: sinankul@bayburt.edu.tr (Sinan Kul)

Received 27 September 2020; Received in revised form 16 December 2020; Accepted 18 December 2020

Available Online 21 December 2020

Doi: <https://doi.org/10.35208/ert.800721>

© Yildiz Technical University, Environmental Engineering Department. All rights reserved.

production; production was 40 000 tons in 1990 and reached 240 000 tons in 2018 [5]. Additionally, pistachio cultivation entered a new era with the Southeast Anatolia Project (GAP). With irrigation conditions, the opportunity to cultivate pistachio developed, and new facilities will be offered in addition to present facilities and hence, production amounts will increase further in future years.

The maturity period for pistachio is the second half of August to the beginning of September in hot regions like Gaziantep and Şanlıurfa. Harvesting in these regions begins at the end of August and continues until the end of September. In Turkey, the mechanization level for pistachio harvesting and processing is at very low levels and these processes are based on hand labor

[7]. After the harvest, pistachio is picked and transported to drying areas, or exhibition areas. From the time when the fruit is picked from the tree until entering the depot for storage, the granulation, sorting and drying processes are called exhibition processes [8].

In order for pistachio to become a useable product, the dry red skins must be softened and loosened and this process occurs with water or steam. There are 6 separate stages of soaking, roasting, washing and stripping, separating empty and full nuts, drying and cracking during stripping the pistachio of the red outer skin. The flow scheme for the pistachio processing industry in Turkey is shown in Fig 1 [9].

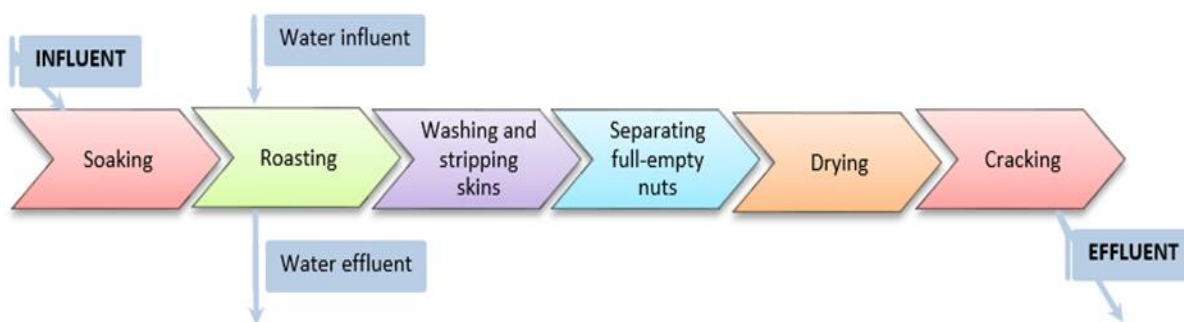


Fig 1. Flow scheme for the pistachio processing industry

Industries processing pistachio have variations in product amount linked to pistachio amounts in winter and summer seasons. The result of investigations and research identified that the roasting and stripping stage uses mean 100 m³ water daily and that 1 ton of pistachio produces 20 m³ wastewater. This proportion may vary linked to the size of the processing facility. Pistachio industry wastewater contains high organic matter content, organic matter with high pollutant qualities like dense suspended solids and polyphenols. Literature research revealed a limited number of studies about treatment of wastewater from industries processing pistachio [10, 11].

The coagulation-flocculation process is used for removal of ions dissolved in water, color, turbidity and suspended solid matter, harmful bacteria and proteins, material creating flavor or odor, algae and plankton during treatment of drinking water and wastewater [12]. Coagulation is fully linked to the dosage of coagulant and pH of the medium. For aluminum salts, optimum coagulation occurs at pH 5-7, while for iron salts it occurs at pH 4-10. In these types of coagulation processes, colloids are held within hydrated polymeric structures. The most commonly used coagulant in water and wastewater treatment processes is alum (Al₂(SO₄)₃·18H₂O), with alum flocs least soluble at pH 7. Below pH 7.6, flocs have positive load, while above pH 8.2 the load is negative. Iron salts are commonly used as coagulant. Insoluble aqueous iron oxide forms in the interval from pH 3-13. At acidic pH values, flocs have positive load, while at alkali pH values flocs have negative load, with mixed loads in the interval pH 6.5-8. The presence of anions in the medium affects the degree of flocculation. Sulfate ions increase

flocculation in acidic conditions, while they lower it in alkali conditions. Chloride ions increase flocculation degree by an amount at both acidic and basic pH values [13].

This study was carried out in two stages; in the first stage of the study, wastewater characterization of wastewater originating from the pistachio industry was primarily completed, and in the second stage, chemical pre-treatment studies were completed. There are limited studies related to treatment of wastewater from industries processing pistachio in the literature. Studies about this topic will contribute to the Turkish and global literature in addition to offering a technological and economic choice for treatment of pistachio processing industry wastewater in Turkey.

2. MATERIALS AND METHODS

2.1. Chemical material, clay and wastewater

All chemicals used in the study were obtained commercially (Merck and Sigma quality). Clay used to assist coagulants and as adsorbent was natural clay from Narman county in Erzurum quarried by Anka Nanoteknoloji Ltd. The mineral was initially dried naturally, then in a 110 °C oven for 4 hours, then ground and sieved using ASTM standard sieves and clay with 0.5 mm dimensions was used in this study. Pistachio wastewater used in the study was obtained from a pistachio processing factory located in Gaziantep province.

2.2. Experimental system

The first section of the study used a jar test setup for pre-treatment. The jar test was completed with slow mixing of 25 rpm to rapid mixing of 300 rpm. For the jar test setup, each 800 mL flask contained 10% diluted pistachio wastewater and the dilution rate was noted

during calculations. pH was set with NaOH and H₂SO₄. Coagulation-flocculation processes were completed with a variety of chemicals. After the precipitation process, samples taken from the supernatant portion were observed for removal of %COD, %SS and %TP of organic pollutants. The jar test setup used in the study is given in Fig 2.

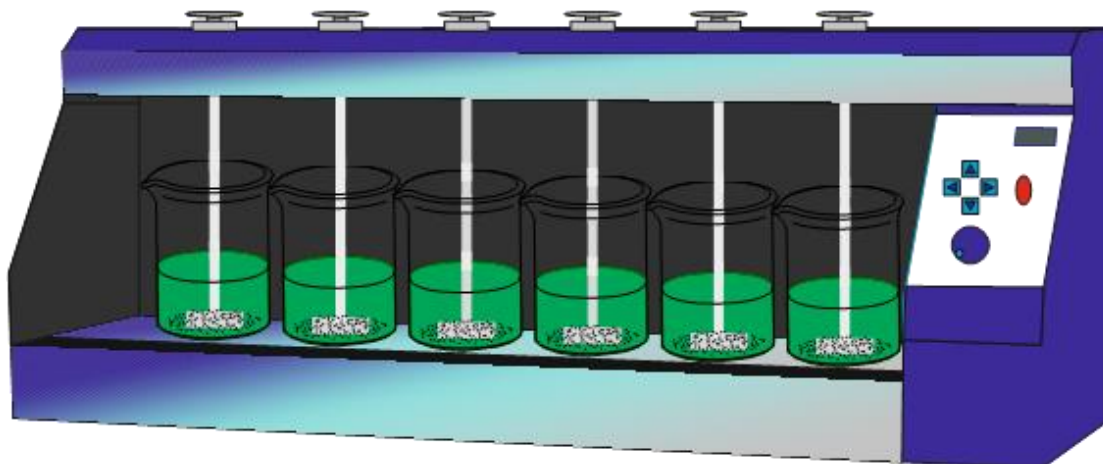


Fig 2. Experiment setup

2.3. Chemical analysis

During the study, samples prepared according to methods stated in the standard methods were heated in a thermoreactor (WTW marka CR3000 model) for 2 hours at $148 \pm 2^\circ\text{C}$ and absorbance values were read at 600 nm with a spectrophotometer (Spekol 1100, Carl Zeiss Technology) to identify COD concentrations [14]. For SS measurements, measurements were taken spectrophotometrically with a Spekol 1100 (Carl Zeiss Technology) brand spectrophotometer at 525 nm wavelength. Additionally, to confirm accuracy, measurements were taken gravimetrically as stated in the standard methods [14]. Total phenol was detected with the Folin-Ciocalteu method [15] with phenol concentration measured spectrophotometrically using the 4-aminoantiprin method [16]. NH₃ concentration was examined with a Thermo Orion brand 290 A+ ion selective electrode. Additionally, it was investigated colorimetrically with Merck brand commercial kit number 14752 with a spectrophotometer. Oil and grease measurements were performed using a 'oil-grease petrol-hydrocarbon' measurement device (Wilksir HATR-T2). The pH and temperature in the reactors were recorded and measured continuously with the aid of a WTW brand multiline P4 model multiparameter measuring device according to electrometric methods. According to the membrane electrode method, the dissolved oxygen amount in the sample was read by dipping the oximeter probe into the sample [14]. Nitrate and nitrite concentration measurements were taken with a Dionex ICS 3000 brand ion chromatography device. Phosphate analysis used ammonium vanadomolybdate with absorbance measurements read at 400 nm wavelength with a spectrophotometer. Total organic carbon and total nitrogen measurements were performed using a Teldyne-Tekmar Apollo 9000 TOC-TN analysis device.

3. RESULTS AND DISCUSSION

3.1. Characterization of pistachio wastewater

The results of studies found that wastewater from the pistachio industry contained high degree of pollutants and hence should definitely be treated before discharge into the receiving environment. Discharge should occur after standards for receiving environments stated in the Water Pollution Control Directive (WPCD) are met. Wastewater from the pistachio industry were obtained in two different periods and from different operations, with the analysis results for identification of pollutant parameters contained in wastewater shown in Table 1.

3.2. Chemical treatment of wastewater from pilot facility

The first procedure in the study left wastewater obtained from pistachio processing facilities to precipitate without any treatment for different durations. After the simple precipitation procedure, results for samples taken from the upper sections of the wastewater are shown in Fig 3.

As seen in the graph given in Fig 3, removal efficiency rapidly increased up to 1 hour and then no particular change was observed. At the end of the first hour of the chemical precipitation procedure, SS, COD, TSS, turbidity and oil-grease removal efficiencies were 82%, 26%, 43%, 70% and 65% with these values reaching 89%, 40%, 62%, 82% and 68%, respectively, at the end of 12 hours. The obtained results show the wastewater has good simple precipitation features, and application of a preliminary precipitation procedure will have significant positive effect on the treatability of the wastewater.

Table 1. Characterization of wastewater obtained from the pistachio industry

Parameters measured	Unit	1st Period	2nd Period
TCOD	mg L ⁻¹	20 891	15 700
SCOD	mg L ⁻¹	9 137	4 520
PCOD	mg L ⁻¹	11 754	11 184
SS	mg L ⁻¹	9 600	6 100
TSS	mg L ⁻¹	16 384	11 710
TOC	mg L ⁻¹	3 410	3 225
TN	mg L ⁻¹	125.5	116
BOD (Final BOD)	mg L ⁻¹	3 742	3 074
Total phenol	mg L ⁻¹	1 750	354.34
Phenol	mg L ⁻¹	52.26	13.45
Ammonia	mg L ⁻¹	1.31	1.02
Oil-grease	mg L ⁻¹	11.37	9.6
pH	-	5.99	5.5
Temperature	°C	18	18
Conductivity	ms cm ⁻¹	2.69	2.67
Turbidity	NTU	995	990
Cl ⁻	mg L ⁻¹	-	290.67
NO ₃ ⁻	mg L ⁻¹	-	0.61
SO ₄ ²⁻	mg L ⁻¹	-	37.32
PO ₄ ³⁻	mg L ⁻¹	-	6.7
Na ⁺	mg L ⁻¹	-	337.79
NH ₄ ⁺	mg L ⁻¹	-	2.58
K ⁺	mg L ⁻¹	-	650.8
Mg ⁺	mg L ⁻¹	-	24.18
Ca ⁺	mg L ⁻¹	-	121.127

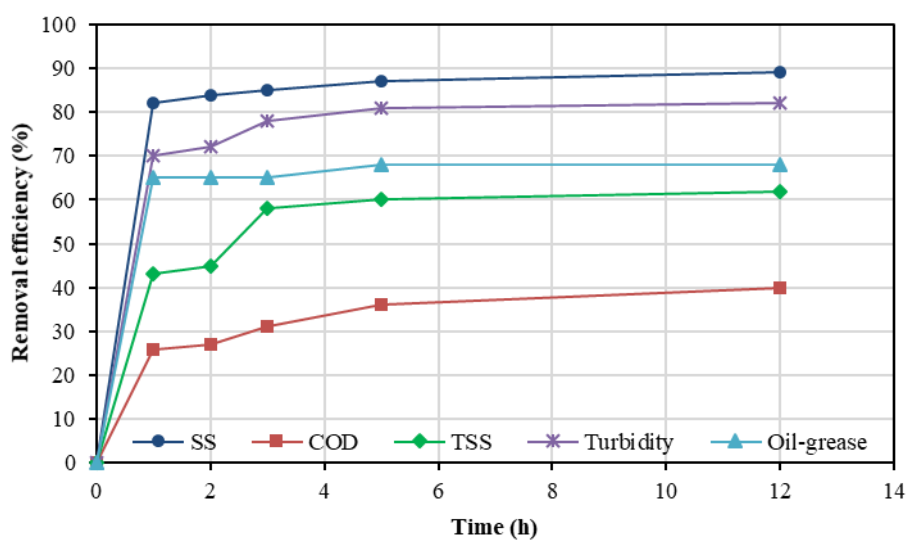


Fig 3. SS, COD, TSS, turbidity and oil-grease removal efficiencies with different precipitation durations

3.3. Effect of coagulant type on treatment efficiency

Studies investigating the effect of coagulant type on removal efficiency in chemical treatment experiments for wastewater were completed by adding different coagulant material to wastewater in reactors in the experiment system shown in Fig 2. In the experiments, 500 mL wastewater placed in 6 flasks with 800 mL volume and dosed the wastewater with the chosen coagulants. For pH setting, 1 N H₂SO₄ or 1 N NaOH was chosen. After the precipitation procedure, samples taken from the upper section of wastewater had COD, SS and TP removal efficiencies calculated. Within the scope of these experiments, montmorillonite clay, AlCl₃, Al₂(SO₄)₃, Fe₂(SO₄)₃ and FeCl₃ were used. Also,

the best pH interval, optimum coagulant type and dosage were investigated.

In the first stage of the chemical coagulation study, studies were performed to determine the appropriate precipitation duration under the same conditions. In this study, 1 g L⁻¹ coagulant dosage was added to each jar, with the pH value of 6.5. The jars were stirred at 300 rpm for a rapid mix period of 3 minutes and it was followed by a slow mix period of 15 minutes at 25 rpm. After that, the samples were taken at different precipitation times of 30 minutes, 1 hour, 2 hour and 3 hours and analyzed for SS, COD and TP to determine the removal efficiencies. The results were shown in Fig 4.

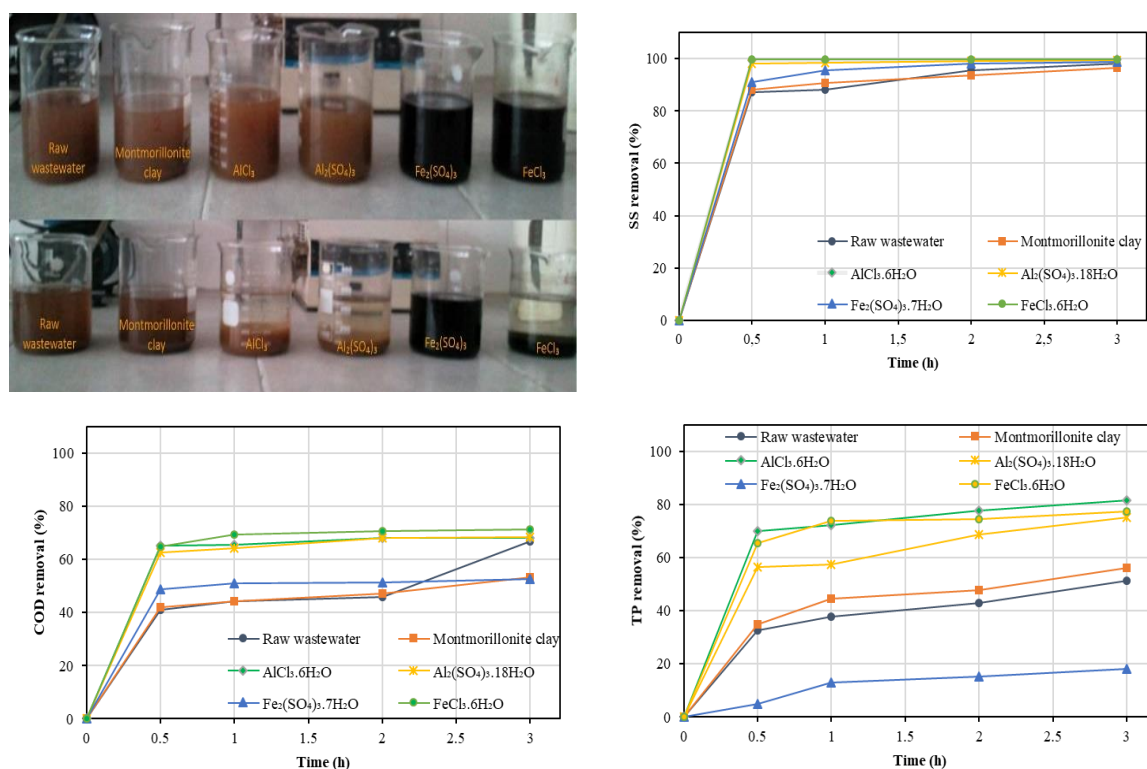


Fig 4. Situation after 30 min when different coagulants are used and effect of different coagulants on SS, COD and TP removal efficiency

As shown in Fig 4, at the end of the 30 min precipitation procedure, AlCl₃, Al₂(SO₄)₃ and FeCl₃ can be seen to cause a significantly positive difference in turbidity. When Fig 4 is investigated, experiments performed at pH 6.5 with 1 g L⁻¹ coagulant dosage obtained highest removal efficiencies for SS and COD of 99.8% and 71.3% with FeCl₃, while highest removal efficiency for TP was determined as 81.5% with AlCl₃. Studies observed that high removal efficiency was observed up to 30 min; however, there was no further removal after 30 min. As a result, the ideal precipitation duration was determined as 30 min. Reduction of surface load in jar test experiments performed without the addition of coagulant material did not have repulsion potential in electrical double layer due to the presence of electrolytes with opposite charge in the medium and it is thought the desired treatment efficiency could not be obtained as a result. In the study, the treatment

efficiency for montmorillonite clay and Fe₂(SO₄)₃ were clearly observed to be low. As a result, in remaining studies, the use of these two coagulants was discontinued.

3.4. Effect of coagulant dosage on removal efficiency

In this stage the effect of coagulant dosage was investigated in chemical coagulation studies and experiments continued with the three coagulants of AlCl₃, Al₂(SO₄)₃ and FeCl₃ with best efficiency in the first stage. Each reactor had 0.5, 1 and 2 g of coagulant material added with pH set to 6.5 and mixing rate was 3 min of rapid mixing at 300 rpm, then 15 min of slow mixing at 25 rpm and then 30 min precipitation procedure. The SS, COD and TP removal efficiencies for the coagulant type and amount can be seen in Fig 5.

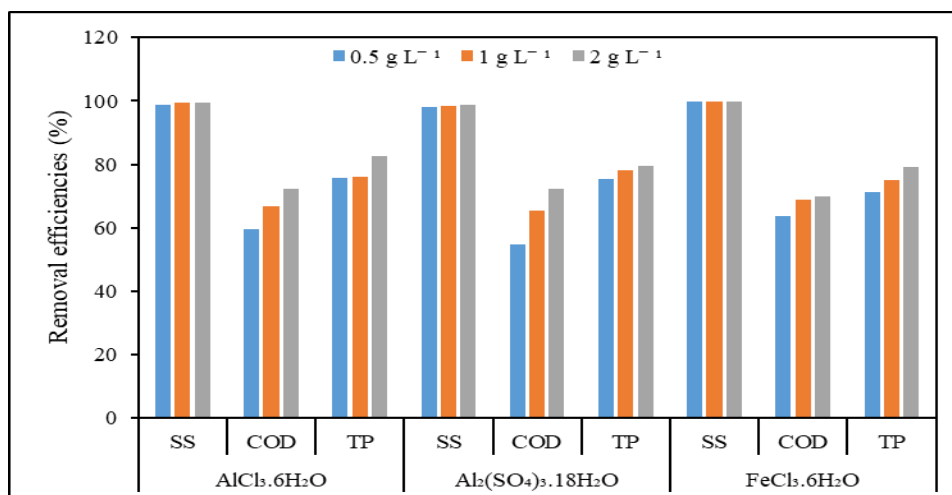


Fig 5. Effect of different AlCl₃, Al₂(SO₄)₃ and FeCl₃ dosage on SS, COD and TP removal efficiency

Fig 5 shows that AlCl₃ had highest SS, COD and TP removal efficiencies with 2 g L⁻¹ coagulant of 99.6%, 72.4% and 82.6%; for Al₂(SO₄)₃ highest SS, COD and TP removal efficiencies were obtained with 2 g L⁻¹ of 98.8%, 72.4% and 79.5%; while for FeCl₃ the highest SS, COD and TP removal efficiencies were obtained with 2 g L⁻¹ of 99.8%, 69.8% and 79.2%, respectively. The use of higher amounts of coagulant than the optimum coagulant dose causes other unwanted problems during wastewater treatment. Considering the wastewater amount and experimental setup, there was very little difference between coagulant doses in these experiments in laboratory conditions. If it is considered that in real applications kilograms of coagulant are used, the importance of the identification of optimum coagulant dose is understood. As a result,

when Fig 5 is investigated, the optimum dosage for the three coagulants was identified as 1 g L⁻¹.

3.5. Effect of pH change on treatment efficiency

To research the effect of pH variation, coagulants with 1 g L⁻¹ dosage were used with rapid mixing at 300 rpm for 3 min, slow mixing at 25 rpm for 15 min and 30 min precipitation with experiments performed with pH values from 1-12. For pH setting, 1 N H₂SO₄ or 1 N NaOH solutions were used to set the pH to values from 1-12. Fig 6 shows the variations over time for SS, COD and TP removal efficiencies for the appropriate pH interval of the coagulants used (AlCl₃, Al₂(SO₄)₃ and FeCl₃).

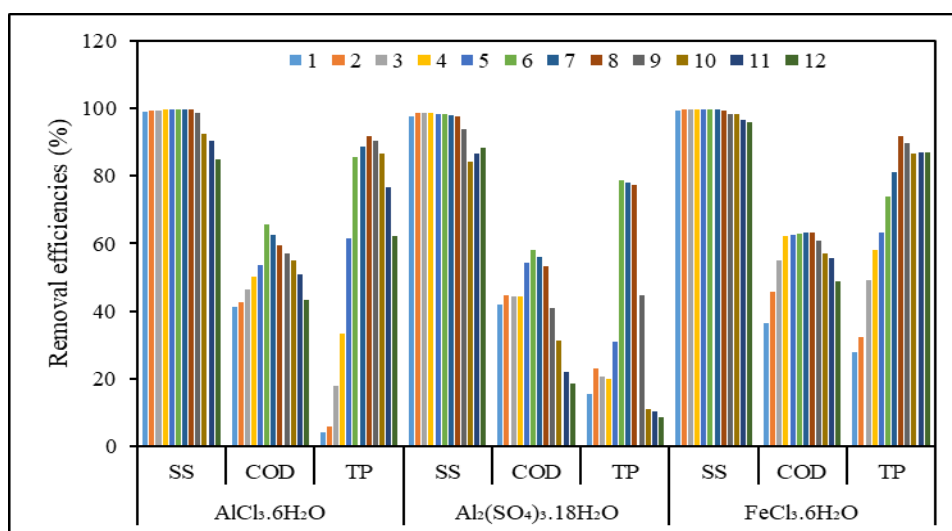


Fig 6. Effect of AlCl₃, Al₂(SO₄)₃ and FeCl₃ coagulants used at different pH values on SS, COD and TP removal efficiencies

As seen in Fig 6, during pH optimization, for AlCl₃ the SS removal efficiency was 99.6%, COD removal efficiency was 65.8% and total phenol removal efficiency was 85.5% at the optimum pH 6. For Al₂(SO₄)₃, SS removal efficiency was 98.4%, COD removal efficiency was 58.1% and total phenol

removal efficiency was 78.8% at the optimum pH value of 6. Finally, for FeCl₃ the SS removal efficiency was 99.3%, COD removal efficiency was 63.4% and total phenol removal efficiency 91.8% at the optimum pH of 8. If the pre-treatment of pistachio processing industry wastewater using chemical coagulant matter operates

at low pH, flocs with better precipitating properties were obtained. At high pH, weak flocs formed and it was determined that suspended matter was found in the supernatant portion. As a result, the desired treatment efficiency could not be reached at high pH values. Due to chemical treatability studies, AlCl_3 provided better results with maximum SS, COD and TP removal efficiencies found with coagulant dosage 1 g L^{-1} , pH 6, mixing rate of 300 rpm for 3 min and 25 rpm for 15 min and 30 min precipitation.

4. CONCLUSIONS

Though Turkey is 3rd in the world in terms of pistachio processing industries, the number of companies with production from modern facilities is very few. Wastewater from these industries contribute significantly to pollution of natural environments. In this study, chemical precipitation was used to determine the optimum treatment conditions for treatability of pistachio processing industry wastewater with high COD content.

The significant toxic pollutant of pistachio processing industry wastewater was firstly characterized and in the second stage chemical pre-treatment studies were performed. The chemical treatability studies used clay, AlCl_3 , $\text{Al}_2(\text{SO}_4)_3$, $\text{Fe}_2(\text{SO}_4)_3$ and FeCl_3 as coagulants. The results of the chemical treatability experiments identified AlCl_3 as the best coagulant. At optimum dosage and optimum pH, AlCl_3 provided 99.6% SS removal efficiency, 65.8% COD removal efficiency and 85.5% TP removal efficiency. The results obtained from the experiments and recommendations are listed below.

- When pre-treatment studies applied a simple precipitation procedure, the SS removal efficiency was 82%, COD removal efficiency was 26%, TSS removal efficiency was 43%, turbidity removal efficiency was 70% and oil-grease removal efficiency was 65% at the end of one hour. These results show that wastewater has good simple precipitation properties. It was understood that if preliminary precipitation is applied, there will be significant positive effect on treatability of the wastewater.

- Chemical treatability studies used montmorillonite clay, AlCl_3 , $\text{Al}_2(\text{SO}_4)_3$, $\text{Fe}_2(\text{SO}_4)_3$ and FeCl_3 as coagulants. At the end of experiments, optimum coagulant dosages, optimum precipitation duration, optimum pH values and the obtained COD, SS and TP removal efficiencies were determined. Detection of optimum coagulant dosage used 0.5 , 1 and 2 g L^{-1} coagulant, identification of optimum precipitation duration used 30 min, 1 hour, 2 hour and 3 hours and optimum pH detection used values from pH 1-12 for chemical treatment experiments. The results of the chemical treatability experiments found optimum dosage was 1 g L^{-1} for the three coagulants and optimum pH values were 6 for AlCl_3 and $\text{Al}_2(\text{SO}_4)_3$ and 8 for FeCl_3 . At optimum dosage and pH values, AlCl_3 provided 99.6%, $\text{Al}_2(\text{SO}_4)_3$ provided 98.4% and FeCl_3 provided 99.3% SS removal efficiency with pH values of 6 for AlCl_3 and $\text{Al}_2(\text{SO}_4)_3$ and 8 for FeCl_3 . At optimum dosage and optimum pH values AlCl_3 gave 65.8%, $\text{Al}_2(\text{SO}_4)_3$ gave 58.1% and

FeCl_3 gave 63.4% for COD removal efficiencies. At optimum dosage and optimum pH values AlCl_3 gave 85.5%, $\text{Al}_2(\text{SO}_4)_3$ gave 78.8% and FeCl_3 gave 91.8% for TP removal efficiencies. The coagulant providing best results compared to other chemicals was identified as AlCl_3 .

- For selection of chemicals to be used as coagulant, though the highest removal was obtained with AlCl_3 , it was concluded that AlCl_3 may not be suitable at high pH values due to not forming stable structures. However, the desired efficiency can be reached for pre-treatment at low pH. When compared with other chemicals, the most appropriate coagulant for COD, SS and TP removal is AlCl_3 . After AlCl_3 , the order is FeCl_3 , $\text{Al}_2(\text{SO}_4)_3$, clay and $\text{Fe}_2(\text{SO}_4)_3$. After the coagulation-flocculation procedure for pistachio wastewater, it can be seen that high removal efficiencies were achieved from the color of the discharge water.

- It is thought this study will be a guide to more comprehensive treatment studies for pistachio processing industry wastewater.

ACKNOWLEDGEMENT

This research was supported by Atatürk University Scientific Research Projects (BAP) Coordination Unit within the scope of Project No: 2011/421. Also, we would like to thank to Atatürk University Department of Environmental Engineering and all employees.

REFERENCES

- [1]. İ. Dağdeviren and İ. Erdoğan, "Pistachio Cultivation, Growing Techniques of Plants in Wet Conditions in the GAP Region" (in Turkish), *T.C. Başbakanlık Köy Hizmetleri Genel Müdürlüğü Şanlıurfa Araştırma Enstitüsü*, 1996.
- [2]. Lemaistre, J., *Le pistachier: étude bibliographique*, Fruits, 14(2), pp. 57-77, 1959.
- [3]. S. Özbek and M. Ayfer, "In Turkey Pistachio (*Pistacia vera* L.) rootstocks and graft technique" (in Turkish), *Ankara University Faculty of Agriculture Yearbook*, 4, pp. 189-214, 1959.
- [4]. B.E. Ak ve H. Kaşka, "A Research on the Effect of Dense Planting on Yield in Pistachio Cultivation" (in Turkish), *Türkiye 1. Ulusal Bahçe Bitkileri Kongresi, İzmir*, Vol. 1, pp. 163-166, 1992.
- [5]. The FAOSTAT website. [Online], Available: (2020) Production quantities of Pistachios by country(1994-2018) <http://www.fao.org/faostat/en/#data/QC/visualize>.
- [6]. S. Arpacı, H. Tekin and H. Atlı, "Spreading Areas of wild Pistacia species in Turkey", Siti Project Progress Report (in Turkish), *Antepfıstığı Araştırma Enstitüsü Müdürlüğü, Gaziantep*, 1997.
- [7]. H.S. Atlı and S. Arpacı, "Harvesting Pistachio, in Pistachio Cultivation" (in Turkish), *Antepfıstığı Araştırma Enstitüsü Müdürlüğü, Gaziantep*, 2001.
- [8]. R. Karaca, "Pistachio Harvest Processing Technique and Storage, Pistachio Growing

- Technique" (in Turkish), *Antepfıstığı Araştırma Enstitüsü Müdürlüğü*, Vol. 4, pp. 89-103, 1995.
- [9]. A. Sabancı and M. Çelik, "Machine features used in mechanization and evaluation processes in pistachio production" (in Turkish), *Tarımsal Mekanizasyon*, Vol. 9, pp. 58-70, 1985.
- [10]. A.E. Yılmaz and Z. Köksal, "The Investigation of Parameters Affecting on Treatment of Pistachio Processing Industry Waste Water by Continuous Electrocoagulation Process", *Journal of the Institute of Science and Technology*, 7(1), pp. 95-103, 2017.
- [11]. M. Türkyılmaz, "Treatment of Pistachio Processing Plant Wastewater by UV/Chlorine Advanced Oxidation Process", *Selçuk University, Graduate School of Natural and Applied Science*, 2016.
- [12]. F. Şengül and E. Küçükgül, "Physical Chemical Basic Processes and Processes in Environmental Engineering" (in Turkish), *DEÜ Mühendislik Fakültesi Basım Ünitesi*, 253, 1995.
- [13]. W.W. Eckenfelder, "Industrial Water Pollution Control", *MC Graw-Hill*, 1989.
- [14]. APHA, Standard methods for the examination of water and wastewater, American Public Health Association (APHA), Washington, DC, USA, 2005.
- [15]. M.R. Rover and R.C. Brown, "Quantification of total phenols in bio-oil using the Folin-Ciocalteu method", *Journal of Analytical and Applied Pyrolysis*, Vol. 104, pp. 366-371, 2013.
- [16]. L. Clesceri, "Standard methods for the biooxidation of phenol", *Biotechnology and Bioengineering*, 1989.



RESEARCH ARTICLE

Assessment of toxic and essential metals in fish feed ingredients available in different areas of Bangladesh

Biraj Saha^{1,*} , Md. Abdul Mottalib¹ , A. N. M. Al-Razee² 

¹ Institute of Leather Engineering and Technology, University of Dhaka, Hazaribagh, Dhaka-1209, BANGLADESH

² Department of Analytical Chemistry & Environmental Science, Training Institute for Chemical Industries, Polash, Narsingdi-1611, BANGLADESH

ABSTRACT

Contamination of heavy metals in fish feed ingredients is regarded as a major crisis globally especially in developing countries because it may be the source of toxicity in the food chain. Fish farming in Bangladesh is growing very rapidly and fish available in the markets are mostly coming from fish farms where fish farmers mostly use commercial fish feeds manufacturing with different ingredients. In this study, several types of ingredients based on different origins were collected from several areas and after measuring dry weight these were digested by a mixture of acids. This study is concerned to access the toxic and essential metals in different fish feed ingredients which are frequently used to produce commercial fish feed in Bangladesh. The concentration (mg kg^{-1} dry weight) range of toxic metals such as; Pb (0.56- 1.73), Cd (0.12-0.97), Cr (0.15-0.88), As (BDL), Hg (BDL), Ni (1.10-2.50) and essential metals such as; Fe (13.57-48.96), Cu (10.11-28.09), Zn (10.60-26.25), Na (12.07-35.00), K (13.06-28.97), Ca (10.00-47.96) in selected fish feed ingredients were recorded by Inductive Coupled Plasma Optical Emission Spectroscopy (ICP-OES, Optima 7000DV) with significant variation ($P < 0.05$). The analyzed toxic and essential metal concentrations in most of the ingredients were within the safe limit proposed by World Health Organization, Food and Agricultural Organization and European Union indicating no health risk.

Keywords: Essential metal, fish feed ingredients, health risk, toxic metal

1. INTRODUCTION

Bangladesh has one of the highest population densities and is also the 7th most populous country in the world. A large number of folks directly or indirectly rely on agriculture [1]. Aquaculture and fisheries are one of the major sectors of agricultural activities and play a significant role to boost the country's economy by ensuring fish demand and encouraging the establishment of a large number of by-product industries which have a great contribution to the national economy, giving 3.69% to the Gross Domestic Product (GDP) of this country's economy and 22.60% to the agricultural GDP [1, 2].

Civilization rapidity, high population rate and inclination to industrialization, developing countries are becoming the shelter of many of the world's most contaminated air, water and solid waste problems.

Previous studies have reported that the level of particular heavy metals is increasing in water bodies around the world, especially in rivers. The industrial procurement and waste generated from these industries are mainly responsible for this worldwide pollution [3]. Bangladesh is widely recognized for producing leather from raw hides and skins and the tanning industries are highly reliable to chrome tanning method which is liable for chromium pollution both in liquid and solid waste. Moreover, groundwater is polluted severely due to arsenic contamination in many regions of this land [4, 5]. Industrial disposals and mining extraction can be a potential source of heavy metal exposure in the aquatic ambiance [6]. Besides, environmental contaminants in food processed with fishes and even in fish have become a global concern. Due to high biological accumulation and magnification rate, heavy metal contamination in fish can impose a detrimental

Corresponding Author: biraj.saha533@yahoo.com (Biraj Saha)

Received 10 December 2020; Received in revised form 20 December 2020; Accepted 21 December 2020

Available Online 25 December 2020

Doi: <https://doi.org/10.35208/ert.838481>

© Yildiz Technical University, Environmental Engineering Department. All rights reserved.

effect on human health [7]. Exposure of metals in water bodies has attracted global concern because of its exuberance, consistency and environmental toxicity. Pollution because of toxic metals has a detrimental health effect on invertebrates, fish, and humans. Cultivated fishes and aquacultures largely depend on artificial feeds. Commercial feed manufacturers failed to fulfill the standards required for cultivated fish production, and the origin of ingredients for the manufacturing of the feeds tends to be contaminated with heavy metals and other pollutants [8, 9]. The common sources of fish feed ingredients are maize, rice, rice polish, wheat, soybean grits, mustard oil cake, coconut oil cake, lentil bran, molasses, etc. [10].

Bangladesh is well known for the cultivation of fish to fulfill the protein demand of the countrymen and fishes are the most pivotal organisms in the aquatic food chain, which are very sensitive to metal contamination. Different metals are accumulated in fish tissues at different concentration levels. The metal concentration differs from fish to fish due to the affinity of metals to fish tissues, uptake rate, extraction and absorption rate [11, 12]. Metals such as Pb, Cd, As, Hg, Cr are toxic as well as accumulation of these metals for a long period in the bodies of aquatic organisms may be responsible for severe diseases [13]. Heavy metal toxicity can be responsible for mental distress and nervousness, energy declining, and blood composition irregularity, breakdown of the function of lungs, kidneys, liver and other vital organs [14]. The adverse effect of metals when intakes above the standard levels can be considered as chronic or acute toxic, and heavy metals can be regarded as neurological toxic, carcinogenic, mutagenic. The primary diseases of humans related to toxic metals such as; Cd, Pb, As, Hg consumption may cause vomiting, convulsions, immobility, ataxia, hemoglobinuria, gastrointestinal diseases, stomatitis, tremor, diarrhea, depression and respiratory diseases [15].

Essential metals are needed in trace amounts for the proper ramification of enzyme profile, hemoglobin development and vitamin production in humans [16]. Iron helps to bind, transport, and spread oxygen into the flow of blood in animals. Some of the trace elements control important biological processes [17]. Zinc and copper are essential to life. It plays a vital role in lipid, protein and carbohydrate metabolism. Copper is involved in iron metabolism, the formation of bones, connective tissues and maintaining the integrity of the myelin sheath of nerve fibers. The deficiencies of zinc and copper cause growth retardation of animals [18, 19]. Sodium and Potassium are the prime dietary metal requirements of humans to keep a good balance of physical fluids system and to active nerve and muscle properly [20], [21]. Calcium is a key nutrient in the human body that mainly helps the bones rebuild properly and stay strong [22]. Although essential metals play important physiological and biochemical roles in the body and either their deficiency or excess can lead to disturbance of metabolism and therefore causes to create various diseases [23]. Since raw materials of different origins are used to produce commercial fish feeds, proper observing for heavy metal accumulation

in feeds will have to go a far way for manufacturing standard feeds that will help to produce a large number of cultivated fishes and keep humans safe from different diseases [24].

Though several studies are done previously on heavy metal determination in fishes, we focused to identify the preliminary sources of these metals in fish tissues. Besides, along with heavy metals, we assessed the concentration of essential metals in the different fish feed ingredients which are regularly used by feed producers around the country. Consequently, this study was designed to find the concentration of toxic metals (Pb, Cd, Cr, As, Hg, Ni) and essential metals (Fe, Cu, Zn, Na, K, Ca) in selected fish feed ingredients available in the local market of Bangladesh.

2. MATERIALS AND METHODS

2.1. Sample collection

Samples of feed ingredients were collected from different renowned fish feed manufacturing companies located in Bangladesh. Ten major feed ingredients including carbohydrate (Wheat, maize, rice), animal origin (Chicken Bone, Fat) and plant origin (Mustard oil cake, Linseed, Duck Weed, Water hyacinth) were collected for their assessment of heavy metal contents. All homogeneous samples were collected in an insulated small container that was dry and clean without any leakages. Each sample was labeled with proper name, weight, physical type (animal or vegetable origin), and collection date by using a waterproof marking pen on a strip of masking tape (WHO, 2002) [25].

2.2. Digestion and analysis

All collected fish feed ingredient samples were cut into small species and dried in a micro-oven at 105°C until a constant weight was achieved and finally powdered. Samples also were dried in a similar way 1 g of the homogenate of each sample (dry weight) was taken into a quick fit round bottom flask and a 15 mL mixture of concentrated HNO₃, H₂SO₄ and HClO₄ in (4:1:1; v/v) was added into the flask. A condenser was set up with the flask and the mixture was stirred at 85°C for 3 hours until the proper digestion was completed and the solution became clear [26]. Then the digested samples stayed to cool for 30 minutes. Filtration of all digested samples was done with Whitman no. 42 filter paper and the filtration was transferred into the volumetric flask, then 20 mL deionized water was added and rinsed well and finally diluted to 50 mL with deionized water. Samples were stored at ambient temperature until metal analysis. All chemicals used were Merck, Germany analytical grade, including standard stock solutions of known concentrations of different metals. The entire samples were analyzed by Inductive Coupled Plasma-Optical Emission Spectroscopy (ICP-OES) with the following detection limit [Table 1].

Table 1. Information about the ICP-OES spectrometer

Metals	Wavelength (nm)	Detection limit (mg kg ⁻¹)	Assigned Value (mg kg ⁻¹)	Obtained Value (mg kg ⁻¹)	Percent Recovery (%)
Pb	220.35	0.01	0.50	0.4815	96.3
Cd	228.80	0.001	0.50	0.4923	98.5
Cr	267.71	0.001	0.50	0.4693	93.4
As	193.69	0.01	0.50	0.5132	102.6
Hg	253.65	0.01	0.50	0.5242	104.8
Ni	245.78	0.01	0.50	0.4953	99.06
Fe	238.21	0.001	0.50	0.5232	104.6
Cu	327.39	0.001	0.50	0.5245	104.7
Zn	206.20	0.001	0.50	0.4876	97.5
Na	245.65	0.01	0.50	0.5123	102.5
K	213.45	0.01	0.50	0.4987	99.7
Ca	220.34	0.01	0.50	0.5143	102.8

2.3. Statistical analysis

All statistical analyses were performed using Microsoft Excel (version 2016). The Pearson Correlation Coefficient in the present study is also done to calculate the interrelationships among the analyzed elements at a level of > 0.5 or < -0.5. A positive value indicates, one metal increase in value, other value also rises. Besides, negative value implies the opposite relationship. If the value is greater than 0.8, there is a strong relationship between the two variables whereas if the value is lesser than 0.5 means a weak relationship. Analysis of variance (Two-way ANOVA) and correlation matrix was employed to examine the statistical significance of differences in the mean concentration of metals in the collected fish feed ingredients. A probability level of $P < 0.05$ was considered statistically significant [27].

3. RESULTS AND DISCUSSION

The summary of the concentrations of toxic metals such as Pb, Cd, Cr, As, Hg and Ni found in different commercial fish feed ingredients are presented in Table 2. Table 3 shows that the highest concentration of Pb was 1.73 mg kg⁻¹ found in chicken bone and the lowest concentration (2.15 mg kg⁻¹) was in Animal fat. The mean concentration of Pb in these selected ingredients was 1.05 mg kg⁻¹ which is lower than the permissible limit of 5.0 mg kg⁻¹ proposed by (WHO/FAO, 2004) [28] [Fig 1] but the recorded result for Pb in the present study was higher than the previously recorded value which was 3.19 mg kg⁻¹ and 4.18 mg kg⁻¹ respectively [30, 31]. The mean concentration of Pb in the present study was lower than 0.30 mg kg⁻¹ reported by Adeniji et al. [10].

Table 2. Concentration of toxic metals (mg kg⁻¹ dry weight) in different fish feed ingredients

No	Ingredients	Pb	Cd	Cr	As	Hg	Ni
01	Wheat	0.80	0.12	0.63	BDL	BDL	1.50
02	Maize	1.11	0.97	0.50	BDL	BDL	1.10
03	Duck Weed	1.05	0.43	0.33	BDL	BDL	2.50
04	Water- hyacinth	1.13	0.70	0.40	BDL	BDL	2.50
05	Linseed	1.07	0.13	0.18	BDL	BDL	2.00
06	Rice & Rice bran	0.76	0.40	0.15	BDL	BDL	1.50
07	Mustard oil cake	1.13	0.18	0.68	BDL	BDL	1.70
08	Molasses	1.15	0.83	0.40	BDL	BDL	1.60
09	Chicken Bone	1.73	0.58	0.88	BDL	BDL	1.80
10	Animal Fat (cow)	0.56	0.15	0.63	BDL	BDL	1.40
Safe Limit (mg kg ⁻¹)	FAO/WHO, 2004 [28]	5.00	1.00	1.00	1.00	0.50	----
	EU, 2010 [29]	2.00	2.00	1.00	2.00	1.00	----

BDL= Below Detection Limit; FAO= Food and Agricultural Organization; WHO= World Health Organization; EU= European Union.

Table 3. Statistical data analysis of toxic metals

Statistical data analysis of Toxic Metals						
Metals	Pb	Cd	Cr	As	Hg	Ni
Maximum value	1.73	0.97	0.88	---	---	2.50
Minimum value	0.56	0.12	0.15	---	---	1.10
Mean value	1.05	0.45	0.48	---	---	1.76
Standard Deviation	0.31	0.31	0.23	---	---	0.46
P value	0.003*	0.001*	0.008*	---	---	0.60
F value	0.71	0.21	0.76	---	---	1.12
F-critical value	0.20	0.28	0.43	---	---	1.64
Adeniji et al. [10]	0.30	0.50	0.20	---	---	
Alexieva1 et al. [30]	3.19	0.54	1.53	0.108	.0002	3.07
Islam et al. [31]	4.18	0.32	3.5	1.00	----	2.70

*Significant at P< 0.05

The mean concentration of Cd in these selected ingredients was 0.45 mg kg⁻¹ which is beyond the safe limit of 1 mg kg⁻¹ [28] and 2 mg kg⁻¹ [29] [Fig 1]. The maximum Cd concentration was 0.97 mg kg⁻¹ recorded in Maize whereas the least content was 0.12 mg kg⁻¹ found in Wheat. The average Cd content was 0.32 mg kg⁻¹ in a previous study reported by Islam et al. [31], Adeniji et al., [10] and Alexieva1 et al. [30] found Cd content 0.50 mg kg⁻¹ and 0.54 mg kg⁻¹ respectively in their study which was higher than the present study. A noticeable amount of Cr was found in Chicken bone, Animal fat and Mustard oil cake. The highest concentration of Cr was 0.88 mg kg⁻¹ recorded in Chicken bone and the lowest concentration was 0.15 mg kg⁻¹ in Rice and Rice bran. The recorded mean value of Cr was 0.48 mg kg⁻¹ within the maximum limit of 1.00 mg kg⁻¹ [28, 29] [Fig 1]. Islam et al. [31] and

Alexieval et al. [30] found the Cr concentration 3.50 mg kg⁻¹ and 0.54 mg kg⁻¹ in their study which is higher than the present study but the mean concentration of Cr in this study was higher than 0.20 mg kg⁻¹ recorded by Adeniji et al. [10]. As and Hg concentration was below detection limit whereas the maximum limit 1.00 mg kg⁻¹ for each metal proposed by WHO/FAO, 2004 [28] and EU, 2010 [29] though some studies traced the concentration of As and Hg in their study. The highest concentration of Ni (2.50 mg kg⁻¹) was found in Water hyacinth and Linseed and the lowest concentration (1.10 mg kg⁻¹) was recorded in Maize. The average concentration of Ni was 1.76 mg kg⁻¹, which is lower than 3.07 mg kg⁻¹ and 2.70 mg kg⁻¹ in the two separate studies carried out by Alexieva1 et al. [30] and Islam et al. [31].

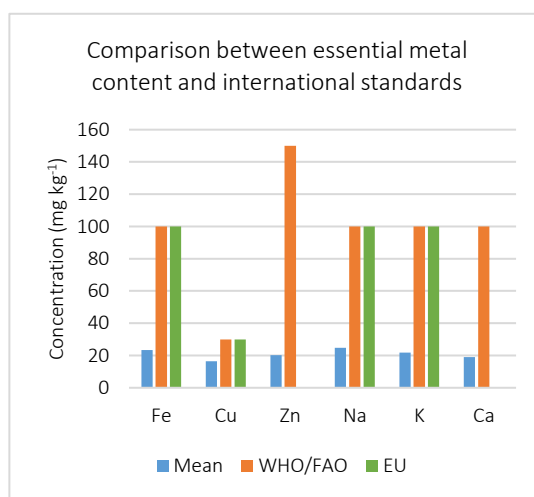
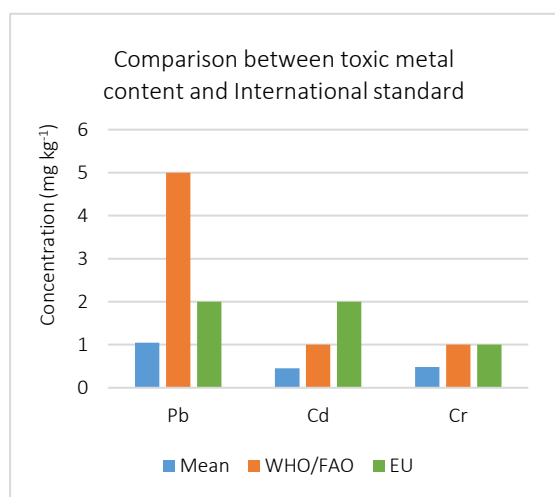


Fig 1. Comparison between recorded content of traced metals and international Safe limit

The concentration of essential metals such as; Fe, Cu, Zn, Na, K and Ca in selected fish feed ingredients are represented in Table 4. Table 5 summarizes that the highest concentration of Fe was 48.96 mg kg⁻¹ recorded in the chicken bone which is considered as animal origin whereas the lowest concentration of Fe

was 13.57 mg kg⁻¹ found in Linseed as plant origin. The average concentration of Fe was 23.30 mg kg⁻¹ which is within the safe limit of 100 mg kg⁻¹ proposed by FAO, 2016 [32] and EU, 2010 [29] [Fig 1] as well as the found average value of Fe in the present study is lower than 34.78 mg kg⁻¹ in a past study by Godfred et

al., 2020. The average concentration of Cu was 16.41 mg kg⁻¹ in this study whereas 29.00 mg kg⁻¹ Cu was found in a study by Roy et al.[33]. The recorded value

in the present study was in the acceptable limit of 30 mg kg⁻¹ stated by FAO, 2016 [32]and EU, 2010 [29] [Fig 1].

Table 4. Concentration of essential metals (mg kg⁻¹ - dry weight) in different fish feed ingredients

No	Ingredients	Fe	Cu	Zn	Na	K	Ca
01	Wheat	27.57	15.72	15.15	35.00	27.00	18.10
02	Maize	28.70	10.11	14.23	31.10	13.06	16.50
03	Duck Weed	18.73	18.37	24.27	29.00	24.30	10.00
04	Water- hyacinth	18.30	19.40	24.27	14.00	15.34	10.07
05	Linseed	13.57	11.80	25.00	24.00	27.80	12.62
06	Rice & Rice bran	19.40	17.98	26.25	23.30	17.65	19.06
07	Mustard oil cake	33.70	16.90	14.57	26.83	21.34	12.69
08	Molasses	33.08	15.08	23.08	30.60	27.12	24.16
09	Chicken Bone	48.96.	28.09	23.78	21.67	28.97	47.96
10	Animal Fat (cow)	16.67	10.67	10.60	12.07	15.78	18.41
Safe Limit (mg kg ⁻¹)	WHO, 2004 & FAO, 2016 [28, 32]	100	30	150	100	100	100
	EU, 2010 [29]	100	30	100	100	---

Table 5. Statistical data analysis of essential metals

Statistical data analysis of Essential Metals						
Metals	Fe	Cu	Zn	Na	K	Ca
Maximum value	48.96	28.09	26.25	35.00	28.97	47.96
Minimum value	13.57	10.11	10.60	12.07	13.06	10.00
Mean value	23.30	16.41	20.12	24.76	21.84	18.96
Standard Deviation	10.22	5.25	5.76	7.38	5.97	11.12
P-value	0.005*	0.07	0.001*	0.004*	0.003*	0.50
F-value	0.31	0.85	0.61	0.47	0.53	1.16
F-critical value	0.15	1.38	0.21	0.12		1.49
Roy et al., 2019 [33]	----	29.00	24.50	---	---	----
Godfred et al., 2020 [34]	34.78	----	14.95	---	---	----

The highest concentration of Cu (28.09 mg kg⁻¹) was found in Chicken bone and the lowest concentration (10.11 mg kg⁻¹) was recorded in Maize. The average concentration of Zn was 20.12 mg kg⁻¹ in this study which is within the permissible limit of 150 mg kg⁻¹ proposed by WHO, 2004 [28] [Fig 1] and it is higher than 14.95 mg kg⁻¹ recorded Godfred et al. [34] and lower than 24.50 mg kg⁻¹ reported by Roy et al. [33]. The highest concentration of Na was 35.00 mg g⁻¹ found in Wheat and the lowest concentration was 12.07 mg kg⁻¹ in Animal fat recorded in Wheat. The average concentration of Na was 24.76 mg kg⁻¹ in the present study which is within the maximum limit of 100 mg kg⁻¹ proposed by WHO and EU [Fig 1]. The highest concentration of K and Ca was 28.97 mg kg⁻¹ and 47.96 mg kg⁻¹ both in Chicken bone. The average

value of K and Ca was recorded 21.84 mg kg⁻¹ and 18.96 mg kg⁻¹ respectively in the present study which is acceptable according to the safe limit of 100 mg kg⁻¹ WHO and EU [Fig 1].

Table 3 and Table 5 indicates, there is a significant variation (P<0.05) in metal concentration in all fish feed ingredients as P-value is lower than α value (0.05) except for the recorded concentration of Ni, Cu and Ca. Besides, the present study also found that F-critical values were lower than F-value which also indicated that there was significant variation in the concentration of Pb, Cd, Cr, Fe, Zn, Na and K. In contrast, P-value is higher than α value (0.05) and F-critical value is higher than F value in the concentration of Ni, Cu and Ca.

Table 6. Pearson correlation coefficient of selected metals in fish feed ingredients

	Pb	Cd	Cr	Ni	Fe	Cu	Zn	Na	K	Ca
Pb	1									
Cd	0.27	1								
Cr	0.50*	0.32	1							
Ni	0.14	-0.31	-0.27	1						
Fe	0.18	0.24	0.65*	0.17	1					
Cu	0.50*	-0.14	0.37	0.43	0.65*	1				
Zn	0.01	-0.08	-0.01	0.60*	0.36	0.51*	1			
Na	-0.15	-0.15	-0.06	0.33	-0.52	-0.58	0.62*	1		
K	-0.30	0.11	-0.73	0.06	-0.44	-0.26	0.16	0.37	1	
Ca	0.59*	0.57*	0.52*	-0.13	0.36	0.52*	0.02	0.03	-0.16	1

The Pearson Correlation Coefficient in the present study is used to describe the interrelationships between the elements analyzed at a level of > 0.5 or < -0.5 which are significantly correlated. Table 6 summarizes a high positive correlation between Pb-Cr (0.50), Pb- Ca (0.59) and Fe-Cu (0.65) which indicates a similar source of these metals in fish feed ingredients. The correlation between Pb-Cu, Cd-Ca, Cr-Fe, Ni-Zn, Zn-Na were above 0.5 and positively correlated. In Contrast, Cr-K, Fe-Na and Cu-Na are weakly correlated as their values were less than -0.5.

4. CONCLUSIONS

Overall, the total mean toxic and essential metal concentration of all fish feed ingredients in this study revealed an order of Ni>Pb>Cr>Cd>As, Hg and Na>Fe>K>Zn>Ca>Cu. A significant amount of all selected metals was assessed in different fish feed ingredients in this study. However, the recorded result revealed that the concentration of Pb, Cd, Cr, As, Hg, Ni, Fe, Cu, Zn, Na, K, Ca in the selected fish feed ingredients was within the permissible limit of WHO/FAO and EU and indicating no risk for fish cultivation as well as for human health in future. This study recorded that there was significant variation (P<0.05) in metal concentration in each fish feed ingredients. Since it is impossible to completely eliminate the presence of undesirable contaminant due to the environment so, regular training and enlightenment programs should be given to farmers, feed producers on the need for proper storage and handling of fish feed ingredients as these will reduce or preventing where possible the level of toxic metals in feed ingredients, fish and human the ultimate consumer. Policymakers, food regulator authority, farm owners can take initiative to check the quality and origin of ingredients which will use to manufacture the commercial feeds for fish cultivation in Bangladesh.

ACKNOWLEDGMENTS

The authors would like to acknowledge Institute of Leather Engineering and Technology, University of Dhaka, Bangladesh for the technical support to conduct this research. There is no conflict of interest among the authors.

REFERENCES

- [1]. P.R. Das, M.K. Hossain, B.S. Sarker, A. Parvin, S.S. Das, M. Moniruzzaman and B. Saha, "Heavy Metals in Farm Sediments, Feeds and Bioaccumulation of Some Selected Heavy Metals in Various Tissues of Farmed Pangasius hypophthalmus in Bangladesh," *Fisheries and Aquaculture Journal*, Vol. 8, pp. 1-8, 2017.
- [2]. FRSS, Fisheries resources survey system (FRSS). Fisheries statistical report of Bangladesh: Department of Fisheries, pp. 1-57, 2015.
- [3]. J. Tariq, M. Ashraf and M. Afzal, "Pollution status of the Indus River, Pakistan, through heavy metal and macronutrient contents of fish, sediment and water," *Water Research*, Vol. 30, pp. 1337-1344, 1996.
- [4]. M.S. Islam, M. Azizul and M.M. Hossain, "Propagation of Heavy Metals in Poultry Feed Production in Bangladesh," *Bangladesh Journal of Science*, Vol. 42, pp. 465-474, 2007.
- [5]. B. Saha, M.A. Mottalib and A.N.M Al-Razee, "Assessment of selected heavy metals concentration in different brands of fish feed available in Bangladesh," *Journal Bangladesh Academy of Science*, Vol. 42, pp. 207-210, 2018.
- [6]. B. Gumgum, E. Unlu, Z. Tez and Z. Gulsun, "Heavy metal pollution in water, sediment and fish from the Tigris River in Turkey," *Chemosphere*, Vol. 1, pp. 290, 1994.
- [7]. A. Bahar, Yilmaz, Mustafa, K. Sangun, D. Yaglioglu and C. Turan, "Metals major, essential to non-essential composition of the different tissues of

- three demersal fish species from Iskenderun Bay, Turkey," *Food Chemistry*, Vol. 123, pp. 410-415, 2015.
- [8]. G.M. Kundu, M. Alauddin, M.S. Akter, M.S. Khan and M.M. Islam, "Metal contamination of commercial fish feed and quality aspects of farmed tilapia (*Oreochromis niloticus*) in Bangladesh," *BioResearch communications*, Vol. 3, pp. 345-353, 2017.
- [9]. I. Sen, A. Shandil and V. Shrivastava, "Study for determination of heavy metals in fish species of the river Yamuna (Delhi) by inductively coupled plasma-optical emission spectroscopy (ICP-OES)," *Advances in Applied Science Research*, Vol. 2, pp. 161-166, 2011.
- [10]. C.A. Adeniji and O.O. Okedeyi, "Preliminary Assessment of Heavy Metal Concentrations in Selected Fish Feed Ingredients in Nigeria," *Journal of Fisheries & Livestock Production*, Vol. 5, pp. 1-4, 2017.
- [11]. P. Kotz, H.H. Preez and J.H. Vuren, "Bioaccumulation of copper and zinc in *Oreochromis mossambicus* and *Clarias gariepinus*, from the Olifants River, Mpumalanga, South Africa," *Water SA*, Vol. 25, pp. 99-110, 1999.
- [12]. S.E. Abalaka, S.I. Enem, I.S. Idoko, N.A. Sani, O.Z. Tenuche, S.A. Ejeh and W.K. Sambo, "Heavy Metals Bioaccumulation and Health Risks with Associated Histopathological Changes in *Clarias gariepinus* from the Kado Fish Market, Abuja, Nigeria," *Journal of Health and Pollution*, Vol. 7, pp. 66-72, 2017.
- [13]. J.O. Duruibe, M.O.C. Gwuegbu and J.N. Egwurugwu, "Heavy metal pollution and human biotoxic effects," *International Journal of Physical Sciences*, Vol. 2, pp. 112-118, 2007.
- [14]. P.B. Tchounwou, B.A. Wilson, A.A. Abdelghani, A.B. Ishaque, A.K. Patlolla, "Differential cytotoxicity and gene expression in human liver carcinoma (HepG2) cells exposed to arsenic trioxide and monosodium acid methanearsonate (MSMA)," *International Journal of Molecular Sciences*, Vol. 3, pp. 1117-1132, 2002.
- [15]. D. McCluggage, "Heavy metal poisoning," Colorado, USA: NCS Magazine.
- [16]. M.A. Mottalib, G. Zilani, T.I. Suman, T. Ahmed and S. Islam, "Assessment of trace metals in consumer chickens in Bangladesh," *Journal of Health and Pollution*, Vol. 8, pp. 1-10, 2018.
- [17]. L. Prashanth, K.K. Kattapagari, R.T. Chitturi, V.R. Baddam and L.K. Prasad, "A review on role of essential trace elements in health and disease," *Journal of NTR University of Health Science*, Vol. 4, pp. 75-85, 2015.
- [18]. J.K. Chester, "Trace element-gene interaction with particular reference to zinc," *Proceedings of the Nutrition Society*, Vol. 50, pp. 123-129, 1991.
- [19]. D.A. Davis and D.M. Gatlin, "Dietary mineral requirement of fish and marine crustaceans," *Review in Fisheries Science*, Vol. 4, pp. 75-99, 1996.
- [20]. M. Constantin and I. Alexandru, "The role of sodium in the body," *Balneo- Research Journal*, Vol. 2, pp. 71-74, 2011.
- [21]. J.D. Cohen, J.D. Neaton, R.J. Prineas and K.A. Diuretics, "Serum potassium and ventricular arrhythmias in the Multiple Risk Factor Intervention Trial," *The American Journal of Cardiology*, Vol. 60, pp. 548-554, 2005
- [22]. Y.S. Choi, H. Joung and J. Kim, "Evidence for revising calcium dietary reference intakes (DRIs) for Korean elderly," *FASEB Journal*, Vol. 27, pp. 1065, 2013.
- [23]. H. Ali and E. Khan, "Environmental Chemistry and Ecotoxicology of Hazardous Heavy Metals: Environmental Persistence, Toxicity, and Bioaccumulation," *Journal of Chemistry*, pp. 1-14, 2019.
- [24]. R.U. Khan, S. Naz, K. Dhama, M. Saminathan and R. Tiwari, "Modes of action and beneficial applications of chromium in poultry nutrition, production and health: A review," *International Journal of Pharmacology*, Vol. 10, pp. 357-367, 2014.
- [25]. WHO, The world health report: reducing risks, promoting healthy life, World Health Organization, 2002. <https://apps.who.int/iris/handle/10665/42510>
- [26]. S.E. Allen, H.E. Grimshaw and A.P. Rowland, "Chemical Analysis. In: Moore PD, Chapman SB (eds) *Methods in Plant ecology*," Blackwell Scientific Publication, Oxford, pp. 285-344, 1986.
- [27]. M.S. Ahmed, M.M.B. Hasan, M.A. Mottalib, M.N. Alam. and M. Khan, "Translocation of heavy metals from industry into vegetables and crops through water and soil of Mokesh Beel in Bangladesh and their Impact on Human Body," *IOSR Journal of Environmental Science, Toxicology and Food Technology*, Vol. 13, pp. 59-7, 2019.
- [28]. Evaluation of certain food additives and contaminants mercury, lead and cadmium, Joint FAO/WHO Expert Committee on Food Additives. *World Health Organization Technical Report Series*, Vol. 505, pp. 1-32, 2004.
- [29]. Council of the European Union, "Council directive 98/83/EC on the quality of water intended for human consumption," *J Eur Communities*, Vol. 41, pp. 34-54, 2014. <http://eur-lex.europa.eu/legal-content/EN/ALL/?uri=CELEX:31998L0083>
- [30]. D. Alexieva, S. Chobanova, A. Ilchev, "Study on the level of heavy metal contamination in feed materials and compound feed for pigs and poultry in Bulgaria," *Trakia Journal of Sciences*, Vol. 5, pp. 61-66, 2007.
- [31]. M.S. Islam, M.K. Ahmed, M.H.M. Mamun and M. Raknuzzaman, "The concentration, source and potential human health risk of heavy metals in the commonly consumed foods in Bangladesh," *Ecotoxicology and Environmental Safety*, Vol. 122, pp. 462-469, 2015.
- [32]. FAO, 2016, Compilation of legal limits for hazardous substances in fish and fishery

- products, FAO Fisheries Circular No. 764, Food and Agricultural Organization of the United Nations, Rome, pp. 102.
- [33]. P.K. Roy, S.S. Lee, M. Zhang, Y.F. Tsang and K.H. Kim, "Heavy metals in food crops: Health risks, fate, mechanisms, and management," *Environment International*, Vol. 125, pp. 365-385, 2019.
- [34]. S.E. Godfred and M.J. Napoleon, "An Emmanuel. Bioaccumulation of heavy metals concentration in some selected cereals grown near illegal mine Sites at Poyentanga in Wa of the Upper West Region, Ghana," *American Journal of Environmental Science & Technology*, Vol. 4, pp. 1-15, 2020.



RESEARCH ARTICLE

Spatiotemporal modeling of nutrient retention in a tropical semi-arid basin

Saheed A. Raji^{1,2,*}, Shakirudeen Odunuga², Mayowa Fasona²

¹ Federal University of Petroleum Resources Effurun, Department of Environmental Management and Toxicology, NIGERIA

² University of Lagos, Department of Geography, Akoka-Yaba, Lagos, NIGERIA

ABSTRACT

The Sokoto-Rima basin defines the natural and socioeconomic lifeblood of northwestern Nigeria. Its agrarian nature is an indication of significant dependence on the supply of ecosystem services from its various rivers, streams, and wetlands. However, nitrogen (N) and phosphorus (P) constitute a great portion of chemical fertilizers used to enhance crop yields and poor management of these portend great threats for water quality. The overarching objective of this study was to examine the extent of spatial variation of nutrient dynamics in the Sokoto-Rima basin between 1992 and 2015 using the nutrient delivery ratio (NDR) model of InVEST (Integrated Valuation of Ecosystem Service and Tradeoffs) software. Land use/landcover, precipitation, digital elevation, and biophysical variables were the principal datasets employed as model input. The result of the study showed that the surficial N load is almost 15-fold of P in the Sokoto-Rima basin. Over the period of study, cultivated areas and rivers were spatially detected as nutrient sources and sinks respectively. The subsurface nutrient load is dominated by P while the amount of N load is insignificant. The trend of nutrient export is linearly defined: with 0.87% and 1.7% increase in N and P export respectively during 1992-2015. N and P exports vary spatially with a north-south increase-decrease index. Critical length and threshold are highly sensitive to changes in the parameterization of the NDR model. Thus, synergistic cultivation practices such as agroforestry should be extended to existing crop cultivation complexes to curtail nutrient enrichment in the Sokoto-Rima basin and ensure environmental sustainability.

Keywords: Ecosystem services, InVEST, nutrient modeling, semi-arid, Sokoto-Rima basin, spatial variation.

1. INTRODUCTION

One of the numerous ways in which anthropogenic activities alter the natural nutrient cycling of any ecosystem is through land use/landcover changes particularly agricultural expansion [1-2]. The nutrient flow is a vital ecosystem service that controls ecosystem integrity. Any change in the pattern of land use/landcover can disrupt this natural pathway leading to distortions in ecosystem functioning and intactness [4-6]. The non-point sources of nutrient discharge from domestic and agricultural activities constitute a high proportion of human-induced distortions to the natural nutrient flow in any ecosystem [3, 7]. Within tropical systems, particularly in semi-arid areas of the world where agriculture determines the lifeblood of the local economy, this scenario persists. In such agrarian systems, rainwater flows over the landscape washing away natural soil

minerals, animal manure, chemical fertilizers and wastes from domestic sources into abutting streams and rivers [8]. This causes great threat to both human health and welfare [9] as well as aquatic life in the water bodies. Further, it triggers eutrophication of the bodies and general aquatic pollution [10, 11].

Series of measures have been enumerated in literature towards amending this phenomenon. Naturally, vegetated ecosystems can remove pollutants via photosynthetic uptake, tissue storage or via nutrient-fixation mechanisms [12, 13]. Non-polluted soil and wetlands also provide suitable pollution-mitigation by stimulating nutrient storage prior to in-washing into proximate hydrological systems [13-15]. However, in the engagement of pollution control measures within agrarian milieu, nutrient loads are often assessed by estimating the proportion of specific nutrients that are present within identifiable non-point sources across the

Corresponding Author: raji.saheed@fupre.edu.ng (Saheed A. Raji)

Received 19 August 2020; Received in revised form 22 December 2020; Accepted 25 December 2020

Available Online 28 December 2020

Doi: <https://doi.org/10.35208/ert.782409>

© Yildiz Technical University, Environmental Engineering Department. All rights reserved.

landscape [3-4, 8-9]. Two of the most common pollutants in virtually any landscape is nitrogen (N) and phosphorus (P) from different environmental sources [12-14]. N and P impact within cultivated systems are circularly causal. N fixation processes in plants are often boosted by P in certain semi-arid crops thereby increasing level of harvest. Studies across the global semi-arid basins suggest that N and P driven nutrient load exist in higher proportion within cultivated areas than any other land use/landcover classes [13-14]. For instance, Meng et al. [12], stated that 68% of the pollutants within the agricultural region of Fenhe River are N compounds. Hobbie et al. [16], conducted a study across the extensive terrestrial ecosystem of the Mississippi River in the Capitol Region Watershed (CRW) of the United States, and results showed that 22-80% of net N and P inputs from cultivated regions were retained in the basin while the difference was washed downstream. Further, Hahm et al. [15] asserted that semi-arid areas tend to erode nutrients more than forested regions, thus eutrophication and nutrient-filled hydrological bodies subsist downstream.

Geochemical characterisation of semi-arid water bodies such as lakes, streams and rivers have been studied showing heavy nutrient loads with little or no focus on retention capacities [3, 5, 6, 8, 10]. For instance, Adimalla and Venkatayogi [10] stressed that semi-arid soils of the Basara region of India have been polluted by nitrates and phosphates with grave consequences on water users. In addition, Meng et al. [12] asserted that sediment characteristics of agrarian landscapes of the Shanxi Province of China showed that the natural traits of the river systems. Within the context of Nigeria, studies such as [14, 17-20] suggest that the country is not invulnerable to the realities of this problem particularly to water quality and river eutrophication.

Literature has shown that the surface and groundwater quality of the Sokoto-Rima basin has been altered by series of human activities. This has been attributed to industrial effluent discharge into streams [18, 19], and soil enrichment sources [14, 18, 20, 21]. Magami and Sani [14] used the point-based sample collection method to analyse the temporal variations of N and P of Kware Lake with respect to proximate human activities and the result showed that the N and P varies directly with human-induced sedimentation of the freshwater ecosystem. Equally, Raji et al. [18] analysed physicochemical parameters of water samples of the Sokoto River to determine seasonal variations of its water quality. The result showed that the planting season distressed the aggregated physical properties of the river. Adelana et al. [20] examined surface water and groundwater characterisation of the Sokoto-Rima basin with respect to isotopic and geochemical traits, and the outcome of the study showed that low nutrient loads of the identified soil groups varies proportionately with places of intense cultivation. Abubakar and Ipinjolu [21] investigated the level of certain anions of the Argungu River using direct analysis method, and the results showed that the river low pollution status of the nutrient loads were detected in areas of less human disturbance.

In these previous studies on the Sokoto-Rima basin, not much attention has been given to the nutrient cycling and flow which are vital ecosystem services [1-2, 11]. This lacuna has also restricted the identification of key locations of nutrient sources and sinks thus making environmental management of the nutrient cycling difficult. In this study, an attempt is made to narrow these gaps spatially characterising the nutrient delivery pathway of the Sokoto-Rima basin using the Nutrient Delivery Ratio model of InVEST software. This model is generates output of N and P across the landscape via geographic information system (GIS) approach. This approach consequently provides a spatial visualization and variation of the nutrient flow of the Sokoto-Rima basin. Findings of this study can provide a scientific reference for spatiotemporal assessment of nutrient pathway for the semi-arid region of West Africa.

2. MATERIALS AND METHODS

2.1. The study area

The study was conducted in the Nigerian section of the West African transnational hydrological basin known as Sokoto-Rima basin. It is bounded in the north by Niger Republic, and in the west by Benin Republic while in the east and south by Katsina and Niger States of Nigeria. Its geographical location is defined by Latitudes 10°32'35" N to 13°32'55" N and Longitudes 3°30'30" E to 8°1'15" E and the total land area is 94,026.5 km² (Fig. 1). The semi-arid climate of tropical savanna of West Africa dictates the environmental condition of the study area. Precipitation (mostly rainfall) is typically seasonal, quasi-monsoonal in nature; confined to the wet season. Annual rainfall ranges between 350 mm to 895 mm in the northern and southern ends typifying a north-south rainfall increase index. Through the year, diurnal temperature averages 300 C with significant seasonal variability. Vital to nutrient flow is the hydrological network which flows westwards from the eastern highlands and ends southwards into the River Niger. The rock typology is dominated by the basement complex that is spatially restricted to the east. The sedimentary basin of the central and southern axis is activated by the hydrologic and hydraulic activities of the Sokoto and Rima Rivers with several spots of rolling hills (Fig. 1). The population of the Sokoto-Rima basin exemplifies that of an agrarian landscape with low density. According to the National Population Commission of Nigeria, the population of the study area was 6,538,666 in 1991, it increased to 10,238,090 by 2006 with a resultant annual growth rate of 3.11% [27]. The population figure is projected to rise to 15,719,183 by the year 2020 with population density of 167.18 persons per square kilometre. Small-scale and climate-dependent agriculture is the mainstay of the Sokoto-Rima basin. Major crops grown include rice, tomatoes, sorghum, maize, and millet. Others such as soybeans, cowpea and peanuts which are nutrient-fixing crops were cultivated in subsistence scale.

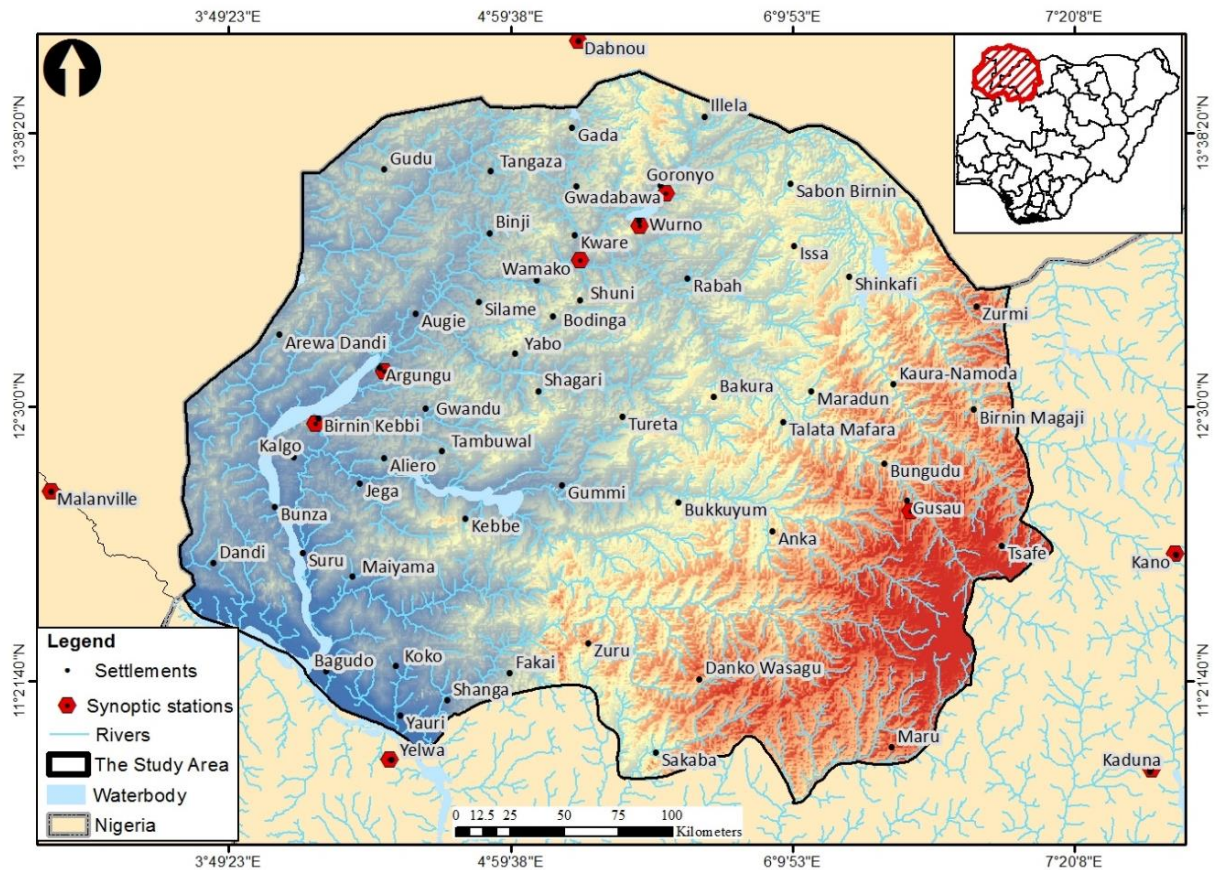


Fig 1. Geographical location of the Sokoto-Rima basin in context of northwestern part of Nigeria with the hydrological network and relief

2.2. Data sources

The land use/landcover data from the Climate Change Initiative (CCI) of the European Space Agency (ESA) was used as data spine for land use/landcover characterization of the study. The pre-classified data has 300 metres spatial resolution with auto-rectified benefits nullifying further image registration and rectification tasks. It has a dynamic range of 32-bit which is wide enough for detection of homogenous land use/landcover classes. It also has regional coverage thus preventing edge-matching errors and continuous phenomenal assessment; an advantage it possesses over existing remotely sensed data sources such as Landsat and Sentinel. Data for the years 1992, 2002, 2012, and 2015 were sourced based on availability at <http://maps.elie.ucl.ac.be/CCI/viewer/profiles.php>.

Nutrient runoff proxy data was based on mean annual rainfall which acquired from climate synoptic stations within and outside the basin to permit proximate geographic coverage. The data were acquired from Sokoto, Yelwa, Birnin Kebbi, Argungu, Gusau, Goronyo, Wurno, Kano, and Kaduna in Nigeria and Malanville in Benin Republic and Niger Dabnou in Niger. Data for the years 1992, 2002, 2012 and 2015 were to match the previously explained landuse/landcover datasets extracted for the study. Data within the Nigerian territory was acquired from the Nigerian Meteorological Agency (NIMET) of Nigeria additional datasets for Benin (Malanville) and Niger (Dabnou) were sourced from Princeton University's Climate

Analytics (PCA) web-portal via https://platform.princetonclimate.com/PCA_Platform/.

Digital Elevation Model (DEM) data was extracted from the West African grid of the ALOS World 3D Digital Surface Model (DSM) version 2.2 data obtained from the digital libraries of Japan Aerospace Exploration Agency (JAXA) through <https://www.eorc.jaxa.jp/>. The data has a 30-metre spatial resolution and a 32-bit quantisation resolution which is sufficient for feature detection consistency.

2.3. Quantifying nutrient retention

The Nutrient Delivery Ratio (NDR) model, an integrated module of the InVEST (Integrated Valuation of Ecosystem Services and Tradeoffs) software package, was employed to spatiotemporally quantify nutrient (nitrogen and phosphorus) retention. InVEST is a free and open-source software package with extensive utility for modeling and assessing diverse ecosystem services principally based on land use/landcover dynamics in conjunction with other environmental variables [1, 11]. The NDR model employs a mass-balance approach to spatially simulate the flow of N and P as influenced by the inherent natural vegetation and other nutrient constraining and stimulating factors. The outcome of the model generates raster datasets that with spatial information about nutrient loads (nutrient sources), exports, and the actual NDR for each of N and P. Data inputs into the NDR model include the prior described data on DEM, land use/landcover, and nutrient runoff.

The associated biophysical parameters are classified into tabulated data which include nutrient loads, retention efficiency, and subsurface proportion for N and P respectively (see Table 1). The software default value of 2.4 for Borselli *K* parameter (calibration

function between hydrologic and sediment flow) was retained while threshold flow accumulation value was set at 10,000 which corresponds to 300 m data resolution. Three outputs were thus modeled from the NDR simulation.

Table 1. Land use/landcover based biophysical variables used for nutrient modeling

Land use/Landcover description	Load (N)	Efficiency (N)	Critical length (N)	Proportion subsurface (N)	Load (P)	Efficiency (P)	Critical length (P)	Proportion subsurface (P)
Cropland	89	0.5	25	0.3	3.57	0.48	15	0.01
Agroforestry	89	0.6	50	0.25	2.48	0.54	15	0
Shrubland	8	0.75	150	0.47	0.93	0.6	25	0
Grassland	8	0.75	150	0.47	0.93	0.6	30	0
Waterbody	2	0.05	10	0.66	0	0.4	15	0
Settlements	10	0.1	10	0.2	2.1	0.26	15	0
Bare surface	5	0.01	10	0.47	0.79	0.26	15	0
Woodland	2.8	0.8	300	0.47	1.4	0.67	20	0

Adapted from [3, 11, 22]

Surface NDR concentrates on the surficial traits of the basin defined by the multiplication delivery factor (downstream nutrient transportation excluding retention) and topographic position of the landscape. Mathematically, this is expressed as:

$$NDR_l = NDR_{0,l} \left(1 + \exp \left(\frac{IC_i - IC_0}{k} \right) \right)^{-1} \quad (1)$$

where: IC_0 and k are calibration parameters, IC_i is topographic index computed from the DEM data, and $NDR_{0,l}$ is the ratio of retained nutrient by pixels downstream the landscape of the basin.

Subsurface NDR which is the second output is based on geographic function of distance decay or the first law of geography which states that closer events are spatially connected than distant events. The subsurface NDR relates with distance to stream and the utmost subsurface nutrient holding and it is defined in equation (2) as:

$$NDR_{subs,1} = 1 - eff_{subs} \left(1 - e^{\frac{-5.l}{l_{subs}}} \right) \quad (2)$$

where: eff_{subs} is the maximum retention efficiency traceable through the subsurface pathway in the multispectral space (retention as a function of biochemical degradation in soils), l_{subs} is the subsurface flow retention length detected at soil maximum capacity (that is the space after which it can be implicit that soil retains nutrient at its maximum capacity), l_i is the distance from the pixel to the stream.

Nutrient export from a given multispectral location is a function of the nutrient load and the NDR, this is further explained in equation (3) as:

$$x_{exp_i} = load_{surf,1} (NDR_{surf,i} + load_{subs,i}) NDR_{subs,i} \quad (3)$$

At the basin level, equation (3) aggregates all the pixels within the multispectral space to give:

$$x_{exp_{tot}} = \sum_i x_{exp_i} \quad (4)$$

where: $load_{surf,1}$ is the surface load at the first pixel, and $NDR_{surf,i}$, $load_{subs,i}$ and $NDR_{subs,i}$ is surface NDR, subsurface nutrient load and subsurface NDR loads respectively while x_{exp_i} is the specific nutrient export, aggregate of which generates the $x_{exp_{tot}}$.

2.4. Sensitivity analysis and uncertainties of the nutrient export

As a test of model performance, sensitivity analysis, was conducted on crucial NDR model parameters particularly on critical length, threshold flow accumulation, Borselli *k* value, load and efficiency functions of each of the land use/landcover classes. This was performed by increasing and decreasing parameter values by 50%, precisely: Borselli *k* parameter varied from the default of 2.4, to 1.2 and 4.8, the critical length was varied from the default value of 90 metres to 45 metres and 180 metres while the threshold flow accumulation was varied from 10,000 (default) to 5,000 and 20,000. The load and efficiency values stated in Table 1 were adjusted $\pm 50\%$ for each of the land use/landcover values.

3. RESULTS AND DISCUSSION

3.1. Nature and dynamics of surface nutrient load of the Sokoto-Rima Basin

Surficial nutrient loads of the Sokoto-Rima basin as defined by the temporal distribution of N and P is displayed in Fig 2. During the period of study, N rose from 1992, peaked in 2012 and plunged slightly in 2015. This shows a linear relation with increasing

mean annual load of 5,667 tonnes increasing at 9.56 tonnes per year. Over the period of assessment, surficial N load increased from 51,736 million tonnes to 513,070 million tonnes.

Spatially, Fig. 3 shows that high N loads of roughly 8.22 kg per kilometre were directly connected to headwaters of the Sokoto-Rima basin throughout the years. The outline of these major water bodies shows that they contribute the least amount of surficial N loads. The baseline year (1992) showed that tributaries of these river networks in the eastern and

northern axis conduit high N loads downstream. In addition, wetlands of the southern axis which were mainly lowlands constitute the highest N loads. By 2002, areas of high N loads were observed in part of central areas with roughly 50% increase in N load while other areas remain unchanged. This observation changed slightly as notable spatial N loads were detected around wetlands close to the major rivers as well as wetlands in the east. By 2015, slight changes were detected.

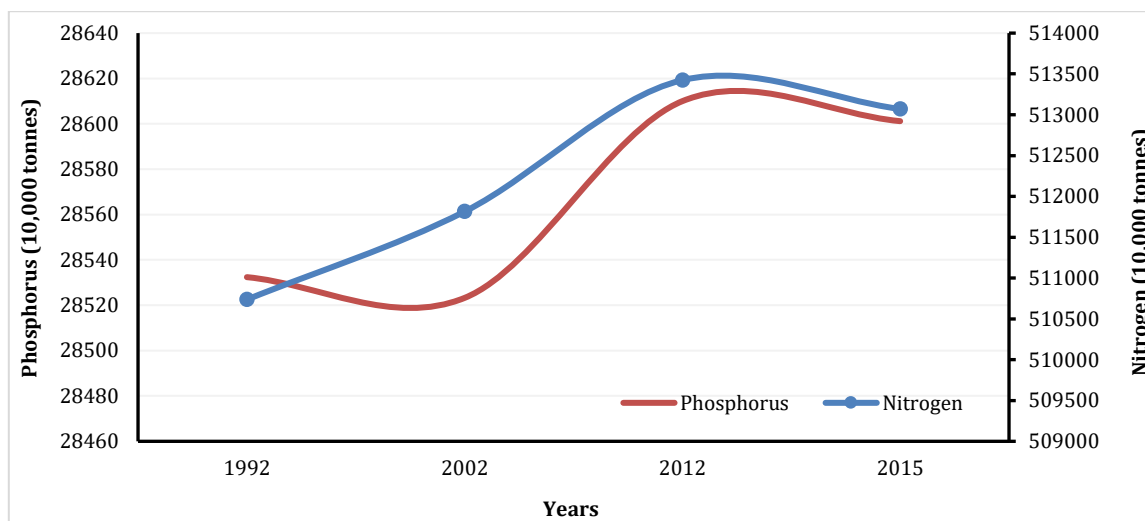


Fig 2. Temporal trend of surface loads of nitrogen and phosphorus of the Sokoto-Rima basin

Surficial P load within the Sokoto-Rima basin increased annually with a mean annual load of 26,103 tonnes per unit area, increasing at a rate of 32 tonnes for every kilometre (Fig 2). Precisely, the baseline value of 28,532 million tonnes increased to 28,601 million tonnes. Its semi-sinusoidal curve pattern showed the level of consumption and the extent of land use/landcover of the Sokoto-Rima basin, an area that is dominated by crop production.

Changes in spatial distribution of surficial P load showed a pattern that is similar to that of N where headwaters of the major streams that define the basin were detected as major sources (Fig 4). On the eastern axis where most of the rivers takes their source accounts for over 70% of the 5.86 million tonnes per km² of P. Areas at the lowest range of P with roughly 0.89 million tonnes are directly proportional to areas of high intense crop cultivation.

These results concurred with the findings of [14, 18 and 20]. Explicitly, [14] claimed that low quantities of nitrate, nitrite, and ammonia (derivatives of N) and orthophosphates in Kware Lake was an indication of fitness of the surface water for multipurpose uses especially during the dry season. [18] stated that seasonal variation of N and P in surface water of the Sokoto River lies between 1.77 mg L⁻¹ and 19.7 mg/litre which is suitable for crop cultivation. [20] indicated that the isotopic classification of the surface waters of the Sokoto-Rima basin in Group IV and V were directly proportional to rainfall input. These suggest that both N and P contribute significantly to

the nature, trend and spatial dynamics of nutrient exchanges within the Sokoto-Rima basin. The results also show further the influence of land use/landcover on the spatial pathway of these nutrients particularly within a low density cultivated semi-arid ecosystem such as the Sokoto-Rima basin.

3.2. Nature and Dynamics of Subsurface Nutrient Load of the Sokoto-Rima Basin

The outcome of subsurface nutrient load returned contrasting results as spatiotemporal dynamics returned differing characterization for each of N and P. First, subsurface load of N in the Sokoto-Rima basin returned no value indicating no retention at this level. This is consistent with the deductions of [22 and 14] who affirmed that N is substantially retained at the surface as a crucial nutrient aiding crop productivity of the semi-arid zone of northern Nigeria. These have been further asserted by [8, 10] in China and India respectively where geochemical analysis of derivatives of N yielded paltry belowground outcomes.

According to [23] accumulated study of P over the centuries has shown a direct correlation with human activities and its impacts on freshwater eutrophication in China. This shows that there are latent chances of subsurface trend of P in an agrarian milieu such as the Sokoto-Rima basin. Fig 5 showed that that P load increased from 2,128.7 million tonnes in 1992 to 2,150.5 million tonnes in 2015, 0.36%

increase with a difference of 7.62 million tonnes. Despite this trend, no spatial variation of subsurface P

was detected an evidence of strong surface load forcing.

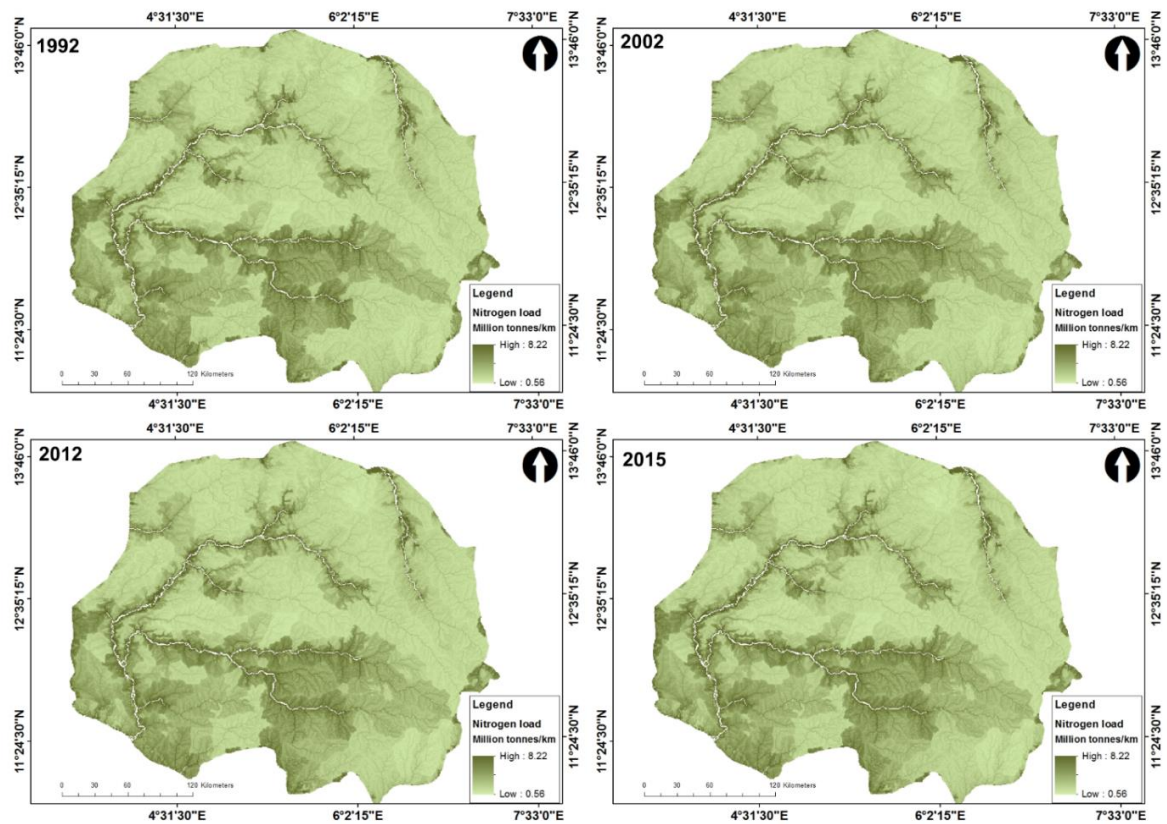


Fig 3. Spatial distribution of surficial nitrogen load in the Sokoto-Rima basin for the years 1992, 2002, 2012 and 2015

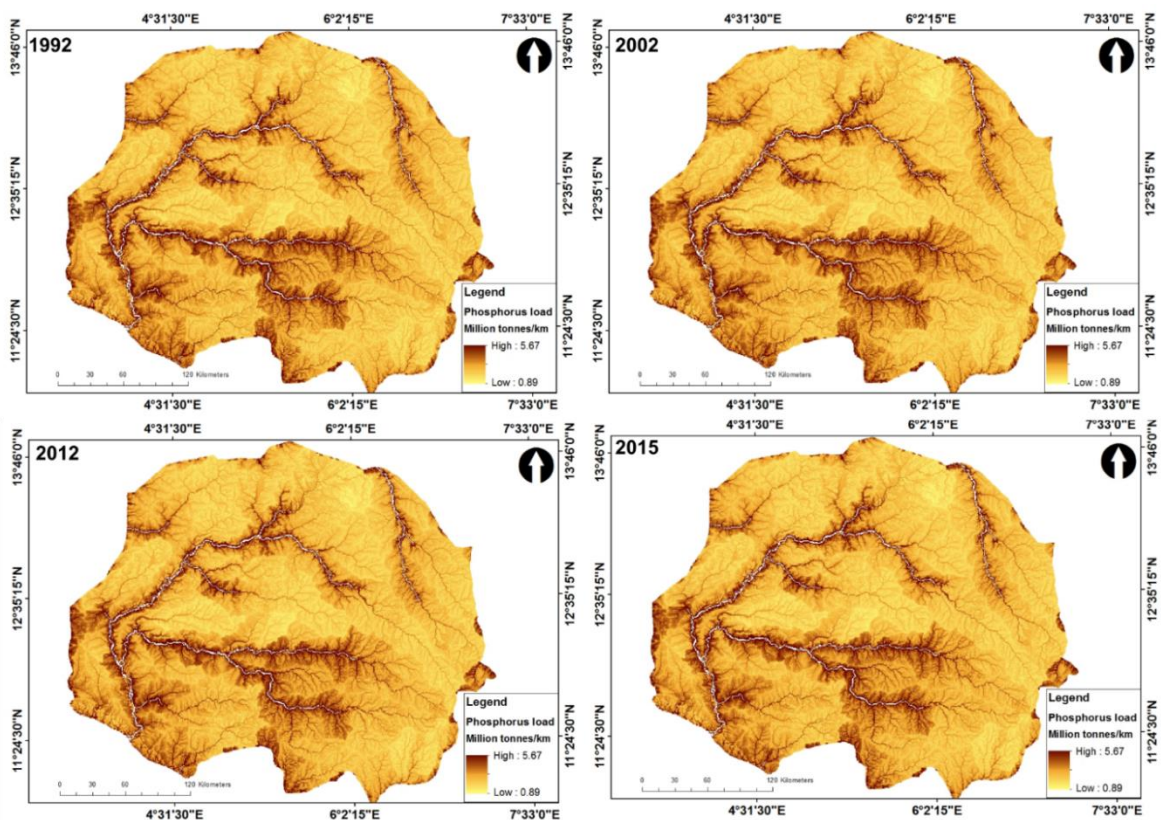


Fig 4. Spatial distribution of surficial phosphorus load in the Sokoto-Rima basin for the years 1992, 2002, 2012 and 2015

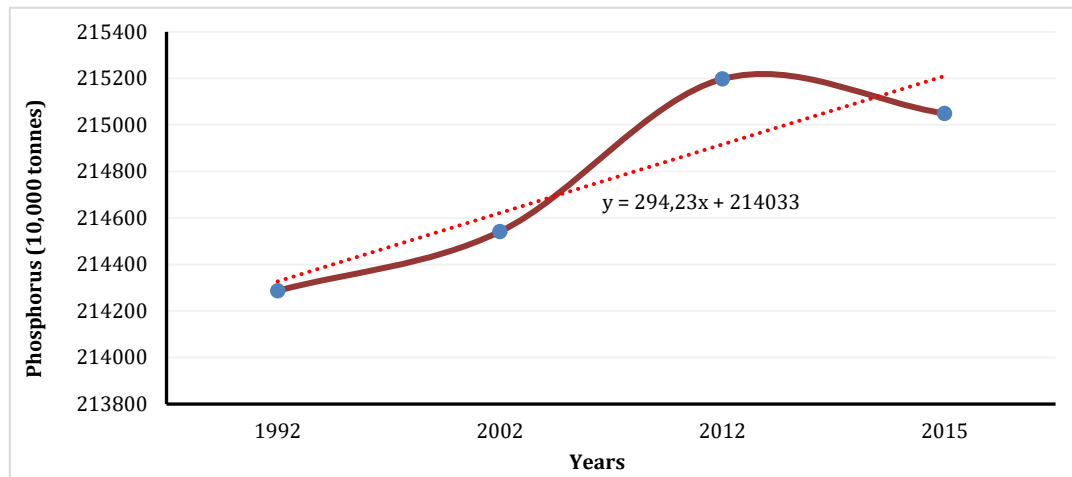


Fig 5. Trend of subsurface phosphorus load of the Sokoto-Rima basin from 1992 to 2015

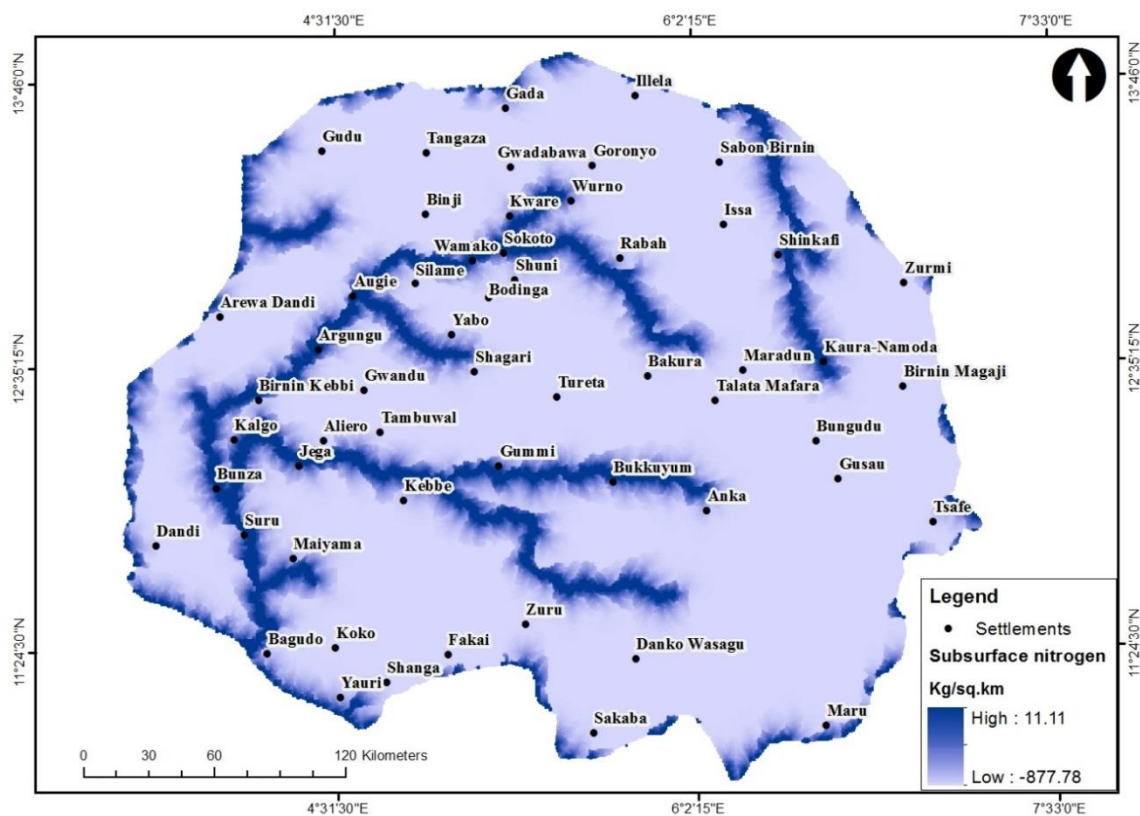


Fig 6. Spatial distribution of subsurface nitrogen loads of Sokoto-Rima basin (1992-2015)

Within the time of this study, no specific spatial variation was detected in the amount of subsurface N loads in the Sokoto-Rima basin, hence the extent of spatial distribution for the year 1992 returned the same as 2015. However, Fig 6 showed that subsurface N loads were spatially restricted to water bodies – rivers, streams and freshwater lakes, with highest values 11.11 kg km⁻². This was followed by the adjoining wetlands with 1.09 kg km⁻². Largely, subsurface N loads were unswervingly influenced by water-bearing land use/landcover classes. This is because N is a vital chemical component of aquatic ecosystems as it contributes extensively to the growth and sustenance of aquatic organisms as part of their

essential feedstock, which is a vital ecosystem service [6, 12]. The deficit range of loads observed in the other areas can be attributed to high uptake of the nutrient as discerned by crop consumption rates [13, 16 22].

3.3. Trend of nutrient export in the Sokoto-Rima Basin

3.3.1. Temporal dynamics of nutrient export

It has been established that nutrient export contributed to the increasing evidence of

eutrophication and sedimentation within freshwater bodies of the Sokoto-Rima basin particularly Lake Kware [14]. It was also noted that N export accounted for over 65% of the nutrient yields observed in the lake [14]. This could be directly associated with increasing intensity of economic and social activities which has resulted in adjustments of the previous natural conditions of the area. Cumulative cultivation of crops and animal husbandry around the lowlands, wetlands and upland areas have led to introduction of nutrients such as fertilizers, herbicides, pesticides, and others in the Sokoto-Rima basin [19-21].

Over the course of this study, N export outweighs P as shown in Table 2 despite the low rate of increase. The magnitude of change showed that from 1992 to 2015, N export increase slightly by 0.87%, compared to 0.65% in 2002, and 0.92% in 2012. A similar pattern was detected for P with 1.7% increase. This observed trend could be traced to the influence of previously acknowledged human activities.

Table 2. Nitrogen and phosphorus export in 1992, 2002, 2012, and 2015

Year	Nutrient export (’000 ton)		Percentage change from baseline	
	Nitrogen	Phosphorus	Nitrogen export	Phosphorus export
1992	15,179.64	4.59	-	-
2002	15,278.19	4.62	0.65	0.74
2012	15,319.76	4.66	0.92	1.70
2015	15,311.09	4.66	0.87	1.70

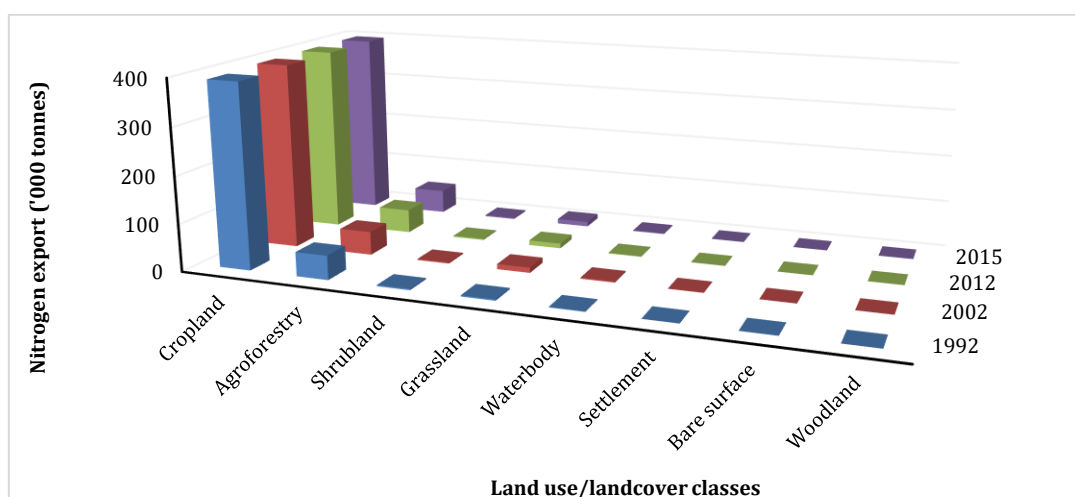


Fig 7. N export of the Sokoto-Rima across the different land use/landcover classes from 1992 to 2015

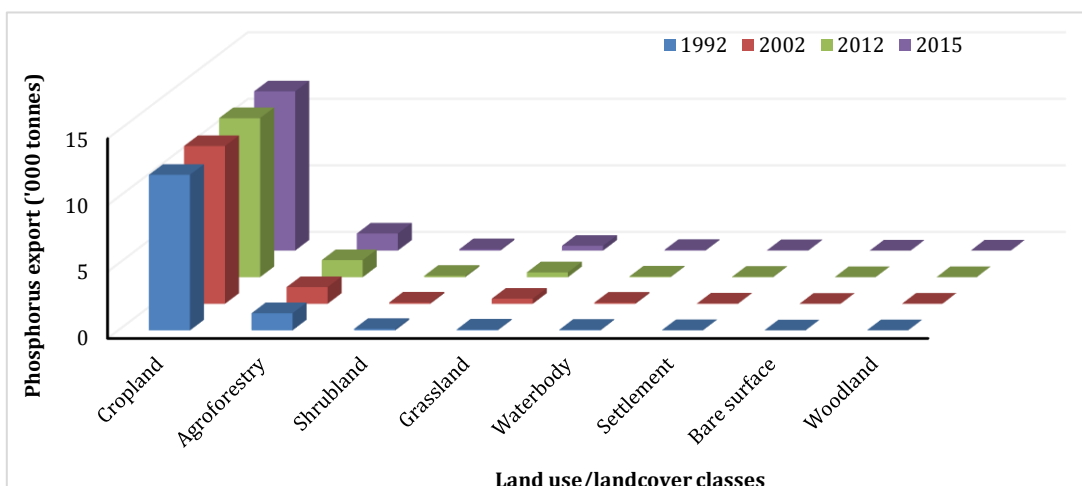


Fig 8. P export of the Sokoto-Rima across the different land use/landcover classes from 1992 to 2015

Land use/landcover influenced the proportion of N and P exported within the Sokoto-Rima basin. Fig 7 and Fig 8 show that cropland influenced nutrient export in the Sokoto-Rima basin with almost 85% of the total amount. This is immediately followed by agroforestry (which is mosaic of cropland and woodland) and grassland while bare surface contributes the least nutrient export. Infinitesimal proportion of nutrients was also exported from settlement. Roughly 90% of N export is sourced from cropland while few amounts are traceable to grassland, shrubland, woodland, and waterbody. This describes the basin N cycle in which cultivated areas determines the nature and pattern of N with respect to low tree density forested areas. [26] have shown that the trend of cropland dominated land use/landcover of the Sokoto-Rima basin will remain unchanged. By implication, this is anticipated to impede not only nutrient export and dynamics but also the attendant ecosystem services.

Fig. 8 specified that the proportion of P exported from the Sokoto-Rima basin is roughly 3-fold less than the magnitude of N. This is also directly related to the anthropogenic activities and limited P storage by the dominant land use/landcover themes [23]. Perring et al. [25] argued that available N inputs in a given terrestrial ecosystem could trigger a coupled increase in other related nutrient elements thereby boosting nutrient cycling. However, the scenario in a semi-arid environment such as the Sokoto-Rima basin where biomass response to increased N is very low, P export is high and co-related to anthropogenic forcing. This justification is proven by Fig 8 where natural land use/landcover contributes the least to P export as the landscape is dominated actively by agrarian influences.

3.3.2. Spatial variation of N and P export

The spatial context of nutrient export of the Sokoto-Rima basin over the period of this study showed dissimilar traits that explain the extent of place-based and location specific variations. In particular, spatial distribution and variation of N export as displayed in Fig 9 showed that N export is relatively unchanged within the period of study (1992-2015). Interval variation, however, depicts some explicitness. From 1992 to 2002, spatial decreases in exported N were detected around wetlands and agroforestry of the north. Spots of decreases were also detected in some parts of the east and the southern swath of the Niger plain where River Sokoto confluences with the Niger River. Local increases can be observed throughout the area with exceptions in the cultivated areas where there were no changes.

The period 2002 to 2012 had slight changes as spatial decreases in N export were detected in areas around the south and some wetland areas of the north. Substantial spatial decreases in N export within the 2012-2015 period could be related to the short space

of spatial comparison. Overall, spatial differences in N exports of the Sokoto-Rima basin remain largely constant with observed declines than increases, and this is analogous to the nature of the area.

The nature of spatial variation in P export returned fluctuating values (Fig 10). Although, P export remained relatively unchanged following similar pattern as that of N. However, there were locational differences across the period of study. The observed spatial trend was such that some areas recorded P increase then decrease later. Specifically, substantial increases were detected in some parts of the north, central and south within the period 1992-2002. The pattern remained relatively unchanged for the period 2002-2012 although some spots of decreases were identified in some eastern location close to water bodies. The period 2012 to 2015 had quasi-constant P export. The aggregate spatial variation of P export showed indications of increase than decrease particularly in areas of agroforestry of the northern axis, and along wetland and extensive floodplains of the south.

3.4. Sensitivity analysis of nutrient export

The linearity function of the equations utilised in deriving the spatial relationships between nutrients and associated parameters suggests a possible degree of sensitivity. This has been justified and substantiated in Fig. 11 which showed the aggregate nutrient export varied considerably with the parameters of the Sokoto-Rima basin. The sensitivity of the nutrient export was greatest for critical length (Crit len) showing the extent of elasticity such that a $\pm 50\%$ adjustment triggers a corresponding 94% decline and 108.76% upsurge in nutrient export. Threshold value (Threshold) demonstrates a converse sensitivity to nutrient exports with a quasi co-equal influence in which a 50% reduction leads to increase in nutrient export while +50% increment yields a reduction up to 95.93%. Load parameters attached to each of the land use/landcover class revealed a direct level of sensitivity out of which cropland returned the highest nutrient export with +50% increment leading to 110.09%. Similar sensitivity pattern was observed for loads for agroforestry and woodland in which positive adjustment in parameter value leads to direct change in nutrient exports. It can be summed that nutrient efficiency factor across the land use/landcover spectrum largely has direct influence on change in nutrient export where cropland and woodland possess the most dynamic influences (Fig. 11).

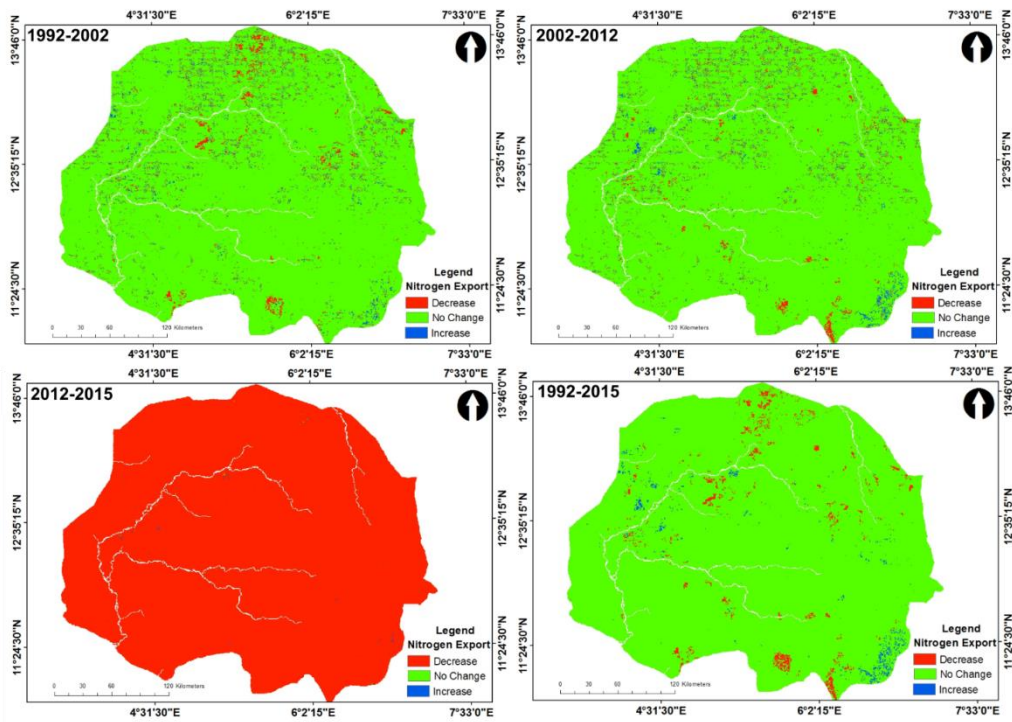


Fig 9. Spatiotemporal variation of nitrogen export in the Sokoto-Rima basin from 1992 to 2015 with specific interval differences (1992 to 2002, 2002 to 2012, 2012 to 2015 and cumulative spatial difference)

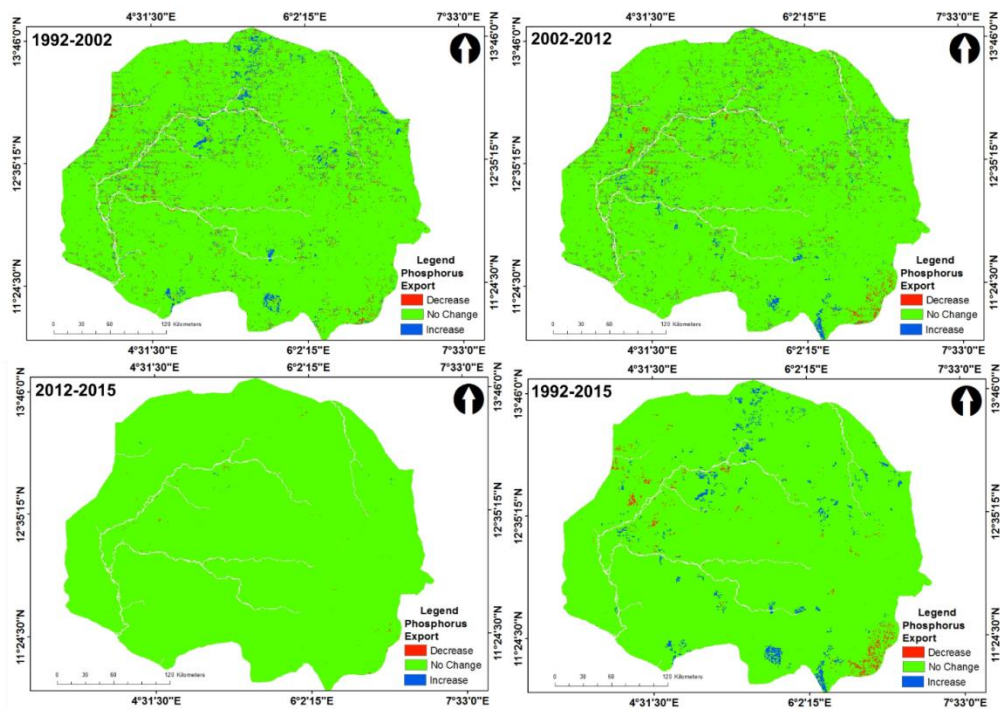


Fig 10. Spatiotemporal variation of P export in the Sokoto-Rima basin from 1992 to 2015 with specific interval differences (1992 to 2002, 2002 to 2012, 2012 to 2015 and accumulative spatial difference)

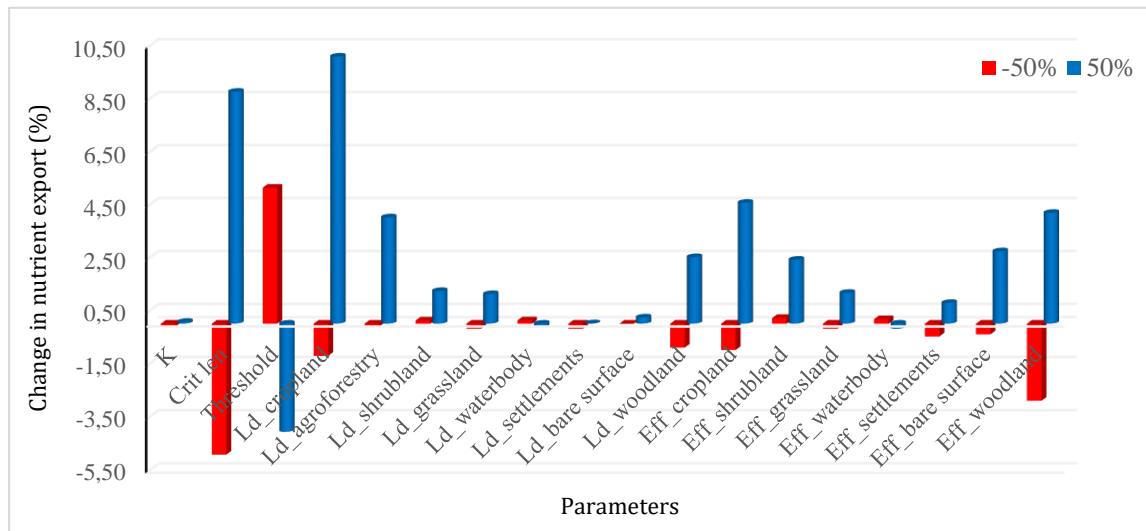


Fig 11. Sensitivity as depicted by response of the aggregate nutrient export to a $\pm 50\%$ change in selected input parameters for the entire Sokoto-Rima basin. K depicts Borselli factor, crit len (critical length, in Table 1), Ld and Eff stand for loads and efficiency for respective land use/landcover classes

3.5. Localized context for nutrient cycle

Nutrient cycling pathway is place-based and context-specific. It is significantly influenced by natural and anthropogenic factors. Given that the Sokoto-Rima basin is predominantly agrarian, the spatial organization of settlements is such that it is buffered by crop production complexes which stretches to wetlands and plains throughout the area. Accordingly, farmland fertilization accounts for N and P enrichment in the Sokoto-Rima basin. Related factors such as weathering of farm wastes, domestic wastes and sewage from townships and bucolic communities as well as animal droppings formed the sources of nutrients. These are usually washed into rivers and streams via surface runoffs from cultivated fields, animal production pens and the usage of animal

wastes for soil enrichment. These are often washed into open water bodies leading to eutrophication problems which have been recorded in the Sokoto-Rima basin [17-20]. This scenario formed the basis of the graphical illustration of River Zamfara (Fig 12) where farmlands and buildings flanked the stream. The persistence of this scenario will lead to uncoordinated and unabated water quality issues for the entire Sokoto-Rima basin. It also calls for the consistent monitoring and improvement of existing land uses that stimulates likely cases of water pollution from domestic and land cultivation areas. The need for regulations on water environment, pollution prevention and environmental protection is therefore vital to mitigate this trend.

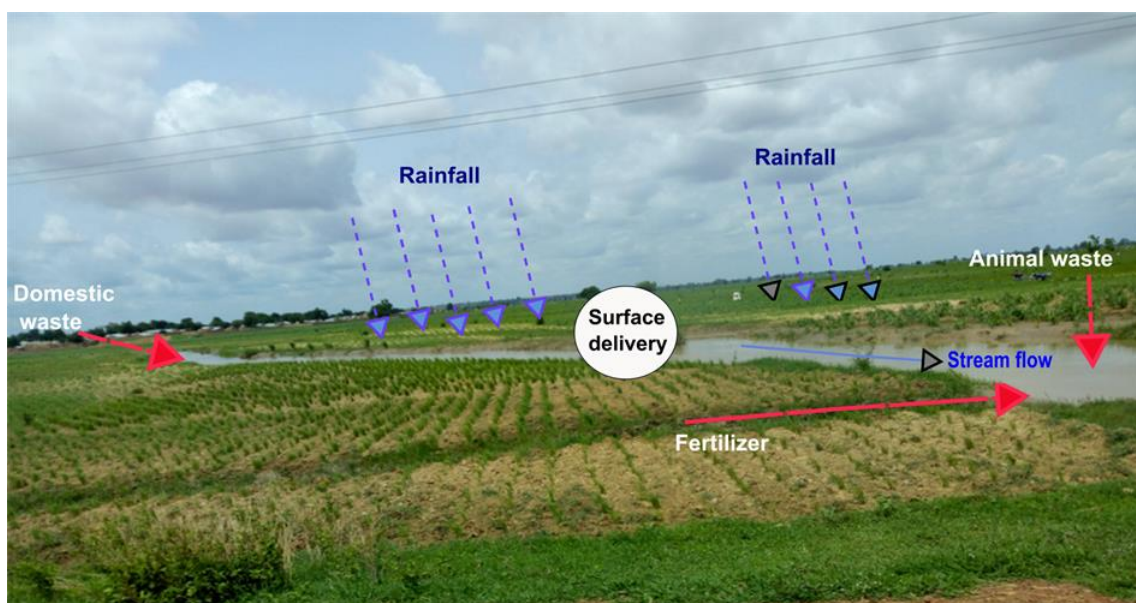


Fig 12. Pathway of nutrient flow and cycling in the along the section of River Zamfara a vital water body within the Sokoto-Rima basin. The blue arrow shows natural feature input source while the red arrow indicate the anthropogenic source of both nitrogen and phosphorus

4. CONCLUSIONS

This study has shown that amounts of surficial N outweighs P in the Sokoto-Rima basin by almost 15-fold with linear increment trend from 1992 to 2015. Also, spatial distribution showed that both nutrients were directly proportional to crop cultivation areas while water bodies particularly the major rivers were identified as sinks. As established in literature within the semi-arid regions of the world, subsurface nutrient loads of N and P loads produced different output in which N returned no trend while P returned linear increasing trend. Spatially, N loads were restricted to water bodies and P returned no spatial characterisation and variation. Nutrient exports also showed spatiotemporal variations with large amounts of N exports were observed compared to P. Cropland and agroforestry influenced roughly 90% of the amount of nutrient exported thus establishing a firm human-nature nexus in the amount of nutrient exported.

Management of this emerging nutrient enrichment of the landscape of the Sokoto-Rima basin require a synergistic approach whereby the intensity of crop cultivation is integrated with the nutrient sink approach. For instance, agroforestry and woodland advancement schemes will aid the control of the direct influence of cropland on nutrient adjustment at the local space. This approach will engender managed nutrient cycling close to reality. Within this context, the Nigerian section of the West African Great Green Wall programme aimed at curtailing the impact of the Sahara desert encroachment, can be locally adjusted as community-based approach to enhance natural ecosystem services and by extension improve environmental resource appraisal within the Sokoto-Rima basin [20, 21].

Sensitivity analysis of the InVEST model adopted for this study revealed some level of uncertainties in the predictive abilities of the model despite its innovative theory and simplified approach. This shows that more extensive studies on model calibration processes, consideration of high-resolution land use/landcover datasets, influence of parameterization should be considered vital. Model parameterisation of the InVEST model should therefore consider inclusion of ecological and physicochemical processes that are less cumbersome for model output interpretation. Addition of material elements within a given ecosystem space such as potassium (K) will further enhance the understanding of nutrient cycling. It will also improve the spatial simulation of multiple nutrients within any ecosystem. These measures are needed within the context of emerging science of nutrient modeling in consideration of natural and anthropogenic factors and forcing.

ACKNOWLEDGEMENTS

We thank the Natural Capital Project for granting access to download the InVEST software package. The efforts of the European Space Agency (ESA) and the Japanese Aerospace Exploration Agency (JAXA) in providing data access were kindly also acknowledged. We also appreciate the two anonymous reviewers

who provided constructive comments to improve the paper.

REFERENCES

- [1]. Millennium Ecosystem Assessment (MA), Ecosystem and Human Well-Being: Synthesis, Island Press, Washington DC. 2005a.
- [2]. Millennium Ecosystem Assessment (MA). Ecosystem and Human Well-Being: Biodiversity Synthesis, Island Press, Washington DC. 2005b.
- [3]. J. W. Redhead, L. May, T. H. Oliver, P. Hamel, R. Sharp, and J. M. Bullock, "National scale evaluation of the InVEST nutrient retention model in the United Kingdom," *Science of the Total Environment*, Vol. 610-611, pp. 666-677, 2018.
<https://doi.org/10.1016/j.scitotenv.2017.08.092> PMID: 28826113.
- [4]. S. Salata, G. Garnero, C. A. Barbieri, and C. Giaimo, "The integration of ecosystem services in planning: An evaluation of the nutrient retention model using InVEST software," *Land*, Vol 6, No. 48, 2017.
- [5]. E. M. Bennett, W. Cramer, A. Begossi, G. Cundill, S. Díaz, B. N. Egoh, I. R. Geijendorffer, I. R., C. B. Crug, S. Lavorel, E. Lazos, L. Lebel, B. Martin-Lopez, P. Meyfroidt, H. A. Mooney, J. L. Nel, U. Pascual, K. Payet, N. P. Harguindeguy, ... and G. Woodward, "Linking biodiversity, ecosystem services, and human well-being: three challenges for designing research for sustainability," *Current Opinion in Environmental Sustainability*, Vol 14, pp. 76 - 85, 2015.
- [6]. A. G., Power, "Ecosystem services and agriculture: Tradeoffs and synergies," *Philosophical Transactions of the Royal Society B*, Vol 365 No 1554, pp 2959-2971, 2010.
- [7]. P. Hamel, R. Chaplin-Kramer, S. Sim, and C. Mueller, "A new approach to modeling the sediment retention service (InVEST 3.0): Case study of the Cape Fear catchment, North Carolina, USA," *Science of the Total Environment*, Vol 524-525, pp. 166-177, 2015.
- [8]. Y Xue, J. Song, Y. Zhang, F. Kong, M. Wen, and G. Zhang, "Nitrate pollution and preliminary source identification of surface water in a semi-arid river basin, using isotopic and hydrochemical approaches," *Water*, Vol 8, pp 328, 2018.
- [9]. B. L. Keeler, S. Polasky, K. A. Brauman, K. A. Johnson, J. C. Finlay, A. O. Neill, K. Kovacs, B. Dalzell "Linking water quality and well-being for improved assessment and valuation of ecosystem services," *Proceedings of the National Academy of Sciences of the United States of America*, Vol. 109, pp. 18619-18624, 2012.
- [10]. N. Adimalla, S. Venkatayogi, "Geochemical characterization and evaluation of groundwater suitability for domestic and agricultural utility in semi-arid region of Basara, Telangana State, South India," *Applied Water Science*, Vol 8 (44), 2018.

- [11]. R. Sharp, H. T. Tallis, T. Ricketts, A. D. Guerry, S. A. Wood, R. Chaplin-Kramer, E. Nelson, D. Ennaanay, ... and J. Douglass, "InVEST 3.5.0. User's Guide. The Natural Capital Project" Stanford University. 2018.
- [12]. Z. Meng, Y. Yang, Z. Qin, and L. Huang, "Evaluating temporal and spatial variation in nitrogen sources along the lower reach of Fenhe River (Shanxi Province, China) using stable isotope and hydrochemical tracers," *Water*, Vol 10, pp. 231, 2018.
- [13]. Z. Tang, W. Xu, G. Zhou, Y. Bai, J. Li, X. Tang, D. Chen, Q. Liu, W. Ma, G. Xiong, H. He, N. He, Y. Guo, Q. Guo, J. Zhu, W. Han, H. Hu, J. Fang, and Z. Xie, "Patterns of plant carbon, nitrogen, and phosphorus concentration in relation to productivity in China's terrestrial ecosystems," *Proceedings of the National Academy of Sciences of the United States of America*, Vol 115, pp. 4033-4038, 2018.
- [14]. I. M. Magami and I. Sani, "Spatiotemporal sediment nutrient dynamics of Kware Lake, Nigeria," *Path of Science*, Vol. 5, pp. 3001-3006, 2019.
- [15]. W. J. Hahm, C. S. Riebe, C. E. Lukens, and S. Araki, "Bedrock composition regulates mountain ecosystems and landscape evolution," *Proceedings of the National Academy of Sciences of the United States of America*, Vol 111, pp. 3338-3343, 2014.
- [16]. S. E. Hobbie, J. C. Finlay, B. D. Janke, D. A. Nidzgorski, D. B. Millet, and L. A. Baker, "Contrasting nitrogen and phosphorus budgets in urban watersheds and implications for managing urban water pollution", *Proceedings of the National Academy of Sciences of the United States of America*, Vol 114, pp. 4177 - 4182, 2016.
- [17]. A. Galadima, Z. N. Garba, L. Leke, M. N. Almustapha, I. K. Adam, "Domestic water pollution among local communities in Nigeria --- Causes and consequences," *European Journal of Scientific Research*, Vol 52, pp. 592-603, 2011.
- [18]. M. I. O. Raji, Y. K. E. Ibrahim, B. A. Tytler, J. O. Ehinmidu, "Physicochemical characteristics of water samples collected from River Sokoto, Northwestern Nigeria," *Atmospheric and Climate Sciences*, Vol 5, pp. 194-199, 2015.
- [19]. A. M. Taiwo, O. O. Olujimi, O. Bamgbose and T. A. Arowolo, "Surface Water Quality Monitoring in Nigeria: Situational Analysis and Future Management Strategy". Water Quality Monitoring and Assessment, [D. Voudouris (ed.)], InTech, 2012. Available: <http://www.intechopen.com/books/water-quality-monitoring-and-assessment/surface-water-quality-monitoring-in-nigeria-situational-analysis-and-futuremanagement-strategy> (Accessed 28 July 2020).
- [20]. S. M. A. Adelana, P. I. Olasehinde and P.Vrbka, "Isotope and geochemical characterization of surface and subsurface waters in the semi-arid Sokoto Basin, Nigeria," *African Journal of Science and Technology*, Vol 4 (2), pp. 76-85, 2003.
- [21]. M. Abubakar, and J. K. Ipinjolu, "Levels of some anions in Sokoto-Rima River system in Northwestern Nigeria," *Journal of Research in Forestry, Wildlife and Environmental*, Vol 7 (1), pp. 23-39, 2015.
- [22]. B. D. Tarfa, I. Y. Amapu, C. K. Daudu, U. L. Arunah, I. A. Shero, A. S. Isah, A. A. Yakubu, N. Abdu, N. Tawa, A. T. Raymond, B. P. Marinus, U. E. Haratu and O. O. Ugbabe, "Optimizing fertilizer use within the context of integrated soil fertility management in Nigeria," In C. S. Wortmann, & K. Sones (eds.), *Fertilizer Use Optimization in Sub-Saharan Africa*, pp. 148-163, 2017. Nairobi: CAB International. Available: <http://africasoilhealth.cabi.org/wp-content/uploads/2017/03/Optimizing-Fertilizer-ISFM-in-Nigeria-Ch-12-high-res.pdf> (Accessed 24 December 2019).
- [23]. X. Liu, H. Sheng, S. Jiang, Z. Yuan, C. Zhang, and J. J. Elser, "Intensification of phosphorus cycling in China since the 1600s", *Proceedings of the National Academy of Sciences of the United States of America*, Vol 113 (10), pp. 2609-2614, 2015. Available: www.pnas.org/cgi/doi/10.1073/pnas.1519554113 (Accessed 28 July 2020).
- [24]. T. Maavara, C. T. Parsons, C. Ridenour, S. Stojanovic, H. H. Dürr, H. R. Powley, and P. Van Cappellen, "Global phosphorus retention by river damming", *Proceedings of the National Academy of Sciences of the United States of America*, Vol 112 (51) pp. 15603-15608, 2015. Available: www.pnas.org/cgi/doi/10.1073/pnas.1511797112 (Accessed 28 July 2020).
- [25]. M. P. Perring, L. O. Hedin, S. A. Levin, M. McGroddy, and C. de Mazancourt, "Increased plant growth from nitrogen addition should conserve phosphorus in terrestrial ecosystems", *Proceedings of the National Academy of Sciences of the United States of America*, Vol 105 (6) pp. 1971-1976, 2008. Available: www.pnas.org/cgi/doi/10.1073/pnas.0711618105 (Accessed 28 July 2020).
- [26]. S. A. Raji, M. Fasona, and S. Odunuga, "Simulating future ecosystem services of the Sokoto-Rima basin as influenced by geo-environmental factors", *Turkish Journal of Remote Sensing and GIS*, Vol 1 (2) pp. 106-124, 2020.
- [27]. National Bureau of Statistics, Annual Abstract of Statistics, Federal Government of Nigeria, Abuja, pp. 569, 2017.